The Dissertation Committee for Diana Paulina Zamora Olivares Certifies that this is the approved version of the following dissertation:

Differential Sensing of Kinases

Committee:

Eric V. Anslyn, Supervisor

Kevin Dalby

Jennifer Brodbelt

Guonbing Dong

Christopher W. Bielawski

Hung-Wen Liu

Differential Sensing of Kinases

by

Diana Paulina Zamora Olivares, B.S.

Dissertation

Presented to the Faculty of the Graduate School of

The University of Texas at Austin

in Partial Fulfillment

of the Requirements

for the Degree of

Doctor of Philosophy

The University of Texas at Austin

May 2014

Dedication

This dissertation is dedicated to:

My family

My father who showed me the importance of education and perseverance

My mother who showed me the value of hard work and kindness

My kind and great brother

To my loving husband, Adam Garland who has fulfilled my life with happiness

Acknowledgements

I would first and foremost like to acknowledge my advisor, Eric Anslyn, for his support and guidance, both professionally and personally during this last five years. I admire Eric as a researcher, professor, and as a human being. His kindness, creativity, and passion for science and life have influenced my professional career. He has been an exceptional mentor whose support has been present through success and failure. I would also like to acknowledge Dr. Kevin Dalby who has provided with valuable support and insight. I feel very grateful and fortunate to have been given the opportunity to study under the insight of such brilliant scientists. I would like to thank the past and present members of the Anslyn group: Michelle Adams, a dear friend who taught me how to run my first HPLC and LDA; Leo Joyce, who helped me during my transition to the USA; Lei You, who guided me with my first synthetic procedures during my first project; Alona Himali who taught me about peptide chemistry; Jiney Jose, who guided me during my second project; Alex Gade, who has been a wonderful co-worker and friend. I have been fortunate to develop a wonderful friendship with Hannah Jo and Helen Seifert with whom I have shared a great time. I would also like to thank the following group members Dr. Youjun "Charles" Yang, Ryota Saito, Amanda Hargrove, Justin Dragna, Jeff Pruet, Reid Long, and Pedro Metola. I would also like to mention my gratitude to Dr. Tamer Kaoud (College of Pharmacy, UT-Austin), for his friendship and particular insight that has provided throughout my studies. Michelle Gadush (Proteomics facility), who provided with valuable guidance in peptide synthesis. I would also like to thank my undergraduate advisors, Hulme Rios-Guerra (FESC-UNAM) and Guillermo Ceballos-Reyes (ESM-IPN), who awakened and guided my curiosity for Chemistry. This work was

supported by the CONACYT Fellowship No.212537. This work would not have been possible without the love and support of my family and close friends. To my husband Adam Garland – for your love and friendship, you are the best; graduate school gave me the best present of my life, meeting such a wonderful person to spend my life with. To my mom and dad – who have encouraged me to pursue my dreams despite the obstacles, I am truly grateful for your love, wisdom and for setting such a great example for me to follow over the years. To Uncle Frank – your unconditional love and support has been a pillar toward the success of my graduate studies. To Bobbie – you helped me to make this dream possible, thank you for believing in and for encouraging pursuing my goals. To Edgar, Ingrid and Leo – our talks and laughs have been the sun of my days. To my new family Frank, Chris, Rebecca, Janet, Michael, Jamey, Jack, Ian and Theo – who have become a wonderful part of my life, sharing together marvelous moments of happiness.

Differential Sensing of Kinases

Diana Paulina Zamora Olivares, Ph.D.

The University of Texas at Austin, 2014

Supervisor: Eric V. Anslyn

During the last decade, organic and supramolecular chemistry in combination with analytical and fluorescent-based sensing methods have led to the development of chemical biology tools to study protein phosphorylation *in vitro*. However, further challenges remain present to develop better chemical approaches that can allow us to understand the activation/inhibition of specific kinase pathways.

To avoid the tedious process of developing individual highly selective receptors, the use of differential sensing techniques has been growing in the supramolecular chemistry field. This sensing protocol exploits the interactions between target analytes and a library of cross-reactive receptors to create a response pattern that is unique for individual analytes or different mixtures thereof. Using this approach, one obtains a distinct fingerprint of composite signals produced by the sensor elements allowing for discrimination of different kinases *in vitro* and in complex mixtures such as cell lysates.

The main emphasis of this work sought to expand the current optical-based detection systems of phosphorylated proteins to include a new pattern-based recognition method for a new class of protein kinases. To this end, the synthesis of chemosensors and peptide-based biosensors was pursued to detect and differentiate relevant mitogen-

activated protein (MAP) kinases which represent targets of pharmaceutical interest. Further, this research included the quantitative detection of MAP kinases and corresponding inhibitors using a combination of pattern recognition approaches with new chemometric tools.

Table of Contents

List of Tables

List of Figures

List of Schemes

Chapter 1: Optical-Based Sensing Methods for the Detection of Phosphorylated Protein Kinases

1.1 Introduction

The coordinated activity of enzymes, substrates, ligand molecules and metal ions within cells follows a systematic network of modulated signals, producing the necessary metabolic processes for the appropriate balance of cellular functions. Among the diverse post-translational modifications implicated in cellular signaling pathways, the phosphorylation and dephosphorylation of proteins are two of the most important and prevalent processes in eukaryotic cells. Phosphorylation and dephosphorylation are regulated by protein kinases and protein phosphatases, respectively. Interestingly, it has been found that nearly 30% of all human proteins are phosphorylated at any time, while about 500 different protein kinases participate in this process.[1]

Traditional methods have evolved into more efficient and versatile tools to study the dynamics of protein phosphorylation. Over the last decade, organic and supramolecular chemistry in combination with analytical and fluorescence-based sensing methods have led to the development of chemical biology tools to study protein phosphorylation *in vitro*. However, further challenges remain present to develop better chemical approaches that can allow us to understand the activation/inhibition of specific kinase pathways.

Herein, we review on the progress toward the development of new chemical biology tools to sense phosphorylation events on peptides and proteins. The focus is placed on the synthesis of chemosensors in combination with the application of differential sensing

methods. Afterwards, we discuss the detection and differentiation of phosphorylated Mitogen-activated protein (MAP) kinases and their dynamic active/inactive states in complex mixtures such as cell lysates.

1.1.1 Protein Phosphorylation

Reversible phosphorylation of proteins is one of the most important regulatory processes in cell function. Chemically, it is considered a covalent modification reaction, where the γ-phosphoryl group of 5'-Adenosine TriPhosphate (ATP) is transferred to the hydroxyl group of the amino acids tyrosine, threonine and/or serine increasing the hydrophilic properties of the protein (**Figure 1.1**).[2] This event acts as a "switch on", leading to conformational changes in the protein, which are correlated with protein-protein interactions following a cellular signaling pathway. Protein phosphorylation regulates a wide range of cellular processes involved in metabolic pathways such as cell growth, proliferation and differentiation, membrane transport, mitosis, and apoptosis.[3] Previous studies have shown that mutations and aberrant kinases can induce overexpression of the protein substrate, causing abnormalities in the cellular processes and leading to negative outcomes such as cancer, neurodegenerative and inflammatory diseases, diabetes mellitus, endocrinological disorders, and hematological malignances.[3-5]

Most importantly, academic institutions and drug companies have made a substantial effort in order to understand the correlation between the dynamics of aberrant kinases and early cancer onset. Thus, developing new sensing methods that can establish a correlation

between kinase activity and a fluorescent substrate that modulates its signal upon phosphorylation remains a challenging task. The creation of such methods could potentially allow for the development of protein-kinase inhibitors that target a specific group of kinases for therapeutic purposes.[4]

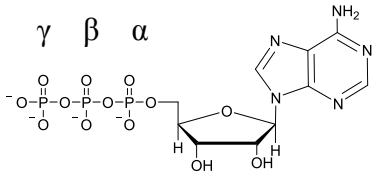

5'-Adenosin triphosphate (ATP)

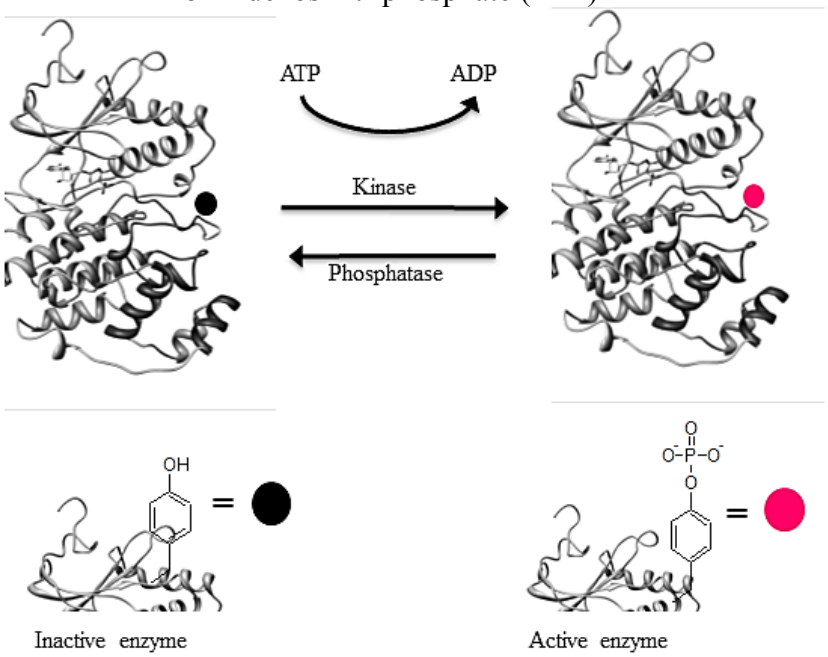

Figure 1.1: *Protein phosphorylation reaction*. Graphic representation of the phosphorylation event of a protein substrate where a kinase transfers the γ-phosphoryl group of ATP to the hydroxyl group of the amino acid tyrosine.

1.1.2 History of Protein Kinases

In the 1950s, kinase activity was first observed when Eugene Kennedy described a liver enzyme capable of catalyzing the phosphorylation of casein using radioactive ATP.[6] Afterwards, Edwin G. Krebs and Edmond H. Fisher discovered the dynamic reversible transformation of phosphorylase a to phosphorylase b in the presence of Mg-ATP. Krebs and Fisher gave the name phosphorylase kinase to the enzyme that was responsible to catalyze the transfer of the γ-phosphoryl group of ATP to a particular serine residue in phosphorylase b.[7] Their pioneering discoveries earned Ed Fisher and Ed Krebs the Nobel Prize in 1992.

However, it took several decades for researchers to become aware of the importance of protein phosphorylation. At the end of the 1960s, protein phosphorylation was still thought of as a single and specialized mechanism to regulate glycogen metabolism. It was during the 1970s and 1980s that several kinases were discovered and correlated with other cellular functions such as glycolysis and lipolysis in liver, heart-muscle relaxation and contractibility.[8] Soon afterwards, some protein kinases such as epidermal growth factor (EGF) were discovered to be specific tyrosine kinases.[9] Additionally, most of the threonine/serine kinases and their regulatory mechanisms were discovered during the late 1970s.[8]

The first connections between malfunctioning kinases and disease were made in the late 1970s. Castagna discovered tumor-activators that were analogous to the second messenger diacylglycerol responsible for the activation of protein kinase C.[10] In the

twenty-first century, protein kinases have become one of the major target groups of enzymes in drug discovery after G-protein-coupled receptors.[4]

1.2 Protein Kinase Classification

More recently, Manning *et al.* categorized the human kinome to discover a total of 518 human protein kinases. The human kinome is first classified in two major kinase groups. The first group is a single super-family that encompasses 478 eukaryotic protein kinases (ePKs), which are categorized based on the sequence similarity of their catalytic domain. These (ePKs) conventional protein kinases are divided into 388 protein-serine/threonine kinases and 90 protein-tyrosine kinases. The second kinase group includes 40 atypical protein kinases (aPKs) which are found in thirteen families. These aPKs present biochemical kinase activity, but they lack sequence similarity to the ePK group. This new kinome database is encoded by 2% of all the human genome.[11]

The 518 human kinases were also classified into nine major groups according to the sequence similarity of their catalytic domain and biological functions. Each group is divided into families and subfamilies. **CMGC** group 1 containing CDK, MAPK, GSK3, CLK families; **AGC** group 2 containing PKA, PKG, PKC families; **TK** Tyrosine kinase group 3; **TKL** Tyrosine kinase-like group 4; **CAMK** Calcium/calmodulin-dependent protein kinase group 5; **CK1** Casein kinase 1 group 6; **STE** Homologs of yeast Sterile 7 group 7, Sterile 11, Sterile 20 kinases. For instance, the following dendogram can quickly help to identify kinase groups whose members are only phosphorylated substrates with

tyrosine residues (TK or TKL), while enzymes in the other groups are phosphorylated serine and threonine residues (**Figure 1.2**).[11]

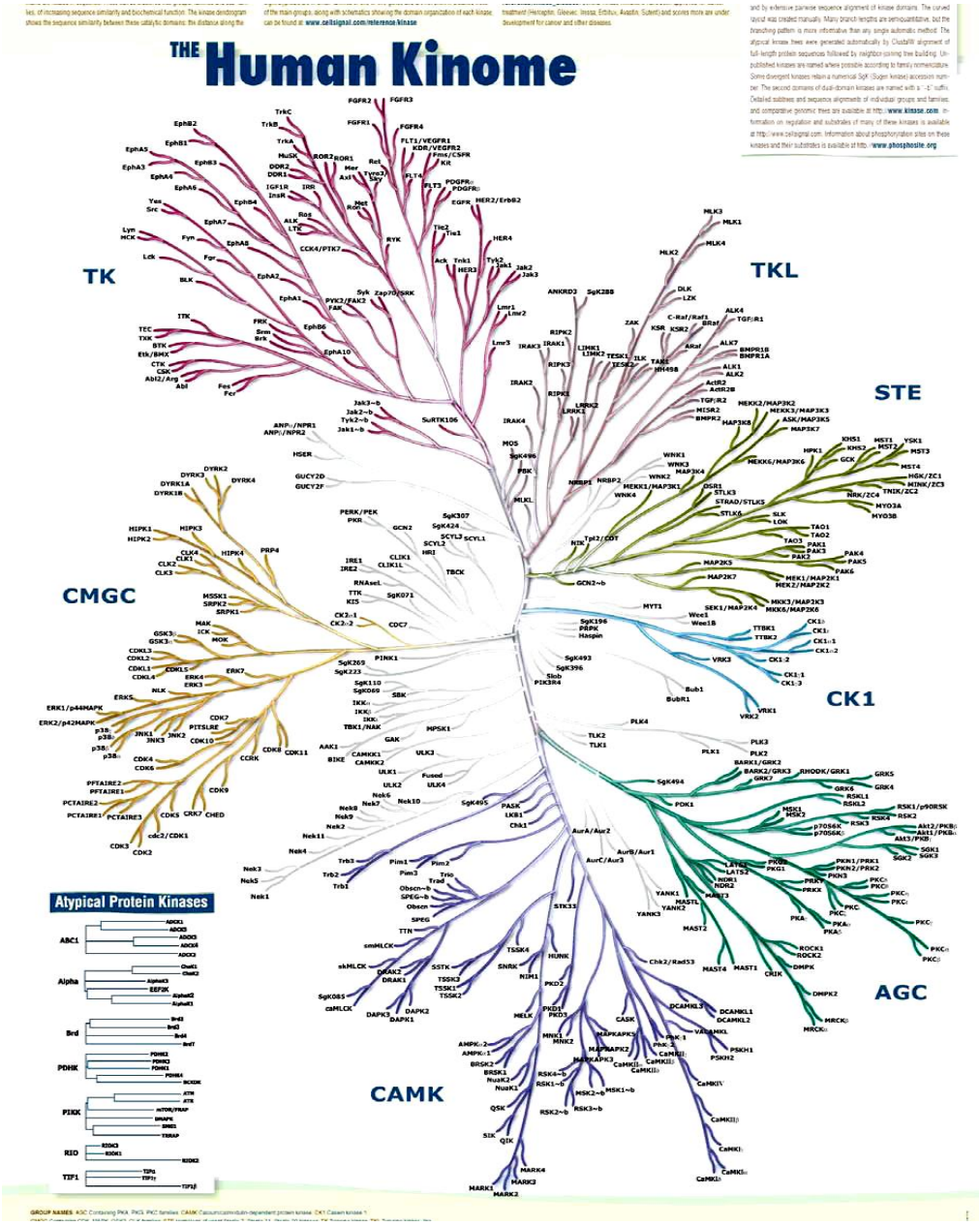

Figure 1.2: *Major groups of human protein kinases*. Kinome dendogram showing seven major groups of kinases, which are also divided in families and subfamilies. (Reproduced from Ref. 11. © Science, 2000)

1.3 Mitogen-Activated Protein Kinases (MAPK)

In the late 1980s, a protein kinase identified as insulin-stimulated protein kinase was found to phosphorylate microtubule-associated protein-2 (MAP2). Later on, it was found that the activation of insulin-stimulated protein kinase required the presence of mitogens and growth factors, changing the name to mitogen-activated protein kinase (MAPK).

The MAP kinase family is composed of serine/threonine kinases that are members of the CMGC kinase group, which were named according to the initials of some members of this group. The MAP kinase family is classified in subfamilies called extracellular signal-regulated kinases ERK1 and ERK2; the c-Jun N-terminal kinases, JNK1, JNK2, JNK/3; and four p38 enzymes p38α, p38β, p38γ and p38δ.[3]

External factors activate the cell-surface receptors which result in a cell signal cascade of events that promote activation of the MAP kinase module MAPKKK-MAPKK-MAPK (**Figure 1.3**). On this module, MAPKKK and MAPKK are known as upper kinases or upstream activating kinases that need to be active through the MAPK cascade, which in turn signal the activation or phosphorylation of MAPKs. ERK, c-Jun and p38 MAP kinases translate these signals into modulation of gene expression and regulation of cell function such as cell growth, proliferation, differentiation and apoptosis.[12]

MAP kinases catalyze the phosphorylation of substrates that contain serine/threonine residues on the consensus PX(S/T)-P motif. Their downstream MAPK substrates constitute other protein kinases, transcription factors, phospholipases and cytoskeletal

proteins.[13] In general, MAP kinases are responsible for key cellular functions such as gene expression, mitosis, regulation of apoptosis and the cell cycle, cytokine production and inflammatory responses.

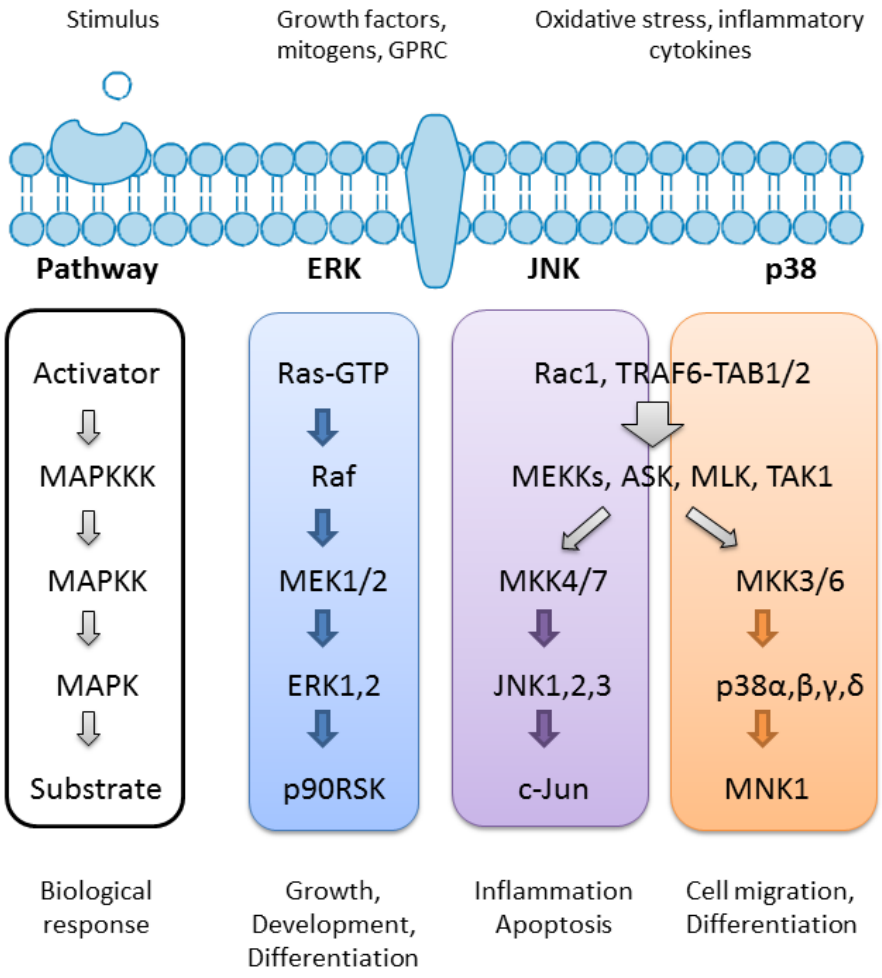

Figure 1.3: *Mitogen-activated protein kinase module***.** Graphical representation of the conventional ERK, JNK and p38 upstream and downstream signaling cascades.

1.3.1 Activation of MAP Kinases

The most essential requirement for MAP kinase activation is the dual phosphorylation of the threonine (Thr) and tyrosine (Tyr) residues present in a particular segment called the Thr-Xaa-Tyr (TXY) motif. This dual phosphorylation motif TXY is located on the activation loop of MAP kinases (**Figure 1.4**). The phosphorylation of both amino acids promotes conformational changes stabilized by electrostatic interactions within the loop. Conformational rearrangements of MAP kinase structure involved loop reorientation, lobe closure, α_C helix orientation and C-terminal reorganization.[14] The structural changes of the catalytic site and the ATP binding groups create the recognition site for the protein substrate.

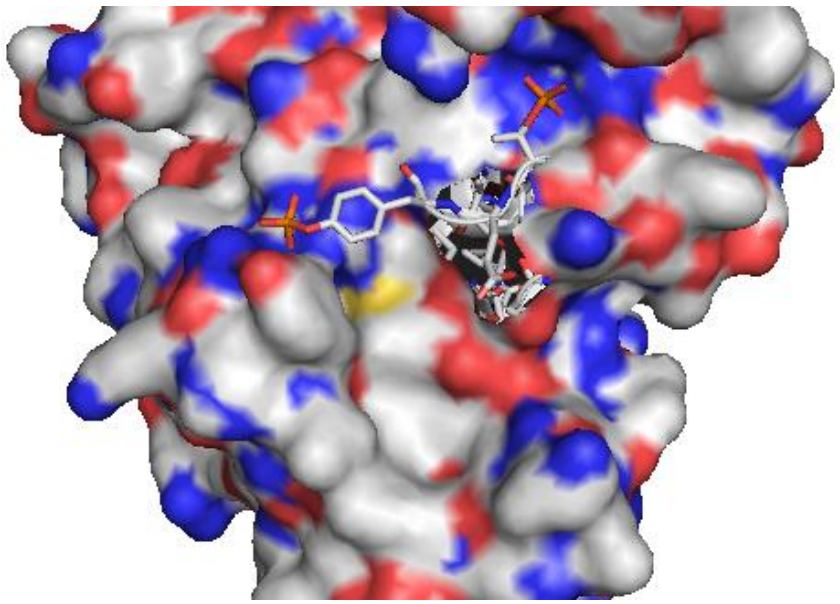

Figure 1.4: *Active protein structure of ERK2 (PBD ID: 2ERK).* ERK1/2 presenting dual phosphorylation on the ^{183}T-E-Y^{185}motif located on the activation loop. The electrostatic interactions between negatively charged phosphoryl groups and positively charged arginine residues induce conformational changes on activated MAP kinases.

1.3.2 ERK, JNK and p38 MAP Kinases

1.3.2.1 *Extracellular Signal-Regulated Kinases*

Extracellular signal regulated kinases ERK1 and ERK2 are 43 and 41 kDa respectively, and are considered isoforms because they share 83% of their amino acid sequence. The ERK pathway is mainly initiated by stimulation of growth factors, hormones, virus infection or carcinogens. Important functions of the ERK cascade involve the regulation of meiosis, mitosis, cell migration and antiapoptotic signals.[12]

After extracellular stimuli signal through the cell surface plasma membrane, the ERK cascade (Ras, Raf-1, MEK1/2, ERK1/2) starts with the activation of GTP-bound Ras which in turn promotes Raf association with the plasma membrane (**Figure 1.5**). Then Raf phosphorylates MAP kinases MEK1 and MEK2. ERK1 and ERK2 are activated by dual phosphorylation of the TEY (^{183}Thr-Glu-Tyr^{185}) motif by dual-specificity upstream kinases MEK1 and MEK2.[15]After activation, Both ERK1 and ERK2 translocate from the cytosol to the nucleus, where they phosphorylate several important substrates, such as transcription factors Ets-1, Elk-1, c-Myc and more. ERKs also activate the ribosomal S6 protein kinase (p90RSK), responsible for signal transduction and activation of other ribosomal proteins.[16],[17]

The structural differences between active and inactive ERK2 have been intensively studied in the past two decades. Dual phosphorylation of Thr-183 and Tyr-185 promotes conformational rearrangements stabilized by electrostatic interactions between the negatively charged phosphoryl groups and the positively charged arginine residues.[18]

There is an important association between the duration of ERK signaling and abnormal cell behavior. Unregulated ERK cascade activation by growth factors and *Ras* oncogene can lead to sustained ERK1 and ERK2 activity, resulting in the suppression of signals that control the cell cycle and cell survival.[19]

1.3.2.2 c-Jun N-Terminal Kinases and p38MAP Kinases

JNK and p38 MAP kinases are also identified as stress-activated protein kinases (SAPK). In most cases, JNK and p38 cascades are simultaneously activated by cellular and environmental stress such as DNA damage, ischemia, UV irradiation, changes in osmolality, oxidative stress and heat shock. Likewise, different cytokines such as tumor necrosis factors (TFN) which are responsible for programmed cell death can cause activation of JNK and p38 kinases. Anomalies on JNK gene expression are involved in different diseases such as diabetes (Type 1 and 2), cardiovascular diseases, arthritis, Alzheimer's and Parkinson's diseases.[20]

The JNK signaling pathway turns on different cellular functions, including differentiation, cell growth, transportation and apoptosis.[19] There are three isoforms in the JNK subfamily (JNK1, JNK2 and JNK3) which are activated by dual phosphorylation of the TPY (Thr-Pro-Tyr) motif within the activation loop.[21] The JNK cascade (MKK4/7, JNK, c-Jun) starts with activation of the upstream kinases MKK4 and MKK7 by upstream activators ASK, MLK, TAK, among others. MKK4 and MKK7 are dual-specificity kinases that phosphorylate threonine and tyrosine residues on JNK isoforms, which in turn activate the transcription factor c-Jun (**Figure 1.3**).[22]

Due to its prevalent role in cell migration and apoptosis, JNK activation can trigger tumor proliferation or tumor suppression. C-Jun acts as a transcriptional repressor of the gene p53, which is responsible for tumor suppression. The oncogenic function of JNK cascade induces the sustained activation of c-Jun which promotes cell proliferation and cell cycle progression. In addition, the C-Jun oncogene has been highly expressed in most carcinoma cells.[23,24]

Instead, the proapoptotic functions of the JNK cascade can restrict Ras-induced tumor progress by inhibition of proliferation, inhibition of angiogenesis or promotion of apoptosis. JNKs initiate apoptosis in response to many different types of stress such as γ-irradiation, ischemia/reperfusion injury in heart attacks, protein synthesis inhibitors (anisomycin) and inflammatory cytokines. Particularly, chemotherapeutic agents require JNK participation to induce apoptosis.[25,26]

Different isoforms have been identified in the p38-MAPK subfamily: p38α, β, γ and δ, including ERK6 which was recently identified.[27]Analogous to the JNK cascade, MKK3 and MKK6 are also phosphorylated by upstream kinases ASK, MLK and TAK. Dual upstream kinases MKK3 and MKK6 phosphorylate p38-MAP kinases on the TGY (Thr-Gly-Tyr) motif. Different target proteins such as transcription factors, kinases or phosphatases (MEF2, ATF-2, MSK1/2) are activated by p38-MAPKs.[28]

Similar to JNK signaling pathways, the p38-MAPK cascade is involved in several cellular functions such as differentiation, proliferation, cytokine secretion and gene expression. Likewise, p38-MAPK signaling presents antagonistic roles. It is required for

apoptosis and cell survival, depending on the cell type and associated environmental stress.[19]

1.3.3 Ras Proteins and MAPK Signaling Pathway

Unregulated MAPK signaling pathways can trigger the development of tumor initiation and progression, as well as the processes of invasion and metastasis.[19] The following MAP kinases, ERKs, JNKs and p38s have been recognized to play an essential role in controlling cell migration through the regulation of the module Ras/Raf/MAPK (**Figure 1.5**), and migration is remarkably important in leading metastatic processes. Substantial experimental data has shown that aberrant activation of Ras proteins is responsible for the development of the malignant phenotype in a variety of cancer cells.[29]

Extracellular ligands bind to the cell surface plasma membrane receptors. These interactions cause guanine nucleotide exchange factors (GEFs) to activate and regulate the cycle between inactive guanosine diphosphate GDP-bound and active guanosine triphosphate GTP-bound forms (**Figure 1.6**). *Ras* proteins are located in the inner face of the plasma membrane and their activity is regulated by the GDP-bound/GTP-bound nucleotide exchange.[30] GTP-bound Ras binds to a broad variety of effector proteins (Raf serine/threonine kinases, PI3K lipid kinases) to stimulate different intracellular signaling pathways. Particularly, the ERK-MAPK protein kinase cascade has been associated to the development of *Ras* oncogenesis. Sustained signaling of mutationally activated Ras at residues 12, 13 and 16 is present in almost 30% of all known human cancers.[31] The manner in which Ras is involved in the deregulation of the cell cycle process and

promotion of cell survival has been well documented; additionally, much emphasis has been placed in the understanding on how Ras promotes metastasis.[30]

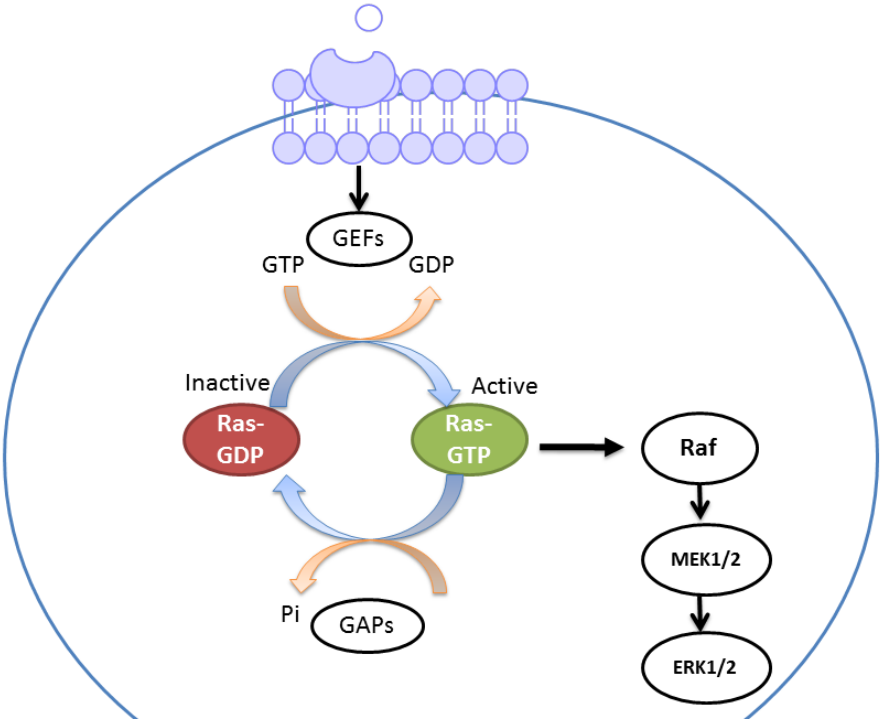

Figure 1.5: *Activation of Ras /Raf/MAPK signaling pathway.* External stimuli cause the activation of guanine nucleotide exchange factors (GEFs), which in turn replace inactive Ras-GDP to active Ras-GTP. GTPase –activating proteins (GAPs) regulate the hydrolysis of Ras-GTP back to the inactive form. Active GTP-bound Ras stimulates intracellular Ras/Raf/MAPK signaling.

Traditional Methods Used to Study Kinase Activity

1.3.4 Radioactivity-Based Assay

Conventional methods to study the activation state of kinases are associated with some drawbacks such as time-consuming and expensive protein purification protocols for *in vitro* assays, which lack spatial-temporal resolution. The phosphotransfer of radioactive isotope γ^{32} P-ATP to a substrate is monitored by scintillation counting.[32] Even though radioactive-based assays are efficient and sensitive, they present additional setbacks: 1) they require special handling for safety reasons, 2) this method generates radioactive waste, 3) these assays cannot be used for high-throughput analysis due to their inherent endpoint nature,4) these methods are not practical when working with cell lysates, and 5) sub-physiological concentrations of ATP (10-50 μM) are required for the assay to avoid dilution of γ^{32}P-ATP.[33]

1.3.5 Immunoblotting

Alternatively, endogenous kinase activity can be detected by performing in-gel assays. Western blotting analysis is still a powerful semi-quantitative analytical technique to detect specific kinases in cells from cell cultures or tissues.[34] After sample preparation, the first step separates the proteins from the sample using gel electrophoresis, where a small sample volume with the kinase protein is loaded into wells in a polyacrylamide gel membrane. (**Figure 1.6**) Then, the gel is introduced into a blotting tank that is filled up with detergent. After voltage is applied along the gel, proteins migrate through the gel at

different speeds. The proteins are separated based on their isoelectric point, molecular weight or electric charge.[35] For the second step, the gel is placed on top of a nitrocellulose or polyvinylidene difluoride (PVDF) membrane which possesses a strong affinity for proteins inside another blotting tank. Usually an electrical current is applied to the blotting tank in order to transfer the proteins to the thin membrane (**Figure 1.7**).[35] After the transfer process, a blocking step is performed before the addition of an antibody.

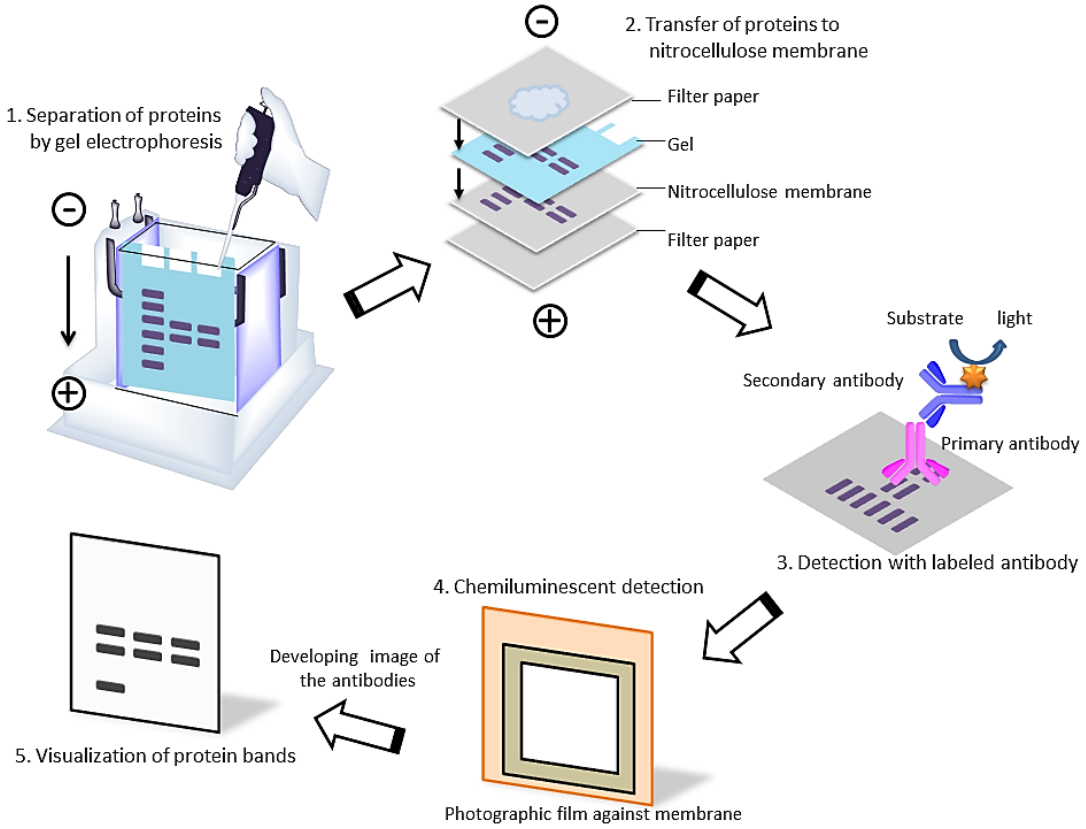

Figure 1.6: *Immunoblotting process*. Schematic representation of Western blot method for the detection of phosphorylated protein kinases.

Considering that the membrane has the same affinity for the antibody and the protein targets, the membrane is first incubated with a diluted solution of protein such as non-fat dry milk or bovine serum albumin (BSA) to avoid non-specific interactions between the antibody and the PVDF membrane. Then, a second diluted solution, which contains a primary antibody (0.5-5 µg/mL) for a specific kinase, with small percentage of detergent and powdered milk or BSA, is added to the membrane and incubated for 30 min to

overnight. A subsequent washing step is done to remove unbound primary antibodies. Then, the secondary antibody, which is directed at a specific portion of the primary antibody (known as anti-mouse or anti-goat, etc) is incubated with the membrane. These antibodies or monoclonal antibodies are produced by rabbits or mice, or in cells respectively. The secondary antibody is attached to biotin or to a reporter enzyme such as horseradish peroxidase.[36] Finally, a substrate for the enzyme is added to the membrane producing luminescent light in proportion to the amount of phosphorylated or non-phosphorylated kinases. A sheet of photographic film is placed on top of the membrane, and the film is passed through a photo developing machine. The film provides clear visualization and shows short bands that represent individual kinases on that sample.

Even though immunoblotting is a non-radioactive labeling approach and can detect phosphorylation states of kinases using phospho-specific antibodies, several steps are necessary throughout the process, which makes it time-consuming and expensive. Another limitation is that several kinases have many phosphorylation sites to which specific antibodies are not available.[37] In general, the major limitation of radio-labeling and immunoblotting assays is that they do not allow for real-time detection of kinase activity within cellular processes with normal or modified expression in cell extracts or living cells.

1.4 Fluorescence-Based Sensing Methods to Study Protein Phosphorylation

1.4.1 Fluorescence Sensing

The use of fluorescence spectroscopy as an analytical tool has seen greater spread in the last decade due to its versatility in fundamental research within different fields in medicine and biotechnology. In this context, fluorescence-based probes that can report fluorescence changes upon phosphorylation are rapidly increasing in number. Fluorescence is preferred over other spectroscopic methods such as absorbance due to its high sensitivity (1000-fold higher), selectivity, short detection times, and biocompatibility.[38] Likewise, fluorescence-based chemosensors have become powerful tools to monitor phosphorylation events not only in purified kinases but also while in their native cellular environment, allowing for quantification of kinase activity with temporal and spatial resolution.

Fluorescence is a photophysical process that takes place when a molecule is irradiated with UV/vis light, resulting in the emission of light from a singlet excited state. First, the exposure of a molecule to light at an appropriate wavelength promotes the absorption of a photon which in turn excites an electron from the ground state S_0 (taking place from the highest occupied molecular orbital, HOMO), to a higher energy orbital. This electron is promoted to the lowest unoccupied molecular orbital (LUMO) in the molecule; this excited state is known as the singlet state S_1 where the spin is conserved by light excitation (**Figure 1.8**). Then, energy is released as radiationless transitions when the electron relaxes from a higher to a lower vibrational level within the S_1 electronic state.

Next, fluorescence emission occurs when the excited molecule relaxes from the excited singlet state to the ground state releasing excess energy in the form of photons.[39]

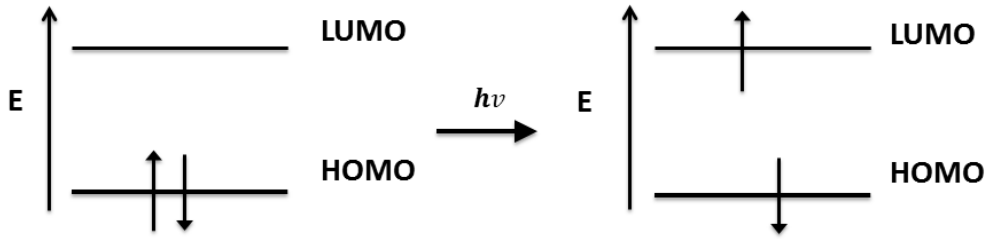

Figure 1.7. *One representation of a molecular orbital diagram.* Promotion of an electron occurs from the HOMO to the LUMO after light excitation.

Once in the ground state, the molecule can undergo repeating absorption-emission cycles giving continuous signaling photons, which is the origin for the high sensitivity of this technique. Nevertheless, excited molecules can follow different pathways to release the obtained energy; thermal deactivation, intersystem crossing followed phosphorescence, or interactions of the excited state molecule with other molecules resulting in electron transfer shown in the Jablonski diagram (**Figure 1.8**).[40]

The intrinsic properties of fluorescence, including anisotropy, FRET, PET quenching, environment sensitivity and metal-ion enhancement have allowed for the design of a wide variety of kinase sensors.

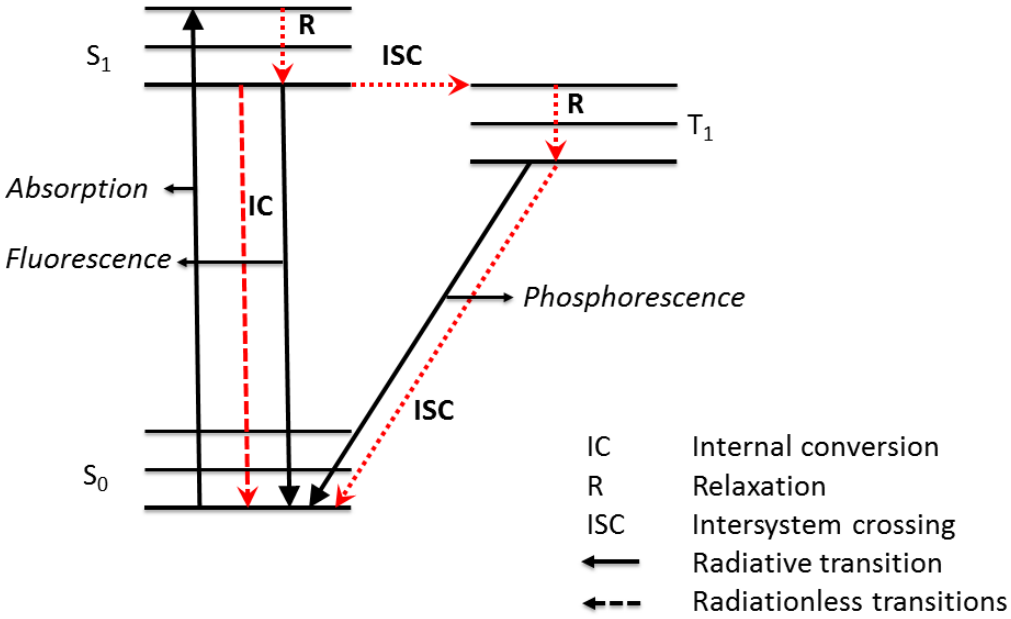

Figure 1.8: *One representation of a Jablonski diagram.* Summary of the several electronic and vibrational states, and photophysical processes observed in the singlet and triplet excited states.

1.4.2 FRET-Based Protein Biosensors

Forster resonance energy transfer (FRET) is a distance dependent process wherein nonradioactive energy is transferred from a donor to an acceptor. Cyan fluorescent protein (CFP) and yellow fluorescent protein (YFP) were used as a donor-acceptor pair because of their photostability and sensitivity. Usually FRET sensors present a modular design including a peptide substrate to target a kinase, a flexible linker, a phosphopeptide binding domain (PBD), and two fluorescent proteins (FPs) attached to the N- and C-termini. Upon phosphorylation the PDB binds to the phosphorylated fragment, bringing both FPs together into close proximity, resulting in an intramolecular FRET event.[41]

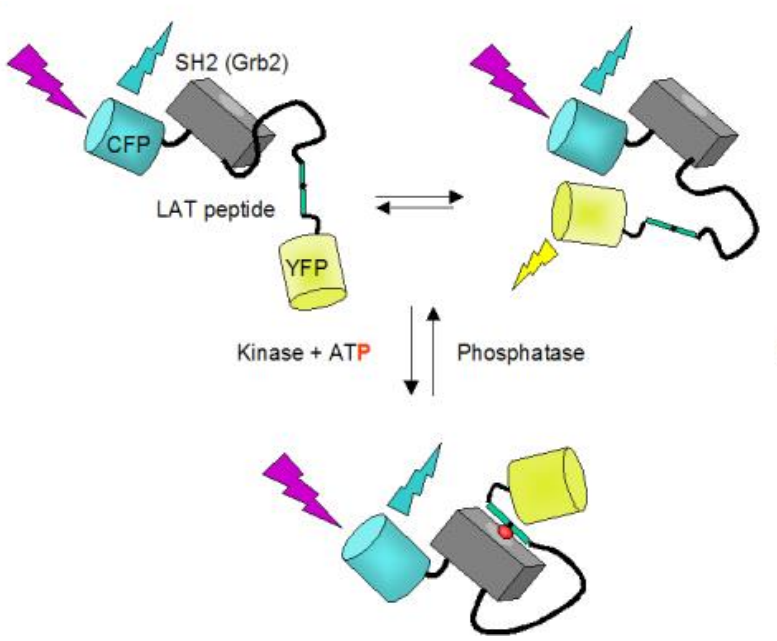

Figure 1.9: *Modular design of FRET-based biosensors*. Schematic representation of the Reporter of Zap-70 activity, including the peptide substrate, a linker, FRET resporters: Cyan fluorescent protein (CFP) and yellow fluorescent protein (TFP). (Reproduced from Ref.46. © PloS ONE, 2008)

As an example, Lellouch*et al.*[42] designed a genetic encoded biosensor called ROZA (Reporter of Zap-70 activity) to detect phosphorylation events of tyrosine kinase ZAP-70 in Jurkat T-cell membrane receptors. ROZA sensors were produced using peptide substrates for ZAP-70 that contained tyrosine residues Tyr132, Tyr175 and Tyr195. The peptide substrates were linked to the respective SH2 domain of mouse Grb2 for Y175 and Y195 (**Figure 1.9**). Several variants of ROZA were generated by varying the peptide substrate, the length of the linker, and the SH2 fragment. The sequence that resulted in the most significant FRET change due to efficient phosphorylation was incorporated to a peptide containing 13 *N*-terminal residues of mouse Lck to restrict its location to the

plasma membrane of Jurkat T- cells. Upon addition of a phosphatase inhibitor which reveals tyrosine kinase activity to the ROZA-expressing Jurkat cells, kinase activity was observed by a decrease of the 535 nm/470 nm ratio corresponding to the FRET signal. Jurkat T-cells expressing ROZA were examined by immunoblotting to prove that the observed FRET changes were due to ZAP-70 dependent phosphorylation. Additionally, treatment of the transfected T-cells with a kinase inhibitor for ZAP-70 resulted in the inhibition of ROZA phosphorylation. Remarkably, subcellular localization of ZAP-70 clusters was observed in Jurkat cell conjugates due to probe localization in the plasma membrane.

1.4.3 Environmentally-Sensitive Peptide Sensors

Environment-sensitive biosensors present a fluorophore that exhibits different spectroscopic properties such as shifts in the emission wavelength, fluorescence lifetimes, and quantum yields in response to changes in solvent polarity of their immediate environment. Solvatochromic fluorophores usually present large excited-state dipole moments, displaying weak fluorescence emission and low quantum yields in aqueous media. In contrast, fluorophores display high fluorescence signals in non-polar solvents or when linked into hydrophobic pockets in proteins. Typical solvatochromic fluorophores include 4-dimethylamino phthalimide (4-DMAP, **1.1**), PRODAN (**1.2**), DANSYL (**1.3**) or 7-nitrobenz-2-oxa-1,3-diazole (NBD, **1.4**).[40,43]

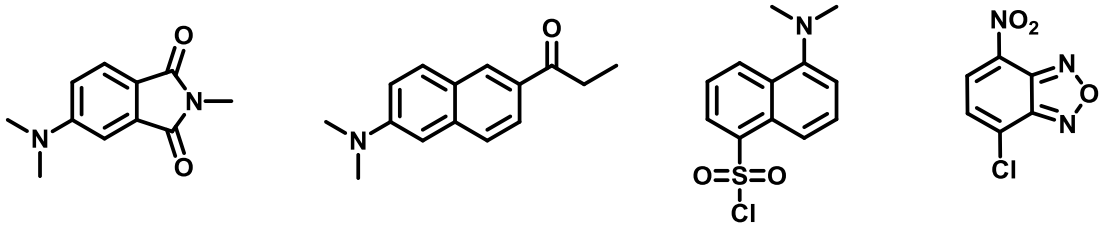

1.1 **1.2** **1.3** **1.4**

Typical environment-sensitive kinase sensors contain a substrate recognition site and a fluorophore linked to amino acid side chains in close proximity to the phosphorylation site (one to five residues apart). As a result of kinase activity, the inserted phosphoryl group changes the local polarity of the fluorophore, altering its spectroscopic properties.

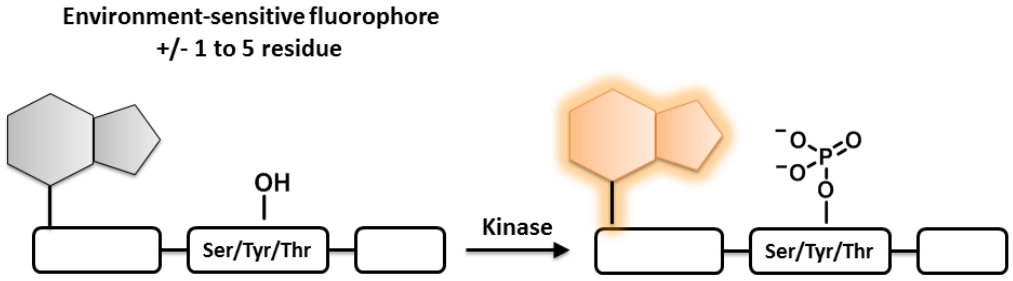

Figure 1.10: *General mechanism of environment-sensitive kinase sensors.* The presence of the phosphoryl group modifies the local surroundings of the adjacent solvatochromic fluorophore. The fluorophore is attached to the peptide chain which is one to five residues apart from the phosphorylation site, enhancing the fluorescent signal.

This strategy led Lawrence *et al*.[44] to build a library of peptides containing different environmentally-sensitive fluorophores (**1.5**, **1.6**, **1.7**) to study the phosphorylation reaction of tyrosine peptide substrates with Src protein kinase in the presence of the Lck SH2 domain. The SH2 protein-binding domain has the ability to recognize phosphorylated serine and tyrosine residues; likewise, the presence of the SH2 domain is expected to cause polarity changes in the environment of phosphorylated peptides during recognition. Therefore, the phosphorylated peptides **1.9** were anticipated to present a selectively fluorescent enhancement compared to their nonphosphorylated counterparts **1.8**, when interacting with the Lck SH2 domain (**Figure 1.11**). The three fluorophores were first linked to (*L*)-2,3-diaminopropionic acid (Dap)**1.10** and (*L*)-2,4-diaminobutyric acid (Dab)**1.11** to give a total of six different fluorophore-Dap/Dab residues. Successively, these residues were coupled at four different sites along different Src peptide substrates, which in turn were assessed by their fluorescent response in the presence of Src protein kinase and Lck SH2 domain. Peptides with Dap-**1.5** and Dab-**1.5** positioned at residues +3 and +4 sites produced the largest increase in fluorescent signal. The authors further assessed additional peptide substrates derived from Rink resin containing Dap-**1.6** and Dab-**1.5** positioned at +1 and +4 residues on the peptide sequence, respectively. A dissociation constant of 2.1 μM was found for peptide Dap-**1.6**. A concentration-dependent experiment was performed to assure that the fluorescent signal was only produced in the presence of the Lck SH2 domain after phosphorylation. The concentration of Lck SH2 domain was increased from 0 to 32 μM, where saturation

was achieved at 16 μM. Moreover, the addition of a phosphotyrosine phosphatase after completion of the phosphorylation reaction by Src kinase produced a decrease in the fluorescence intensity to the initial value. This study highlights a new kinase sensing method wherein the fluorophore site attachment does not require a fixed spatial relationship with respect to the phosphorylated residue.

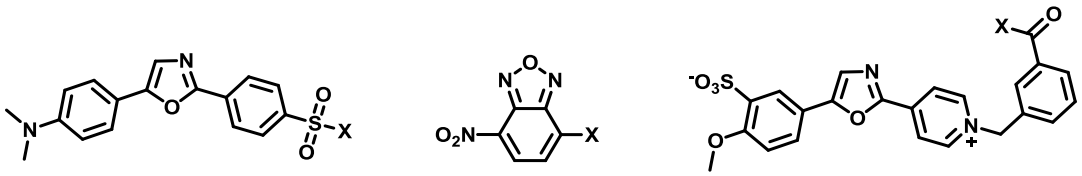

1.5 **1.6** **1.7**

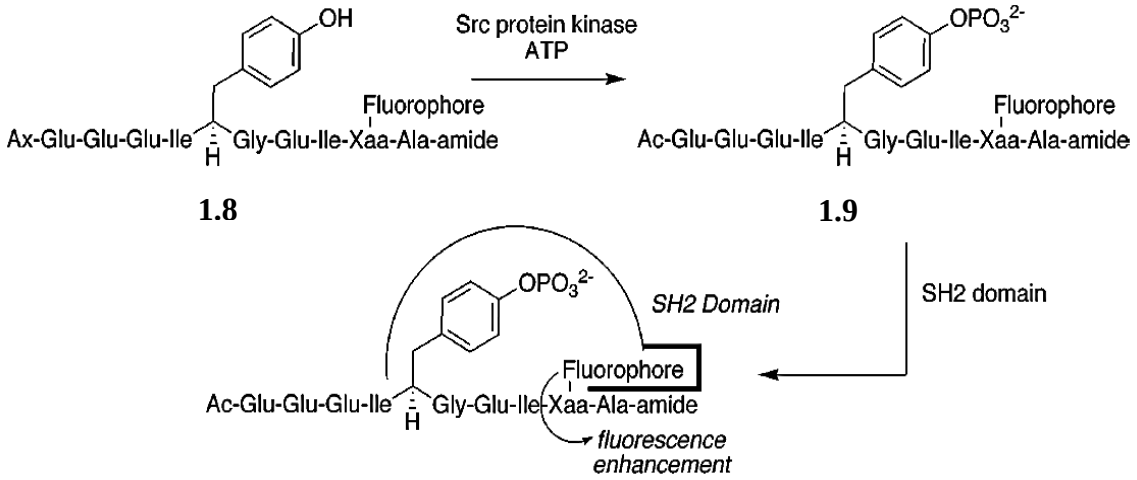

1.8 **1.9**

Figure 1.11: *Kinase sensing approach using environmentally-sensitive fluorophores from Lawrence et al*. Src protein kinase catalyzing the phosphorylation reaction of tyrosine peptide substrates containing fluorophores **1.5**, **1.6**, and **1.7**, which become fluorescent in the presence of SH2 binding domain. (Reproduced from Ref.48. © Journal of American Chemistry Society, 2005)

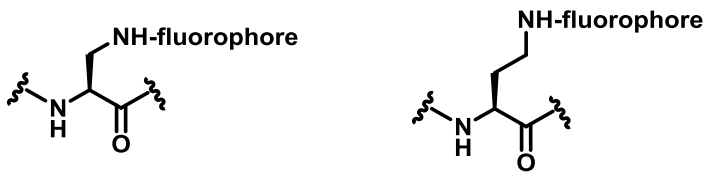

1.10 **1.11**

Ac-Glu-Glu-Glu-Ile-Tyr-Gly-Glu-Ile-Glu-Ala-NHCH$_2$CH$_2$SH

P+1 +2 +3 +4

1.4.4 Metal Ion-Based Fluorescence Sensing

1.4.4.1 Zinc Chemosensors

Research in supramolecular chemistry has led to the development of chemosensors capable of detecting with high selectivity and affinity phosphorylated peptides and proteins under physiological conditions. These phosphate ion chemosensors are designed on the bases of the model *fluorophore-spacer-receptor*, in which a covalent spacer separates the analyte-binding receptor and the fluorophore.[39] The main binding force between host-guest interactions derives from metal-ligand coordination chemistry, producing emission signaling changes upon binding the target analyte. The turn-on strategy is based on the photoinduced electron transfer (PET) mechanism. Herein, the receptor unit works as an electron donor when the analyte is absent, quenching the fluorophore excited state. Upon formation of the phosphate anion–receptor complex, electron transfer is prevented and the fluorescence is restored.[45]

Hamachi and co-workers have built a wide variety of chemosensors using zinc(II)dipicolylamine Zn(DPA) as a molecular recognition moiety for phosphate anions. The artificial receptors **1.12** and **1.13** contain an anthracene fluorophore core linked to two Zn(DPA) units.[46] Binding studies showed that both chemosensors present high selectivity towards phosphate species in the presence of other anions such as sulfate, nitrate, acetate and carboxylates. The binding events were measured with fluorescence titrations. Apparent affinity constants on the order of 10^4-10^5 M^{-1} were obtained for receptors **1.12** and **1.13** with adenosine nucleotides, phosphate monoesters and phospho-

L-tyrosine.[47] Interestingly, the addition of dimethyl phosphate or cyclic AMP did not cause any fluorescence change in the emission spectra of the chemosensors. Furthermore, the mono substituted Zn(DPA) anthracene **1.14** did not present fluorescence changes in the presence of the previous phosphate species. ^{1}H-NMR studies and X-ray crystallographic analysis of receptor **1.13** and phenyl phosphate revealed the cooperative participation of both Zn(DPA) units, with each metal cation coordinating with a phosphate oxygen atom. The authors found that fluorescence enhancement upon addition of phosphate species to these chemosensors arises from the second zinc cation complexed with the benzylic amine of the DPA unit. Hence, this increased metal-ligand interaction diminishes the intrinsic PET quenching of the anthracene fluorescence by the benzylic amine.[48]

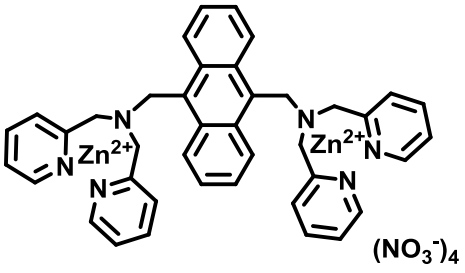

1.12

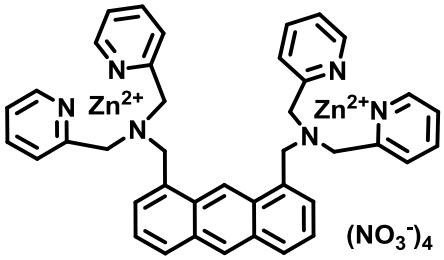

1.13

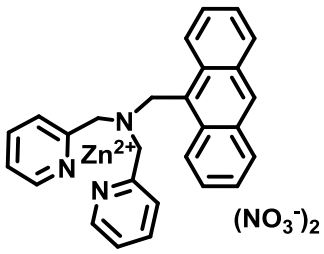

1.14

Further studies by Hamachi and co-workers showed that the two Zn(DPA) moieties of **1.12** and **1.13** interact with various phosphorylated peptides but not with their non-phosphorylated counterparts in aqueous solution at neutral pH. Fluorescence spectroscopy was used to measure binding constants of **1.12** and **1.13** with peptide substrates **1.15a** and **1.15d** to find K_a values ranging from 10^4 to 10^7 M^{-1}. On the other hand, no binding event was observed for non-phosphorylated peptide **1.15g**. The receptors were found to preferentially bind to the negatively charged phosphorylated peptides compared to the positively charged one **1.15c** containing arginine residues. The binding selectivity was ascribed to charge repulsion between the zinc cations and the arginine side chains. Additional binding studies with phosphorylated peptides **1.15a-f** proved that the affinity of the receptors depends on the peptide sequence and the total charge of the peptide. The receptors bind more strongly to the phosphorylated peptides that contain increasing negative charge **1.15a** and **1.15b** with K_a values of 10^6 to 10^7 M^{-1}.[48]

a: Glu-Glu-Glu-Ile-pTyr-Glu-Glu-Phe-Asp
b: Asp-Glu-Glu-Ile-pTyr-Gly-Glu-Phe-Phe
c: Arg-Arg-Phe-Gly-pSer-Ile-Arg-Arg-Phe
d: Lys-Ser-Gly-pTyr-Leu-Ser-Ser-Glu
e: Ala-Glu-Glu-Ile-pTyr-Gly-Val-Leu-Phe
f: Ala-Arg-Arg-Gly-pSer-Ile-Ala-Ala-Phe
g: Glu-Glu-Glu-Ile-Tyr-Glu-Glu-Phe-Asp

1.15

In addition, the same group used receptor **1.13** to monitor the dephosphorylation reaction catalyzed by the protein tyrosine phosphatase 1B (PTP1B) and its correspondent phosphorylated peptide substrate AspAlaAspGlu-**pTyr**-LeuIleProAsnAsnGly. The kinetic assay showed that the fluorescence intensity of **1.13** decreased with the addition of PTP1B over time.[48] Receptor **1.12** was also found to be a useful staining agent allowing for the selective identification of phospho-proteins in SDS-PAGE gel. Emission bands were observed only for phospho-ovalbumin and phospho-α-casein, but not for the non-phosphorylated proteins β-galactosidase, bovine serum albumin, avidin and lysozyme.[49]

Despite the high sensitivity and different applications reported by the previously described receptors; **1.12** and **1.13** are not useful to monitor kinase-catalyzed phosphorylation reactions. The strong binding affinity towards other phosphorylated entities such as ATP, which is required in a phosphorylation assay, interferes in the binding between the chemosensors and phosphorylated peptide substrates or proteins.

To overcome this situation, Hamachi and co-workers designed a very highly selective hybrid biosensor, where a similar dinuclear zinc receptor was incorporated into the phosphoprotein binding site of the M15C-WW mutant protein, allowing them to monitor kinase-catalyzed phosphorylation.[50] The Zn(DPA) chemosensor derivative **1.16** was synthesized using a stilbazole linker to attach a maleimide group. The WW binding domain derived from protein Pin1 was used to covalently attach receptor **1.16** using the thiol group of the cysteine residue. Relevant bis-phosphorylated peptides enclosing sequences that are usually recognized by the Pin1 WW domain were titrated into the

hybrid biosensor. High affinity constants $K_a > 10^6$ M^{-1} were measured for peptide **1.17a** using fluorescence titrations under physiological conditions. Additionally, no binding was observed for mono-phosphorylated substrates **1.17b-d**. Thus, two main requirements were needed to achieve high affinity and selectivity by the biosensor. Firstly, the consensus sequence of the peptide substrate needed to be originally recognized by the Pin1 WW domain. Secondly, one of the phospho-recognition sites was occupied by one of the phosphorylated residues, while the second phosphorylated amino acid residue needed to be located at a particular distance to be recognized by the chemosensor binding region.[51]

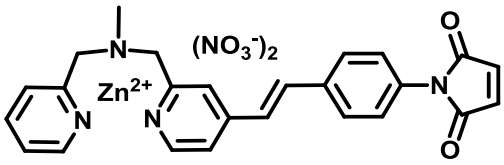

1.16

a: His-Tyr-**pSer**-Pro-Tyr-**pSer**- Pro-Ser
b: His-Tyr-Ser-Pro-Ser-Tyr-**pSer**-Pro-Tyr-**pSer**- Pro-Ser
c: His-Tyr-Ser-Pro-Ser-Tyr-**pSer**-Pro-Tyr-Ser- Pro-Ser
d: His-Tyr-Ser-Pro-Ser-Tyr-Ser-Pro-Tyr-**pSer**- Pro-Ser

1.17

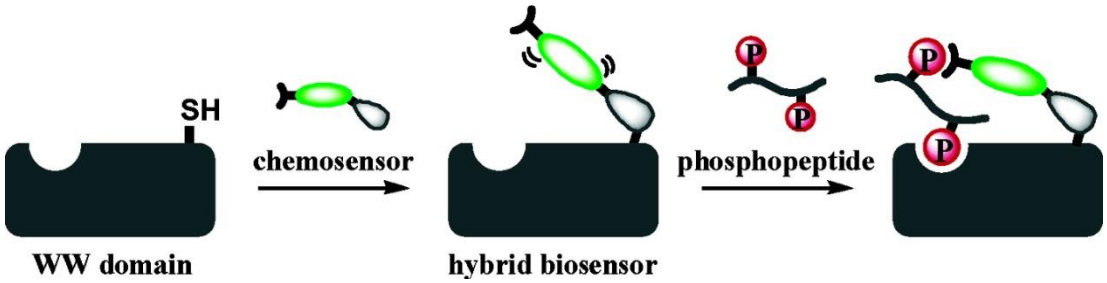

Figure 1.12: *Sensing approach using hybrid biosensor from Hamachi et al*. Pin1 WW domain biosensor recognizing bis-phosphorylated peptide. (Reproduced from Ref. 55. © Journal of American Chemistry Society, 2007.)

More recently, a different strategy was followed by Hamachi *et al.* developing BODIPY-based chemosensor **1.18**. The receptor contains a BODIPY fluorescence scaffold attached to two Zn(Dpa) units. Fluorescent titrations were used to measure dissociation constants. Chemosensor **1.18** was found to have high selectivity towards *i*+4 bis-phosphorylated peptides **1.19a** and **1.19c**. Dissociation constants of 43 μM were found for peptide substrate **1.19a** in the absence of ATP. Interestingly, the K_d changed to 150 μM when **1.19a** was added to the receptor in the presence of ATP. Moreover, no binding event was observed for mono-phosphorylated peptide **1.19b**. The receptor bound preferentially to peptide **1.19c**, whose sequence was bearing a negative net charge. An increase in the fluorescence intensity of up to 1.5 fold was found for **1.19c** compared to **1.19a**. A binding affinity of 8.5 μM was found in the presence of ATP. Thus, chemosensor **1.18** was used to monitor the kinase-catalyzed reaction with glycogen synthase kinase 3β (GSK3β), which is involved in insulin signaling and neurofibrillary tangles in brain tissue. A fluorescent enhancement of 2-fold was found for peptide **1.19b** in the presence of GSK3β protein and the receptor after 60 min. In addition, an inhibitor assay was

carried out in the presence of GSK3β inhibitor **1.20**. The formation of **1.19c** was suppressed to 13%, showing a decrease in the fluorescence intensity of the receptor in the presence of 0.5 μM of **1.20** and GSK3β.[52] In further biosensing applications, receptor **1.18** was found useful as a fluorescent staining agent. Hyperphosphorylated proteins were selectively detected in hippocampus tissue after 10 min of incubation with 10 μM of **1.18**.[53]

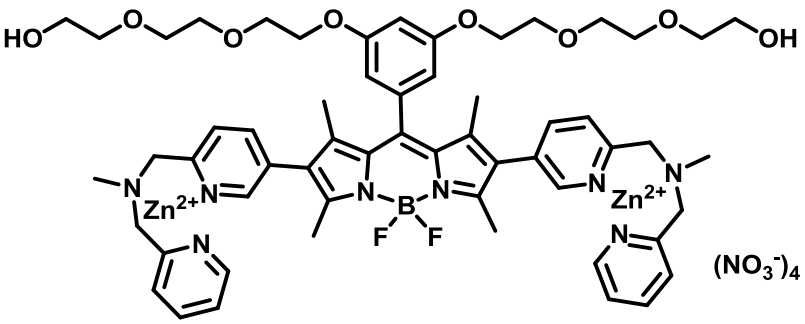

1.18

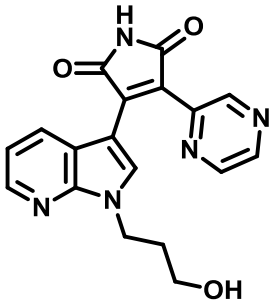

1.20

a: Tyr-Ala-Val-Val-Arg-**pTyr**-Pro-Pro-Lys-**pSer**-Pro-Ser-Ser
b: Tyr-Ala-Val-Val-Glu-**pTyr**-Pro-Pro-Glu-**pSer**-Pro-Ser-Ser
c: Tyr-Ala-Val-Val-Glu-Tyr-Pro-Pro-Glu-pSer-Pro-Ser-Ser

1.19

More recently, chemosensor **1.21** was studied by Gunning and co-workers. This receptor contains a pyrene fluorophore covalently attached to a Zn-cyclen macrocycle. The turn-on fluorescence signal resulted from the π-π stacking of two receptor units forming an excimer reporter upon the binding to bis-phosphorylated peptides and proteins. Analogous to Hamachi's receptor design, Zn(II) was used as coordination metal for the molecular recognition of phosphoryl groups. Fluorescent titrations showed that receptor **1.21** selectively binds to bis-phosphorylated peptides containing Ala-pTyr-pTyr-Ala-Ala motifs, resulting in a 2:1 sensor-peptide stoichiometry. An affinity constant of K_a= 4.3 M^{-1} and limit of detection of 0.6 μM were measured using fluorescence titrations under physiological conditions. The addition of mono-phosphorylated peptides did not cause significant changes in the emission spectra of the receptor. In further studies, excimer formation was induced by the incubation of the sensor with full-length proteins *α*- and *β*- casein containing bis-phosphorylated motifs. Sensor **1.21** was also used as a fluorescent staining agent in polyacrylamide gel, showing high selectivity towards proteins with bis-phosphorylated sequences.

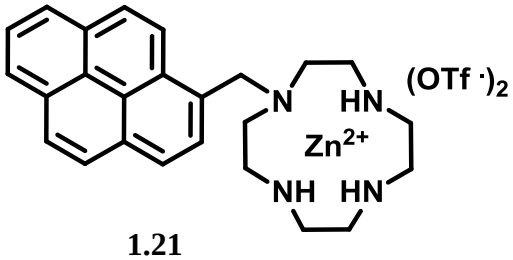

1.21

1.4.4.2 Chelation-Sensitive Peptide Sensors

Imperiali and co-workers have extensively developed peptide-based sensors that work based on the chelation-enhanced fluorescence process. The peptides are covalently attached to the sulfonamide-oxine (SOX) fluorophore which chelates Mg^{2+} ions in the presence of a phosphoryl group. These SOX-peptide sensors have been widely used in a variety of kinase assays due to their high compatibility with non-physiological Mg^{2+} levels. Additionally, this method is applicable for the detection of serine, threonine and tyrosine kinase activity.[38] The non-phosphorylated SOX-peptides present low metal ion affinity, displaying low or no fluorescence. However, upon phosphorylation the peptide increases its affinity for Mg^{2+} metal ion, resulting in chelation-enhanced fluorescence (λ_{ex} = 360 nm, λ_{em} = 485 nm).[54]

The first synthesized SOX-peptides were designed with three organized segments (**Figure 1.13A**) using a β-turn focused design (BTF). A) SOX-amino acid placed +/- 2 residues apart from the phosphorylation site, 2) a kinase recognition unit including the amino acid to be phosphorylated, and 3) a β-turn peptide sequence between the SOX-amino acid and the recognition unit, allowing preorganization of the binding site to interact with Mg^{2+}.[54] The peptide sensors were successfully used to assess kinase activity *in vitro* and in cell extracts. However, the β-turn requirement limits the application of this design to small peptide fragments rather than full peptide recognition sequences, due to the conformational constraint of the β-turn moiety.

To circumvent the β-turn limitation, a different strategy known as the recognition focused domain (RFD) approach was used (**Figure 1.13B**), where the SOX fluorophore was incorporated by alkylation of the cysteine residue to afford a C-SOX peptide sensor. The C-SOX design allowed for the insertion of extended substrate sequences to maximize the specificity by the target kinase. This RFD approach was used to monitor the phosphorylation of several relevant substrates of protein kinase C (PKC), protein kinase A (PKA), sarcoma kinase (Src), and insulin receptor kinase (IRK). The C-SOX peptides were used in 96 well plates, allowing for high-throughput measurements of multiple kinases and obtaining significant kinetic parameters.[55]

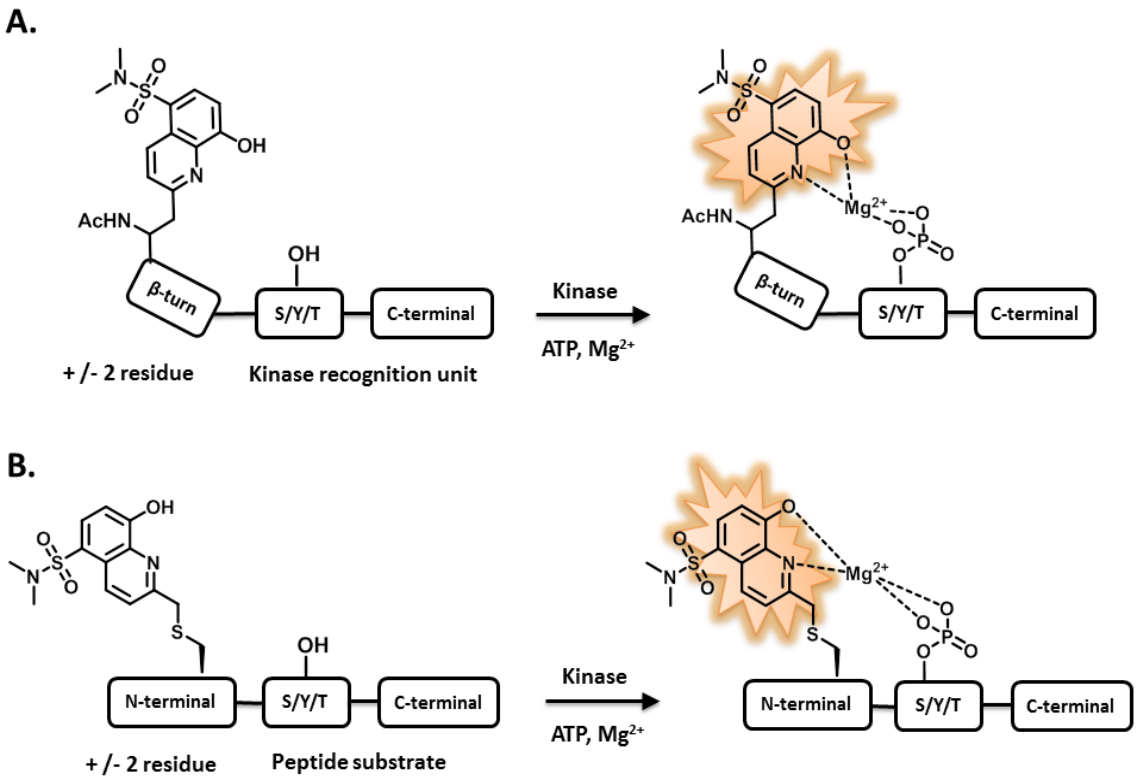

Figure 1.13: *Kinase sensing approach using SOX-peptide sensors from Imperiali et al*. A) β-turn focused (BTF) design. B) Recognition focused domain (RFD) design. The affinity for Mg^{2+} is increased upon phosphorylation of Ser, Tyr or Thr residues, and the SOX-amino acid undergoes chelation-enhanced fluorescent.

1.4.5 Concluding Remarks for Fluorescent Chemosensors

The main requirement for the correct performance of the aforementioned chemosensors and biosensor systems is the existence of high molecular complementarity to afford high affinity and specificity to target specific peptides or proteins. The design process of these fluorescence-based sensors has been inspired by the study of the binding sites of phosphate-recognition proteins. Additionally, computer modeling has been used to improve host-guest interactions by assuring that the structure of the receptors maximizes the expected interactions with the phosphoryl groups. However, these traditional lock-and-key based sensors have been designed to target one specific type of protein analyte, due to their inherent molecular complexity. Using the lock-and-key model, an individual chemosensor has to be developed and can only detect one analyte. In this context, detection of proteins remains a major task due to their composite nature and the required neutral aqueous conditions for their structural stability. Thereby, additional detection methods that can identify protein entities and the variation of their concentrations as biological markers can serve as powerful tools to assess cellular responses to external factors, pathological conditions, or as screening for kinase inhibitors.

1.4.6 The Pattern-Based Recognition Approach

As an alternative to the highly specific chemosensors described above there is the approach of differential sensing which is inspired by the human olfactory and gustatory senses. These biological entities use an array of cross-reactive receptor proteins which interact with their analytes through differential binding or cross-reactive reactions, creating a unique response pattern that is recognized as a particular smell or taste. This biological model has encouraged supramolecular chemists to develop differential sensing arrays that mimic these sensory systems.[56] Thereby, a sensing array is composed of a collective assembly of differential receptors. In the field of Supramolecular Analytical Chemistry, differential sensing is commonly used to describe the binding form of the receptor elements in the array. Herein, the individual sensors present moderate affinity and selectivity, binding differently to each analyte through non-specific interactions. Hence, each receptor can interact with several analytes, but each receptor binds the targets differently from the other receptors. Using this approach, one obtains a distinct fingerprint of composite optical signal produced by the sensor elements, allowing for detection and differentiation of different challenging biomolecules, including proteins.[57] This approach overcomes the tedious process of planning and developing highly selective binding recognition sites on the receptors. Less synthetic effort is needed to build receptors that can distinguish between structurally analogous analytes. In addition, less time is consumed synthesizing a new host for every analyte, considering the structural and dynamic complexity of proteins.[58]

1.4.6.1 Chemometric Analysis in Differential Sensing

In practice, the fingerprint refers to the convoluted data consisting of absorbance or fluorescence signals, which can be difficult to analyze by the naked eye. Sensing arrays usually need a variety of receptors to obtain a good discriminatory response, thus the information that is acquired from these arrays becomes intrinsically multivariate. Thereby, the use of differential sensing arrays conveys the need of statistical tools to interpret and analyze multivariate datasets. Chemometric analytical methods have been implemented to resolve this task. Mathematical and statistical methods such as principal component analysis (PCA),[59] linear discriminant analysis (LDA),[60] and hierarchical cluster analysis (HCA)[59] are typically used for the qualitative or semi-quantitative analysis of the data set. Likewise, artificial neural networks (ANN),[61] and support vector machines (SVM)[62] have been successfully employed for the quantitative analysis of the multivariate data, in addition to analyte identification.

In general, PCA and LDA are considered statistical treatments, which through a combination of mathematical functions and correlation matrixes reinterpret the multivariate data from the array, and produce a different dataset with reduced dimensionality. In both cases, the variance contained in the original dataset is the major statistical characteristic that is preserved during the chemometric analysis. As a result, the observations (hosts and fluorescence dataset) are correlated with the variables (analytes), leading to the detection and visualization of the pattern responses in the data input. Mathematically, PCA creates a series of orthogonal axes that convert the original dataset

to a new coordinate system. The greatest extent of variance within the dataset is represented by the first coordinate, known as the first principal component. The second and third principal components represent the amount of decreasing variance. As a result, plots of lower dimensionality are obtained that usually show the first, second and third principal components, which separate out different clusters of analogous data.

PCA is an unsupervised method or clustering analysis method, where the response patterns are obtained without additional information about the classes of analytes prior to the implementation of the PCA algorithm. On the other hand, supervised statistical approaches require prior identification of the analyte before operation of the chemometric algorithms. LDA is a supervised technique essentially used for analyte classification and dimensionality reduction. A different mathematical model is developed during LDA operation, where the discriminant functions maximize the variance between differing classes of analytes, while minimizing the variance within each analyte class. Analogously, LDA plots are obtained by discriminant factors, separating clusters of data with similar identity along the orthogonal axes. A validation process is required at the end of the analysis to evaluate the confidence of analyte discrimination by the implemented model. The leave-one-out or jack-knife analysis is the most common cross-validation approach where one data point is left out at a time from the dataset, and the mathematical functions are recalculated in the absence of the removed point. The previously omitted data point is then used to assess the mathematical model by treating the point as an unknown, and predicting which analyte class it fits in. This operation is

repeated until every data point is removed and categorized, where the classification ability of the model is represented by the correct placement of all analytes.

Analysis of multivariate data with nonlinear relationships between the values that are measured and the values that are known is achieved by using ANN, which is a more advanced computational model. This method was inspired by the central nervous system, where interconnected sets of neurons form a network. ANNs can establish relationships between known and observed data, conveying confidence levels to the experimental trends. The input data is first entered into a program and then computed by mathematical functions. An output value is generated by a different function in the same program. These functions transform and correlate the input information that is passed along the network to the derived output signals. Thus, an ANN is considered an adaptive model that generates a nonlinear mapping between input values and output data.

Recently, SVMs have emerged as a powerful tool to process multivariate data analysis. This model is mainly applied to datasets with different classes that cannot be separated using linear planes. SVM is a supervised method used for analyte classification, where mathematical functions separate the classes by mapping the inputs into a different dimensional space. This method is capable of classifying any type of multivariate data due to the variety of functions that can be applied to obtain linear correlations between the variables. These functions are known as kernel, and can be linear, polynomial, Gaussian-based functions, and so on. These kernel functions are used to transform the input data in different categories using a different dimensional space that linearly

separates the classes. A different operator or hyperplane is created in this higher-dimensional space, maximizing the separation or margin between the two classes. The maximum-margin hyperplane is the largest distance between the hyperplanes that separate the data points of the two categories. This gap should be as wide as possible to maximize the resolution between the two categories. New data points are then mapped into the training data with higher-dimensional space, and predicted to belong to a class according to which side of the margin they fit in.

1.4.6.2 Differential Sensing of Proteins

Different protein-detecting arrays have been developed in the last decade for the detection of different classes of proteins. These cross-reactive receptors are composed by large molecular scaffolds such as supramolecular structures, DNA base pairs or nanoparticles, containing different recognition motifs to enhance receptor-protein surface interactions. Our group and others[63-65] have traditionally generated differential receptors that incorporate two main structural features. Firstly, a core host structure is designed to contribute to the enhancement of the binding affinity between receptor and protein analyte. The host scaffold is additionally used to form a pre-organized binding site which can interact with different protein surfaces. Secondly, variable recognition moieties such as peptidic arms, metal centers, DNA strands or fluorophores are covalently or non-covalently attached to the core unit, imparting the desirable differential binding. These libraries of receptors have been successfully elaborated using a rational design of molecular recognition units capable of interacting with protein surfaces through

hydrogen-bonding, hydrophobic effects and ion pairing. Hydrophilic groups have been introduced to increase the selectivity towards different proteins, and to assure the appropriate solubility of the receptors under physiological conditions. Additionally, host-guest complementarity is generally achieved through electrostatic interactions by incorporation of peptide-based ligands. These sensing arrays have been able to detect structurally similar proteins which also presented different conformational characteristics in solution, and in the presence of complex mixtures.

Anslyn and co-workers developed a combinatorial library of peptide-based receptors to differentiate proteins and glycoproteins. The library of receptors was built using a hexasubstituted benzene core with two appended peptidic arms (**1.22**). This pinwheel scaffold was used for the formation of a prearranged binding cavity. The tripeptide arms were diversified by incorporating all natural amino acids (except Cys) to provide differential binding, using the side chains for distinctive hydrogen-bonding, ion pairing and hydrophobic interactions. The receptors also contained boronic acids to give preferential binding towards glycoproteins. A combinatorial library of 19^3 resin bound receptors was created, where 29 receptors were arbitrarily chosen, and incorporated into the array. The protein analytes were firstly added to the array, followed by the addition of bromopyrogallol red indicator (**1.23**).

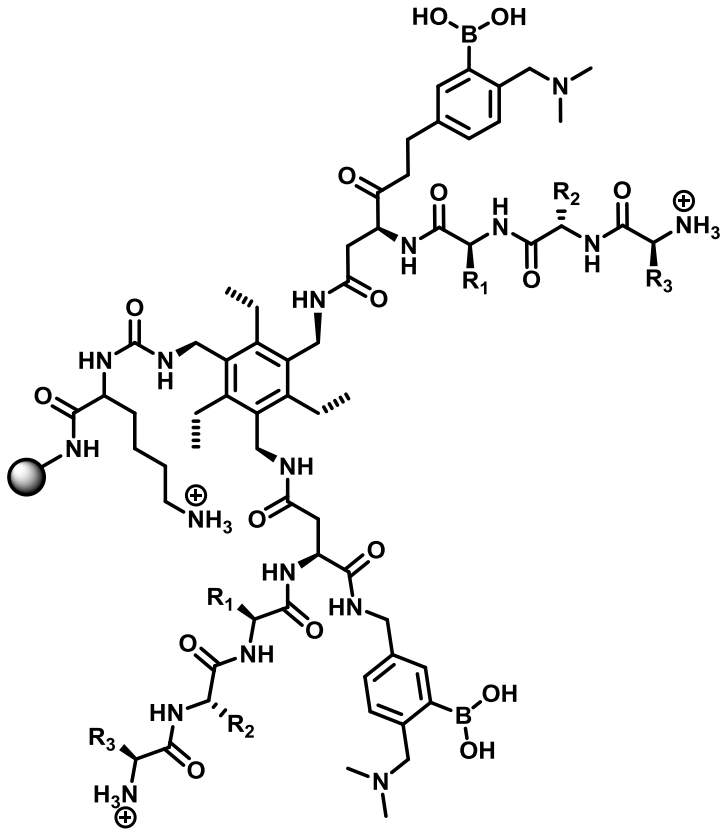

1.22

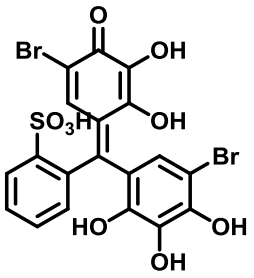

1.23

Kinetic indicator-uptake studies were done to obtain the respective slopes of each of the 29 receptors. The slopes were converted to single data points, and analyzed using PCA. This sensing array successfully differentiated glycoproteins ovalbumin and fetuin and the other proteins elastin, bovine serum albumin and lysozyme at 355 μM concentration. Seven of the 29 receptors were sequenced by Edman degradation, and were found to have the greatest contribution in the discrimination of the proteins. This study established the use of differential peptide-based receptors to provide a wide range of binding modes, and successfully detect and differentiate large biomolecules.

Hamilton and co-workers developed a library of fluorescent tetraphenylporphyrin receptors (**1.24**) capable of differentiating metal and nonmetal-containing proteins.[64] Different peptidic arms with basic, acidic and aromatic residues were attached to the porphyrin receptors. The hydrophobic porphyrin scaffolds were used to impart good binding affinity, while the side chains of the amino acids were used to impart different selectivity by varying the total charge of the receptors. The combination of five different amino acid derivatives with the porphyrin cores resulted in the formation of 35 porphyrin sensors. Different protein targets such as basic cytochrome c, acidic ferredoxin, lysozyme and lactalbumin were studied using this array. The fluorescence of the porphyrin sensors was quenched upon addition of the proteins, which could be also observed by the naked eye. The metal-containing proteins, cytochrome c and ferredoxin gave the most representative differentiation due to their inherent charge and hydrophobic distribution on their respective surfaces. Furthermore, the iron metal incorporated in these paramagnetic proteins produced additional quenching of the fluorescence of the receptors. Alternatively, the fluorescent changes produced by neutral proteins lysozyme and lactalbumin were presumably derived from differential association with polar and nonpolar surfaces. The obtained fluorescent pattern responses lead to the identification of each of the four analytes. From the previous library receptor, eight porphyrin receptors were chosen to develop a second array to differentiate metal and nonmetal protein mixtures. Chemometric analysis was used to analyze the obtained fluorescence pattern, and showed good differentiation of the ten analyte mixtures.

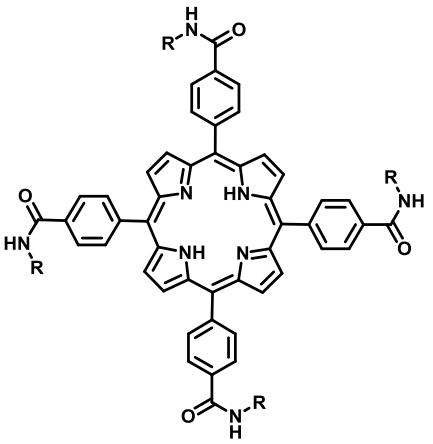

1.24

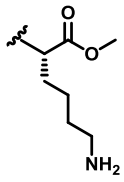

Lys

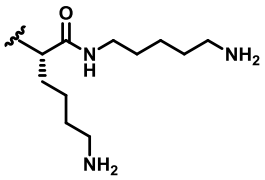

Lys-1,5-Pentanediamine

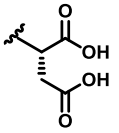

Asp

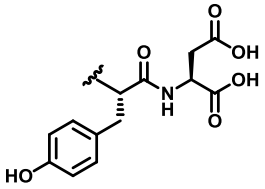

Tyr-Asp

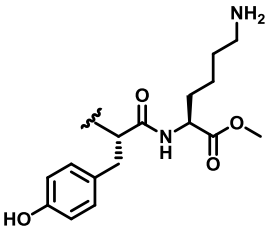

Tyr-Lys

A different strategy was followed by Hamilton *et al.*,[66] developing an array of receptors based on fluorescent DNA G-quadruplexes with protein-binding fragments. The G-rich strands (**1.25**) were functionalized with three different fluorophores, pyrene (**1.26**), fluorescein (**1.27**) and tamra (**1.28**). Each fluorophore was chosen due to their convenient spectral overlap within them. Pyrene displayed excimer formation when forming π-π stacking (**1.29**), whose emission overlapped with the excitation spectra other two fluorophores. Four emission signatures were produced by direct excitation of each fluorophore, and by the induction of a FRET process from fluorescein and tamra which are a well-known donor-acceptor pair. Five protein analytes were studied using this array, including melittin, avidin, histone, heme and myelin basic protein. A distinctive fluorescence pattern was obtained upon addition of the protein targets to the G-quadruplex ensemble. Several photophysical events such as fluorescence quenching, interruption of the π-π stacking formation, and differences in FRET were ascribed to

produce the differential fluorescence pattern due to the effect of the peptide side chains on the protein surfaces. These fluorescent pattern responses allowed for the identification of the five protein analytes using PCA (**Figure 1.14**).

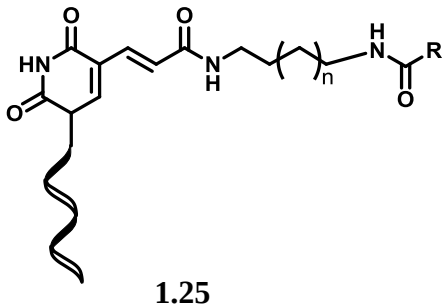

1.25

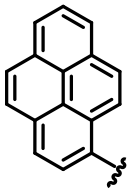

1.26

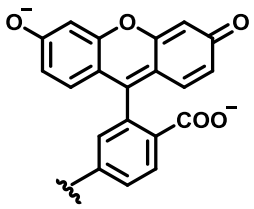

1.27

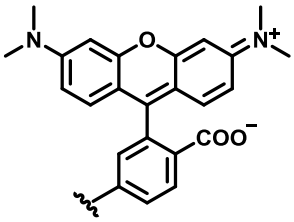

1.28

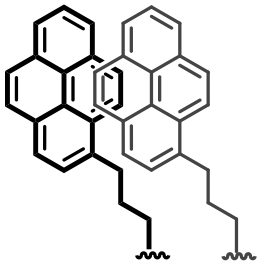

1.29

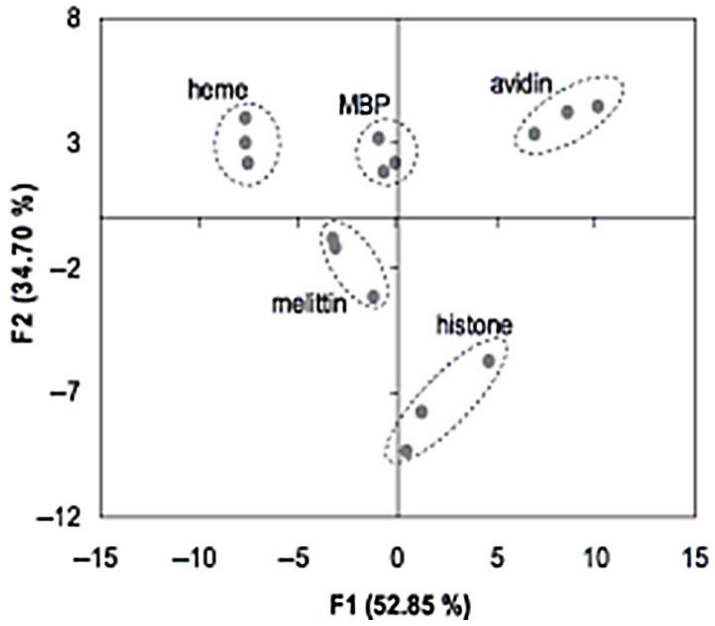

Figure 1.14: *Discrimination of five proteins with DNA G-quadruplexe sensing array from Hamilton et al*. PCA plot of hemoglobin, melittin, avidin, histone, and myelin basic proteins at 500 nM concentration. (Reproduced from Ref. 63. © WILEY-VCH, 2009.)

Rotello *et al.*[67] developed a different type of sensing array using gold nanoparticles (AuNPs) functionalized with different chemical structures. An improved feature of this array is the use of both synthetic and biomolecular elements, which were introduced to mimic multivalent interactions of biomacromolecules. The incorporation of green fluorescent protein (GFP) as a fluorescent reporter for the binding event improved the biocompatibility of the system. The protein-protein surface interactions were improved using the nanoparticle-GFP receptor complex, allowing the system to reach low detection limits. Different sensor elements were synthesized using five AuNPs with ligand varying in hydrophobicity, hydrogen-bonding ability and aromaticity. The

nanoparticle-GFP receptor conjugates were formed due to the electrostatic complementarity between the cationic surface of the AuNPs and the negatively charged GFP, resulting in fluorescence quenching of the GFP. Five protein targets were used for this study, including fibrinogen, transferrin, IgG, human serum albumin and α-antitrypsin. The addition of the protein analytes to the nanoparticle-GFP complex mixtures produced either a positive response where the fluorescence was restored when the GFP was displaced by the analytes; or a negative response as a consequence of protein-GFP aggregation. The five serum proteins were successfully discriminated at 25 nM concentration using this sensing array. In further studies, the previous serum proteins were also differentiated at 500 nM physiological concentration when added to a complex mixture of human serum (**Figure 1.15**).

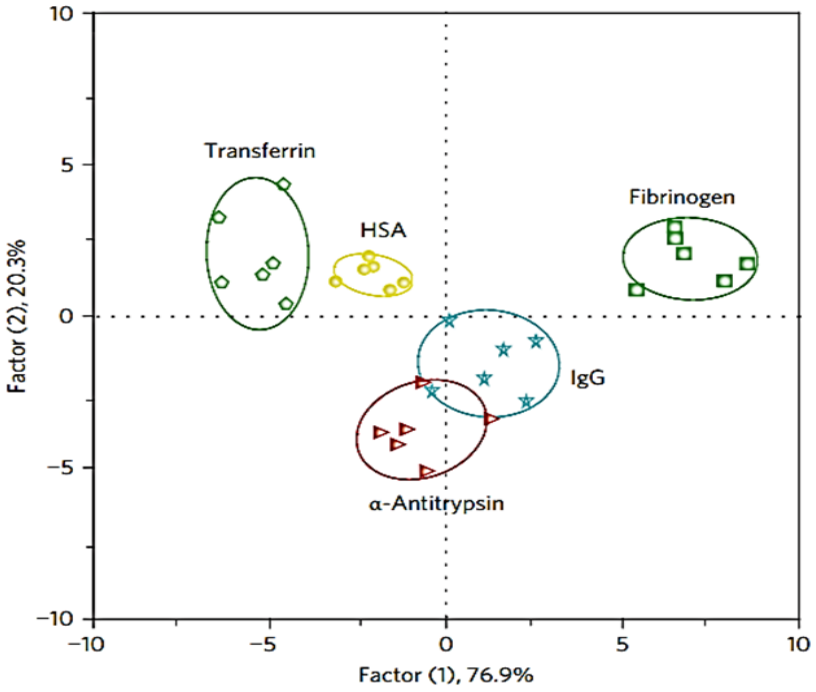

Figure 1.15: *Discrimination of serum proteins with nanoparticle sensing array from Rotello et al*. LDA plot of fibrinogen, transferrin, IgG, human serum albumin and α-antitrypsin at 500 nM concentration. (Reproduced from Ref. 64. © Nature Publishing Group, 2009.)

More recently, Rotello and co-workers improved the previous nanoparticle-based sensing method.[65] The surface of the cationic AuNPs was linked to different ligands with different physicochemical properties to impart differential binding toward protein surfaces. Additionally, different fluorescent conjugated polymers and GFP were used as reporters for the binding event upon addition of the protein targets. The anionic polymers (**1.30, 1.31**) were conjugated to oligo(ethylene glycol) chains to improve the solubility and to avoid aggregation problems. The sensing ensemble was formed using a combination of six different AuNPs, GFP and three fluorescent polymers. The receptor-

reporter complexes were mainly bound due to strong charge complementarity. A remarkable range of 12 proteins were differentiated using this nanoparticle sensing ensemble. Upon addition of the protein analytes to the array, changes in fluorescence emission were obtained due to the displacement of the reporters from the AuNPs. The obtained fluorescence pattern was analyzed using LDA, showing good clustering and differentiation of the individual proteins.

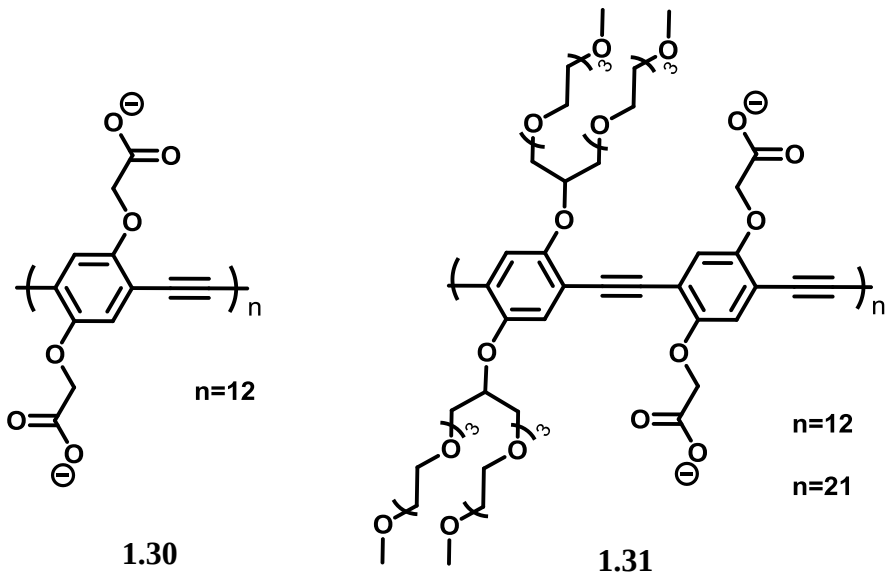

1.30 **1.31**

1.4.7 Concluding Remarks for Differential Sensing of Proteins

In summary, the previous examples have shown that proteins can be successfully detected and differentiated under physiological conditions using a combination of differential sensing and chemometric tools. Each of the aforementioned array sensing systems distinguished different classes of proteins by including different receptor-

indicator complexes in their respective arrays. Different receptor designs were developed to obtain the appropriate cross-reactive library of receptors for the arrays. These receptor varieties used a combination of specific interactions and differential binding to classify protein analytes. The pattern-based recognition approach has proven to be effective for protein sensing, extending its differential sensing power to the discrimination of protein mixtures.

1.5 SUMMARY AND OUTLOOK

Protein phosphorylation is one of the most remarkable events for the correct performance of cellular activity. MAP Kinases are one of the most important families of proteins in cancer research. X-ray crystallography and computational models have revealed the notable similarity and complexity of MAPK conformational structure. Traditionally, radioactive-based assays with ATP and antibodies have functioned with inherently high selectivity to detect the phosphorylation state of MAP kinases. In the last decade, a variety of fluorescence-based sensing methods have been developed to study protein phosphorylation. Each researcher had a different approach for developing an appropriate biosensor or chemosensor for different types of phosphorylated peptides or proteins. The lock-and-key model relied on biosensors or chemosensors with high selectivity and specificity. Some examples used a peptide or protein substrate which was functionalized with a fluorophore located in close proximity to the phosphorylation site, reporting the binding event. Other examples developed small artificial chemosensors that contain recognition moieties towards phosphoryl groups on peptides/proteins. Using this

approach only one receptor can be used to target one particular protein. The synthesis of this type of receptors has been evidently challenging for chemists. The introduction of the pattern recognition approach which combines differential sensing and chemometrics has shown that single highly selective receptors may not be required for certain studies. Instead, differential receptor arrays with low selectivity can be used which mimic the mammalian senses of taste and smell through cross-reactive interactions. The above-mentioned arrays encompassed receptors that incorporate different binding modes within each receptor. A general large scaffold was first incorporated into the receptor, targeting the general properties of the protein surface such as hydrophobicity, charge, and aromaticity; and enhancing the binding affinity. Then, different binding moieties were added to the scaffold to impart differential binding. The cross-reactive interactions between the library of receptors and analytes, allowed the detection and differentiation of different proteins with the same array. Finally, the power of differential sensing arrays has enabled the detection of proteins in complex mixtures.

To the best of our knowledge, phosphorylated proteins and particularly MAP kinases have not been yet detected using the pattern-based recognition approach. Our group and others have established the basis to use this method to study the activity of MAP kinases *in vitro* and in cell lysates. In the following chapters, the development of new differential sensing methods and their application for protein phosphorylation and MAPKs will be discussed.

Chapter 2: In-Situ Generation of Differential Sensors that Fingerprint Kinases and the Cellular Response to their Expression

2.1 ABSTRACT

Mitogen activated protein (MAP) kinases are responsible for many cellular functions, and their malfunction manifests itself in several human diseases. Usually, monitoring the phosphorylation states of MAP kinases in-vitro requires the preparation and purification of the proteins or western blotting. Herein, we report an array sensing approach for the differentiation of MAP kinases and their phosphorylated counterparts in-vitro. This technique utilizes a library of differential receptors created in-situ containing peptides known for affinity to MAP kinases, and a Zn(II)–dipicolylamine complex that binds phosphate groups on proteins. An indicator-displacement assay signals the binding of the individual receptors to the kinases, while chemometrics is used to create a fingerprint for the kinases and their state of activity. For example, linear discriminant analysis correctly identified kinase activity with a classification accuracy of 97.5% in-vitro, while the cellular response to kinase expression was classified with 100% accuracy.

2.2 INTRODUCTION

Protein phosphorylation is a pivotal post-translational modification that regulates intracellular signaling networks, gene transcription, and cell growth in eukaryotic cells.[11] The specific phosphorylation of serine, threonine, and tyrosine residues controls the enzymatic activity of a diverse range of kinases. For example, the mitogen-activated protein (MAP) family of kinases triggers key cell-signaling pathways, thus regulating a variety of cellular responses, such as mitosis, cell differentiation, the cell cycle, and apoptosis.[13,68] Aberrant MAP kinase activity is associated with human diseases, such as inflammatory response, hematologic malignancies, and cancer.[5,69] Of the MAP kinases, several are associated with these disease states, including extracellular signal regulated kinases (ERK1/2), the c-Jun N-terminal kinases (JNK1/2/3), and p38 MAPK α, β, γ, and δ.[70]

Simple and efficient protein phosphorylation detection methods, as well as techniques to qualitatively assess cellular changes in response to the phosphorylation, could serve as tools to monitor cell status, kinase activity, and as screens for potential inhibitors.[5,13,68-70] While many approaches involve antibodies and radioactivity-based assays,[71] optical-based sensing methods to detect phosphorylation events are advancing rapidly.[72-74] Efforts in this area have focused on the development of receptors whose responses are sensitive, as well as being functional in physiological environments.[75,76] For instance, the chelation-enhanced fluorescence strategy popularized by Imperiali using a sulfonamido oxime (SOX) fluorophore is a leading approach.[77] Phosphorylation of

Ser/Thr residues enhances the affinity of SOX with magnesium, and as a result increases the fluorescence of SOX.[78]

Other groups are working to create supramolecular receptors as kinase chemosensors.[79,80] Hamachi and co-workers studied chemosensor **2.1**, which contains two units of zinc-dipicolylamine Zn(DPA).[81] In aqueous solution at neutral pH, the two Zn(Dpa) moieties of **2.1** interact with various phosphopeptides (K_a values ranging from 10^4 to 10^7 M^{-1}),[82] but not with their nonphosphorylated counterparts. Additionally, the same group designed a highly selective hybrid biosensor,[50] where a similar dinuclear zinc receptor was incorporated into the phosphoprotein binding site of M15C-WW mutant protein, allowing them to monitor kinase-catalyzed phosphorylation.

While the Hamachi and Imperiali detection systems selectively bind to and signal phosphorylation, it is necessary to synthesize a different receptor to be selective for each phosphorylated target. Further, in some cases it may be desirable to characterize an overall change in cell signaling pathways and the detection of a specific phosphorylation event is not necessarily indicative of other cellular changes. To avoid the tedious process of developing individual highly selective receptors, the use of differential sensing techniques has been growing in the supramolecular chemistry field. This sensing protocol exploits the interactions between target analytes and a library of cross-reactive receptors to create a response pattern that is unique for individual analytes, or different mixtures thereof.[83,84] Using this approach, one obtains a distinct fingerprint of composite signals produced by the sensor elements, allowing for discrimination of different challenging

analytes.[57] Our group,[85] and others,[64-67] have used differential sensing for the analysis of various pure peptides and proteins. For example, we recently reported a pattern-based approach to discriminate phosphorylated tripeptides. A library of cross-reactive receptors was derived from a tris(2-pyridylmethyl)amine unit conjugated to guanidinium ligands and random tripeptides (**2.2**). Five different tripeptides, three metals, and three indicators led to 45 receptors, imparting cross-reactivity to the array, allowing chemometric-based differentiation of the targets.[86] Hence, as the next step in extending differential sensing to the detection of post-translational modifications, we envisioned that differential sensing could also be used to pattern protein phosphorylation events, and thereby fingerprint kinases *in vitro*. Furthermore, we also sought to challenge the methodology with a real-life test and examine its utility in complex mixtures, specifically cell extracts. In cell extracts, the technique would necessarily be responding to changes in distributions of protein modifications that result from activating a kinase pathway.

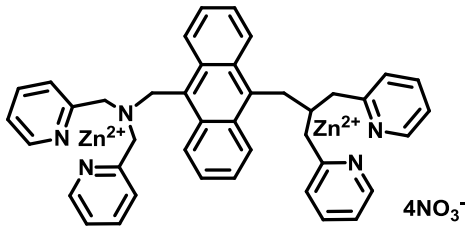

2.1

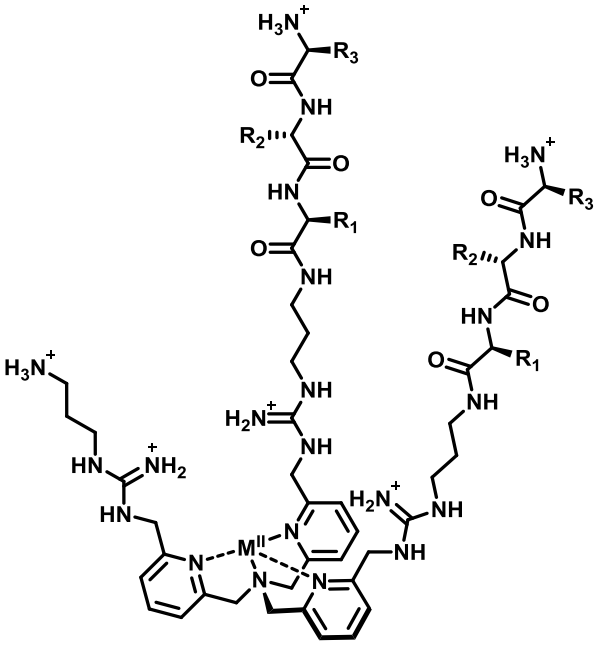

2.2

2.3 RESULTS AND DISCUSSION

2.3.1 Design Criteria

To pattern kinases and cellular responses to their activation we first considered the use of library **2.2**. However, the synthetic complexity of **2.2** is daunting, and hence we set another goal, that of creating a general method by which a suite of receptors could be generated simply by mixing components *in-situ*. The conjugate addition reaction of thiols to different conjugate acceptors caught our attention because of its recent use for drug discovery.[87] The reaction involves the 1,4-addition of sulfhydryl groups to an enone, which takes place rapidly in water at room temperature.[88,89] For our purposes the differential receptor library was based on the functionalization of 1,3,5-

triacryloylhexahydro-1,3,5-triazine (**2.3**) which has been shown by Son (**Scheme 2.1**), to be an attractive conjugate acceptor scaffold for creating tripodal systems.[90]

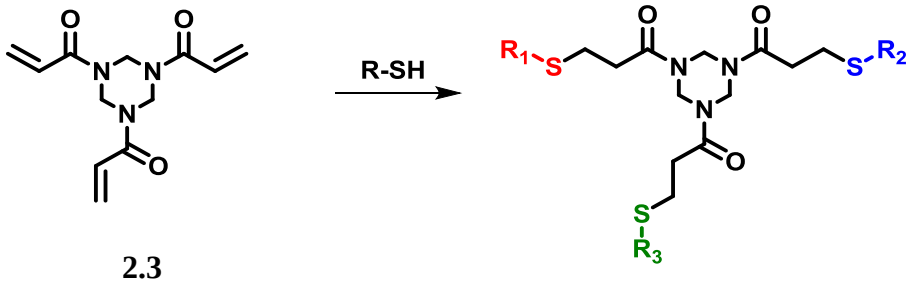

2.3

Scheme 2.1: *Thiol-ene 1,4-addition of sulfhydryl groups to a conjugate acceptor.*

To pursue our objectives, specific components of the tripodal receptor library were chosen. First, we created component **2.4** (**Figure 2.1**). This compound carries a nucleophilic thiol for use in **Scheme 2.1**, as well as Hamachi's proven phosphate binding bis-Zn(DPA) unit (the synthesis of **2.4** is described in detail in the Supporting Information). Second, because our group has previously shown that peptides provide differential binding towards different analytes,[91] we synthesized by SPPS techniques two peptides with known affinities to the MAP kinases. For example, ERK-2 phosphorylates the transcription factor Ets-1 at Thr-38 with high specificity.[92] Residues 31-35 (PVDAC) are in close proximity to the phosphorylation site of Ets-1.[93] Hence, the PVDAC sequence (**2.5**), when incorporated into a receptor library, was expected to impart cross-reactivity between ERK-2 and other kinases. In addition, continuing with this design strategy, we followed the lead of Dalby, who reported the modular peptide substrate Sub-F, which is phosphorylated by ERK-2 when docking with the F-recruitment site (FRS) of

this enzyme.[94] The KALIC peptide (**2.6**) derives from a linker that separates the C-terminal WXWP binding motif from the MAP kinase phosphorylation site of sub-F peptide. Therefore, such a linker is expected to bind but have low specificity. Lastly, dithiothreitol (**2.7**) was envisioned as a linker that would add to two different scaffolds (**2.3**), resulting in oligomerization, such as dimers, trimers or even larger receptors. When mixtures of three equivalents of these four components are added to **2.3**, a mixture of receptors is created. By varying which components are combined together in the individual wells of a multi-well plate, each well contains a unique set of receptors, thereby creating the diversity and cross-reactivity needed in a differential sensing scheme simply by mixing the components.

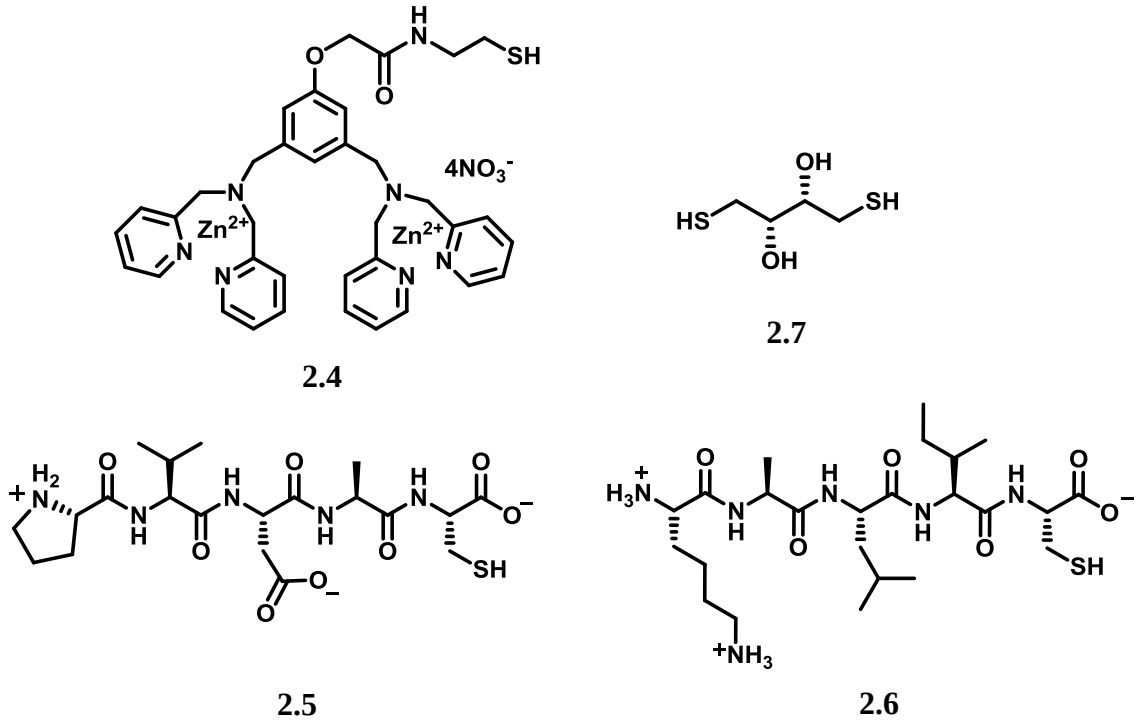

Figure 2.1: *Structure of the receptor library components.* Bis-Zn(DPA) receptor (**2.4**), DTT (**2.7**), and designed peptides **2.5** and **2.6** with cysteine residues used to generate our *in-situ* created cross-reactive array for the discrimination of MAP kinases.

2.3.2 Determination of the Optimal Ratio of Fluorophore to Receptor

For the creation of an optical-signaling protocol that reports the binding of the suite of receptors to the kinases, we turned to indicator displacement assays (IDAs). In an IDA, the receptor interacts with the indicator through non-covalent interactions, and the indicator is displaced from the receptor when it is replaced by the analyte, inducing a signal modulation.[95] IDAs have several advantages when using differential sensing: 1) fluorescent indicators can be easily incorporated to impart optical signal changes, 2) they

are modular, meaning that different combinations of receptors and indicators are created simply by mixing, 3) the receptor-indicator stoichiometries can be adjusted to optimize the optical response and the threshold concentration for signaling,[96] and 4), one avoids the synthesis of several indicator-linked receptors.[97] To signal peptide and protein binding events to our receptors, the coumarin-based indicator **2.8** was chosen due to its high solubility under physiological conditions, and previous binding studies with zinc coordination compounds.[98,99]

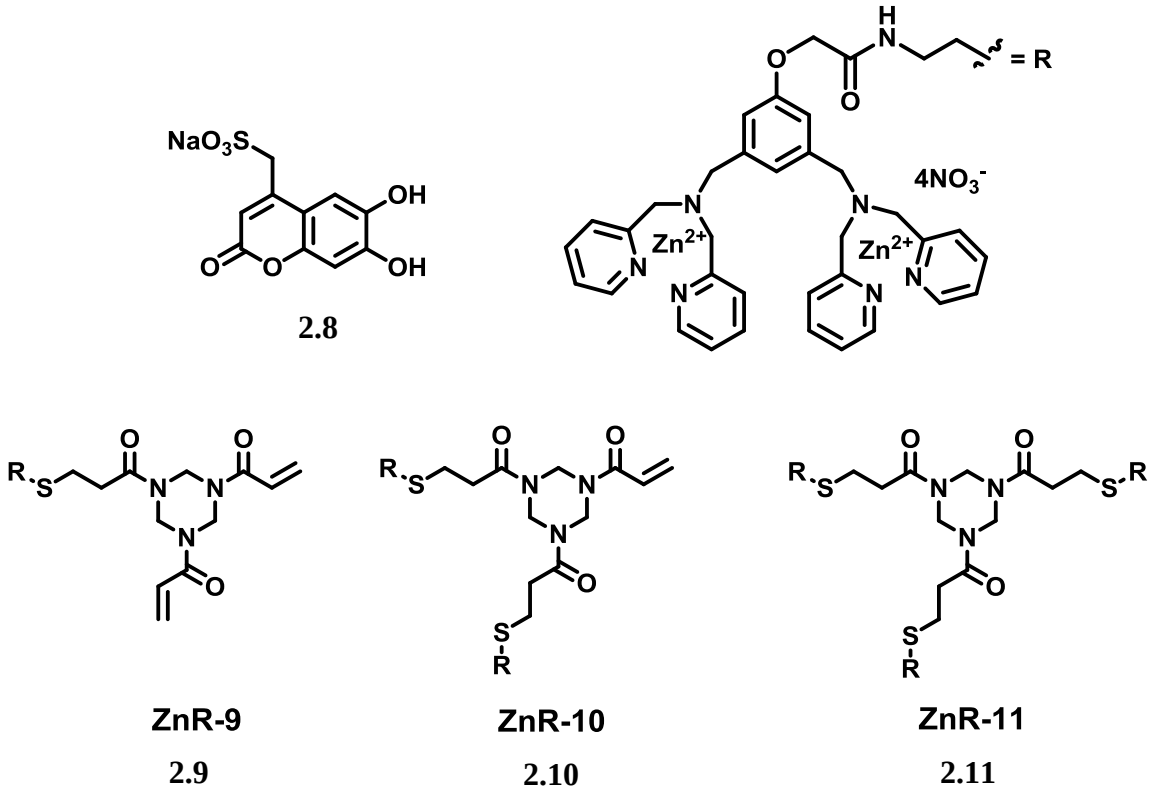

Figure 2.2: *Chemical structures of components in the sensing ensemble*. Coumarin-based indicator (**2.8**) and bis-Zn(DPA) chemosensors ZnR-9 (**2.9**), ZnR-10 (**2.10**), and ZnR-11 (**2.11**).

To test our IDA strategy, and to probe for any differential interactions of our general receptor design with phosphoproteins, receptor ZnR-10 (**2.10**) was synthesized. This receptor was used to model the behavior of all receptors in the array; it carries two of the bis-Zn(DPA) units and one underivatized site. First, fluorescence titrations in HEPES buffer were performed to optimize the correct receptor to indicator ratio. To study the binding of indicator **2.8** to ZnR-10, 750 µL of 100 µM **2.8** in HEPES buffer in a septum-capped glass cuvette (Starna cells) was titrated with aliquots of at least 5 µL, using 100 µL Hamilton microsyringe, of a solution of 250 µM ZnR-10 and 100 µM **2.8** in HEPES buffer. The spectra at 357 to 644 nm were recorded after each addition with an excitation wavelength of 347 nm. The fluorescence values at the maximum wavelength (475 nm) were obtained after each aliquot. The addition of receptor ZnR-10 into a solution of **2.8** resulted in a concentration-dependent quenching of the fluorescence emission of **2.8** (**Figure 2.3A**), and a 1:2 receptor-indicator binding stoichiometry was found. The change in fluorescent intensity at 475 nm was plotted against increasing concentration of host (**Figure 2.3B**) which determined the ratio of ZnR-10 to indicator to be used in the following binding assays with peptides and proteins.

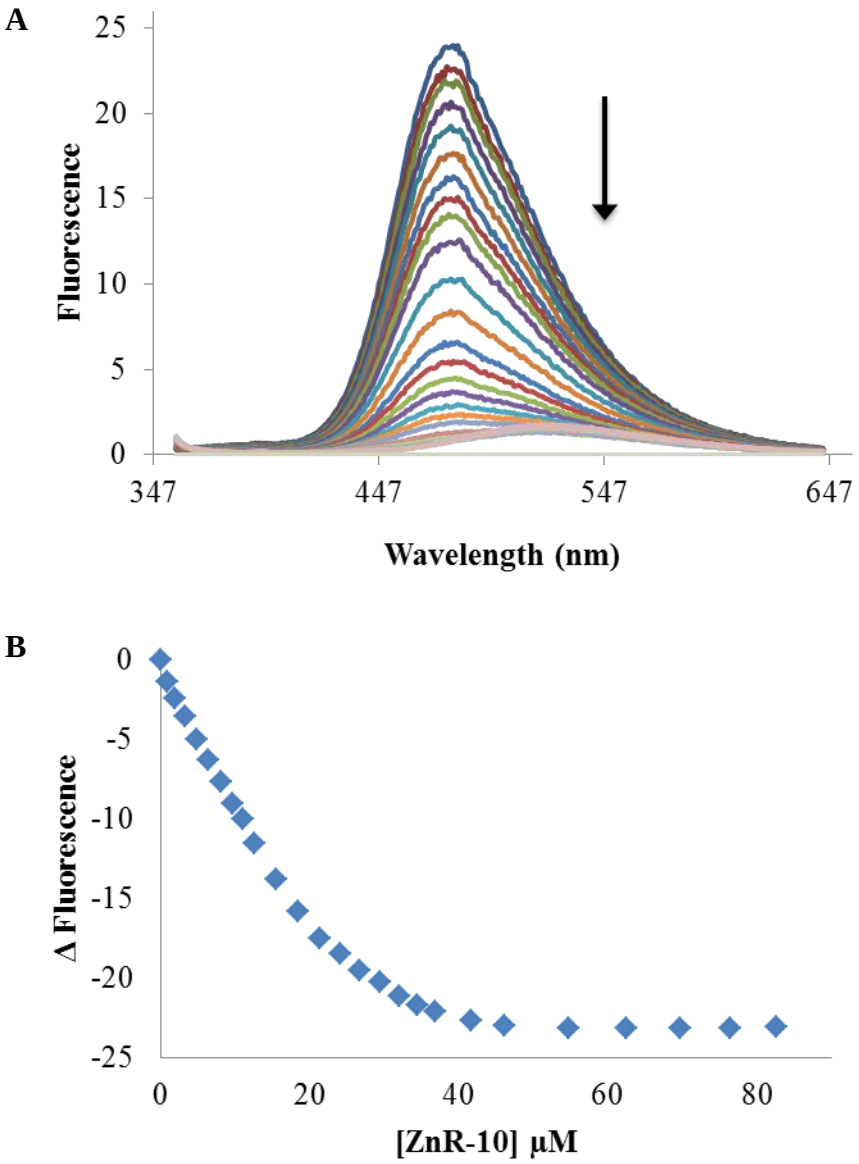

Figure 2.3: *Binding of coumarin-based indicator to receptor ZnR-10.* (A) Addition of **ZnR-10** (0 - 82 µM) to Indicator (100 µM) in 50 mM HEPES, 10 mM NaCl Buffer, pH=7.4, λ_{ex} 347 nm. (B) Binding isotherm for the binding of indicator to **ZnR-10** of the data in **Figure 2.3A,** fitting 2:1 binding ratio at λ_{em} = 475 nm.

2.3.3 Indicator Displacement Assay Using a Phosphorylated Peptide

To prove our principle for sensing protein phosphorylation, we first targeted a specific phosphorylated peptide. We synthesized Sub-F peptide (YAEPLTPRILAKWEWPA), which is a substrate for ERK-2. Phosphorylation conditions and characterization of sub-F peptide is described in the Supporting Information. In our first IDA, we prepared a 1:2 receptor-indicator complex (ZnR-10: **2.8**) in aqueous solution at pH=7.4 (50 mM HEPES, 10 mM NaCl). Then, in separated experiments fluorescent titrations between peptides with ZnR-10-indicator complex were done. Individual solutions of 36.6 μM ZnR-10 and 100 μM **2.8** in HEPES buffer were titrated with aliquots of 1.92 mM phosphorylated peptide solution and 1.92 mM non-phosphorylated peptide solution, which also contained the receptor-indicator complex. Only the phosphorylated peptide (**Figure 2.4A**) was able to displace the indicator, which resulted in the restoration of the emission intensity at the λ_{max} of **2.8** (**Figure 2.4B**).

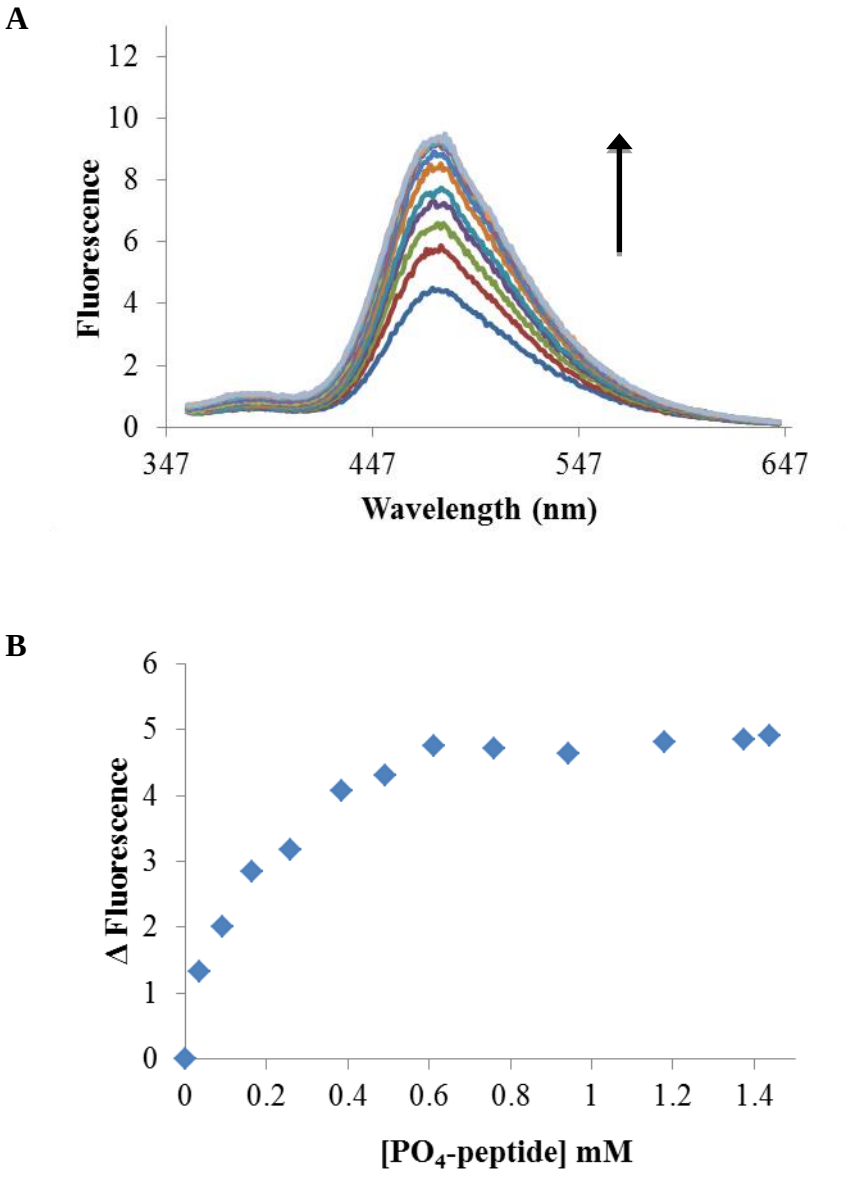

Figure 2.4: *Addition of phosphorylated peptide to indicator-ZnR-10 complex.* Increase in the fluorescence intensity due to displacement of the coumarin indicator. (A) Addition of phosphorylated Sub-F peptide (PO_4-peptide) (0 – 1.37 mM) to **ZnR-10** (36.6 µM), **2.8** (100 µM) in 50 mM HEPES, 10 mM NaCl pH=7.4, λ_{ex} 347 nm. (B) Binding curve of data in **Figure 2.4A** measured at λ_{em} = 475 nm.

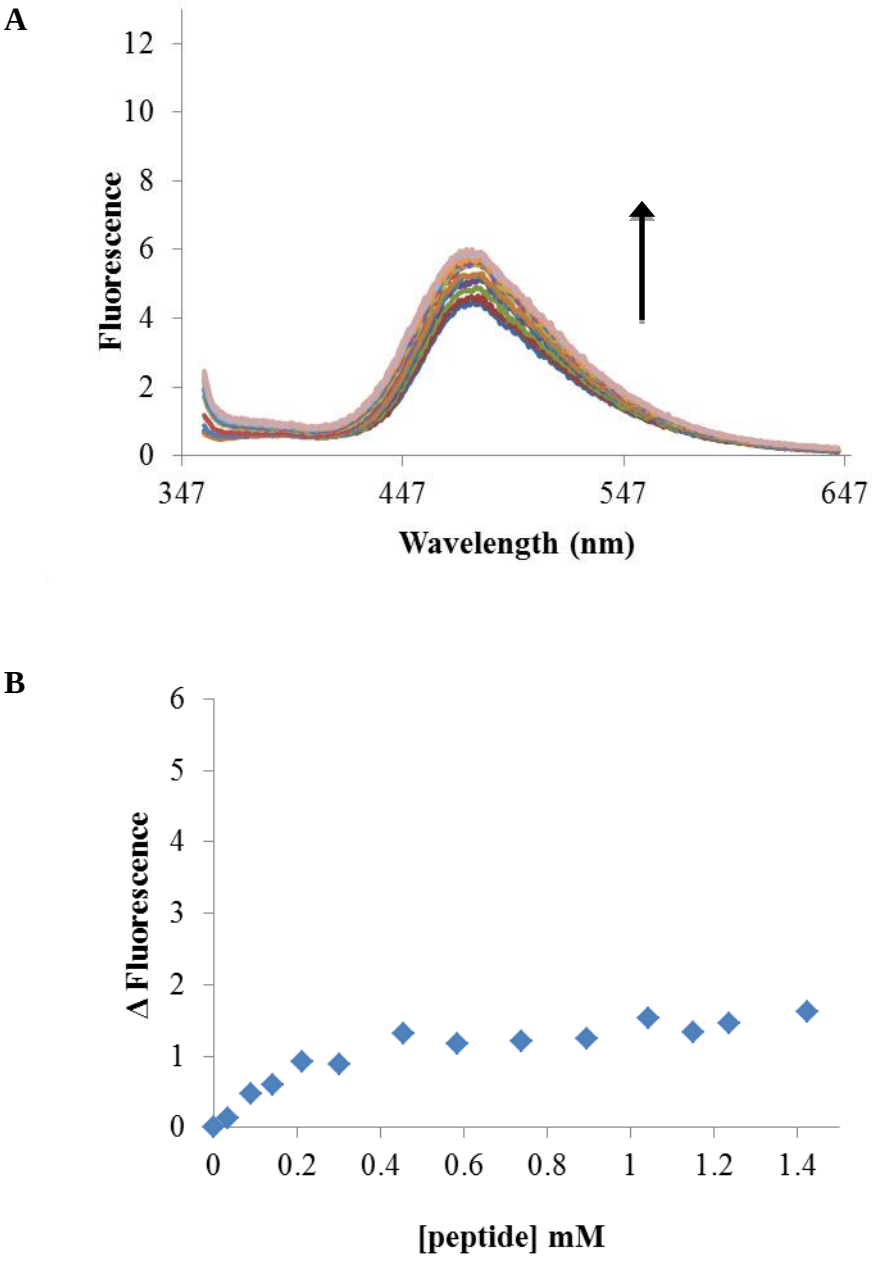

Figure 2.5: *Addition of nonphosphorylated peptide to indicator-ZnR-10 complex.* Increase in the fluorescence intensity due to displacement of the coumarin indicator. (A) Addition of nonphosphorylated Sub-F peptide (0 - 1.42 mM) to **ZnR-10** (36.6 µM) and **2.8** (100 µM)) in 50 mM HEPES, 10 mM NaCl pH=7.4, λ_{ex} 347 nm. (B) Binding curve of data in **Figure 2.5A** measured at λ_{em} = 475 nm.

2.3.4 *In Vitro* Differentiation of Active and Inactive MAP Isoform Kinases

Because it was found that chemosensor ZnR-10 can differentiate between phosphorylated and non-phosphorylated peptides, we anticipated a similar distinction between active and inactive kinases. In separate experiments, phosphorylated ERK-1 and its inactive form were titrated into a 1:2 receptor-indicator complex solution. A significant increase in the fluorescence intensity was observed upon the addition of active ERK-1 (**Figure 2.6A**), compared with the non-phosphorylated analog. Despite an increase in the fluorescence intensity observed in both cases (**Figure 2.6C**), there was a large enough and reproducible difference to encourage us to continue.

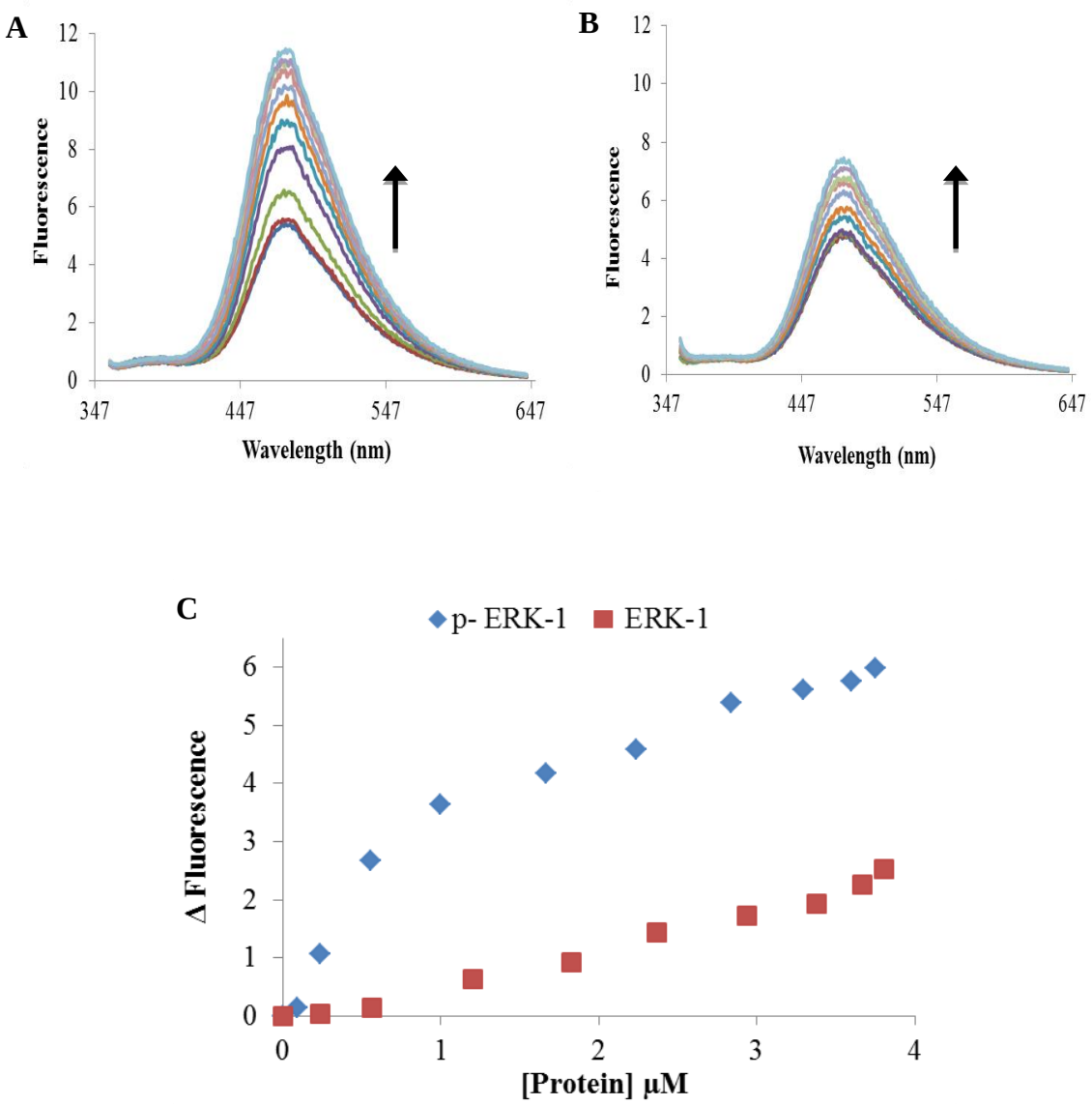

Figure 2.6: *Addition of active and inactive ERK-1 to indicator-ZnR-10 complex.* Increase in the fluorescence intensity due to displacement of the coumarin indicator. (A) Addition of phosphorylated ERK-1 (0 – 3.8 µM p-ERK-1) to **ZnR-10** (36.6 µM) and **2.8** (100 µM) in 50 mM HEPES Buffer, 10 mM NaCl pH=7.4, λ_{ex} 347 nm. (B) Addition of non-phosphorylated ERK-1 (0 – 3.8 µM ERK-1) to **ZnR-10** (36.6 µM) and **2.8** (100 µM) in HEPES Buffer, 10 mM NaCl pH=7.4, λ_{ex} 347 nm. (C) Binding curves of data in **Figures 2.6A** and **2.6B** measured at λ_{em} = 475 nm, respectively.

Hence, our third and final test prior to creating the array was to analyze the response to a different MAP kinase. Starting with ERK-2, an isoform of ERK-1 with 84% identity at the amino acid level,[100] we found that the inactive ERK-2 induces a fluorescence response similar to that of active ERK-2 (**Figure 2.7C**). Although the response of this single receptor to active and inactive ERK-2 are similar, the isotherms are different from those of ERK-1, and potentially other receptors that result from our *in-situ* generated array would be able to differentiate these two ERK-2 species. Hence, these preliminary results showed that this single receptor-indicator system is not only capable of distinguishing active and inactive kinases, but it can also differentiate between close isoforms, and it led credence to the notion that a series of such receptors may lead to a reliable method to classify kinases and their active/inactive forms.

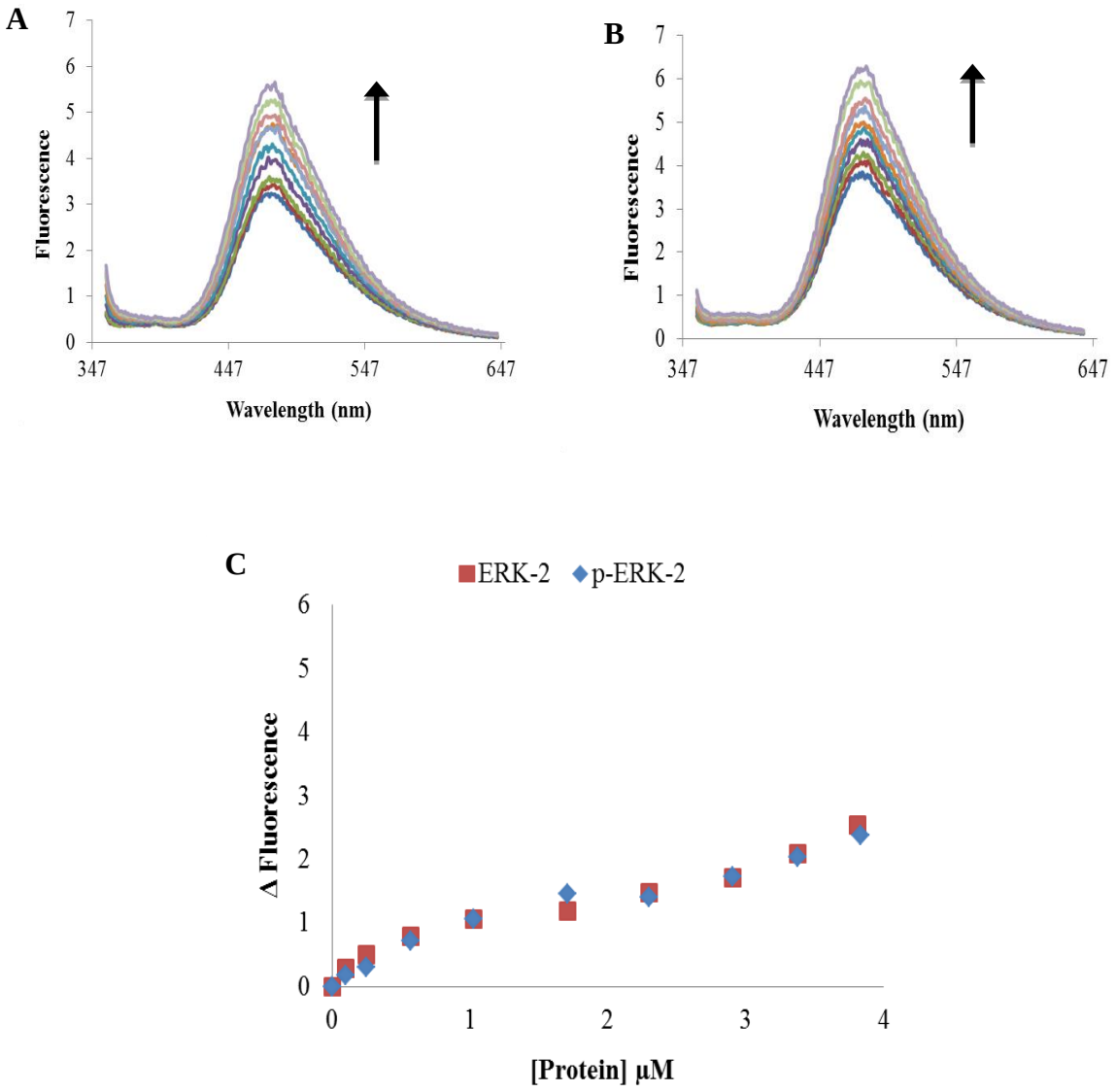

Figure 2.7: *Addition of active and inactive ERK-2 to indicator-ZnR-10 complex.* (A) Addition of phosphorylated ERK-2 (0 – 3.8 µM p-ERK-2) to **ZnR-10** (36.6 µM) and **2.8** (100 µM) in 50 mM HEPES buffer, 10 mM NaCl pH=7.4, λ_{ex} 347 nm. (B) Addition of non-phosphorylated ERK-2 (0 – 3.8 µM ERK-2) to **ZnR-10** (36.6 µM) and **2.8** (100 µM) in 50 mM HEPES, 10 mM NaCl pH=7.4, λ_{ex} 347 nm. (C) Binding curves of data in **Figures 2.7A** and **2.6B** measured at λ_{em} = 475 nm, respectively.

2.3.5 Detection Limit Determination

The standardized analytical method to calculate the limit of detection (LOD), detection limit (DL), limit of quantitation (LOQ) and lower limit of quantitation (LLOQ) requires seven replicates of a blank to calculate the signal noise.[101,102] Part of the background signal will arise from the fluorescence of host-indicator complex without the analyte. Thus, the average of the fluorescence intensity at 475 nm (**Figure 2.8**) was obtained from seven blank replicates in the presence of the host-indicator complex, and the standard deviation was used to substitute in **Equations 2.1** to **2.4**.

$$LOD = x + 3\sigma \qquad \textbf{(Eq. 2.1)}$$

$$LOQ = x + 10\sigma \qquad \textbf{(Eq. 2.2)}$$

$$DL = \frac{3\sigma}{m} \qquad \textbf{(Eq. 2.3)}$$

$$LLOQ = \frac{10\sigma}{m} \qquad \textbf{(Eq. 2.4)}$$

The parameters used in the equations are described as follows: x, blank average; σ, the standard deviation; and *m*, slope value of a calibration curve. **Equation 2.1** has been used to find the limit of detection of the signal. The 3σ method introduced by Kaiser defines the limit of detection which refers to the concentration that will give a signal

three times the standard deviation of the noise.[1] The LOQ is at least ten times the LOD.[102] In addition, **Equation 2.3** has been used to calculate the actual DL which is the minimal concentration of analyte that can be detected, and **Equation 2.4** has been used to find the LLOQ which gives a more accurate value of the minimal amount of phosphorylated ERK-1 that can be measured. The slope (*m*) in **Equation 2.3** and **Equation 2.4** is equivalent to the extinction coefficient (ε) of the fluorophore. Thus, the binding isotherm acquired from the addition of phosphorylated ERK-1 to host-indicator complex (**Figure 2.6A**) was used to obtain the slope value applying the following mathematical method.

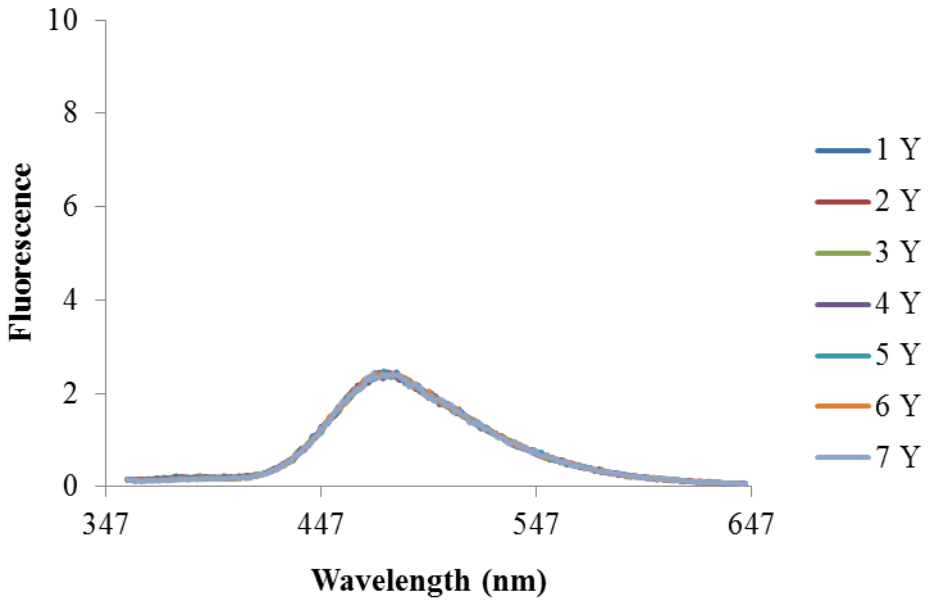

Figure 2.8: *Control experiment with indicator-ZnR-10 complex.* Seven blank measurements of **ZnR-10** (36.6 µM) and **2.8** (100 µM) in 50 mM HEPES Buffer, 10 mM NaCl pH=7.4, λ_{ex} 347 nm.

Igor Pro 6.04 software was used to fit the exponential curve and obtain the corresponding coefficients (**Figure 2.9**) to substitute in **Equation 2.5**. The slope of the fit at x = 0 corresponds to the linear portion of the curve, and so it can be used to find the extinction coefficient. To find this value we simply took the derivative of the fit (**Equation 2.6**) and solved at x = 0.

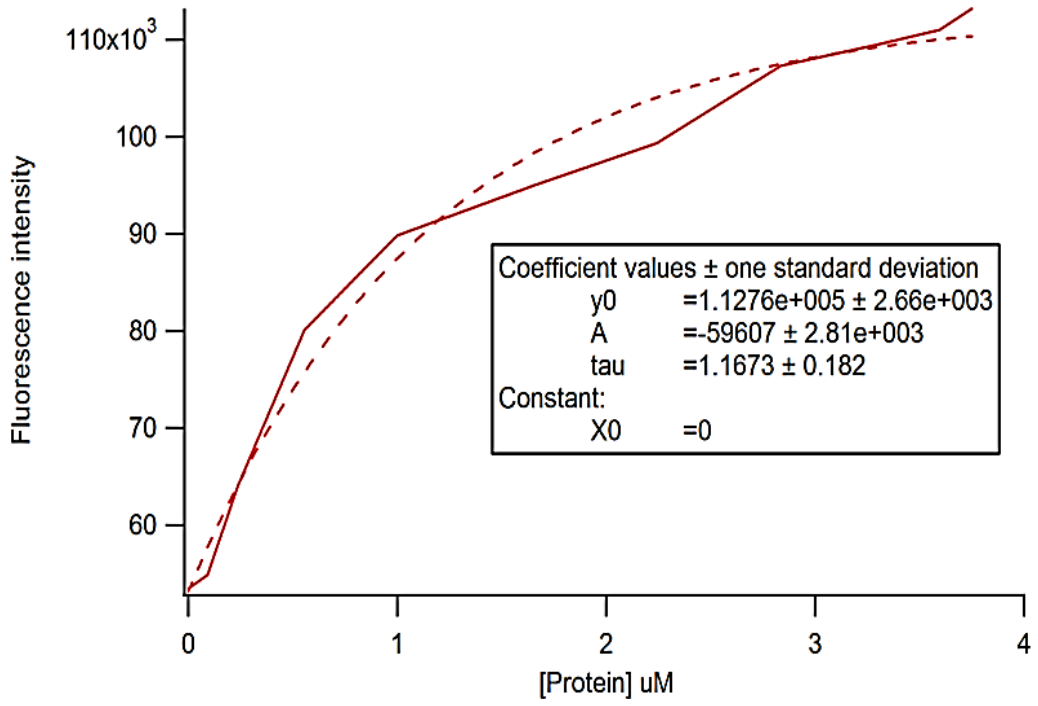

Figure 2.9: *Curve fitting of the binding isotherm of ERK1 to host-indicator complex using Igor Pro.* The red solid line corresponds to the obtained binding isotherm for the binding of phosphorylated ERK-1 to host-indicator complex at λ_{em} = 475 nm from the data in **Figure 2.6A**. The red dot line corresponds to the curve fitting.

$$y = yo + Aexp\left(\frac{-x}{\tau}\right) \quad \textbf{(Eq. 2.5)}$$

$$\frac{dy}{dx} = Aexp\left(\frac{-x}{\tau}\right)\left(\frac{-1}{\tau}\right) \quad \textbf{(Eq. 2.6)}$$

If $\mathbf{x = 0}$ where it is the most linear then:

$$\frac{dy}{dx} = -59607exp\left(\frac{0}{1.1673}\right)\left(\frac{-1}{1.1673}\right)$$

$$\frac{dy}{dx} = \frac{59607}{1.1673} = 51077\ FI/\mu M$$

The value of the slope was found to be m = 51077 $\pm$ 8320 $FI/\mu M$. **Equation 2.7** was used to find the error propagation[4] of the slope, DL and LLOQ:

$$\frac{\delta Q}{Q} = \sqrt{\frac{\delta a^2}{a} + \frac{\delta b^2}{b}} + \cdots \quad \textbf{(Eq. 2.7)}$$

The parameters used in the **Equation 2.7** are described as follows: δa, uncertainties of quantities a; and δb, uncertainties of quantities b.[103] After substituting the values for A and τ and their corresponding uncertainties (from **Figure 2.9**) into **Equation 2.7**, the uncertainty value of the slope was 8320.

Finally, after substituting the slope value into **Equation 2.3** and **Equation 2.4**, the detection limit and the lower limit of detection were 14±2.3 nM and 46±7.5 nM of phosphorylated ERK-1, respectively.

Blank repetitions	Fluorescence at 475 nm
1	23722.7
2	23905
3	23981
4	23439.2
5	23874.6
6	24224
7	23656.9
AVERAGE	*23829.05*
STDEV	*232.94*
Signal detection limit	24527.89
Limit of Quantitation	26158.51
Slope	m = 51077 ±8320
Detection limit	0.0136 ± 0.0022 µM
Lower limit of quantitation	0.0456 ± 0.0074 µM

Table 2.1: *Summary chart showing blank measurements.* SDL, LOQ, DL and LLOQ values of phosphorylated ERK-1.

2.3.6 Sensing Ensemble Construction and Fingerprint of MAPK

To evaluate the ability of the *in-situ* generated cross-reactive receptors to discriminate ERK-1/2, JNK-3 and $p38_{\gamma}$ kinases, we prepared a 384-well plate with receptor-indicator combinations. To generate the sensing ensemble, bis-(DPA) receptors R-9, R-10 and R-11 were synthesized (see Supporting Information), and used to create seven different combinations of hosts (**Table 2.2**). Host H1 contains R-9 (57 µM); Hosts

H2 and H3 contain receptor R-9 (57 μM) which was stirred separately with one equivalent (per free vinyl group) of the correspondent peptide PVDAC or KALIC (57 μM), and DTT (57 μM). Hosts H4 and H5 contain receptor R-10 (39 μM) and Host H6 contains receptor R-10 (39 μM) and DTT (39 μM). Host H7 contains receptor R-11 (35 μM).

Host	1	2	3	4	5	6	7
Type of bis-Zn(DPA) receptor	ZnR-9	ZnR-9	ZnR-9	ZnR-10	ZnR-10	ZnR-10	ZnR-11
Type of Host	R-9 $Zn(NO_3)_2$ Indicator	R-9 PVDAC DTT $Zn(NO_3)_2$ Indicator	R-9 KALIC DTT $Zn(NO_3)_2$ Indicator	R-10 $Zn(NO_3)_2$ Indicator	R-10 $Zn(NO_3)_2$ Indicator	R-10 DTT $Zn(NO_3)_2$ Indicator	R-11 $Zn(NO_3)$ Indicator
Receptor (μM)	57	57	57	39	39	39	35
DTT (μM)	-	57	57	-	-	39	-
PVDAC (μM)	-	57		-	-	-	-
KALIC (μM)	-	-	57	-	-	-	-
$Zn(NO_3)_2$ (μM)	114	114	114	155	155	155	213
Indicator (μM)	57	57	57	57	100	100	124
Equiv.	1:2:1	1:1:1:2:1	1:1:1:2:1	1:4:1.5	1:4:2.5	1:1:4:2.5	1:6:3.5

Table 2.2: *Host concentrations used in the sensing ensemble.*

The order of addition of each of the reagents was important due to the known coordination interactions between sulfhydryl groups and Zn^{2+} metal ions.[104] Therefore, zinc nitrate was the last reagent added in appropriate equivalents according to the number of DPA moieties present in each receptor where the final concentration was 114 μM, 155 μM and 213 μM according to each host (**Table 2.2**). Aliquots of each host solution were loaded into a 384-well plate (32 μL Costar black polystyrene microplate), followed by indicator aliquots according to the number of bis-Zn(DPA) moieties present in each receptor. The final concentrations of indicator were 57 μM of **2.8** to hosts H1-4, 100 μM of **2.8** to hosts H5 and H6, and 124 μM of **2.8** to host H7 in HEPES buffer. Finally, respective aliquots of phosphorylated and non-phosphorylated kinases ERK-1, ERK-2, JNK-3 and $p38_{\gamma}$ were added to each set of host-indicator solutions, so that the final protein concentrations were 4 μM (four replicates each).

Changes in the emission data at the λ_{max} of 8 at pH = 7.4 (475 nm) for each ensemble of the sensor array upon addition of each kinase were recorded using a microplate reader (Biotek Synergy 2). The data generated (4 replicates x 7 host x 8 kinases) were analyzed with the program XLSTAT using linear discriminant analysis (LDA). This chemometric analytical technique simplifies the data set obtained from the sensing array, allowing for differentiation and classification of the response pattern. LDA maximizes the distance between analyte groups while minimizing the distance within an analyte group.[105]

A series of LDA tests were set up with purified and single proteins. First, using the four phosphorylated kinases (ERK-1, ERK-2, JNK-3 and $p38_{\gamma}$), the resulting score plot (**Figure 2.10A**) shows excellent differentiation along the F1 and F2 axes, and good clustering of the experimental replicates at the given concentration. The active kinases are organized along the F1 axes by emission modulation of the sensing ensemble, where isoform ERK-2 is located into the left quadrant and ERK-1 into the right one. The kinases are classified into respective sets with 100% accuracy according to a jackknife analysis.[106] Next, using the same conditions we sought to test the capability of our sensing ensemble to discriminate phosphorylated and non-phosphorylated kinases (ERK-1, ERK-2, JNK-3 and $p38_{\gamma}$). Similar to the previous study, each active and inactive kinase produced a distinctive fluorescence pattern, but with a lower accuracy, 93.5% via a jackknife (**Figure 2.11A**). Although inactive $p38_{\gamma}$ overlaps with active ERK-2, we can clearly distinguish that the active/inactive $p38_{\gamma}$ and ERK-2 proteins are located on opposite sides of the left quadrant. It is also observed that ERK-1/ERK-2 kinases, which have very similar structures, are classified in opposite areas along F1. Furthermore, the phosphorylated isoforms are significantly differentiated from the non-phosphorylated ones, and within themselves, along both F1 and F2 axes. Finally, active and inactive JNK-3 kinases are clearly classified and located on the top right quadrant. A general trend was found, where the active kinases are located on the right side and the inactive ones are located on the left side, except the ERK-2 isoform.

It was found that the protein kinases located on the right side of the score plot displaced indicator **2.8** in the array to a higher extent than those kinases located on the left side of the score plot (**Figure 2.10A** and **2.11A**). A loading plot can be generated along with the LDA score plot, and it gives vectors that represent the host contribution to the differentiation of the kinases (**Figure 2.10B** and **2.11B**).

According to both loading plots, hosts H-1, H-5, H-6 and H-7 which contain single receptors ZnR-9, ZnR-10, ZnR-10 with DTT and ZnR-11 vary significantly in response to both active and inactive kinases, whereas hosts H-2, H-3 and H-4 which contain ZnR-9 with peptides and DTT did not contribute significantly. This result suggests that different extents of bis-Zn(DPA) moieties on the receptors are responsible to maximize the differential binding between active and inactive kinases.

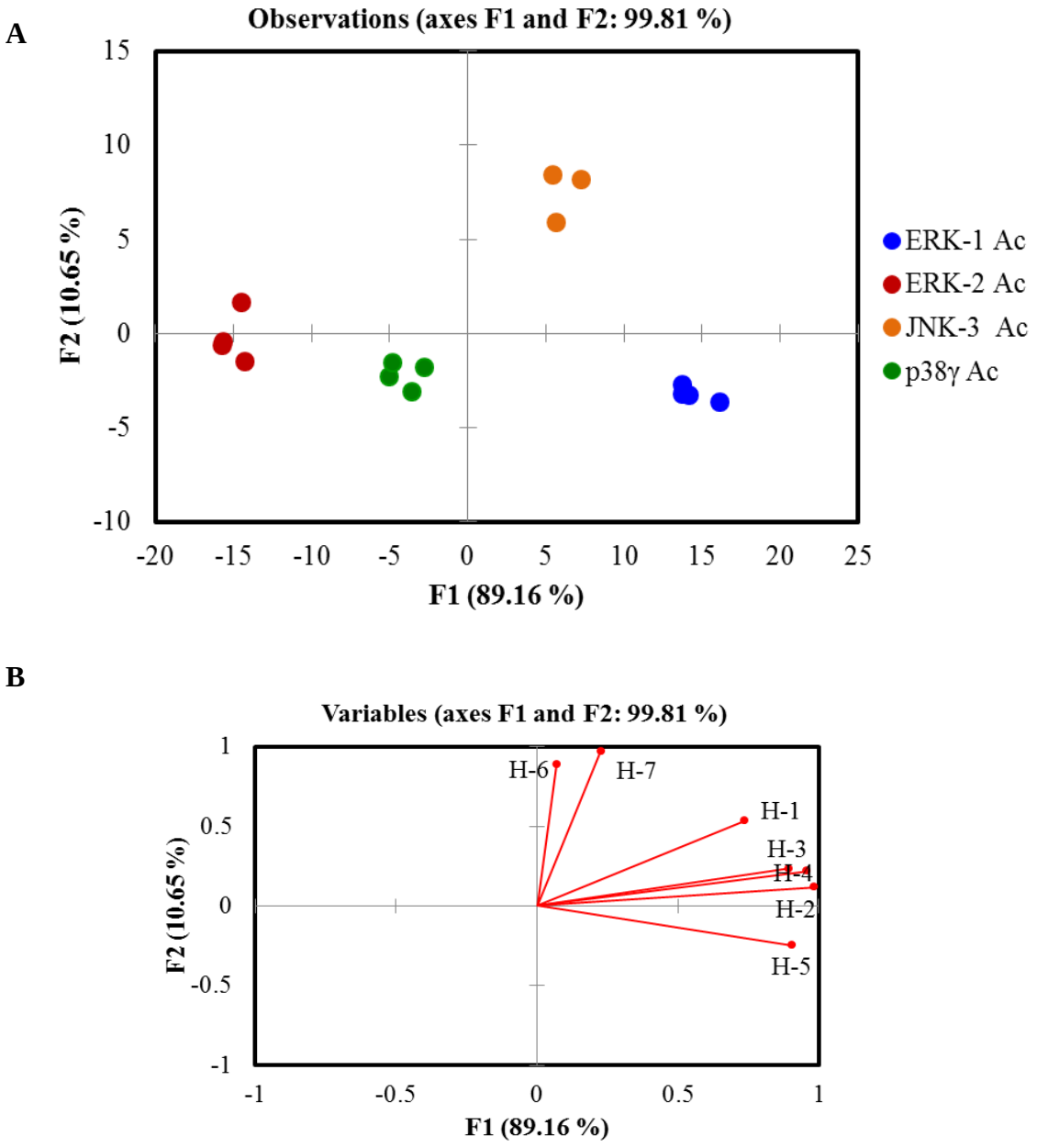

Figure 2.10: *LDA score plot and loading plot of the response from the sensing array showing in-vitro differentiation of active MAP kinases.* (A) LDA score plot and (B) loading plot of the fluorescence response pattern of phosphorylated MAP kinases (ERK-1, ERK-2, JNK-3 and p38$_\gamma$) at 4µM concentration with 100% jack knife analysis. Vectors on the loading plots represent individual host contribution on the array represented by host number.

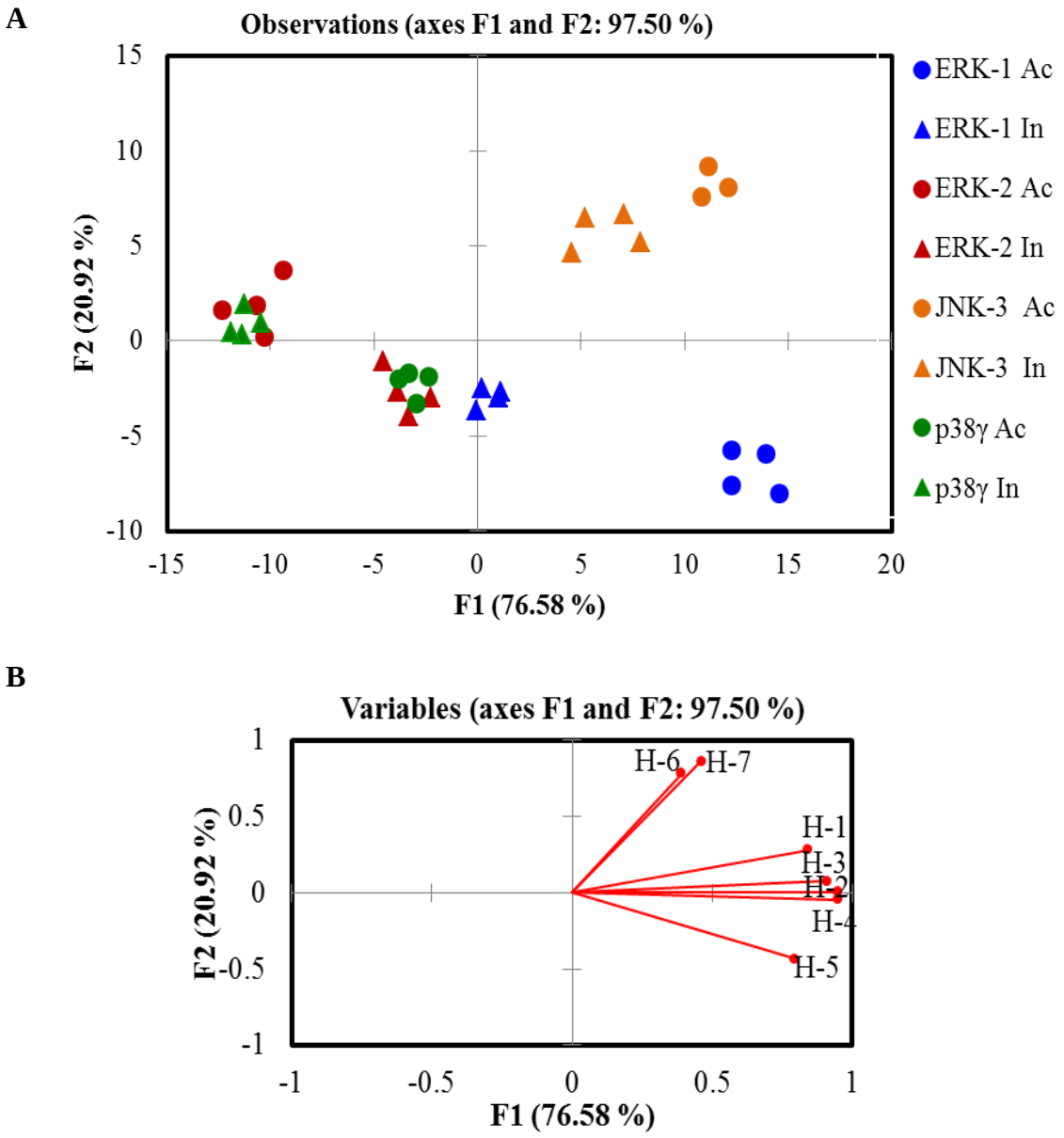

Figure 2.11: *LDA score plot and loading plot of the response from the sensing array showing in-vitro differentiation of active and inactive MAP kinases.* (a) LDA score plot and (B) loading plot of the fluorescence response pattern of phosphorylate (○) and non-phosphorylated (△) kinases (ERK-1, ERK-2, JNK-3 and $p38_{\Upsilon}$) at 4µM concentration with 93.5% jack knife analysis. Vectors on the loading plots represent individual host contribution on the array represented by host number.

2.3.7 Fingerprint of Cell Lysates with Different Cellular Response

After the successful *in-vitro* differentiation of purified active and inactive kinases using LDA of the signals from our array, we explored whether the system could be used to differentiate kinase activity in a complex mixture. To prove the discriminatory properties of our system, we assessed whether the differential receptor library could differentiate HEK293T cells that have differing kinase expression and activity. Because our approach necessarily responds to all phosphorylated proteins, the pattern that arises is a qualitative differentiation of distributions of proteins that change due to a specific profile of kinase activity. For example, differences in the cell line generated by stimulation with anisomycin, epidermal growth factor (EGF), and/or overexpression of ERK-1, would all be reflective of changes resulting from activation of specific pathways. Anisomycin has been reported to activate both JNK and p38 MAPK pathways,[107] and EGF was reported to induce ERK and to a lesser extent the JNK pathway.[108]

Before array analysis, western blot (WB) on lysates was performed to confirm the anticipated changes in these kinases (**Figure 2.12**). The WBs showed an increased activation/phosphorylation of JNK and p38 in the cells that were stimulated with anisomycin if compared to the untreated ones (control cells). Further, the ERK activation/phosphorylation pathway was confirmed to be increased in cells stimulated with EGF when compared to the control. Two other sets of lysates contained HEK293T cells that have ERK1-WT overexpressed, while one of them was also stimulated with

EGF. WB analysis showed that overexpressed ERK-1 was partially phosphorylated. However, induction of the cells with EGF significantly increased its phosphorylation.

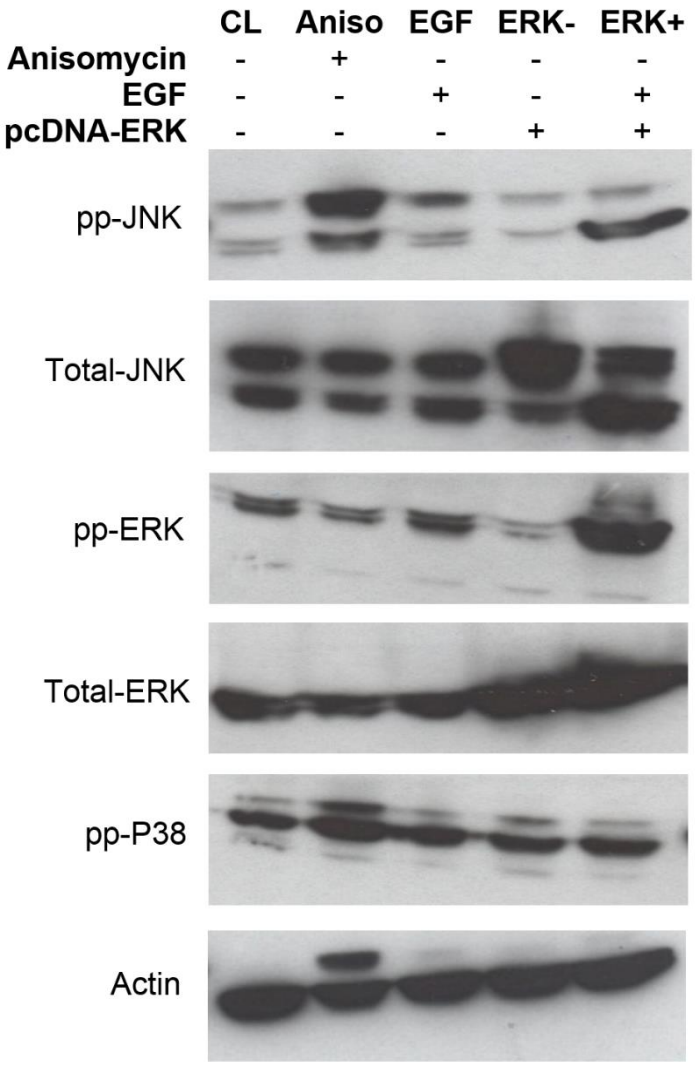

Figure 2.12: *Western Blot analysis of different HEK293 cell lysates*. The JNK pathway was induced by the addition of anisomycin (100 nM) for 5-10 minutes **(Aniso)** or the ERK pathway was induced by the addition of 100 ng/mL EGF **(EGF)** for 30 minutes before lysing the cells. Cells that were transfected with pcDNA-ERK construct to overexpress WT-ERK1, were either induced with 100 ng/mL EGF for 30 minutes before lysis **(ERK+)** or lysed without induction **(ERK-)**. Lysates containing 60 µg of total protein were fractionated by SDS PAGE (10% gel) and subjected to western blot analysis in order to detect the phosphorylated forms of each MAP kinases. (The results were similar in two different experiments)

Cell lysate expression, purification, and activation, are described in the supporting information. HEK293T cell lysates were prepared in CytoBuster™ Protein Extraction Reagent (EMD-Biosciences) after washing in PBS (Invitrogen). The lysates were cleared by centrifugation, and ATP was washed away using Amicon Ultra-0.5 mL Centrifugal Filters. Bradford analysis (Bio-Rad) was used to measure the protein concentration. Discrimination of cell lysates was obtained at total protein concentration according to **Table 2.3**. For the detection, 6 µL of cell lysate was added to the same sensing ensemble and same data analysis was followed.

Cell Lysates	CL	Aniso	EGF	ERK-	ERK+
Total [Protein] mg/mL	3.6	6.0	4.1	1.5	6.2

Table 2.3: *Total protein concentration of each cell lysate.*

The LDA score plot (**Figure 2.13A**) of the fluorescence data showed excellent differentiation between the cells overexpressing ERK-1 (ERK-), cells over-expressing ERK-1 and induced by EGF (ERK+), and control cells along the F1 and F2 axes, and good clustering of the replicates. This result suggests that the variation of the responses is dependent on protein and phospho-protein identity. Furthermore, the LDA score plot (**Figure 2.14A**) of the fluorescence data also showed excellent discrimination of the cells that have ERK induced by EGF (EGF), which are separated along the second principal component (F2) from the cells that have JNK/p38 induced by anisomycin, and separated

from the control cells along the first principal component (F1). This differentiation suggests that the sensing array is able to detect subtle changes in phosphoproteins when cells are stimulated with different activators. These cell extracts are classified into respective sets with 100% accuracy according to a jackknife analysis. Another general trend was found (Figure 6A and 6C), where the induced and/or over-expressed cell lysates are located on the right side of the score plot and the control lysates are located on the left side.

The loading plots (**Figure 2.13B** and **2.14B**) from the analysis showed a broad cross-reactivity from the hosts. In this case, hosts H-1, H-2 and H-3 correspond to the receptors with single ZnR-9, and ZnR-9 with peptides and DTT, which produced a completely different response from hosts H-4 and H-5, which correspond to receptor ZnR-10; and host H-6 and H-7 which encompass receptors ZnR-10 with DTT and ZnR-11, respectively.

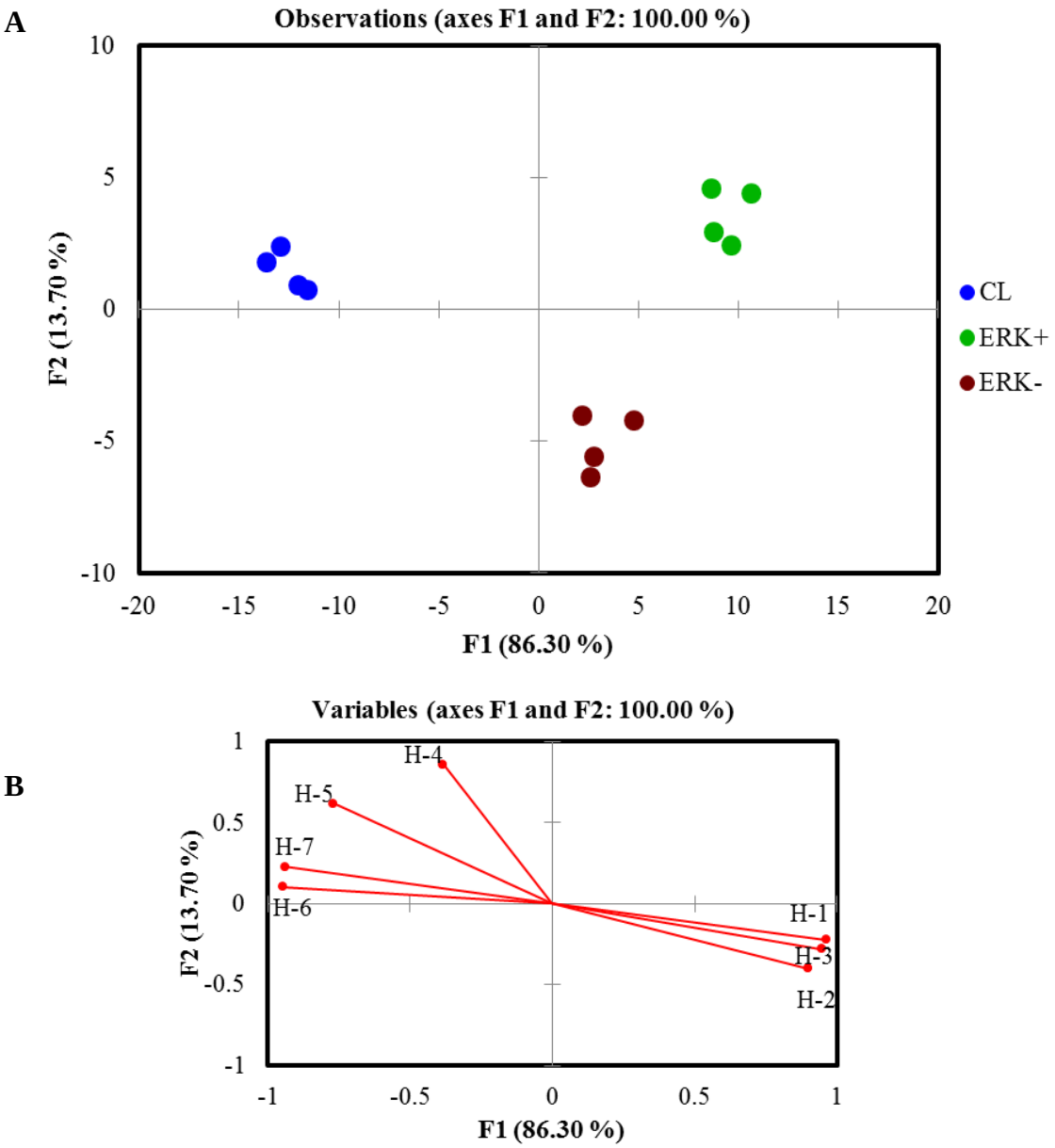

Figure 2.13: *LDA score plot and loading plot of the response from the sensing array showing differentiation of HEK293T cell lysates with differing kinase expression.* (A) LDA score plot and (B) loading plot of the fluorescence response pattern of different sets of stimulated and untreated HEK293T cell lysates with 100% jack knife analysis: control lysate (CL), induced/over-expressed (ERK+), and over-expressed (ERK-).

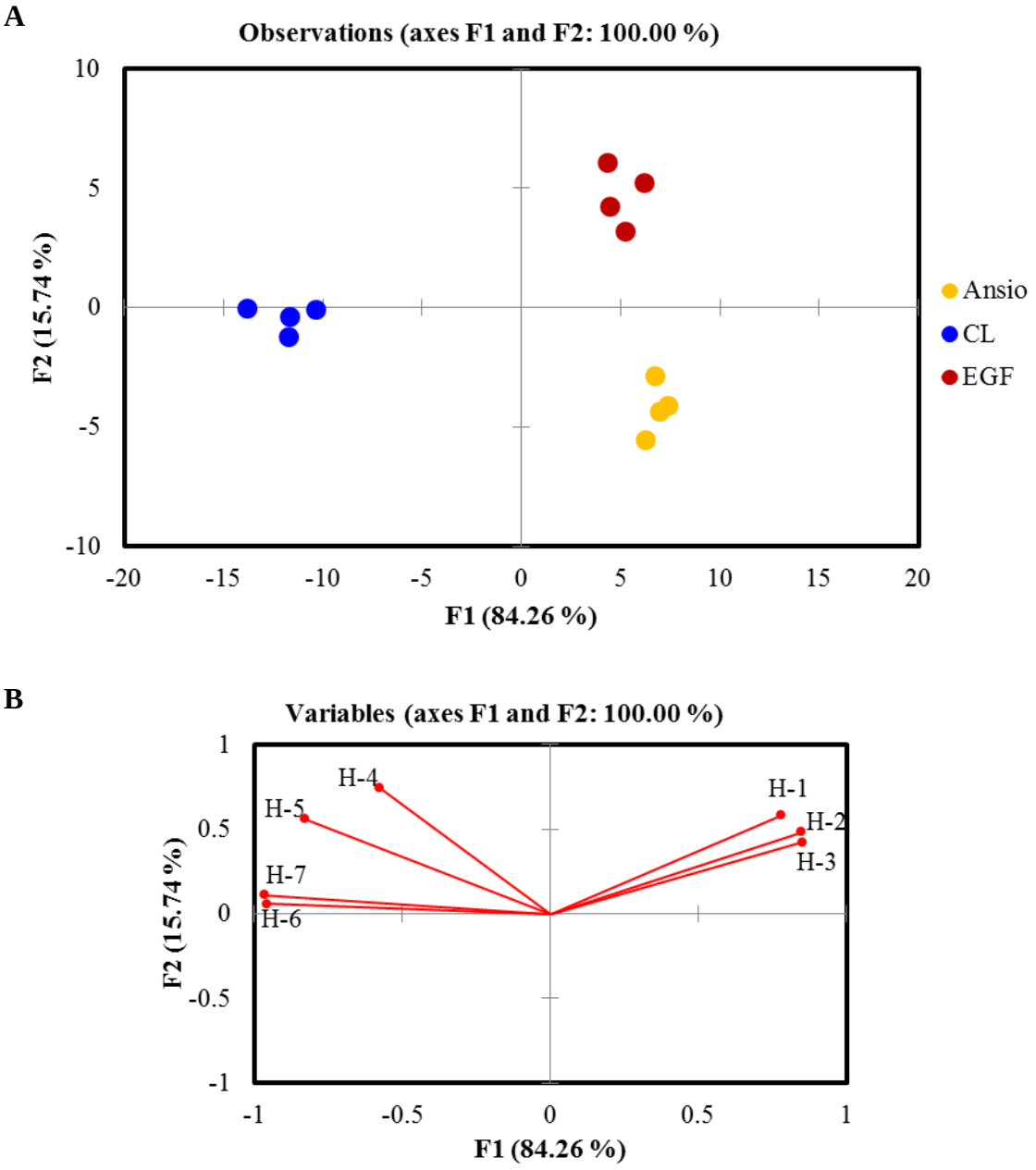

Figure 2.14: *LDA score plot and loading plot of the response from the sensing array showing differentiation of HEK293T cell lysates with differing kinase expression.* (A) LDA score plot and (B) loading plot of the fluorescence response pattern of different sets of stimulated and untreated HEK293T cell lysates with 100% jack knife analysis: control lysate (CL), JNK induced with anisomycin (Ansio), and ERK induction with EGF (EGF).

2.4 CONCLUDING REMARKS

In summary, we have shown that an array of self-assembled synthetic and peptidic elements in combination with an IDA protocol provides cross-reactivity for the differentiation of phosphorylation states on kinases. Significantly, this sensing system is capable of fingerprinting different classes of MAP kinases and cell lysates *in-vitro* at neutral aqueous conditions using chemometric analysis. In this manner, a new pattern recognition approach was derived to target this class of analyte. The ability of this sensing ensemble to differentiate cells that have been induced with different stimulants increases our expectation for the ability of this array to differentiate between different types of cells, such as cells from diseased and non-diseased tissues or even cells from different organs.

2.5 ADDITIONAL AND EXPERIMENTAL INFORMATION

This research has been published as a paper in the *Journal of the American Chemistry Society*.[109]

2.5.1 Materials and General Procedures

Starting materials were purchased from Aldrich Chemical Co., Acros Organics, EM, or TCI, and used without further purification. All solvents were of reagent grade quality and purchased commercially. Compounds **2.13**, **2.14** and **2.15** were prepared according to previous literature procedure.[110] Coumarin-based indicator **2.8** was prepared according to *Smith et al*.[111] All reactions were performed in standard glassware. Evaporation was

done by rotatory evaporation using a standard rotovap equipped with dry ice condenser. TLC analyses were carried out using Silica TLC Plates Aluminum Backing 20 by 20 cm sheet UV active. Column chromatography (CC) was performed using silica gel 60 (230 ± 400 mesh, 0.040 ± 0.063 mm) from Dynamic Adsorbents. Reverse phase purification was done using a Teledyne CombiFlash Companion with C18 RediSep reverse phase columns. Analytical HPLC data was obtained with a Shimadzu HPLC equipped with Gemini C18 column (250 X 10 mm, 5 µm). Solvent A: H_2O with 0.1% v/v TFA; solvent B: CH_3CN with 0.1% v/v TFA. Rate flow: 4 mL/min with an increase gradient 5 to 90% B over 20 min at 254 and 300 nm.

^{1}H and ^{13}C spectra were recorded on Varian DirectDrive or Varian INOVA NMR spectrometers. The NMR spectra were referenced to solvent and the spectroscopic solvents were purchased from Cambridge Isotope Laboratories. Finnigan MAT-VSQ 700 and DSQ spectrometers were used to obtain mass spectra. HR electrospray ionization (ESI) mass spectra were recorded using either Agilent 6530 Accurate-Mass Q-TOF LC/MS or MALDI-TOF (Vogayer, PerSeptive Biosystem).

2.5.2 Synthesis of Dipicolylamine Chemosensor

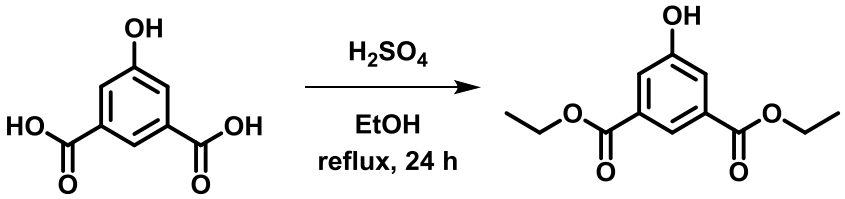

2.12 **2.13**

Diethyl 5-hydroxyisophthalate (**2.13**). Product **2.13** was prepared according to previous literature. White solid, mp: 95-98 °C; ^{1}H NMR (300 MHz, $CDCl_3$): δ 8.18 (s, 1H), 7.80 (s, 2H), 7.36 (s, 1H), 4.37 (q, *J* = 7.1 Hz, 4H), 1.37 (t, *J* = 7.1 Hz, 6H); ^{13}C NMR (300 MHz, $CDCl_3$): δ 166.7, 156.37, 132.00, 122.61, 120.86, 61.67, 14.23; LRMS (m/z): $[M-H]^-$ calcd. for $C_{12}H_{14}O_5$, 237.08; found, 237.08.

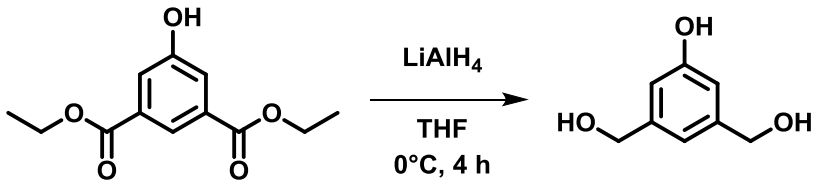

2.13 **2.14**

3,5-Di(hydroxymethyl)phenol (**2.14**). Product **3** was prepared according to previous literature. Clear yellow oil. ^{1}H NMR (300 MHz, [D_6] Acetone): δ 6.78 (s, 1H), 6.72 (s, 2H), 4.51 (s, 4H); ^{13}C NMR (300 MHz, [D_6] Acetone): δ 158.08, 144.29, 116.81, 112.89, 64.52; LRMS (m/z): $[M-H]^-$ calcd. for $C_8H_{10}O_3$, 153.06; found, 152.92; $[M+Formate]^-$ calcd. for $C_9H_{11}O_5$ 199.06; found, 198.92.

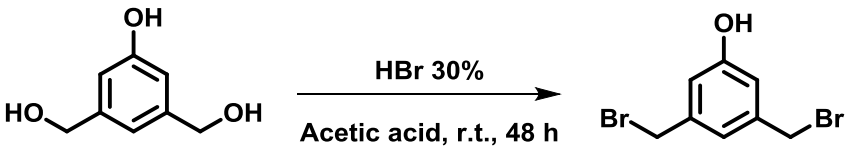

2.14 **2.15**

3,5-bis(bromomethyl)phenol (**2.15**). Product **2.15** was prepared according to previous literature. Brown solid, mp: 75-78 °C; TLC (hexane:ethylacetate, 4:1 v/v): R_f = 0.27; ^{1}H NMR (400 MHz, [D_6] acetone): δ 7.00 (s, 1H), 6.88 (s, 2H), 4.54 (s, 4H); ^{13}C NMR (400 MHz, acetone): δ 158.55, 140.92, 121.83, 116.96, 33.83; LRMS (m/z): $[M+H]^+$ calcd. for $C_8H_8Br_2O$, 279.96; found, 281.

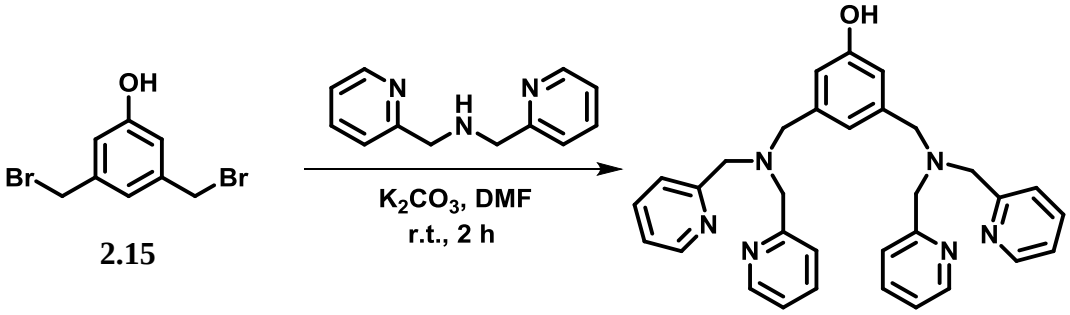

2.15 **2.16**

3,5-bis((bis(pyridin-2-ylmethyl)amino)methyl)phenol (**2.16**). A solution of **2.15** (0.67 g, 2.40 mmol, 1.0 eq), 2,2'-dipicolylamine (1.08 mL, 6.02 mmol, 2.5 eq) and K_2CO_3 (0.39 g, 2.82 mmol, 1.2 eq) in dried DMF (6 mL) was stirred at room temperature during 3 h under nitrogen, monitored by TLC (hexane:ethylacetate, 2:1 v/v). The reaction mixture was neutralized with 20% acetic acid, and the product extracted with DCM (30 mL). The organic layer was washed with $NaHCO_3$, brine and dried over Na_2SO_4, filtered and the solvent evaporated and dried overnight under vacuum. Product **2.16** (0.77 g, 1.50

mmol, 62%) was obtained as a yellow oil; TLC (EtOAc:MeCN:MeOH:H_2O, 6:2:2:2 v/v): R_f = 0.48; Analytical HPLC: Reverse phase C_{18} column. r.t. = 9.58 min; ^{1}H NMR (400 MHz,$CDCl_3$) δ 8.45 – 8.38 (m, 4H), 7.54 (ddd, *J* = 10.1, 9.6, 4.7 Hz, 8H), 7.06 (ddd, *J* = 6.8, 4.9, 1.5 Hz, 4H), 6.99 (s, 1H), 6.76 (s, 2H), 3.74 (s, 8H), 3.52 (s, 4H); ^{13}C NMR (400 MHz, $CDCl_3$) δ 159.65, 157.63, 148.46, 140.54, 136.59, 122.71, 121.96, 119.65, 114.63, 59.76, 58.55. LRMS (m/z): $[M+H]^+$ calcd. for $C_{32}H_{32}N_6O$, 517.26; found, 517.50; $[M+Na]^+$ calcd. for $C_{32}H_{32}N_6NaO$ 539.25; found, 539.50.

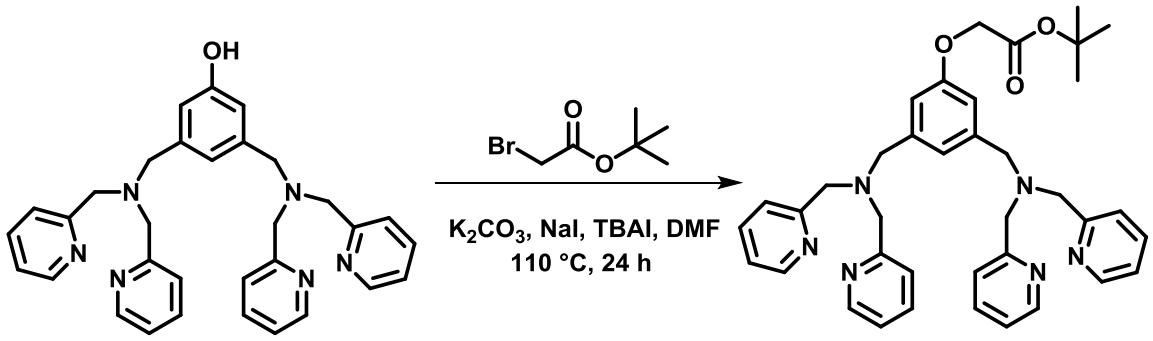

2.16 **2.17**

Tert-butyl 2-(3,5-bis((bis(pyridin-2-ylmethyl)amino)methyl)phenoxy)acetate (**2.17**). Tert-butylbromoacetate (0.087 mL, 0.595 mmol, 1.2 eq), K_2CO_3 (0.41 g, 2.971 mmol, 6.0 eq), NaI (0.037 g, 0.248 mmol, 0.5 eq), tetrabutylammonium iodide (0.091 g, 0.248 mmol, 0.5 eq) and compound **2.16** (0.256 g, 0.495 mmol, 1.0 eq) were reflux in dry DMF (10 mL) at 110 °C for 24 h under nitrogen atmosphere. The reaction mixture was poured into H_2O, extracted with ethylacetate and washed with $NaHCO_3$ and brine. The crude product after evaporation was purified by reverse phase to yield compound **2.17** (0.156 g, 0.248 mmol, 50%) as a transparent oil. Analytical HPLC: Reverse phase C_{18} column. r.t. = 11.24 min;

^{1}H NMR (400 MHz, CD_3CN) δ 8.78 (ddd, *J* = 5.7, 1.5, 0.6 Hz, 4H), 8.27 (td, *J* = 7.9, 1.6 Hz, 4H), 7.77 (dd, *J* = 7.7, 5.9 Hz, 4H), 7.70 (d, *J* = 7.9 Hz, 4H), 6.67 (s, 1H), 6.53 (s, 2H), 4.39 (s, 2H), 4.13 (s, 8H), 3.56 (s, 4H), 1.44 (s, 9H); ^{13}C NMR (400 MHz, CD_3CN) δ 168.60, 158.88, 154.21, 146.53, 143.75, 138.37, 127.76, 126.83, 125.31, 116.52, 82.81, 65.99, 60.11, 57.69, 28.21; HRMS (*m/z*): $[M+H]^+$ calcd. for $C_{38}H_{42}N_6O_3$, 631.33912; found, 631.33964; $[M+Na]^+$ calcd. for $C_{38}H_{42}N_6NaO_3$ 653.32106; found 653.32136.

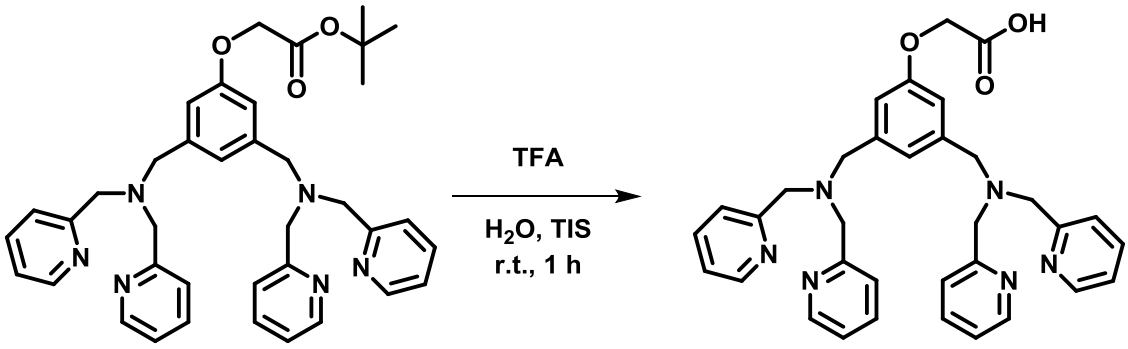

2.17 **2.18**

2-(3,5-bis((bis(pyridin-2-ylmethyl)amino)methyl)phenoxy)acetic acid (**2.18**). A mixture of 20 mL of TFA/ H_2O/TIS (95/2.5/2.5 % v/v) was added to compound **6** (0.100 g, 0.174 mmol). The reaction mixture was stirred for 1 h at room temperature. The solvent was evaporated with high vacuum. The crude product was lyophilized to yield compound **7** (0.085 g, 0.149 mmol, 94%) as brown oil. Analytical HPLC: Reverse phase C_{18} column. r.t. = 9.78 min; ^{1}H NMR (400 MHz, CD_3CN) δ 8.77 (dd, *J* = 5.6, 1.2 Hz, 4H), 8.34 (td, *J* = 7.9, 1.6 Hz, 4H), 7.85 – 7.79 (m, 4H), 7.76 (d, *J* = 8.0 Hz, 4H), 6.58 (s, 1H), 6.46 (s, 2H), 4.49 (s, 2H), 4.14 (s, 8H), 3.48 (s, 4H); ^{13}C NMR (400 MHz, CD_3CN):

δ 170.72, 158.71, 154.00, 147.62, 143.08, 138.49, 128.24, 127.17, 125.45, 116.46, 65.35, 60.18, 57.83. HRMS (*m/z*): $[M+H]^+$ calcd. for $C_{34}H_{34}N_6O_3$, 575.2765; found, 575.2763.

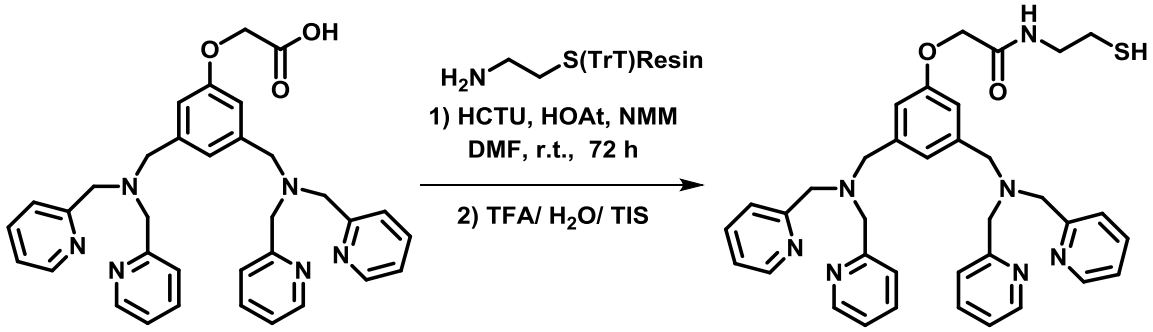

2.18 **2.19**

2-(3,5-bis((bis(pyridin-2-ylmethyl)amino)methyl)phenoxy)-N-2mercaptoethyl)acetamide (**2.19**). Cysteamine 2-chlorotrityl Novabiochem resin (0.106 g, 0.096 mmol, 1.0 eq) was swelled with DMF (5mL) in a solid phase synthesis reactor for 40 min and the solvent was discarded. The mixture containing **7** (0.165 g, 0.287 mmol, 3.0 eq), HOAt (0.039 g, 0.287 mmol, 3.0 eq), HCTU (0.119 g, 0.287 mmol, 3.0 eq), NMM (0.063 mL, 0.574 mmol, 6.0 eq) in DMF (5 mL) was added to the resin. After 72 h of shaking under argon at room temperature, the excess reagents were drained and discarded. The resin was then washed with DMF, DCM and MeOH (5X) and dried under vacuum. The product was cleaved by exposing the resin to TFA/H_2O/TIS (95/2.5/2.5 % v/v) for 20 min. The crude was purified by reverse phase to yield compound **2.19** (0.054 g, 0.085 mmol, 30%) as a pale yellow oil. Analytical HPLC: Reverse phase C_{18} column. r.t. = 10.34 min; ^{1}HNMR (400 MHz, D_2O): δ 8.50 (dd, *J* = 6.1, 1.2 Hz, 4H), 8.29 (td, *J* = 7.9, 1.6 Hz, 4H), 7.81 (d, *J* = 8.0 Hz, 4H), 7.73 (ddd, *J* = 7.5, 5.9, 1.2 Hz, 4H), 6.59 (s,

1H), 6.52 (s, 2H), 4.37 (s, 2H), 4.13 (s, 8H), 3.57 (s, 4H), 3.31 (t, *J* = 6.3 Hz, 2H), 2.50 (t, *J* = 6.3 Hz, 2H); ^{13}C NMR (400 MHz, D_2O): δ 171.10, 157.40, 153.13, 145.97, 142.21, 138.17, 126.92, 125.97, 125.05, 115.79, 66.67, 59.61, 57.11, 41.84, 23.47; HRMS (*m/z*): $[M+H]^+$ calcd. for $C_{36}H_{39}N_7O_2S$, 634.29587; found, 634.29633.

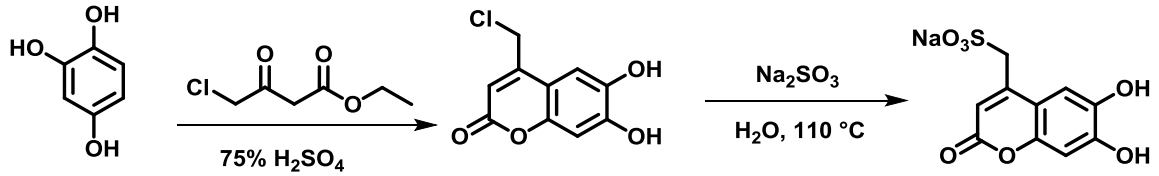

2.20 **2.21** **2.8**

Coumarin-based indicator **2.8** was prepared according to previous literature**.** ^{1}H NMR (400 MHz, D_2O) δ 7.20 (s, 1H), 6.82 (s, 1H), 6.28 (s, 1H), 4.27 (s, 2H). Analytical HPLC: Reverse phase C_{18} column. Increase gradient 5 to 70% B over 15 min at 347 nm. r.t. = 7.68 min.

*Synthesis of receptors R-9 (**2.22**), R-10 (**2.23**) and R-11 (**2.24**).* Thiol-ene conjugate addition reactions of compound **2.19** to 1,3,5-triacryloylhexahydro-1,3,5-triazine (**2.3**).

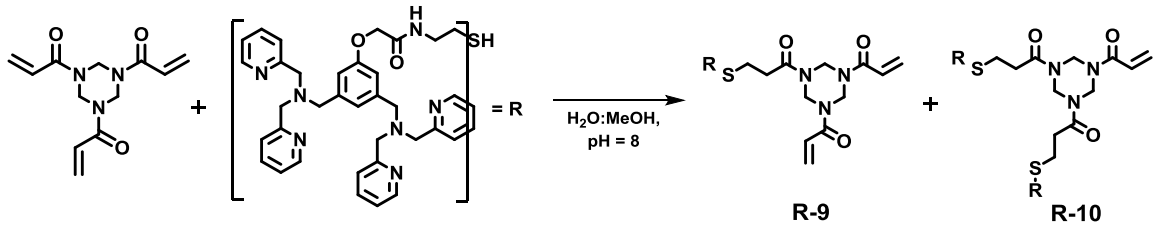

2.3 **2.19** **2.22** **2.23**

Synthesis of compounds R-9 (**2.22**) and R-10 (**2.23**). 1,3,5-triacryloylhexahydro-1,3,5-triazine **2.3** (6 mg, 0.0242 mmol, 1.0 eq) was dissolved in 500 µL of CH_3CN, and then added to a vial containing **2.19** (23 mg, 0.0363 mmol, 1.5 eq). To this mixture, 500 µL of H_2O was added and few beads of K_2CO_3 were added to the reaction mixture to increase pH = 8. The reaction was stirred under nitrogen for 1 h. The reaction mixture was lyophilized. The products were purified using reverse phase chromatography to give R-9 and R-10. Preparative HPLC: Reverse phase C_{18} column. Flow rate 4 mL/min. Solvent A: H_2O with 0.1% v/v TFA; solvent B: CH_3CN with 0.1% v/v TFA. Increase gradient 5% B for 5 min, 5 to 25% B over 35 min, 25 to 90% B over 7 min.

Compound R-9 (12.45 mg, 0.0141 mmol, 59%) was obtained as transparent oil. Analytical HPLC: Reverse phase C_{18} column. r.t. = 10.88 min; ^{1}H NMR (500 MHz, CD_3CN) δ 8.78 (dd, *J* = 5.5, 1.2 Hz, 4H), 8.24 (td, *J* = 7.8, 1.6 Hz, 4H), 7.76 – 7.73 (m, 4H), 7.69 (d, *J* = 8.0 Hz, 4H), 7.27 (t, *J* = 6.0 Hz, 1H), 6.71 (s, 3H), 6.66 (s, 2H), 6.20 (d, *J* = 16.7 Hz, 2H), 5.75 (s, 2H), 5.33 (d, *J* = 32.6 Hz, 6H), 4.30 (s, 2H), 4.15 (s, 8H), 3.63 (s, 4H), 3.41 (dd, *J* = 13.0, 6.6 Hz, 2H), 2.80 – 2.67 (m, 4H), 2.64 (t, *J* = 6.8 Hz, 2H). ^{13}C NMR (500 MHz CD_3CN) δ 168.69, 158.61, 154.40, 146.07, 144.18, 138.54, 129.85,

128.20, 127.57, 126.73, 125.43, 116.75, 67.97, 60.08, 57.72, 39.14, 34.20, 32.10, 27.13. HRMS (*m/z*): $[M+2H]^{+2}$ calcd. for $C_{48}H_{56}N_{10}O_5S$, 442.20724; found, 442.20670.

Compound R-10 (10.16 mg, 0.0067 mmol, 28%) was obtained as transparent oil. Analytical HPLC: Reverse phase C_{18} column. r.t. = 10.85 min; ^{1}H NMR (600 MHz, D_2O, 30% CD_3CN). Water peak was suppressed and compound peaks were referenced to CD_3CN. δ 8.51 (ddd, *J* = 5.6, 1.6, 0.7 Hz, 8H), 8.15 (td, *J* = 7.9, 1.6 Hz, 8H), 7.68 (d, *J* = 8.0 Hz, 8H), 7.65 – 7.61 (m, 8H), 6.74 (s, 2H), 6.66 (s, 5H), 6.11 (d, *J* = 17.0 Hz, 1H), 5.77 (d, *J* = 10.6 Hz, 1H), 5.23 (d, *J* = 30.5 Hz, 6H), 4.36 (s, 2H), 4.10 (s, 16H), 3.68 (s, 8H), 3.35 (t, *J* = 6.6 Hz, 4H), 2.62 (ddd, *J* = 29.6, 22.7, 6.2 Hz, 13H). ^{13}C NMR (500 MHz, CD_3CN) δ 168.73, 158.67, 154.61, 145.24, 144.70, 138.52, 128.11, 127.23, 126.45, 125.34, 116.73, 67.99, 59.99, 57.71, 39.19, 34.20, 32.06, 27.17. HRMS (*m/z*): $[M+2H]^{+2}$ calcd. for $C_{84}H_{97}N_{17}O_7S_2$, 760.36083; found, 760.35934.

Preparation of compound ZnR-10. A solution of MeOH:H_2O (1:1 v/v) was used to dissolve R-10 (0.0046 mmol) and zinc nitrate (0.0185 mmol). The reaction mixture was stirred for 0.5 h. Methanol was removed and the product lyophilized to afford Zn-R10 in quantitative yield. MALDI-TOF: $[M]^+$ calcd. for $C_{84}H_{93}N_{23}O_{25}S_2Zn_4$, 2150.47; found, 2151.09.

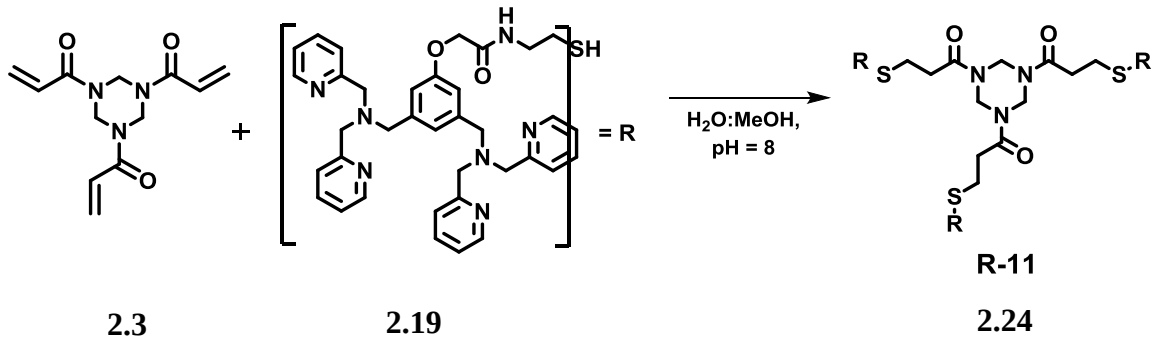

2.3 **2.19** **2.24**

Synthesis of compound R-11 (**2.24**). 1,3,5-triacryloylhexahydro-1,3,5-triazine **2.3** (1 mg, 0.0040 mmol, 1.0 eq) was dissolved in 500 µL of CD_3CN, and then added to a vial containing **2.19** (5 mg, 0.0079 mmol, 1.98 eq). To this mixture, 500 µL of D_2O was added and few beads of K_2CO_3 were added to the reaction mixture to increase pH = 8. The reaction was stirred under nitrogen for 1 h. The reaction mixture was lyophilized. The product was purified using reverse phase chromatography. Preparative HPLC: Reverse phase C_{18} column. Flow rate 4 mL/min. Solvent A: H_2O with 0.1% v/v TFA; solvent B: CH_3CN with 0.1% v/v TFA. Increase gradient 5% B for 5 min, 5 to 25% B over 35 min, 25 to 90% B over 7 min to give R-11 (5 mg, 0.0023 mmol, 58%) as light yellow oil. Analytical HPLC: Reverse phase C_{18} column. r.t. = 10.93 min; ^{1}H NMR (500 MHz, $CDCl_3$) δ 8.50 – 8.46 (m, 12H), 7.61 (td, *J* = 7.7, 1.7 Hz, 12H), 7.53 (d, *J* = 7.8 Hz, 12H), 7.12 – 7.09 (m, 12H), 7.08 (s, 3H), 6.88 (s, 6H), 5.20 (s, 6H), 4.48 (s, 6H), 3.76 (s, 24H), 3.63 (s, 12H), 3.49 (dd, *J* = 12.8, 6.4 Hz, 6H), 2.76 (d, *J* = 10.9 Hz, 9H), 2.66 (t, *J* = 6.7 Hz, 6H); HRMS (*m/z*): $[M+3H]^{+3}$ calcd. for $C_{120}H_{135}N_{24}O_9S_3$, 717.66730; found 717.66860; $[M+3Na]^{+3}$ calcd. for $C_{120}H_{132}N_{24}Na_3O_9S_3$, 739.64924; found, 739.65048;

$[M+2H]^{+2}$ calcd. for $C_{120}H_{134}N_{24}O_9S_3$, 1075.99731; found, 1075.99680; $[M+2Na]^{+2}$ calcd. for $C_{120}H_{132}N_{24}Na_2O_9S_3$, 1097.97925; found, 1097.97953.

2.5.3 Peptide Synthesis

Peptides were synthesized using standard SPPS protocol. Peptide sub-F was synthesized on rink resin (NovaSyn TGR resin) using a peptide synthesizer (CEM Liberty Automated Microwave). Peptides KALIC (**2.5**) and PVDAC (**2.6**) were synthesized with Fmoc-Cys(Trt) Wang resin with a different peptide synthesizer (Prelude by Protein Technology**,** Inc)**.** Coupling reactions used Fmoc-L-amino acid/ HBTU/DIPEA (5:5:10 eq) relative to 1 eq. of pre-loaded resin. Peptides were analyzed by analytical HPLC (Shimadzu HPLC) equipped with Gemini C18 column (250 X 10 mm, 5 µm). Solvent A: H_2O with 0.1% v/v TFA; solvent B: CH_3CN with 0.1% v/v TFA. Rate flow: 4 mL/min with an increase gradient 5 to 95% B over 20 min at 220 nm. Purified peptides were characterized by mass spectrometry using a either MALDI-TOF (Vogayer, PerSeptive Biosystem) or ESI (LCQ, Thermo Finnigan).

Peptide	Peptide Sequence	Mol. Formula	HPLC ret. time (min)	ESI $[M+H]^+$ Calcd.	ESI $[M+H]^+$ found
6	KALIC	$C_{24}H_{46}N_6O_6S$	12.03	547.3	547.4
7	PVDAC	$C_{20}H_{33}N_5O_8S$	11.65	504.2	504.2
				MALDI-TOF $[M]^+$ Calcd.	MALDI-TOF $[M]^+$ found
Sub-F	YAEPLTPR ILAKWEWPA	$C_{101}H_{147}N_{23}O_{25}$	14.20	2082.0938	2082.9874

Table 2.4: *HPLC retention time and MS analysis.*

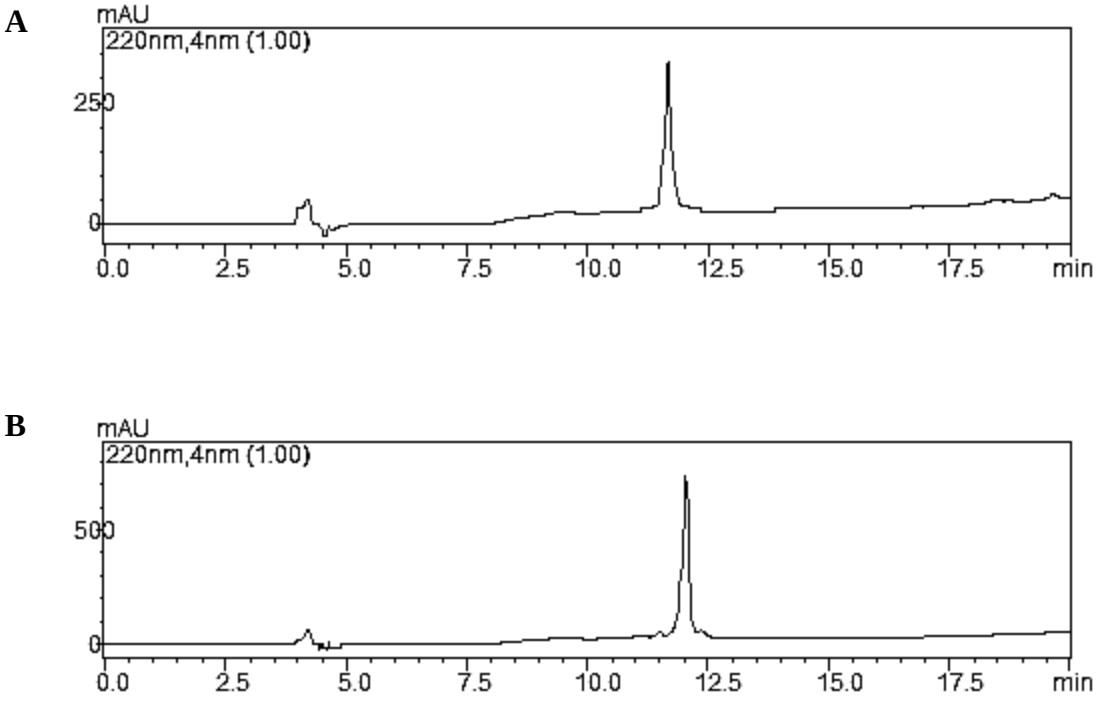

Figure 2.15*:* *HPLC of peptides*. (A) HPLC chromatogram of PVDAC, r.t.=11.65 min (B) HPLC chromatogram of KALIC, r.t.= 12.03 min.

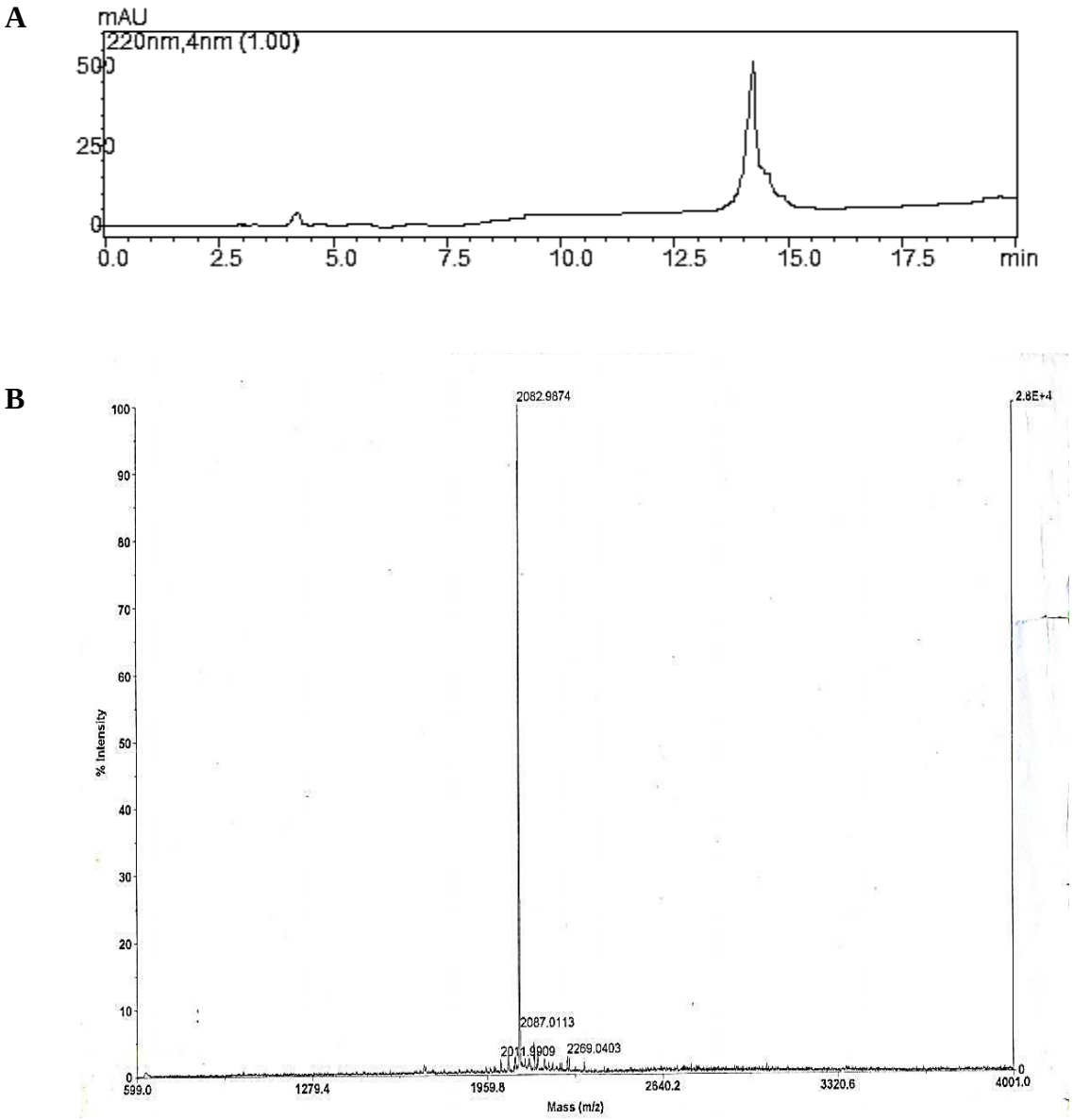

Figure 2.16*:* *HPLC and MS analysis of Sub-F peptide*. (A) HPLC chromatogram of Sub-F peptide, r.t.=14.20 min (B) MALDI-TOF of Sub-F peptide obsd m/z= 2159.57, calcd 2159.34.

2.5.4 Phosphorylation of Sub-F Peptide

Sub-F peptide (166 µM) was phosphorylated using ERK-1 (100 nM), BSA (10 µg/mL), $MgCl_2$ (12 µM), ATP (2mM), DTT (2 mM) in 30 mL Buffer solution (25mM HEPES, 50 mM KCl, 0.1 mM EDTA, 0.1 mM EGTA pH = 7.4) and left overnight at 37°C. The solution was lyophilized and preparative HPLC was performed using a rate flow: 10 mL/min, (A: 0.1% TFA in water; B: 0.1% TFA in acetonitrile). The run started at 5% B (over 10 min), increase to 15% B (over 10 min) and followed by a linear gradient to 45% B (over 20 min). Analytical results: r.t.=13.56 min and MALDI-TOF obsd m/z= 2159.57, calculated 2159.34.

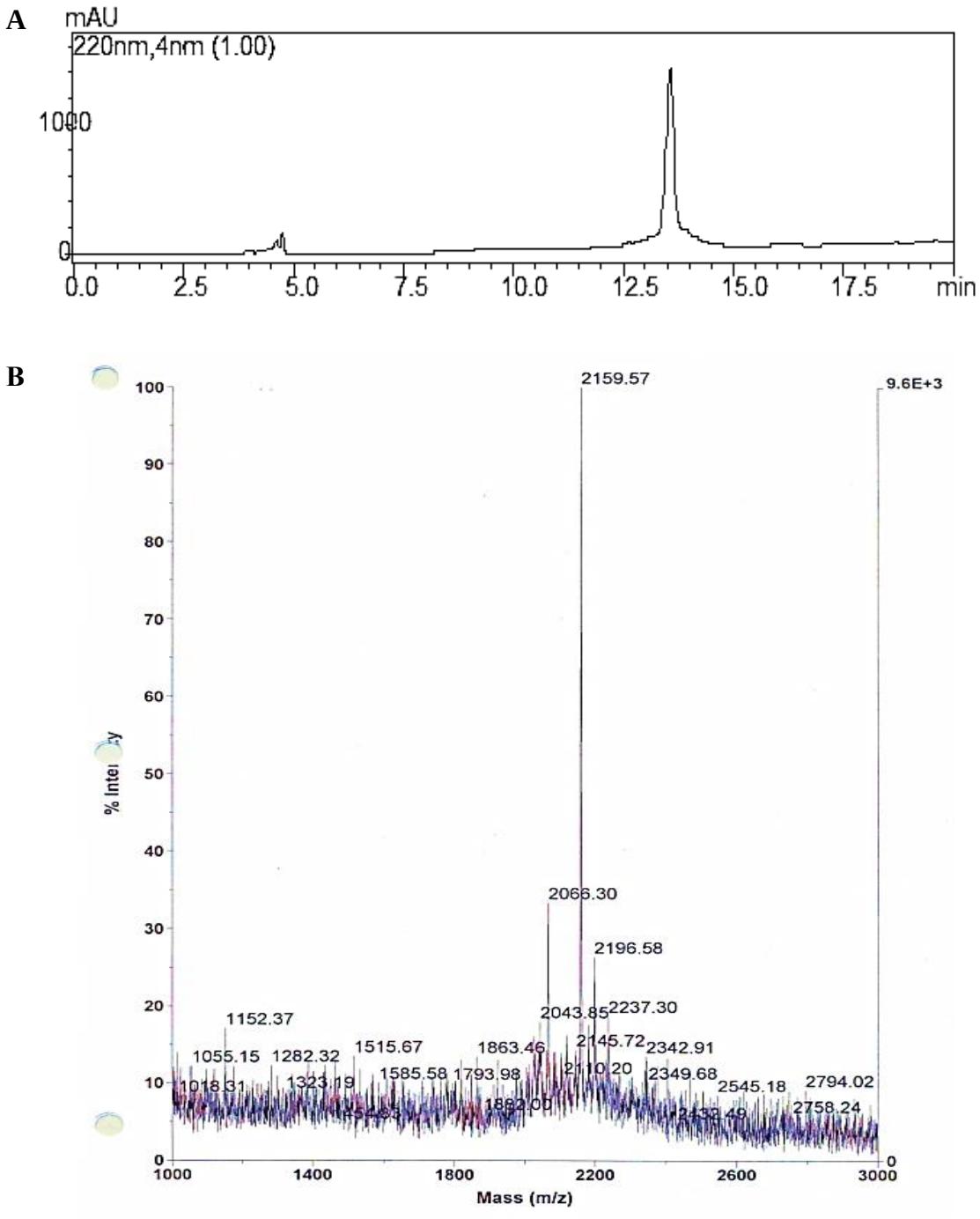

Figure 2.17: *HPLC and MS analysis of phosphorylated Sub-F peptide*. (A) HPLC showing retention rime of r.t. = 13.56 min. (B) MALDI-TOF showing obsd m/z= 2159.57, calculated 2159.34.

2.5.5 Experimental Information

Fluorimeter measurements for all the cuvette assays were done on a PTI fluorimeter with an 814 photomultiplier detection system using a 75W xenon short arc lamp at 25°C in 50 mM HEPES, 10 mM NaCl buffer, pH=7.4. For all the following titrations, the fluorescence spectra were recorded after each addition using the following parameters: Temperature: 25 C. Excitation wavelength: 347 nm. Excitation and emission slit width: 4 nm. Integration time: 0.2 s. Acquisition range: 357-644 nm.

Indicator displacement assays – Fluorescent titrations between **ZnR-10**, indicator **2.8**, and peptides or proteins were done prior to the optimization of the sensing ensemble. A solution of 50 mM HEPES, 10 mM NaCl buffer pH = 7.4 was prepared using deionized water. The solution was filtered and degassed. Several stock solutions were prepared for the following titrations. Receptor **R-10** and $Zn(NO_3)_2$ were first dissolved in 1:1 MeOH-H_2O (v/v) and stir for 30 min to give a 583 µM solution of **ZnR-10**. The receptor solution was freeze dried, lyophilized and re-dissolved in HEPES buffer. Indicator stock solution. Indicator **2.8**was dissolved in HEPES buffer to achieve a concentration of 5 mM. Peptide stock solutions. Sub-F phosphorylated (2.96 mM) and Sub-F non-phosphorylated (2.78 mM) peptides were dissolved in HEPES buffer, respectively. All stock solutions were refrigerated at -20 C. Receptor **ZnR-10**, indicator **2.8** and peptides were individually diluted in HEPES buffer to the correspondent final concentration according to each type of titration.

Uptake indicator titration – Cuvette assay to study the binding of coumarin indicator **2.8** to receptor **ZnR-10** was performed by successively adding a solution of receptor **ZnR-10** (250 µM) into 750 µL solution of indicator **2.8** (100 µM) in HEPES Buffer using 100 µL Hamilton microsyringe.

IDA titration of phosphorylated and non- phosphorylated Sub-F peptide – Cuvette assays to study peptide interaction with the previous sensing ensemble were performed by successively adding concentrated phosphorylated and non- phosphorylated peptide solution (1.92 mM p-peptide; 1.92 mM peptide, respectively) into 160 µL solution of **ZnR-10** (36.6 µM) and **2.8** (100 µM), in HEPES Buffer using 100 µL Hamilton microsyringe.

IDA titration of phosphorylated and non-phosphorylated kinases – Fluorescent titrations between kinases with **ZnR-10**-indicator in different ratios were done separately as follows: 160 µL solution of 36.6 µM **ZnR-10** and 50 µM indicator **2.8,** or a solution of 36.6 µM **ZnR-10** and 100 µM **2.8** in HEPES buffer, were titrated with a correspondent solution of 5 µM phosphorylated or non-phosphorylated kinase p-ERK-1, ERK-1, p-ERK-2, ERK-2, JNK-1 (which also contained the receptor-indicator complex in HEPES buffer) using a 50 µL Hamilton microsyringe. For each **ZnR-10**-indicator ratio at maximum saturation point was chosen as the optimal concentration for the ensemble.

Sensing ensemble – The fluorescence measurements were taken with a Biotek Synergy 2 Multi-Mode Microplate Reader at 25°C in 50 mM HEPES, 10 mM NaCl Buffer, pH=7.4. Costar 384-well black polystyrene plates with flat bottom were used for

all array experiments. To generate the sensing ensemble, receptors R-9, R-10 and R-11 were used to create the seven different hosts. The following stock solutions were prepared as follow: Individual receptors solutions R-9 (283 μM), R-10 (309 μM), R-11 (308 μM) were dissolved in 1:1 MeOH/H_2O (v/v). Peptides PVDAC (365 μM) and KALIC (365 μM), DTT (365 μM) and $Zn(NO_3)_2$ (727 μM) were also dissolved in 1:1 MeOH/H_2O (v/v). Indicator **2.8** (365 μM) was dissolved in HEPES buffer. Aliquots of receptor, peptide and DTT for a 120X volume were mixed for 1 h at pH=7.6 according to **Table 2.2**. Then, $Zn(NO_3)_2$ solution was added according to the number of DPA moieties present in each receptor and stirred for 30 min; the final $Zn(NO_3)_2$ concentrations were 114 μM, 155 μM and 213 μM according to each host. Each host solution was freeze dried, lyophilized, and reconstituted by addition of HEPES buffer when used for the construction of the sensing ensemble.

Indicator aliquots were added according to the number of bis-Zn(DPA) moieties present in each receptor, the final indicator concentrations were 57 μM, 100 μM, and 124 μM according to each host. Finally, separated aliquots of phosphorylated and non-phosphorylated kinases ERK-1, ERK-2, JNK-3 and p38γ (4 μM) were added to each set of host-indicator solutions (four replicates each).

The same sensing ensemble shown in **Table 2.2** was used for the discrimination of HEK293T cell lysates. Aliquots of cell lysate (6 μL) were added to each set of host-indicator solutions (four replicates each). Discrimination of cell lysates was obtained at total protein concentration according to **Table 2.3**. The solutions were brought to a 32 μL

final volume with HEPES buffer. The well plate reader was blanked with HEPES buffer. The 384-well plate were read with a λ_{ex} filter of 360 ± 10 nm and λ_{em} filter of 485 ± 10 nm, using a top 400 mirror. Data collected were analyzed by linear discriminant analysis using XLSTAT 2011 software package.

2.5.6 MAP Kinases and Cell Lysate Expression, Purification and Activation

Expression, Purification and Activation of Tagless MAP Kinases – Tagless *N*-terminal truncated human JNK3α2 (amino acids 39-422 with alanine inserted between amino acids 39 and 40, GenBank accession number NM_138982) was expressed, purified and activated as described previously.[112,113] Activated tagless ERK2 (Rattus norvegicus mitogen activated protein kinase 1, GenBank accession number NM_053842) was expressed, purified and activated as described in *Kaoud et al*.[114] Activated ERK1 were expressed, purified and activated as described in *Callaway et al*.[115] p38MAPKγ was expressed, purified and activated as described previously.[116,117] The activated kinases were all stored in buffer S [25 mM HEPES (pH 7.5), 50 mM KCl, 0.1 mM EDTA, 0.1 mM EGTA, 2 mM DTT and 10-20% (v/v) glycerol] at -80 ºC.

Cell culture – HEK293T cells were maintained in DMEM (Invitrogen) supplemented with 10% (*v/v*) Fetal Bovine Serum (FBS)-US grade (Invitrogen), 2 mM L-glutamine (Invitrogen), 100 UmL^{-1} penicillin (Sigma), and 100 gmL^{-1} streptomycin (Sigma). Cells were cultured in a humidified 5% CO_2 incubator at 37 °C. Cells were seeded in 10 cm plates and incubated till 80-90% confluent and were then treated with anisomycin (50-

100 nM) (MP Biomedicals) for 30 minutes or 100 ng/ml EGF (MP Biomedicals) for 30 minutes. For experiments requiring ERK-1 overexpression, the pcDNA3 vector containing DNA encoding for WT-ERK1 was transfected into HEK293T cells by lipofectamine 2000 (Invitrogen, California, USA) according to the manufacturer's protocol. After 48 hours of transfection, cells were either induced with 100 ng/mL EGF for 30 minutes before lysis or lysed without induction.

Cell lysate preparation and Western blot analysis – HEK293T cell lysates were prepared in CytoBuster™ Protein Extraction Reagent (EMD-Biosciences) after washing in PBS (Invitrogen). The lysates were cleared by centrifugation, and ATP was removed using an Amicon Ultra-0.5 mL Centrifugal Filter. Bradford analysis (Bio-Rad) was used to measure the protein concentration. Lysates containing 60 µg of total protein were fractionated by 10% SDS PAGE (Bio-Rad) and transferred to Hybond-P PVDF Membrane (GE Healthcare). Primary antibodies were incubated overnight at 4 ºC using the following dilutions; 1:2000 anti-phospho-SAPK/JNK (Thr183/Tyr185) (G9) mouse mAb (Cell Signaling Technology); 1:2000 anti-phospho-p44/42 MAPK (ERK1/2) (Thr202/Tyr204) (E10) mouse mAb (Cell Signaling Technology); 1:10,000 anti-phospho-p38α (Thr180/Tyr182), clone 8.78.8 rabbit mAb (Millipore); 1:1000 anti-p44/42 MAPK (Erk1/2) (137F5) rabbit mAb (Cell Signaling Technology); 1:200 anti JNK (D2) mouse mAb (Santa Cruz Biotechnology); and 1:5000 anti-actin, clone 4 mouse mAb (Millipore). Either anti-rabbit (Bio-Rad) or anti-mouse (Bio-Rad) horseradish peroxidase-

conjugated secondary antibodies and Pierce® ECL Western Blotting Reagents (Pierce) were used to develop the blots.

2.5.7 Supplementary Figures

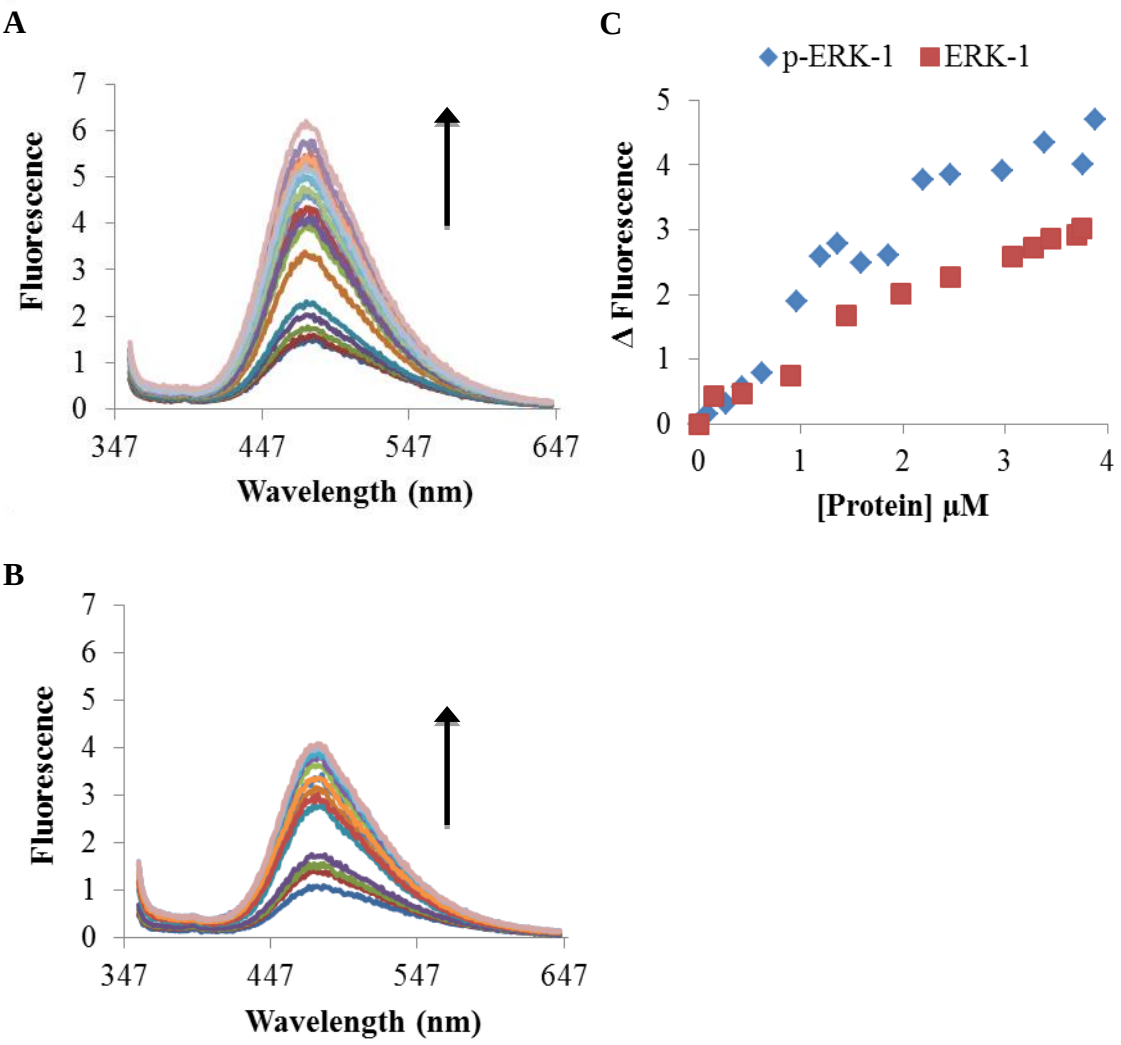

Figure 2.18: *Addition of active and inactive ERK-1 to indicator-ZnR-10 complex.* Increase in the fluorescence intensity due to displacement of the coumarin indicator. (A) Addition of phosphorylated ERK-1 (0 – 3.8 µM p-ERK-1) to **ZnR-10** (36.6 µM) and **2.8** (50 µM) in 50 mM HEPES Buffer, 10 mM NaCl pH=7.4, λ_{ex} 347 nm. (B) Addition of non-phosphorylated ERK-1 (0 – 3.8 µM ERK-1) to **ZnR-10** (36.6 µM) and **2.8** (50 µM) in HEPES Buffer, 10 mM NaCl pH=7.4, λ_{ex} 347 nm. (C) Binding curves of data in **Figures 2.15A** and **2.15B** measured at λ_{em} = 475 nm, respectively.

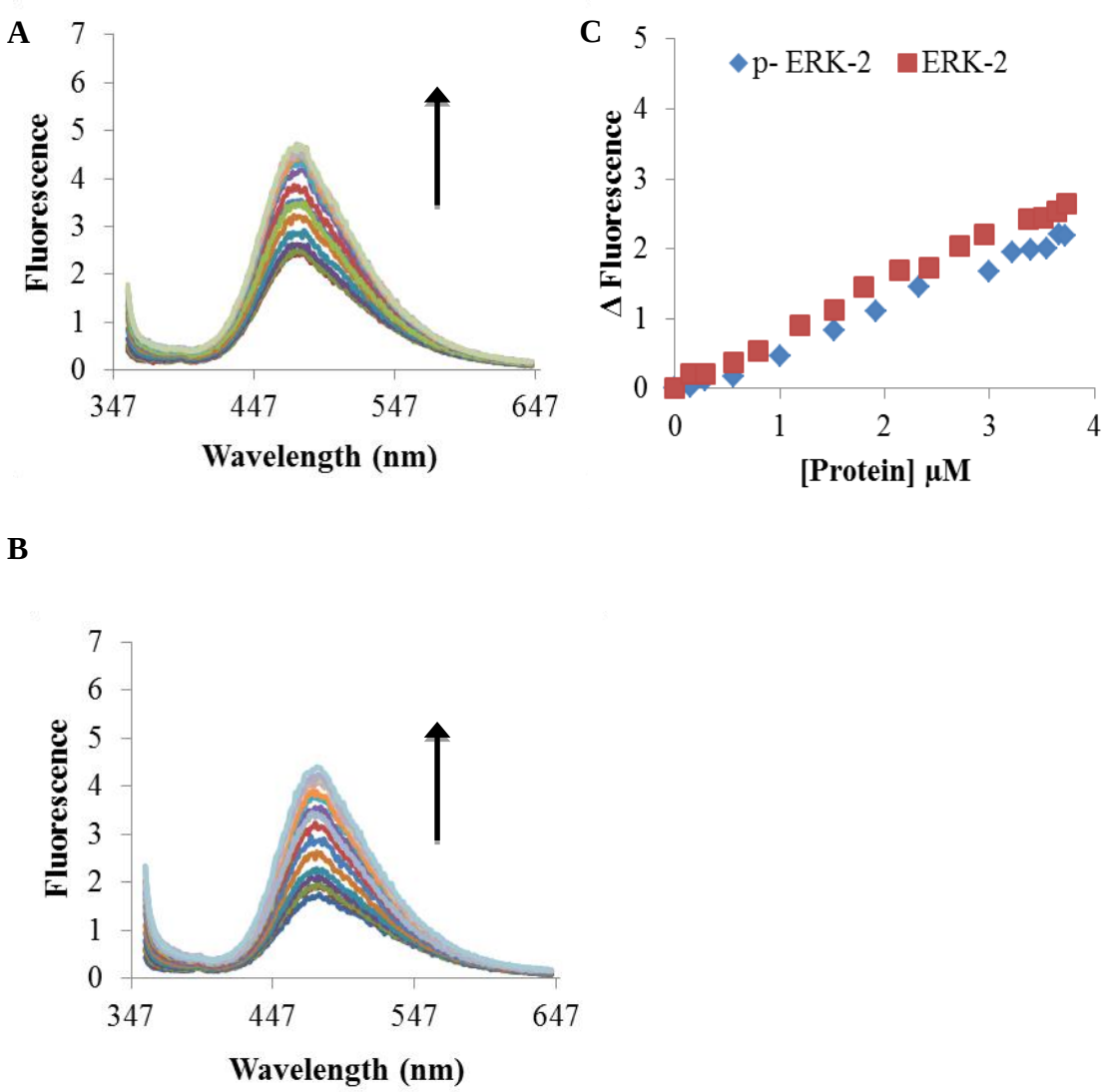

Figure 2.19: *Addition of active and inactive ERK-2 to indicator-ZnR-10 complex.* Increase in the fluorescence intensity due to displacement of the coumarin indicator. (A) Addition of phosphorylated ERK-1 (0 – 3.8 µM p-ERK-2) to **ZnR-10** (36.6 µM) and **2.8** (50 µM) in 50 mM HEPES Buffer, 10 mM NaCl pH=7.4, λ_{ex} 347 nm. (B) Addition of non-phosphorylated ERK-2 (0 – 3.8 µM ERK-1) to **ZnR-10** (36.6 µM) and **2.8** (50 µM) in HEPES Buffer, 10 mM NaCl pH=7.4, λ_{ex} 347 nm. (C) Binding curves of data in **Figures 2.16A** and **2.16B** measured at λ_{em} = 475 nm, respectively.

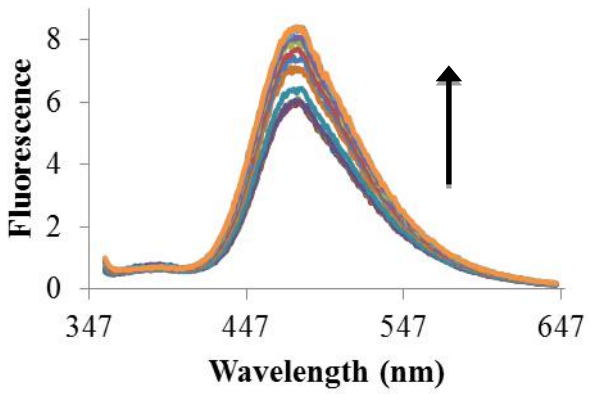

Figure 2.20: *Addition of JNK-3 to indicator-ZnR-10 complex.* Addition of non-phosphorylated JNK-3 (0 – 3.8 µM p-ERK-2) to **ZnR-10** (36.6 µM) and **2.8** (100 µM) in 50 mM HEPES Buffer, 10 mM NaCl pH=7.4, λ_{ex} 347 nm.

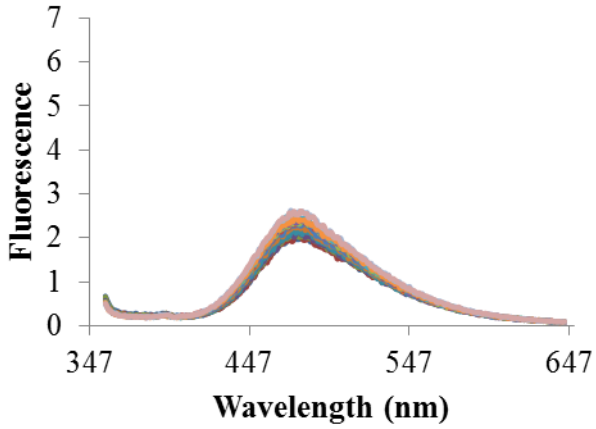

Figure 2.21: *Control experiment.* Addition of HEPES buffer to **ZnR-10** (36.6 µM) and **2.8** (100 µM) in 50 mM HEPES Buffer, 10 mM NaCl pH=7.4, λ_{ex} 347 nm.

Chapter 3: Peptide-Based Sensors for the Differential Sensing and Quantification of MAP Kinases

3.1 INTRODUCTION

The MAPK family that was described in Chapter 1 showed a high degree of similarity in their genome sequence. Interestingly, some members of this family such as ERK2, JNK1 and p38α share about 40 to 50% of sequence identity at the amino acid level.[118] The same protein surface of cognate MAPKs interacts with upstream activators and downstream substrates previously described in Chapter 1. These MAPK activators and protein substrates are recognized by either the catalytic site or by recruitment sites. These additional protein sites convey critical specificity for protein interactions, defining signaling events of MAPK pathways. Recently, researchers have mainly focused on the utility of these recruitment sites to develop new biosensors and detection methods to assess kinase activity. These methods can potentially be used to regulate cellular signaling pathways in MAPKs by developing new small molecule inhibitors targeting these sites. A kinase sensing system which can selectively target a variety of MAPKs with a low limit of detection under physiological conditions is quite challenging to design. The system must be capable of distinguishing from MAPKs from other kinases. Herein, we report a new sensing system which will present differential binding for MAPK sub-families and isoforms under physiological conditions, where the recruitment sites of these proteins are exploited for MAPK detection in solution.

3.2 DOCKING DOMAINS IN MAP KINASES

Members of the MAPK cascade share linear motifs that are responsible for the specificity between MAP kinases, upstream kinases and downstream substrates. This type of interaction is referred to as docking for kinases and phosphatases. Thus, the docking interactions of MAPKs with substrates or ligands occur between modular docking sequences in the substrate and complementary recruitment sites of the kinase. The binding surface of the recruitment sites is separated and distal to the phosphorylation site. The docking interaction refers to the complementarity of the electrostatic or hydrophobic interactions between a protein kinase and its corresponding partner. Substrates contain docking motifs that are recognized as small peptide sequences with few charged and hydrophobic residues.[119]

3.2.1 MAPK Substrates

MAPK substrates present two binding sites in their sequence: a consensus phosphorylation motif and a docking site which is mainly responsible for the wide-ranging selectivity and affinity towards MAPK sub-families (**Figure 3.1**). MAPKs catalyze the phosphorylation of substrates that contain serine/threonine residues that are directly linked to the proline on the carboxyl terminus. This consensus PX(S/T)-P motif is essential for the substrate in order to be phosphorylated by the catalytic site of MAPKs. In addition, MAPKs recognize substrates that contain modular peptide sequences called docking sites which are known as D-site and F-site. The D-sites are the most studied

docking domains, which are also referred as D-motifs, D-domains, DEJL motifs or kinase interaction motifs (KIM). The D-motifs are located in the N-terminus to the conserved Ser/Thr-Pro phosphorylation site. The D-site consists of a cluster of basic residues, a small peptide sequence that acts as a linker followed by a second nearby cluster of hydrophobic residues.[119] The second docking domain also known as DEF domain or F-site presents a characteristic Ψ(X/Ψ)P sequence, where Ψ is an aromatic residue. The F-site has been found in transcription factors (ERK and p38α substrates) and phosphatases. This docking sequence can access and interact with its corresponding kinase pocket only when conformational changes have taken place upon phosphorylation.[120]

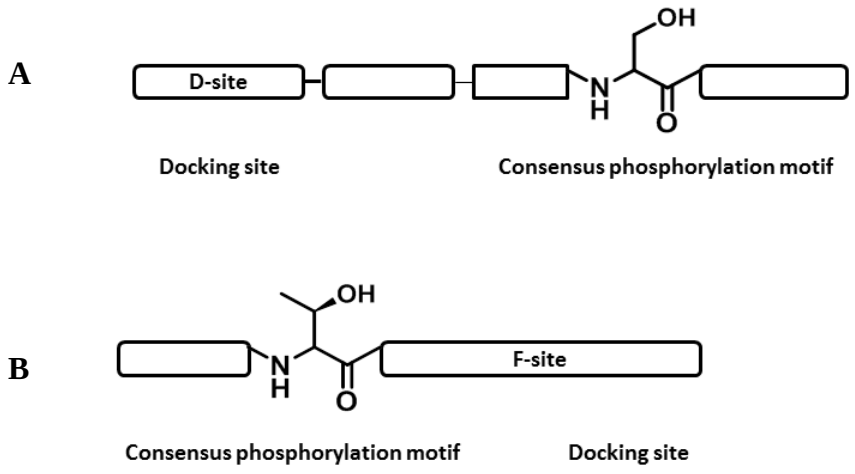

Figure 3.1: *MAPK substrates*. Graphic representation of the different types of MAPK substrates presenting two different binding sites, a phosphorylation site and a distal docking site. (A) The D-site is positioned on the N-terminus of the peptide. (B) The F-site is found on the C-terminus of the peptide substrate.

3.2.2 MAPK Recruitment Sites

Most MAP kinases present two recruitment sites in their structure (**Figure 3.2**). The first one is called the D-motif or D-recruitment site (DRS). It is established that the DRS is an evolutionarily conserved domain among all MAP kinases of different species. This site is the main source of specificity that distinguishes the different subfamilies of MAP kinases. This domain is found on the rear face of the protein, and it is located in the *C*-terminal region. This region is formed by the common docking domain (CD domain), and the docking groove (ED site) which are constituted by hydrophobic residues. The CD domain resides in a cluster of negatively charged residues (Asp-316 and Asp-319) to which hydrophobic and basic residues bind. The ED site has been considered as a potential hydrophobic pocket for drug discovery since this site is considerably different among MAP kinases.[121]

The second recruitment site in MAPKS is called the F-recruitment site (FRS) or FXFP binding site. The FRS is located near the MAP kinase active site and helix G. This site is constituted of hydrophobic residues such as Leu-198, Tyr-231, Leu-232, Leu-235, Ala-258 and Tyr-261, forming a hydrophobic pocket with a preference for hydrophobic residues. Zhang and co-workers have shown that inactive ERK2 has the FRS occupied with residues Phe-181 and Leu-182 which are situated in the activation loop. Upon phosphorylation of ERK2, conformational changes cause activation loop reorientation and its exit from FRS; thereby, the FXFP motif is exposed and F-site substrates can interact with the active ERK2.[122]

Most ERKs, JNKs and p38 substrates present the D-site. Thus, drug discovery on MAP kinase has focused on the development of non-ATP competitive inhibitors since the goal is to target binding sites that exploit the differences on the docking domains instead of targeting the ATP binding site by traditional inhibitors. More recently, computational biology studies and screening of substrate peptide libraries have been implemented based on the modifications of these docking domains to find more non-ATP competitive inhibitors.[123]

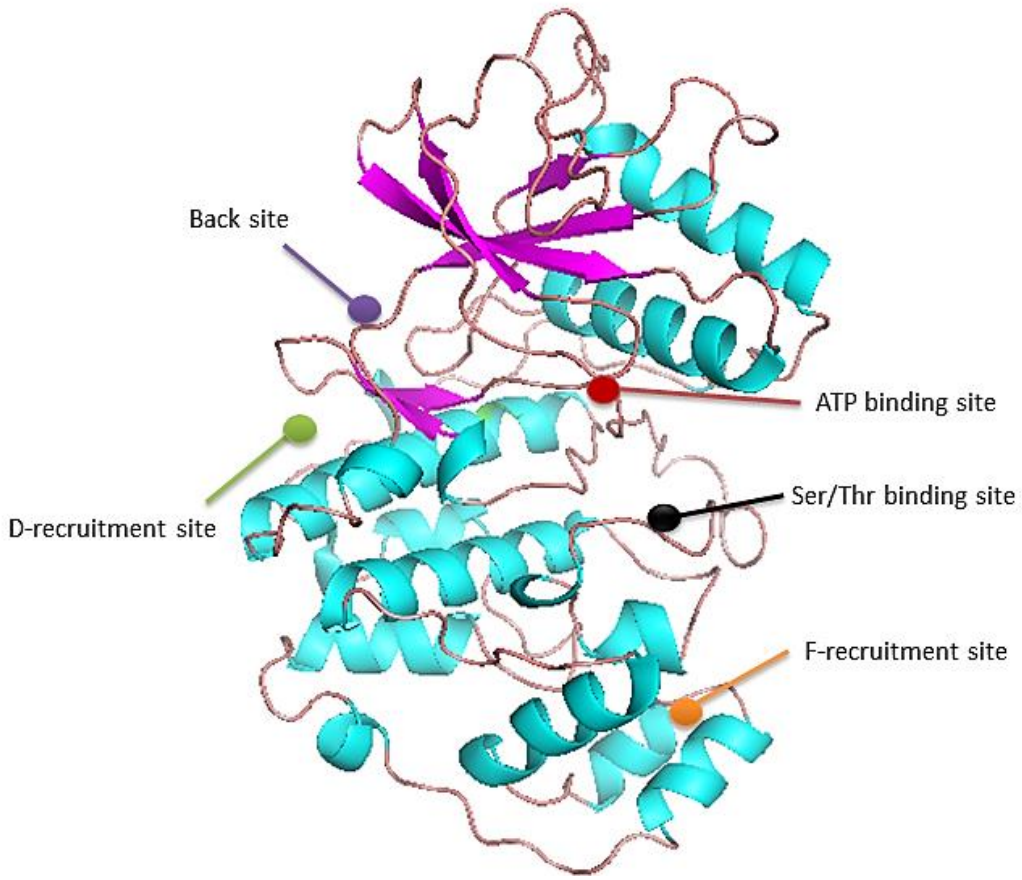

Figure 3.2: *Structure of ERK2 (PDB: 2ERK) showing binding sites***.** Helices are shown in light blue, β-strands are shown in magenta and loops are shown in pink. The D-recruitment site encompasses the common-docking domain (green) and two hydrophobic surface areas. The F-recruitment site (orange) is a hydrophobic pocket with a preference for aromatic residues. The ATP binding site is specified in red. The binding site for substrate with Ser/Thr-Pro motif is indicated in black.

3.3 PREVIOUS STUDIES OF MAPK DOCKING SITES

3.3.1 Modular-Peptide MAPK Substrates

Recently, the docking sites of MAPKs and their mechanism of binding have been the subject of medicinal chemists. Dalby and co-workers used ERK2 as a MAPK model to evaluate the docking interactions of peptide ligands.[124] The interactions between modular docking sequences and the recruitments sites of ERK2 were evaluated using both computational modeling and experimental studies with designed peptides. Two different peptide ligands, Lig-D and Lig-F were synthesized using standard Fmoc-peptide synthesis. Lig-D (FQRKTLQRRNLKGLNLNL) was found to bind the DRS of ERK2. Kinetic studies were performed to study the mechanism of inhibition by Lig-D. The activity of ERK2 was partially inhibited in the presence of Lig-D, decreasing the ability of ERK2 to phosphorylate Ets-1 (residues 1-138) which is an endogenous protein substrate. Lig-F (YAPRAPAKLAFQFPSR) was found to bind to the hydrophobic pocket of FRS. In contrast, Ets-1 was not phosphorylated by ERK2 in the presence of Lig-F, showing a mechanism of competitive inhibition.

In further studies, different modular peptides to target ERK2 were developed based on the previous design, improving the binding interactions of the peptide ligands.[94] The Sub-D peptide (QRKTLQRRNLKGLNLNL-XXX-TGPLSPGPF) was modified by adding a linker and a phosphorylation site to the previous peptide ligand. Sub-D peptide was generated by attaching the C-terminus of the original Lig-D sequence to a flexible linker (X = 6-amino-hexanoic acid), which was also connected to the TGPLSPGPF

sequence (**Figure 3.3**). The consensus phosphorylation site of Sub-F peptide (YAEPLTPRILAKWEWPA) derived from Lig-F, where the conventional FSFG sequence was changed to the WEWP modular docking site.

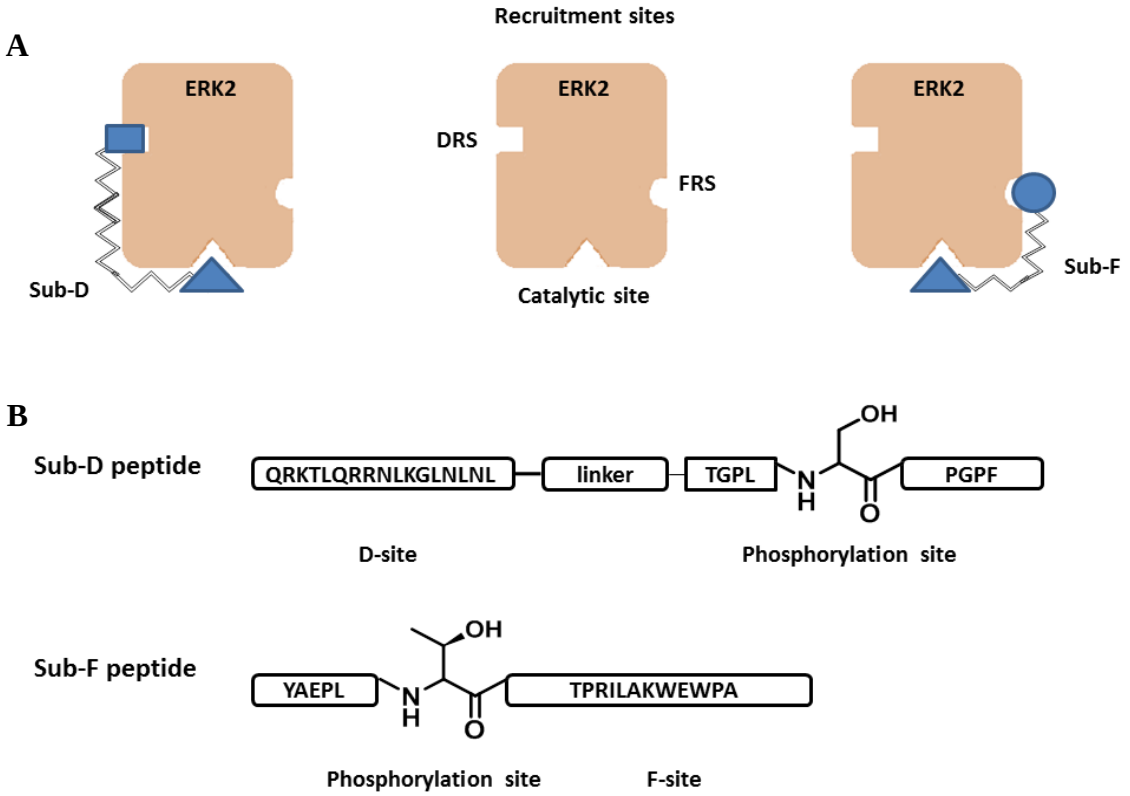

Figure 3.3: *General mechanism of substrate recognition by ERK2 reported by Dalby et al.* Schematic representation of the binding interactions between ERK2 and peptide substrates with different docking sites. (A) Sub-D peptide is recognized by the DRS of ERK2, catalyzing the phosphorylation reaction of the amino acid Ser. Sub-F is recognized by the FRS in ERK, catalyzing the phosphorylation reaction of Thr residue. (B) Sub-D and Sub-F peptide sequences showing the consensus phosphorylation site, and the D-site and F-site, respectively.

Peptide sequences Sub-D and Sub-F were studied using computational modeling. The peptide sequences were virtually constructed and modeled on the surface of ERK2 (**Figure 3.4**). The D-site of the Sub-D peptide presented good docking interactions with the DRS of ERK2. A hydrophobic surface pathway was also found along the surface of ERK2 where the flexible linker can properly interact. The WXWP motif of Sub-F peptide was effectively recognized by the characteristic hydrophobic pocket of the FRS of ERK2. In further application-based studies, kinetic analysis was performed by measuring initial rates of the phosphorylation reaction of sub-D and sub-F substrates with ERK2, using a radioactive assay. Kinetic parameters k_{cat}/K_m 6 x 10^6 M^{-1} s^{-1} and 2 x 10^6 M^{-1} s^{-1} were calculated for Sub-D and Sub-F, respectively. Both peptides were found to be phosphorylated with the same efficiency (6 x 10^6 M^{-1} s^{-1}) compared to the Ets-1 substrate. In addition, the Lig-F was tested as a competitive substrate in the presence of either Sub-D or Sub-F to study allosteric mechanisms. Sub-D was completely phosphorylated by ERK2 in the presence of Lig-F. In contrast, Sub-F peptide was inhibited by the presence of Lig-F. Presumably, the FRS can be used as a drug discovery target for substrate-selective inhibition, where Sub-F peptide could be used for the evaluation of non-ATP competitive inhibitors. These kinetic studies demonstrated that the catalytic activity of ERK2 is not affected by docking peptides that interact with either the FRS or the DRS.

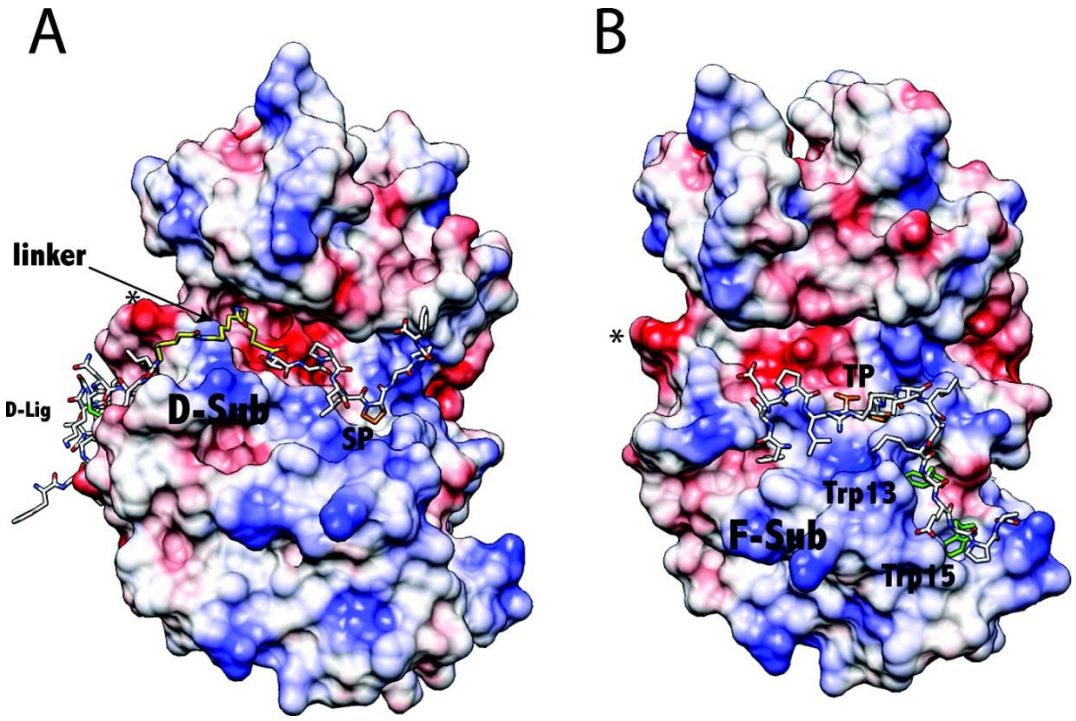

Figure 3.4: *Molecular models of Sub-D and Sub-F peptides bound to ERK2 from Dalby et al.* (A) Sub-D is interacting with the D-recruitment site of ERK2. (B) Sub-F is bound to the F-recruitment site. (Reproduced from Ref. 8. © American Chemical Society, 2011.)

3.3.2 Highly Selective Peptide Sensor

A highly selective SOX-peptide sensor was synthesized by Imperiali and co-workers[125] to study the kinase activity of p38α. Peptide MEF2A-CSox (**3.1**) was designed based on the docking sites of the p38 sub-family. The peptide sensor contained two different modules; the first one had a peptide sequence that was highly selective for the docking sites on p38α. A PEG-linker was used to attach the second module which contained a small sequence including a cysteine residue functionalized with the SOX fluorophore to target the phosphorylation site. The SOX fluorophore was correctly placed in close proximity to the phosphorylation site, enhancing the fluorescence signal upon phosphorylation in the presence of Mg^{2+} ions. The initial rate of phosphorylation of **3.1** was measured in the presence of p38α and other MAP kinases, showing high selectivity for p38α over p38 isoforms and the remaining kinases. Further studies by the same group relied on the use of **3.1** in an assay with HeLa cell lysates. These studies used the broad spectrum staurosporine inhibitor to reduce the background signal from other kinases, increasing the fluorescent signal of p38α activity. Inhibitors of p38α were subsequently added to the cell lysates, reducing the rate of phosphorylation of **3.1**. In additional application-based studies by this group, peptide **3.1** was found to report kinase activity of p38α in different cell lines. The activity of each cell line was corroborated with Western blot analysis, assessing for p38α levels in different cellular environments. These studies demonstrated the ability of peptide sensor **3.1** to measure p38α kinase activity using a

CHEF mechanism upon phosphorylation, detecting changes in the rate of phosphorylation *in vitro* and in cell lysates.

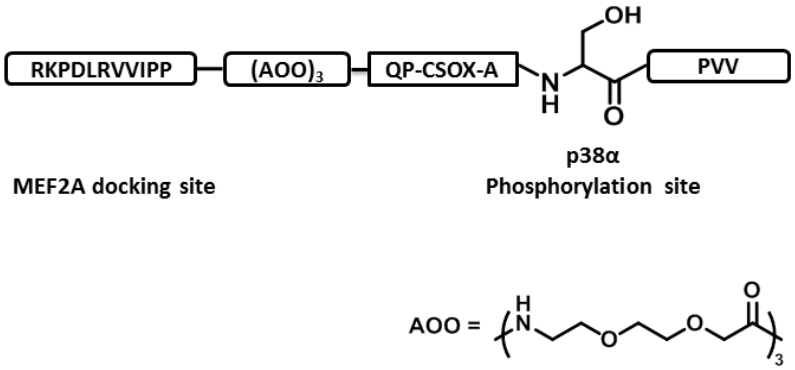

3.1

3.4 MAPK DETECTION WITH A PEPTIDE-BASED SENSING ARRAY

The development of biosensors with high specificity is one of the major challenges in the field of kinase analysis. In nature, closely related substrates will be phosphorylated by several kinases. Experimental assays where the radioactive γ-phosphoryl unit from ATP is transferred to a substrate have been applied to study kinase activity. Western blot analysis with highly specific antibodies is still the primary technique used to quantify kinases. However, these methods can be time-consuming and expensive. This lock-and-key model has been difficult to follow in the case of peptide-based sensors which lack the specificity of docking sites of protein substrates. An additional challenge is the implementation of high-throughput screening to measure altered kinase activity. To overcome this problem, the differential sensing method can enable the detection and differentiation of closely related MAP kinases. Herein, a cross-reactive library of

fluorescent peptides was used to detect and differentiate a wide variety of MAPK isoforms; including ERK1/2, JNK1/2/3 and p38α/β/δ/γ. Changes of kinase concentrations were also semi quantitatively detected using this array sensing approach which discriminating characteristics originated from the recruitment sites of these peptides.

3.4.1 Choosing Peptide Substrates for an Array

Protein substrates are generally difficult to produce in large scale. Thus, peptides can be used as surrogates, simplifying the synthesis and assay assembly. At the structural level, most MAPK substrates incorporate a consensus phosphorylation motif and a docking site in their sequence to be recognized by a variety of MAPKs. Therefore, we followed the leading approach of Dalby by synthesizing modular peptides that contain docking sites. A variety of peptides with distinctive docking sites that presented different affinities and selectivity were thoroughly chosen to develop a library of peptide biosensors (**Figure 3.5**). The following five MAPK peptide substrates Sub-D (**3.2**), MEF2A (**3.3**), NFAT4 (**3.4**), Sub-F (**3.5**) and p38 (**3.6**) presented cross-reactive characteristics to target a wide range of nine different MAPKs. The differential binding strategy consisted of selecting two peptides (Sub-D, MEF2A) with high degrees of affinity towards most MAPK sub-families, including isoforms. Peptide sub-F showed moderate affinity and selectivity for most MAPKs. The remaining two peptides NFAT4 and p38 exhibited higher selectivity towards JNK and p38 sub-families, respectively.

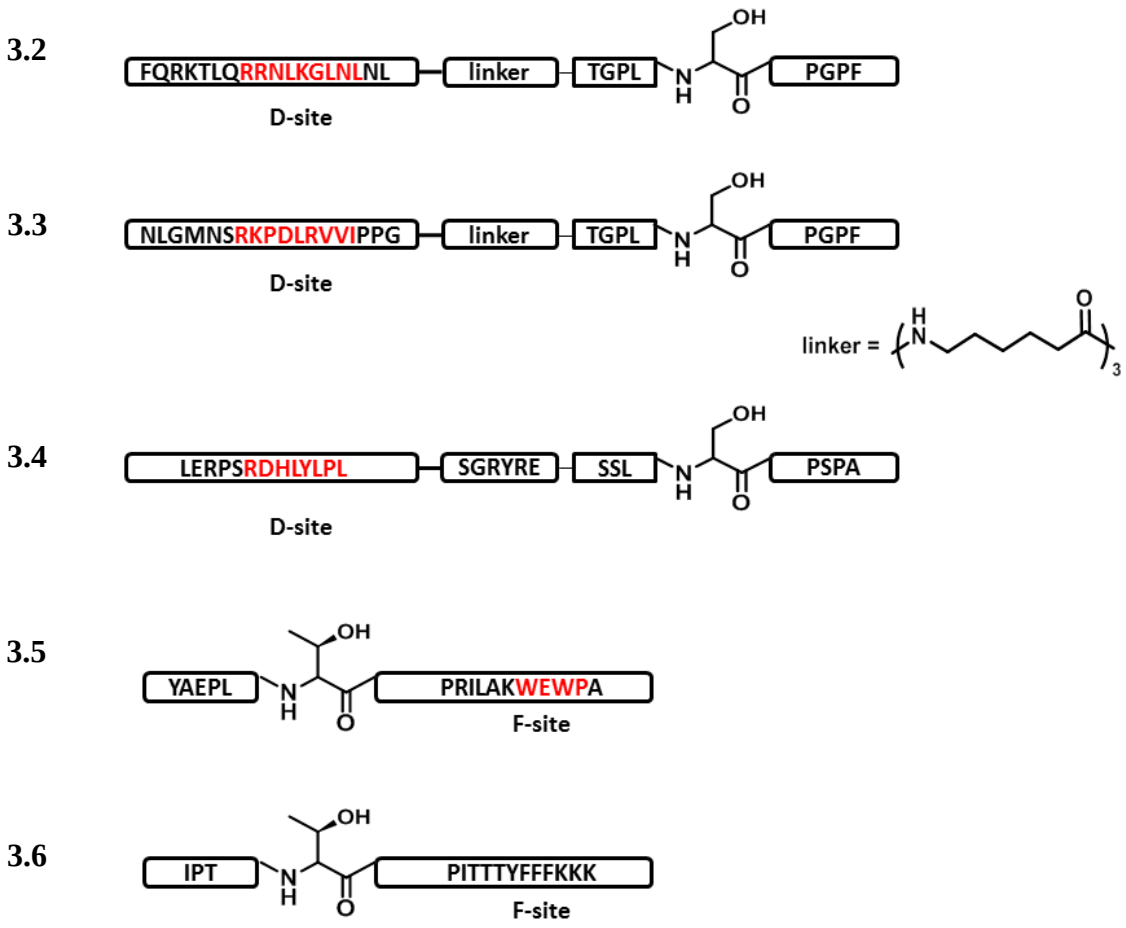

Figure 3.5: *Schematic representation of five MAPK peptide substrates.* Sub-D, MEF2A and NFAT4 peptides contain the D-site which is highlighted in red, and consensus phosphorylation motif with a serine residue. The D-site and phosphorylation site are attached by three 6-aminohexanoic acid groups in Sub-D and MEF2A peptides. Sub-F and p38 peptides contain the F-site which is highlighted in red, and consensus phosphorylation motif with a threonine residue.

3.4.1.1 Sub-D and Sub-F peptides

In the aforementioned study by Dalby and co-workers, ERK2 was recognized by Sub-D and Sub-F peptides with high specificity. Therefore, the modular peptides Sub-D (**3.2**) and Sub-F (**3.5**) reported were chosen due to their ability of recognizing the D-recruitment site and the F-recruitment site, respectively. The D-recruitment site has been recognized in ERK, JNK and p38 kinases, thus it is expected that peptide Sub-D will be phosphorylated by most MAPKs in this study. Furthermore, the F- site has been mainly identified in ERK substrates. Moderate affinity is then expected towards JNK and p38 sub-families.

3.4.1.2 MEF2A and NFAT4 peptides

Recently, Albrecht and co-workers synthesized several docking peptides to study the specificity of linear motifs in known MAPK peptide substrates.[126] These peptides were diversified by varying the region lengths and structural sequence, enhancing the specificity of the D-motif. Particularly, peptides MEF2A (myocyte enhancer factor 2A) and NFAT4 (nuclear factor of activated T cells 4) were included in this study to monitor the binding to ERK2, p38α and JNK1 using fluorescence polarization studies. Both peptides were divided in two different categories according to their binding affinities. MEF2A peptide was first categorized as a peptide with certain selectivity for ERK and p38. Presumably, signaling activation in cells occurs upon phosphorylation of Thr312 and Thr319 residues by ERK2 and p38α. Interestingly, the D-motif of MEF2A peptide

was recognized by both MAPKs. SDS-polyacrylamide gel electrophoresis analysis showed modest discrimination in the binding affinity of MEF2A towards ERK and p38 (**Figure 3.6**).

The second category was formed by peptides with high specificity for JNK. NFAT4 docking peptide was derived from a JNK substrate. Residues Ser163 and Ser165 located in the target site of NFAT4 peptide were only phosphorylated by JNK1 (**Figure 3.6**). Computational models and X-ray crystallography analysis supported charge distribution and structural differences between the surface of JNK docking-site and ERK/p38 surfaces. Interestingly, a charge inversion was found in the D-recruitment site of JNK where a positively charged Lys83 residue is located, whereas both ERK2 and p38α DRS contained a negatively charged Glu residue in the corresponding position. Additionally, the linkage region of NFAT4 is shorter compared to that on MEF2A. Thus, the interactions of long peptide substrates were less compatible with the narrower D-docking site on JNK.

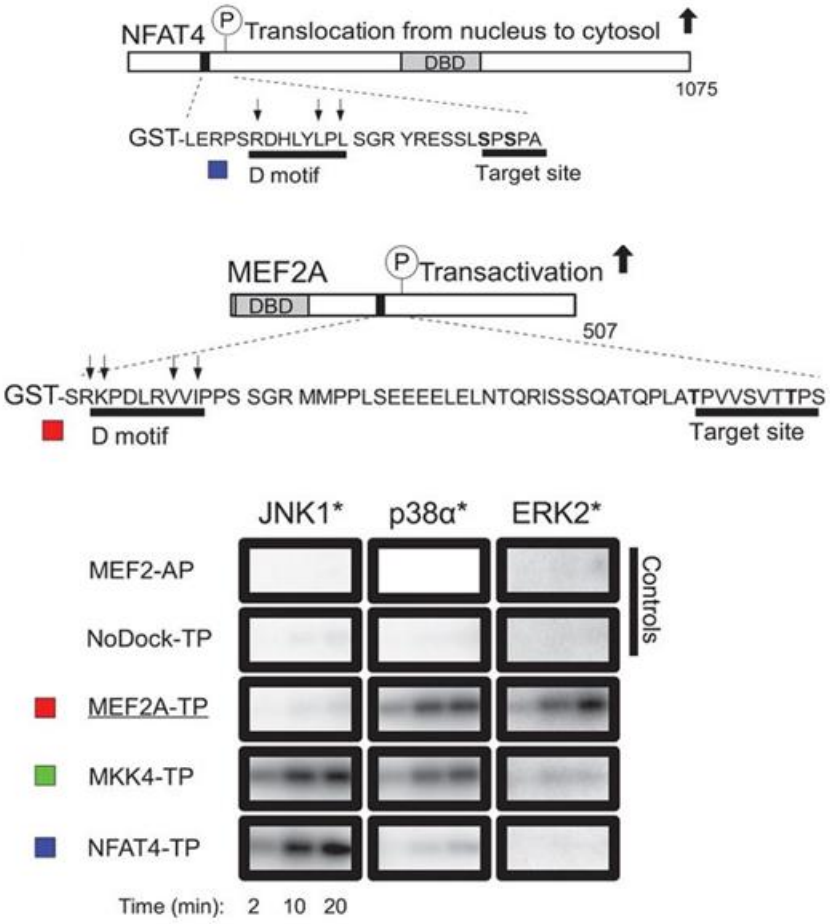

Figure 3.6: *SDS-polyacrylamide gel electrophoresis analysis by Albrecht et al*. (A) MEF2A docking peptide showing the D-motif and target site which are connected by a long sequence of 31 residues. (B) NFAT4 docking peptide presenting the D-motif in close proximity to the phosphorylation site. (C) Gel analysis showing dual selectivity of p38α and ERK2 for MEF2A peptide. NFAT4 is phosphorylated only JNK1, showing high specificity. (Reproduced from Ref. 10. © Science, 2012.)

According to the aforementioned studies, MEF2A peptide was chosen to be part of the differential array of peptides, where MEF2A was expected to bind to ERK and p38 sub-families. The full peptide sequence of MEF2A is shown in **Figure 3.7**, where the target site and the D-motif are connected by a large linkage region of 31 residues, which mainly present negative charge and hydrophilic characteristics. However, this peptide required a difficult synthesis procedure due to the long peptide sequence. To alleviate this synthetic effort, the D-motif was the only docking site that was retained from the original MEF2A peptide, whereas the consensus motif and linkage region were modified for this study. The phosphorylation site (TPVVSVTTPS) of the original sequence of MEF2A was substituted with the same target site used by Sub-D (TGPLSPGPF) which was successfully recognized by ERK2.[124] This target site contained the Thr-Pro motif, which was incorporated in the docking peptides modeled by Dalby *et al.*[94] The flexible linker 6-amino-hexanoic acid was included (previously used for Sub-D), substituting the original 31 residues of the connection region. Thus the new MEF2A peptide (**3.3**) was expected to be recognized by the catalytic site and the D-recruitment sites of ERK and p38 MAPKs.

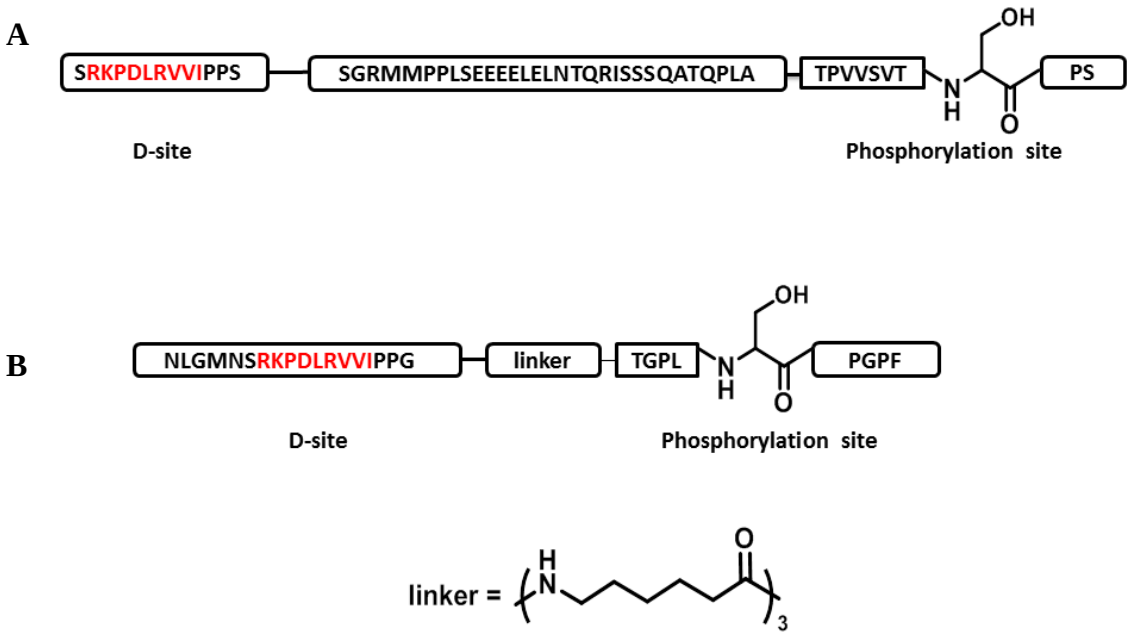

Figure 3.7: *Schematic representation of original MEF2A peptide sequence and MEF2A-modified peptide.* (A) MEF2A docking peptide showing the D-motif and phosphorylation site which are connected by a long sequence of 31 residues reported by Albrecht *et al*. (B) New MEF2A docking peptide (**3.3**) presenting the D-motif from the original sequence. The phosphorylation site (TGPLSPGPF) and the linker were incorporated from the Sub-D peptide model reported by Dalby *et al.*

Additionally, NFAT4 peptide (**3.4**) was chosen as a very selective member of the library of peptide sensors. The linkage region of NFAT4 peptide was only composed of 7 residues. Therefore, NFAT4 peptide was synthesized using the original peptide sequence reported by the Albrecht group. This NFAT4 peptide sequence contains a different D-motif, and a different consensus phosphorylation site compared to Sub-D and MEF2A binding sites. Thus, NFAT4 (**3.4**) was expected to be recognized by the catalytic site and the D-recruitment site of JNK isoforms.

3.4.1.3 p38 Peptide

Pazhanisamy and co-workers studied the activity of p38α with modified peptide substrates that contain a different consensus motif.[127] A peptidic fragment of EGF (endothelial growth factor) protein **3.7a** was chosen as an endogenous substrate to study the kinetic mechanism of p38α-catalyzed reaction in the presence of other competitive peptides. The kinase reaction was measured by HPLC analysis or using spectrometric coupled-enzyme experiments. A set of synthetic substrates **3.7b-e** were designed with different PX(S/T) consensus motifs. Each synthetic peptide contained either a threonine, serine, or tyrosine residue located in a different position and linked to proline. The EGF peptide was phosphorylated on Thr669, reporting a K_m of 840 μM and a k_{cat} of 22.6 s^{-1}. Peptide **3.7b** was found to have a similar k_{cat} compared to **3.7a**, and a K_m value 8-fold lower than that for **3.7a**. The Ser residue next to Pro in **3.7a** was replaced with Thr and Tyr residues in peptides **3.7c** and **3.7d**, respectively. Interestingly, peptides **3.7b** and **3.7c** which contained Ser and Thr at position -1 to Pro were equally phosphorylated, while no

phosphorylation event was observed for **3.7d** which contained Tyr. Additionally, peptide **3.7c** was found to present a K_m value 17-fold lower than that for **3.7a** and a k_{cat} of 8.4 s^{-1}. The Pro residue in peptide **3.7b** was substituted with Ala in peptide **3.7e**, reducing the specific activity although the K_m was not signficantly altered.

a: Lys-Arg-Glu-Leu-Val-Glu-Pro-Leu-**pThr**-Pro-Ser-Gly-Glu-Ala-Pro Asn-Gln-Ala-Leu-Leu-Arg
b: Ile-Pro-Thr-**pSer**-Pro-Ile-Thr-Thr-Thr-Tyr-Phe-Phe-Phe-Lys-Lys-Lys
c: Ile-Pro-Thr-**pThr**-Pro-Ile-Thr-Thr-Thr-Tyr-Phe-Phe-Phe-Lys-Lys-Lys
d: Ile-Pro-Thr-**Tyr**-Pro-Ile-Thr-Thr-Thr-Tyr-Phe-Phe-Phe-Lys-Lys-Lys
e: Ile-Ala-Thr-**pSer**-Pro-Ile-Thr-Thr-Thr-Tyr-Phe-Phe-Phe-Lys-Lys-Lys

3.7

This study highlighted two important characteristics for kinase reactions catalyzed by p38α. (1) Peptides with Ser and Thr residues next to Pro were specifically phosphorylated while no phosphorylation of Tyr was observed in these substrates. (2) The phosphorylation of substrates was not affected by replacing Pro for another hydrophobic residue next to the phosphorylation site. From these studies, peptide **3.7c** was chosen as a very selective member for the library of cross-reactive peptide sensors.

3.4.2 Design of Fluorescent Peptides

Fluorescent peptide-based biosensors are rapidly developing as powerful biological tools to measure kinase activity, as described in Chapter 1. These biosensors display fluorescence changes upon phosphorylation, allowing for a continuous readout in real time. Fluorescent kinase assays can be designed in a high-throughput mode to concomitantly measure kinetic parameters of several protein targets *in vitro*. Thereby, the approach of the Imperiali group was followed by synthesizing SOX-Br **3.14**. Additionally, the Cys residue was incorporated in close proximity to the phosphorylation site. Finally, the Cys residue was then functionalized by attaching the SOX fluorophore through an alkylation reaction, creating the new docking peptides SOX-Sub-D (**3.15**), SOX-MEF2A (**3.16**), SOX-NFAT4 (**3.17**), SOX-Sub-F (**3.18**) and SOX-p38 (**3.19**).

3.4.2.1 Synthesis of Sulfonamido-Oxine (*SOX) Fluorophore*

The fluorophore SOX-Br **3.14** was synthesized through literature procedure with some modifications (**Scheme 3.1**).[128,129] To begin, 2-methylquinolin-8-ol (**3.8**) was obtained commercially. Sulfonation of **3.8** with *chlorosulfonic acid yielded compound* **3.9**, which was used as a crude material for the subsequent reaction. Sulfonamide **3.10** was obtained by treatment of **3.9** and dimethylamine as reported. Compound **3.10** was allowed to react with *tert*-butyldiphenylsilyl chloride to protect the phenolic hydroxyl group on sulfonamide **3.11**. The yield of this reaction was improved by purification of the product through recrystallization with a mixture of methanol and dichloromethane rather

than flash chromatography which produced product decomposition according to previous reports. The following two steps which included oxidation to the aldehyde with selenium dioxide and reduction of the aldehyde to alcohol with sodium borohydride were performed without purification of the intermediate product. The resulting crude material **3.13** was allowed to react with carbon tetrabromide and triphenylphosphine to yield product SOX-Br **3.14.**

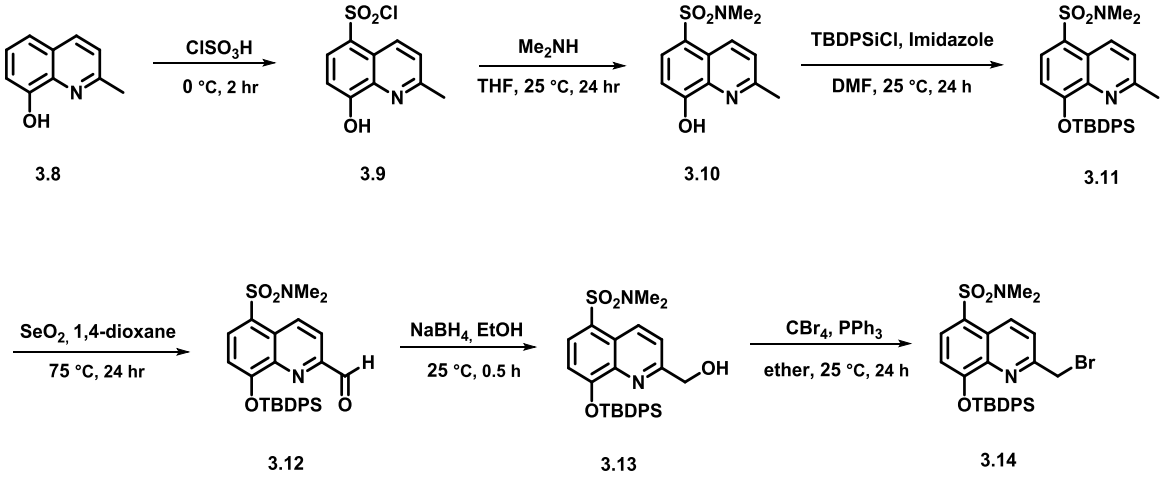

Scheme 3.1: *Synthesis of **3.14***

3.4.2.2 Peptide Functionalization with SOX Fluorophore

The selected modular peptides Sub-D (**3.2**), MEF2A (**3.3**), NFAT4 (**3.4**), Sub-F (**3.5**) and p38 (**3.6**) were synthesized using standard Fmoc-based solid phase peptide synthesis (SPPS). In the aforementioned studies, Imperiali *et al.* showed that a Cys residue on peptide MEF2A can be easily modified by alkylation with the SOX fluorophore.[125] This method was used to install a Cys(Mmt) residue at the P+2 or P-2 position to the phosphorylation site of each peptide as shown in **Scheme 3.2**.

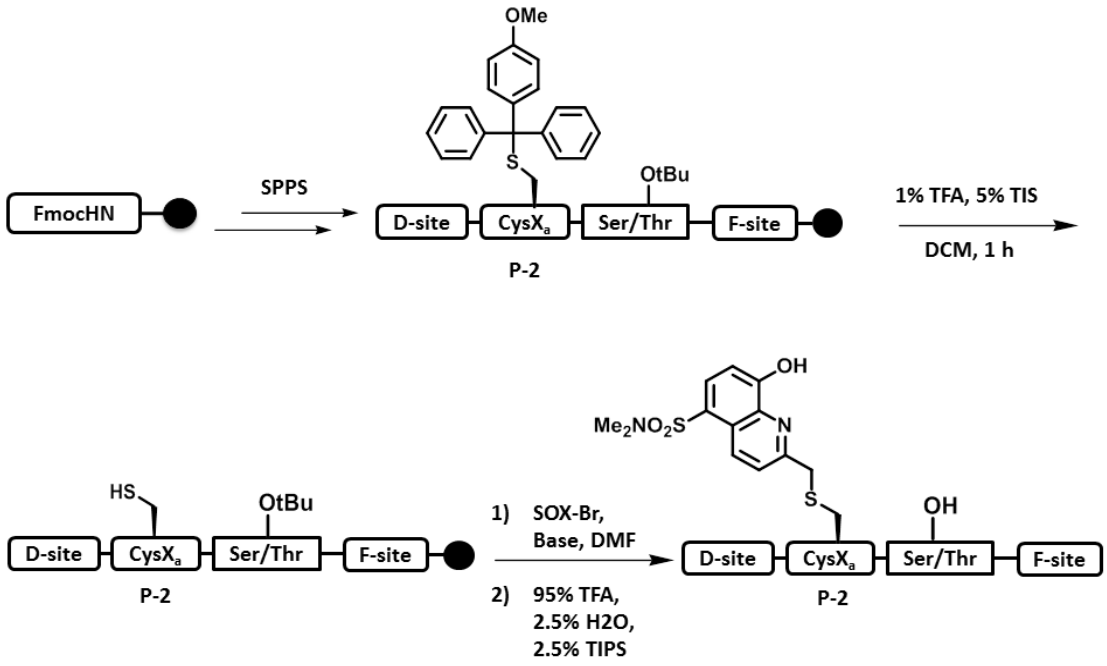

Scheme 3.2: *Deprotection reaction of Mmt group and alkylation of cysteine residue with* ***3.14.***

A selective deprotection of the Cys residue was achieved by cleaving the *p*-methoxytrityl (Mmt) protecting group with a diluted solution of trifluoroacetic acid (TFA) in the presence of triisopropylsilane (TIPS) which was used as a scavenger for Mmt cations. The *tert*-butyl protecting groups on hydroxyl groups were stable under these mild acidic conditions. The alkylation reaction of the Cys residue with SOX-Br **3.14** yielded the desired resin-bound SOX-peptides. The remaining side chains were deprotected using standard cleaving conditions. The SOX-peptides were cleaved from the resin and purified with preparative HPLC, resulting in the modular SOX peptides Sub-D (**3.15**), MEF2A (**3.16**), NFAT4 (**3.17**), Sub-F (**3.18**) and p38 (**3.19**) shown in **Scheme 3.3**.

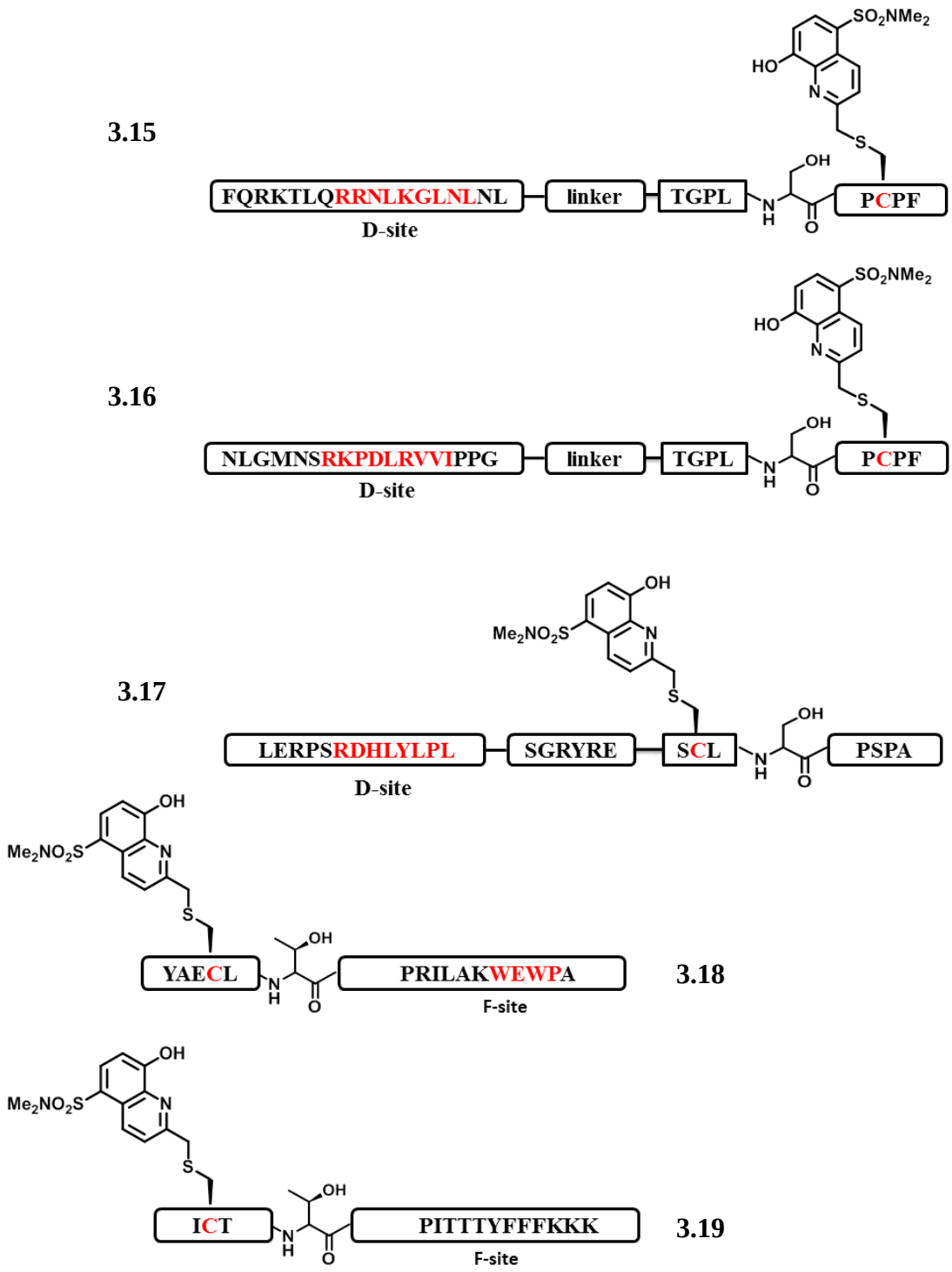

Scheme 3.3: *Schematic representation of modular SOX-peptides.*

3.4.3 Rate Equations for First-Order Phosphorylation Reactions

Continuous fluorescent changes of modular peptides Sub-D (**3.15**), MEF2A (**3.16**), NFAT4 (**3.17**), Sub-F (**3.18**) and p38 (**3.19**) were detected upon phosphorylation with *in vitro* kinases at nanomolar concentrations. Nine isoforms of MAP kinase groups ERK1/2, JNK1/2/3 and p38α/β/γ/δ were added *in vitro* to each SOX-peptide substrate. The phosphorylation reaction was carried out in the presence of ATP and Mg^{2+} to allow for the chelation enhanced fluorescence mechanism. First-order rates of fluorescence increase of SOX-peptide versus time were measured using the method of pre-steady state kinetics. The rate constants were initially analyzed by software curve fitting Igor Pro 6.04. The rate law equations for the first-order phosphorylation reaction of each SOX-peptide in the presence of individual MAPKs are described in **Scheme 3.4**. The concentration of B at time *t* or $[B]_t$ is related to the final concentration of B, $[B]_\infty$ by **Equation 3.1**. The fluorescence of the product ($F_{product}$) or phosphorylated SOX-peptide is directly proportional to [B]. In addition, the fluorescence of the product is also defined by the total fluorescence at time *t* (F_t) and the initial fluorescence of the substrate (F_o). Thus, the fluorescence of the product at any time is defined by **Equation 3.3** which is obtained by substitution of **Equation 3.2** into [B] of **Equation 3.1**. Finally, fluorescence as a function of time can be plotted using **Equation 3.4** which was derived from **Equation 3.3**, reducing the number of variables. The parameters used in the final **Equation 3.4** are described as follows: $F(t)$, fluorescence as a function of time; F_∞, fluorescence of the product; F_o, initial fluorescence of the peptide substrate; k, observed

rate constant; *t*, time. Thereby, the rate constant was obtained using **Equation 3.4** in the curve fitting program.

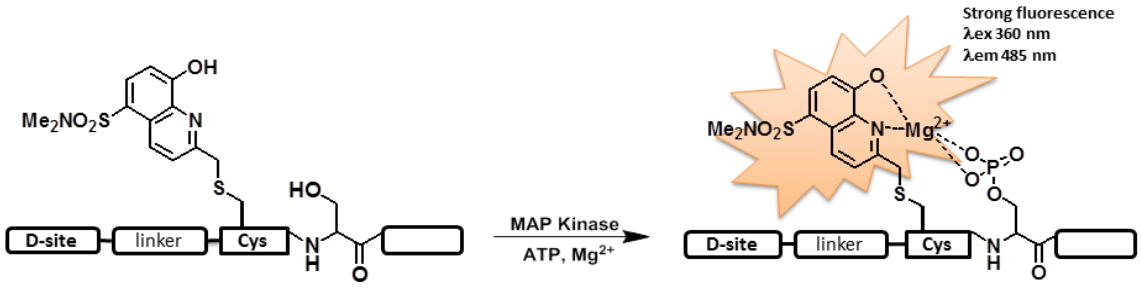

$$A \xrightarrow{k} B$$

$$[B]_t = [B]_\infty\{1 - \exp(-kt)\} \qquad \textbf{(Eq. 3.1)}$$

$$F_{product} \propto [B]$$

$$F_t - F_o \propto [B] \qquad \textbf{(Eq. 3.2)}$$

$$F_t - F_o = (F_\infty - F_o)\{1 - \exp(-kt)\}$$

$$F_t = (F_\infty - F_o)\{1 - \exp(-kt)\} + F_o \qquad \textbf{(Eq. 3.3)}$$

$$\frac{F_\infty - F_t}{F_\infty - F_o} = e^{-kt}$$

$$\boxed{F(t) = F_\infty - (F_\infty - F_o) * \exp(-kt)} \qquad \textbf{(Eq. 3.4)}$$

Scheme 3.4: *Schematic representation of fluorescence changes upon phosphorylation of SOX-peptides*. Parameters in **Equation 3.4**: $F(t)$, fluorescence as a function of time; F_∞, fluorescence of the product; F_o, initial fluorescence of the peptide substrate; k, observed rate constant; *t*, time.

3.5 PRELIMINARY SENSING ARRAY

3.5.1 Sensing Ensemble

A preliminary fluorescence kinase assay was performed to investigate whether an increase of the fluorescent signal would be measurable at 2 µM SOX-peptide concentration. A 96-well plate was prepared using the five SOX-peptides as discriminating variables. The nine MAPK analytes were added to the corresponding well to obtain the following final concentrations ERK1/2 (2 nM), JNK1/2/3 (20 nM) and p38α/β/γ/δ (10 nM). The general layout of the sensing ensemble for all SOX-peptides is shown in **Figure 3.8**, presenting the different volumes (µL) of kinase stock solutions, peptide stock solution and ATP added to each well. The kinase solution contained the corresponding MAP kinase in the presence of DTT (2 mM) and BSA (2.5 µg/mL) for kinase stabilization. The fluorescence intensity of the SOX-peptide was enhanced in the presence of $MgCl_2$ (5 mM) in HEPES buffer. The ATP solution (5 mM) was the last aliquot added to each well, triggering the phosphorylation reaction. Five SOX-peptides, nine MAP kinases and four repetitions were included in this preliminary sensing array.

Detection of Nine MAPKs Using SOX-Peptides											
	Well plate	1	2	3	4	5	6	7	8	9	10
	Analyte	ERK-1	ERK-2	JNK-1	JNK-2	JNK-3	p38-α	p38-β	p38-ϒ	p38-δ	Buffer
SOX Sub-D	A	Smix= 40 Pep= 5 ATP=5	Smix= 40 Pep= 5 ATP=5	Smix= 40 Pep= 5 ATP=5	Smix= 40 Pep= 5 ATP=5	Smix= 40 Pep= 5 ATP=5	Smix= 40 Pep= 5 ATP=5	Smix= 40 Pep= 5 ATP=5	Smix= 40 Pep= 5 ATP=5	Smix= 40 Pep= 5 ATP=5	B= 50
	B	Smix= 40 Pep= 5 ATP=5	Smix= 40 Pep= 5 ATP=5	Smix= 40 Pep= 5 ATP=5	Smix= 40 Pep= 5 ATP=5	Smix= 40 Pep= 5 ATP=5	Smix= 40 Pep= 5 ATP=5	Smix= 40 Pep= 5 ATP=5	Smix= 40 Pep= 5 ATP=5	Smix= 40 Pep= 5 ATP=5	B= 50
	C	Smix= 40 Pep= 5 ATP=5	Smix= 40 Pep= 5 ATP=5	Smix= 40 Pep= 5 ATP=5	Smix= 40 Pep= 5 ATP=5	Smix= 40 Pep= 5 ATP=5	Smix= 40 Pep= 5 ATP=5	Smix= 40 Pep= 5 ATP=5	Smix= 40 Pep= 5 ATP=5	Smix= 40 Pep= 5 ATP=5	B= 50
	D	Smix= 40 Pep= 5 ATP=5	Smix= 40 Pep= 5 ATP=5	Smix= 40 Pep= 5 ATP=5	Smix= 40 Pep= 5 ATP=5	Smix= 40 Pep= 5 ATP=5	Smix= 40 Pep= 5 ATP=5	Smix= 40 Pep= 5 ATP=5	Smix= 40 Pep= 5 ATP=5	Smix= 40 Pep= 5 ATP=5	B= 50

Figure 3.8: *Schematic representation of the sensing ensemble.* Sensing array for the detection of nine MAP kinases: ERK1/2 (2 nM); JNK1/2/3 (20 nM); p38α/β/γ/δ (10 nM) with SOX-Sub-D peptide (2 µM).

3.5.2 Analyzing Rates of Phosphorylation

A continuous increase in the fluorescence intensity over 10 min was observed upon phosphorylation of the SOX-peptides. Changes in the emission data at 485 ± 10 nm of each SOX-peptide at pH = 7.4 upon addition of each MAP kinase were recorded using a microplate reader (Biotek Synergy 2). The observed fluorescence intensity against time was plotted for each MAP kinase and its corresponding SOX-peptide, including four repetitions for each kinase as shown in **Figure 3.9** for SOX-Sub-D and **Figure 3.10** for SOX-NFAT4. The fluorescence increase from the phosphorylated SOX-peptides was sensitive enough to be detected at the given concentrations. The resulting kinetic experiments showed that SOX-Sub-D peptide was efficiently phosphorylated by all the different MAPKs groups. In addition, SOX-MEF2A peptide was phosphorylated by most

MAPK sub-families to different extents (see supplementary material **Figure 3.38 and 3.39**), showing a notable preference from ERK1/2 and the p38 isoforms. Remarkably, ERK1 was found to phosphorylate SOX-Sub-F with higher efficiency compared to ERK2 (supplementary information **Figure 3.40 and 3.41)**. Furthermore, isoforms p38α/γ/δ were also found to phosphorylate SOX-Sub-F. However, no fluorescence increase of SOX-Sub-F was observed in the presence of the JNK sub-family. As estimated from the substrate specificity of NFAT4, the SOX-NFAT4 peptide showed remarkably selectivity towards the JNK group. Interestingly, SOX-NFAT4 peptide was also phosphorylated by p38β, showing a higher phosphorylation efficiency compared to JNK1 and JNK3.

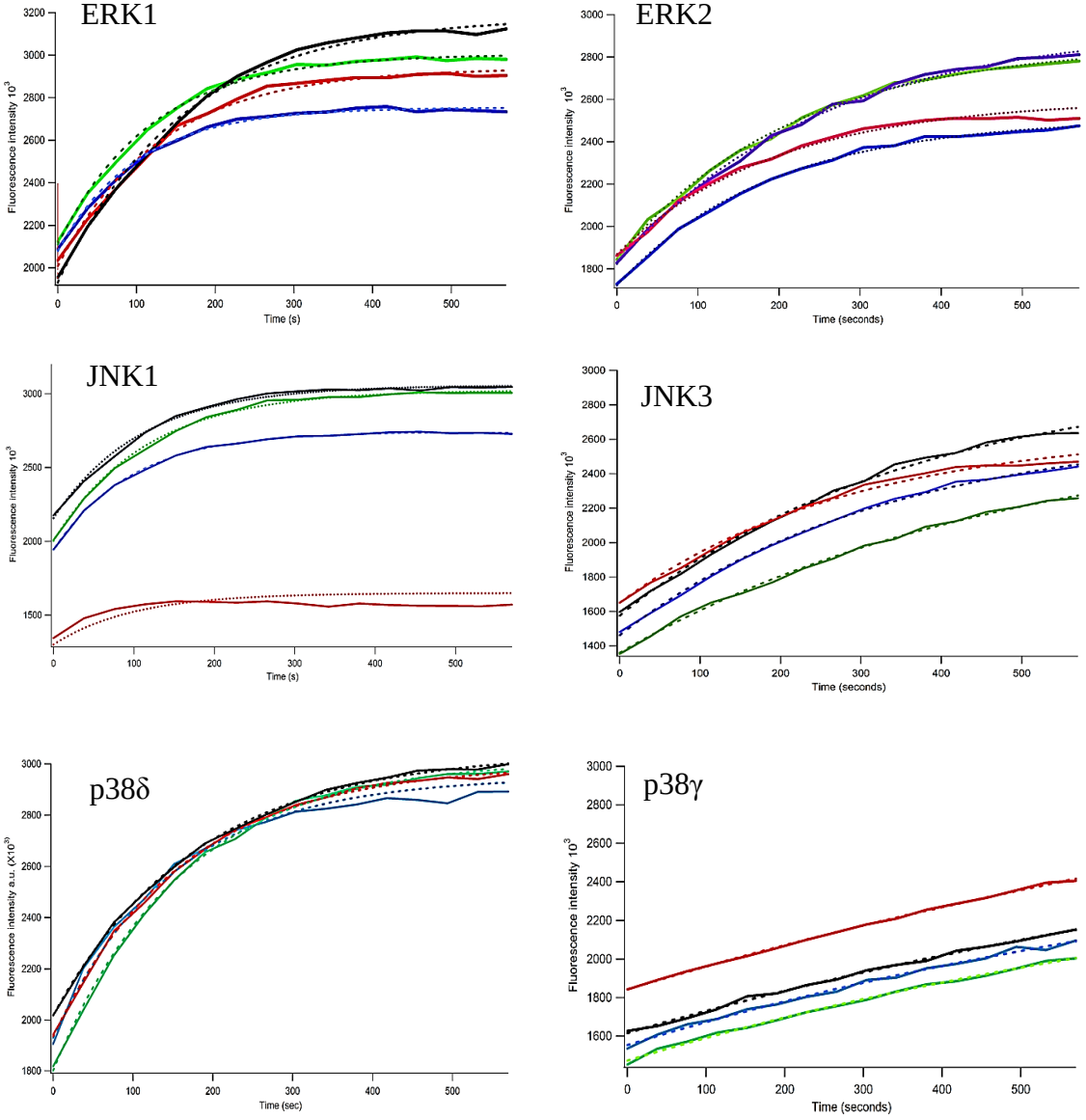

Figure 3.9: *Fit curves of the fluorescence changes of SOX-Sub-D peptide upon phosphorylation with six different MAPKs.* Data collected with 96-well plate half volume, plate reader with λ_{ex} filter of 360 ± 10 nm and λ_{em} filter of 485 ± 10 nm, using a top 400 mirror. Kinase concentrations: ERK1/2 (2 nM), JNK1/2/3 (20 nM) and p38α/β/γ/δ (10 nM) with SOX-peptide (2 µM). Assay buffer: (25mM HEPES, 50mM KCl, 0.1 mM EDTA, 0.1 mM EGTA pH 7.4) with 2 mM DTT, 2.5 µg/mL BSA, 5mM $MgCl_2$, 500 µM ATP at 25°C.

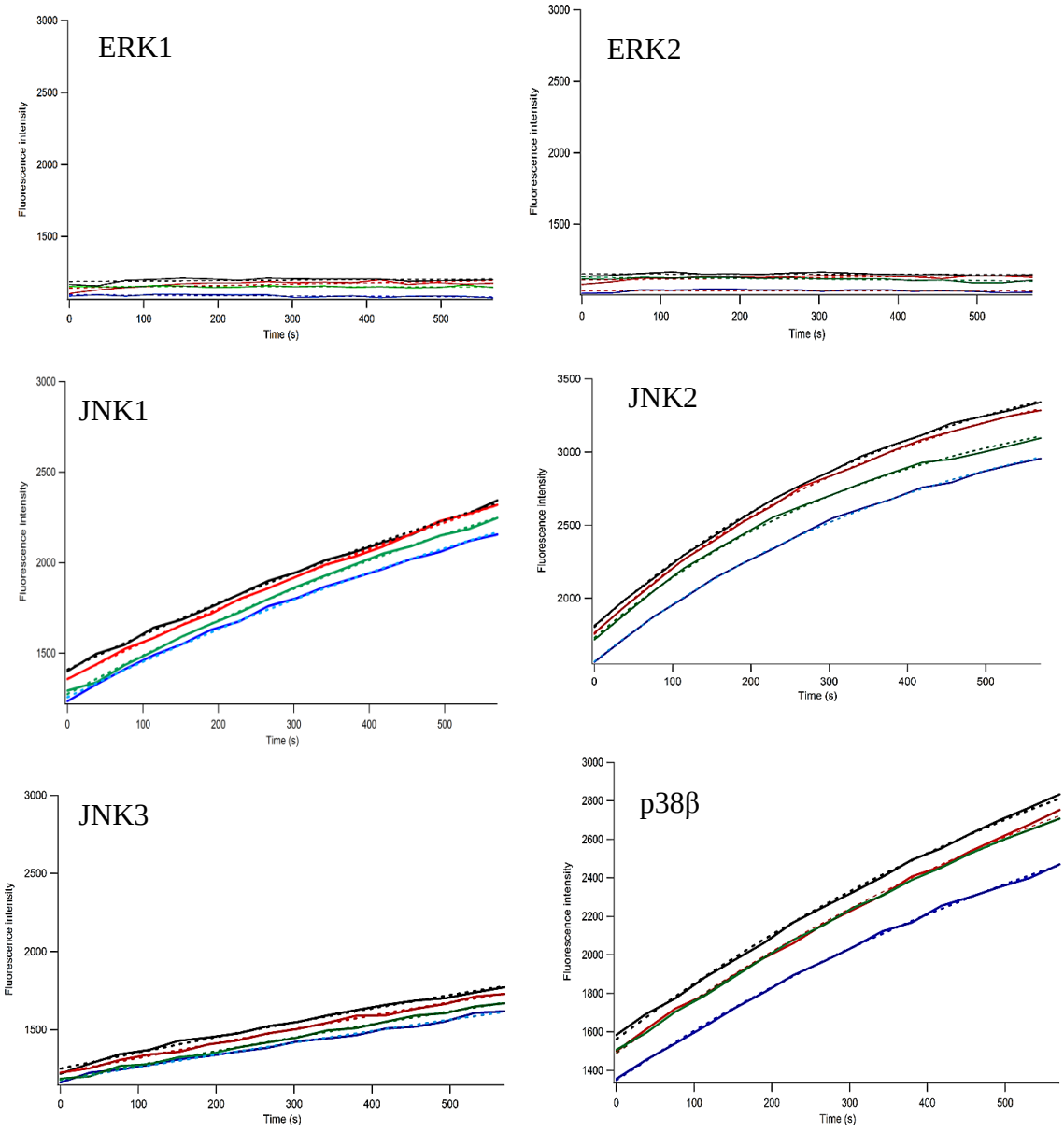

Figure 3.10: *Fit curves of the fluorescence changes of SOX-NFAT4 peptide upon phosphorylation with six different MAPKs.* Data collected with 96-well plate half area, plate reader with λ_{ex} filter of 360 ± 10 nm and λ_{em} filter of 485 ± 10 nm, using a top 400 mirror. Kinase concentrations: ERK1/2 (2 nM), JNK1/2/3 (20 nM) and p38α/β/γ/δ (10 nM) with SOX-peptide (2 µM). Assay buffer: (25mM HEPES, 50mM KCl, 0.1 mM EDTA, 0.1 mM EGTA pH 7.4) with 2 mM DTT, 2.5 µg/mL BSA, 5mM $MgCl_2$, 500 µM ATP at 25°C.

3.5.3 Fingerprint of Nine MAPKs

From these results, it was clearly observed that the rate of phosphorylation is different for each SOX-peptide depending on the MAPK that was used. A total of 180 rate constants were obtained from the phosphorylation of each SOX-peptide using the curve fitting program. The rate constants were used as input data to perform linear discriminant analysis (LDA) using the program XLSTAT. The SOX-peptides were used as discriminatory variables against MAPK analytes. The following LDA plot (**Figure 3.11A**) was obtained using this sensing ensemble. The discriminatory properties of the SOX-peptides showed excellent differentiation of the nine MAPK kinase groups with 62.2% of the variance along the F1 axes, and 28.17% of the variance along the F2 axes. The nine MAPK groups were correctly classified into respective sets with 100% accuracy according to the jack-knife analysis. Each of the MAPK isoforms was classified into their corresponding sub-family group. The JNK group is located on the right side of the LDA plot, whereas the ERK and p38 subfamilies are located on the left side. In addition, ERK1 and ERK2 are distinctly located in the top left quadrant along with p38α and p38δ, while the other isoforms p38β and p38γ are located in the bottom left quadrant. The corresponding loading plot (**Figure 3.11B**) was generated along with the LDA plot, showing the contribution of each SOX-peptide to the differentiation of the nine MAP kinases.

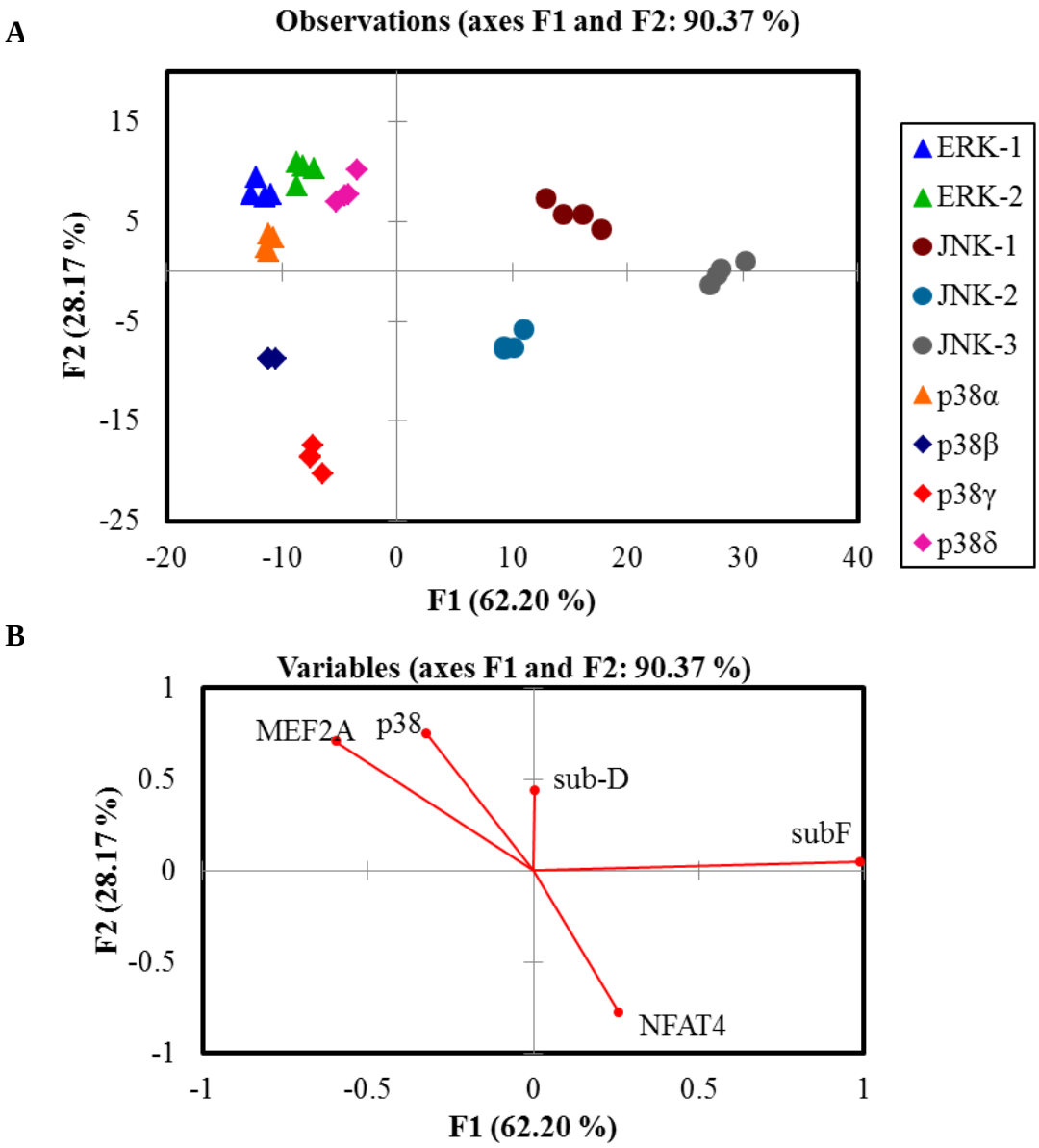

Figure 3.11: *LDA score plots of the response from the SOX-peptides showing in vitro differentiation of nine MAP kinases*. (A) LDA score plot and (B) loading plot of the fluorescence response pattern of phosphorylated MAP kinases. 100% jack knife analysis. Kinase concentrations: ERK1/2 (2 nM), JNK1/2/3 (20 nM) and p38α/β/γ/δ (10 nM) with SOX-peptide (2 µM). Data collected with 96-well plate half area, plate reader with λ_{ex} filter of 360 ± 10 nm and λ_{em} filter of 485 ± 10 nm, using a top 400 mirror. Assay buffer: (25mM HEPES, 50mM KCl, 0.1 mM EDTA, 0.1 mM EGTA pH 7.4) with 2 mM DTT, 2.5 µg/mL BSA, 5mM $MgCl_2$, 500 µM ATP at 25°C.

3.5.4 Analyzing Experimental Kinetic Parameters

The previous kinase sensing array allowed for the detection and differentiation of nine MAP kinase groups which were recognized using only five different SOX-peptide substrates. However, some approximations were made which may need to be more precisely calculated for the accurate implementation of this sensing array system in future experiments. (1) The addition of each of the solutions was manually executed, including the addition of ATP solution. The overall time of ATP addition in the entire plate may be completed within 2 to 3 minutes. This last addition immediately triggers the phosphorylation reaction. Thus, the rate of phosphorylation may not be correctly measured by the time that the plate is introduced into the plate reader. (2) The time range (10 min) may not be long enough to acquire the appropriate exponential curves, and to obtain the rate constants using the curve fitting program. (3) Saturation kinetics have previously been required to obtain correct final fluorescence points which can cause errors in the derived rate constant.[130] The endpoint or final fluorescence (F_∞) is considered an important kinetic parameter that requires experimental determination. In the previous kinase assay, the final fluorescence was automatically calculated by the software program, producing diverse rate constants according to each final fluorescence point within experimental replicates. Consequently, **Equation 3.5** was considered to theoretically determine when the actual reaction time starts, and to estimate the fluorescence endpoint. The endpoint of SOX-Sub-D-peptide was calculated from the corresponding plot that showed the highest fluorescence point, obtaining an average of

the four replicates. This maximal fluorescence value was then constrained in the equation. The parameters used in **Equation 3.5** are described as follows: F_{∞}, highest fluorescence point; F_o, initial fluorescence of the peptide substrate; t_0, 2-3 min time range. The equation was then applied to two experimental runs of SOX-Sub-D peptide, including JNK3 and p38δ. (**Figure 3.12**). The fitting curves (dotted lines) obtained by the software were plotted along with the experimental exponential curves (solid lines), showing the initial reaction time. As shown in the graphs, the phosphorylation reaction took place during the first 2-3 min range after the addition of ATP, displaying an important portion of the kinetic data during this time. Furthermore, the plot of SOX-Sub-D with JNK3 (**Figure 3.12A**) showed that saturation was not achieved during this overall time range (10 min), suggesting that the endpoint was not properly calculated. This result suggested that the maximal average values could be miscalculated for SOX-peptides with no saturation kinetics in further experiments. As a result, the experimental rate constants from this sensing array may be unreliable for the acquired MAPK fingerprint.

$$F(t) = F_{\infty} - (F_{\infty} - F_o) * \exp(-k(t + to)) \qquad \textbf{(Eq. 3.5)}$$

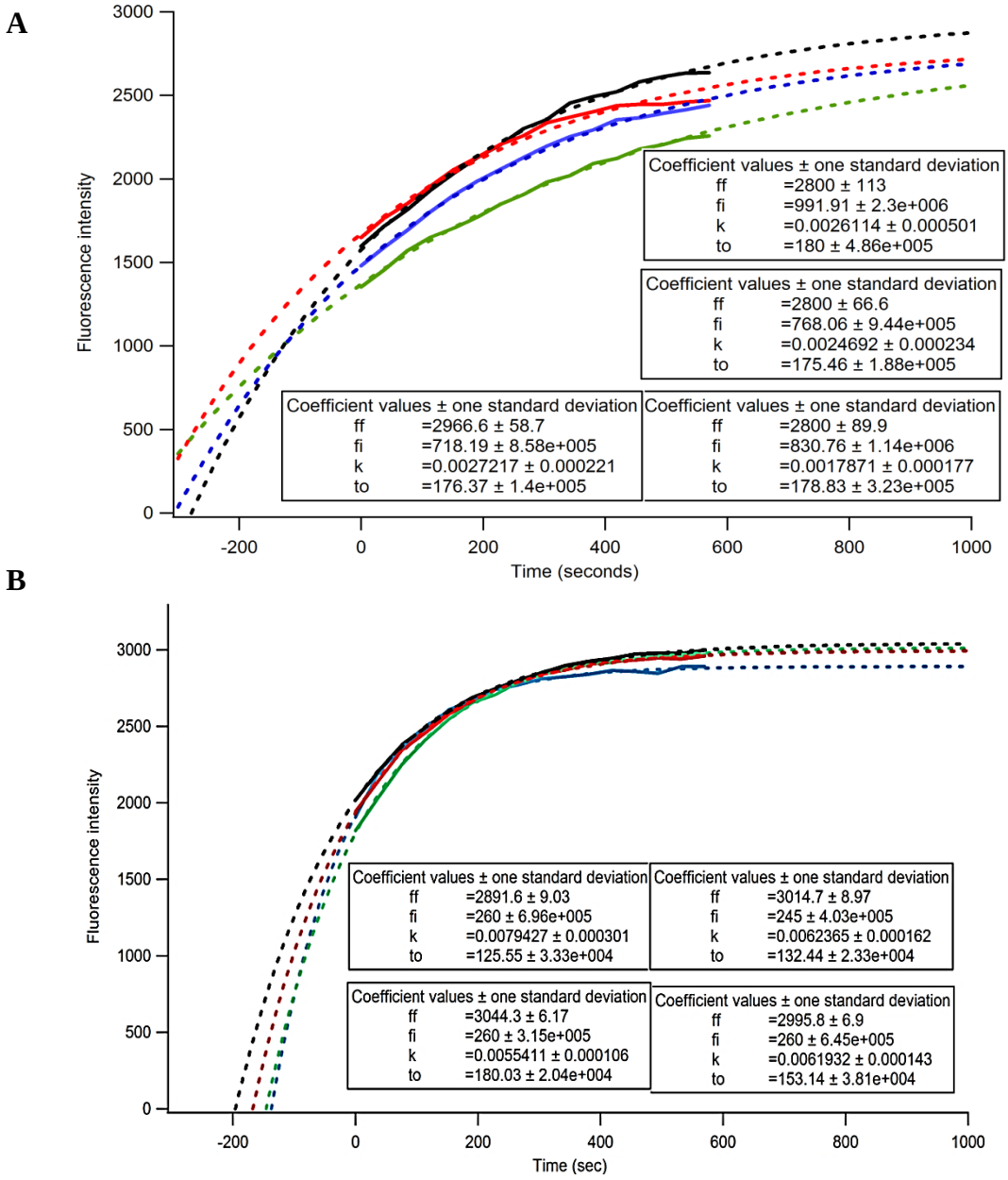

Figure 3.12: *Experimental exponential curves (solid lines) and fitting curves (dotted lines) showing a fluorescence increase of SOX-Sub-D vs time using Igor Pro 6.04.* (A) Fluorescent increase of SOX-sub-D peptide with JNK3. (B) Fluorescent increase of SOX-sub-D peptide with p38δ.

3.6 OPTIMIZING SENSING ARRAY

3.6.1 Sensing Ensemble

To improve the reliability of this peptide-based sensing array, a different microplate reader (Tecan Infinite 500) with an automatic internal injector was used to perform the following kinase assay. The general layout of the sensing ensemble for the five SOX-peptides is shown in **Figure 3.13**. Changes in the emission data at 485 ± 10 nm of each SOX-peptide were measured upon addition of ATP in HEPES buffer at pH = 7.4. Alternatively, three MAPK analytes were chosen for this preliminary experiment, including ERK-1, JNK3 and p38γ. The concentration of these kinases was changed to lower the limit of detection using 1/4 of the previous concentrations to obtain the following final concentrations ERK1 (0.5 nM), JNK3 (5 nM) and p38γ (2.5 nM) in the sensing ensemble. The volumes (μL) of kinase solution, and peptide solution were manually added. The 5 μL ATP aliquot was dispensed by the internal injector to each well using a speed of 300μL/sec. The time range was changed to 20 min to allow for saturation kinetics. **Equation 3.4** was again used to fit the exponential curves, where the fluorescence endpoint at 20 min was calculated from the average of the four experimental replicates. The resulting kinetic data was analyzed with OriginPro curve fitting program to obtain the rate constants.

Preliminary experiment for the detection of small concentrations of MAPK groups												
Well plate	1	2	3	4	5	6	7	8	9	10	11	12
	Sub-F peptide				*p38 peptide*				*NFAT4 peptide*			
Analyte	**ERK-1 0.5 nM**	**JNK-3 5 nM**	**p38γ 2.5 nM**	**Buffer**	**ERK-1 0.5 nM**	**JNK-3 5 nM**	**p38γ 2.5 nM**	**Buffer**	**ERK-1 0.5 nM**	**JNK-3 5 nM**	**p38γ 2.5 nM**	**Buffer**
A	*Smix= 40 Pep= 5 ATP=5*	*Smix= 40 Pep= 5 ATP=5*	*Smix= 40 Pep= 5 ATP=5*	B= 50	*Smix= 40 Pep= 5 ATP=5*	*Smix= 40 Pep= 5 ATP=5*	*Smix= 40 Pep= 5 ATP=5*	B= 50	*Smix= 40 Pep= 5 ATP=5*	*Smix= 40 Pep= 5 ATP=5*	*Smix= 40 Pep= 5 ATP=5*	B= 50
B	*Smix= 40 Pep= 5 ATP=5*	*Smix= 40 Pep= 5 ATP=5*	*Smix= 40 Pep= 5 ATP=5*	B= 50	*Smix= 40 Pep= 5 ATP=5*	*Smix= 40 Pep= 5 ATP=5*	*Smix= 40 Pep= 5 ATP=5*	B= 50	*Smix= 40 Pep= 5 ATP=5*	*Smix= 40 Pep= 5 ATP=5*	*Smix= 40 Pep= 5 ATP=5*	B= 50
C	*Smix= 40 Pep= 5 ATP=5*	*Smix= 40 Pep= 5 ATP=5*	*Smix= 40 Pep= 5 ATP=5*	B= 50	*Smix= 40 Pep= 5 ATP=5*	*Smix= 40 Pep= 5 ATP=5*	*Smix= 40 Pep= 5 ATP=5*	B= 50	*Smix= 40 Pep= 5 ATP=5*	*Smix= 40 Pep= 5 ATP=5*	*Smix= 40 Pep= 5 ATP=5*	B= 50
D	*Smix= 40 Pep= 5 ATP=5*	*Smix= 40 Pep= 5 ATP=5*	*Smix= 40 Pep= 5 ATP=5*	B= 50	*Smix= 40 Pep= 5 ATP=5*	*Smix= 40 Pep= 5 ATP=5*	*Smix= 40 Pep= 5 ATP=5*	B= 50	*Smix= 40 Pep= 5 ATP=5*	*Smix= 40 Pep= 5 ATP=5*	*Smix= 40 Pep= 5 ATP=5*	B= 50
	MEF2A peptide				*Sub-D peptide*							
Analyte	**ERK-1 0.5 nM**	**JNK-3 5 nM**	**p38γ 2.5 nM**	**Buffer**	**ERK-1 0.5 nM**	**JNK-3 5 nM**	**p38γ 2.5 nM**	**Buffer**				
E	*Smix= 40 Pep= 5 ATP=5*	*Smix= 40 Pep= 5 ATP=5*	*Smix= 40 Pep= 5 ATP=5*	B= 50	*Smix= 40 Pep= 5 ATP=5*	*Smix= 40 Pep= 5 ATP=5*	*Smix= 40 Pep= 5 ATP=5*	B= 50				
F	*Smix= 40 Pep= 5 ATP=5*	*Smix= 40 Pep= 5 ATP=5*	*Smix= 40 Pep= 5 ATP=5*	B= 50	*Smix= 40 Pep= 5 ATP=5*	*Smix= 40 Pep= 5 ATP=5*	*Smix= 40 Pep= 5 ATP=5*	B= 50				
G	*Smix= 40 Pep= 5 ATP=5*	*Smix= 40 Pep= 5 ATP=5*	*Smix= 40 Pep= 5 ATP=5*	B= 50	*Smix= 40 Pep= 5 ATP=5*	*Smix= 40 Pep= 5 ATP=5*	*Smix= 40 Pep= 5 ATP=5*	B= 50				
H	*Smix= 40 Pep= 5 ATP=5*	*Smix= 40 Pep= 5 ATP=5*	*Smix= 40 Pep= 5 ATP=5*	B= 50	*Smix= 40 Pep= 5 ATP=5*	*Smix= 40 Pep= 5 ATP=5*	*Smix= 40 Pep= 5 ATP=5*	B= 50				

Figure 3.13: *Schematic representation of the sensing ensemble.* Sensing array for the detection of three MAP kinases: ERK1 (0.5 nM), JNK3 (5 nM) and p38γ (2.5 nM) with five SOX-peptides (2 μM).

3.6.2 Analyzing Rates of Phosphorylation

As expected the same rates of phosphorylation of the five SOX-peptides were observed in the presence of each MAPK upon addition of ATP. Four experimental replicates of the fluorescence intensity versus time were plotted for individual MAP kinase with each SOX-peptide as shown in **Figure 3.14**. Interestingly, saturation kinetics were nearly achieved for each peptide in the presence of ERK1, JNK3 or p38γ over 20 minutes. In addition, the SOX-peptides were efficiently phosphorylated using lower kinase concentrations. The same fluorescence increase pattern (Supplementary information **Figures 3.40, 3.41** and **3.42**) was observed within each MAPK sub-family, where SOX-sub-D was phosphorylated by the three groups. ERK1 efficiently phosphorylated SOX-MEF2A with respect to JNK3 and p38γ. In contrast, SOX-Sub-F was efficiently phosphorylated by p38γ, while no phosphorylation event was observed by JNK3. In addition, SOX-NFAT4 was only phosphorylated by JNK3. However, no phosphorylation of SOX-p38 peptide was observed using the three MAPKs.

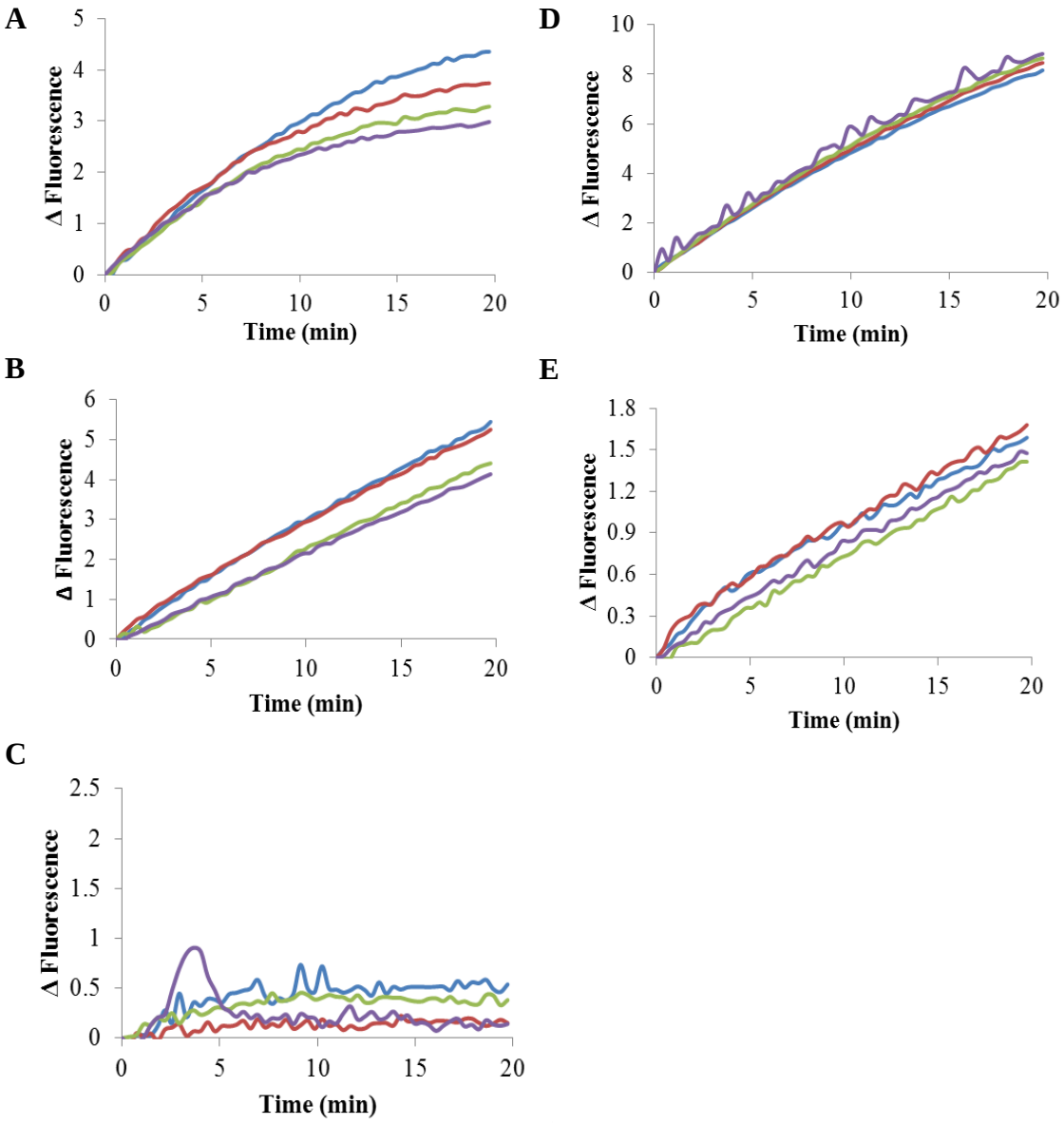

Figure 3.14: *Fluorescence changes of SOX-peptides upon phosphorylation with MAPKs.* (A) SOX-Sub-D with ERK1 (0.5 nM). (B) SOX-Sub-F with p38γ (2.5 nM). (C) SOX-p38 peptide with p38γ (2.5 nM). (D) SOX-MEF2A with ERK1 (0.5 nM). (E) SOX-NFAT4 with JNK3 (5 nM). Kinase concentrations: ERK1 (0.5 nM), JNK3 (5 nM) and p38γ (2.5 nM) with five SOX-peptides (2 µM). Data collected with 96-well plate half area, plate reader with λ_{ex} filter of 340 ± 35 nm and λ_{em} filter of 485 ± 20 nm. Assay buffer: (25mM HEPES, 50mM KCl, 0.1 mM EDTA, 0.1 mM EGTA pH 7.4) with 2 mM DTT, 2.5 µg/mL BSA, 5mM $MgCl_2$, 500 µM ATP at 25°C.

3.6.3 Fingerprint of MAPK Groups

As expected, the following LDA plot in **Figure 3.15** was acquired from this sensing array, showing excellent differentiation between the MAPK groups. In this LDA plot 80.9% of the data was discriminated along the F1 axes and 19% of differentiation was found along the F2 axes. This LDA plot presented 100% jack-knife analysis, signifying satisfactory clustering of the replicates. Interestingly, the same MAPK group pattern was obtained with respect to the previous LDA plot for the nine kinases. JNK3 was again placed on the right quadrant of the LDA plot. However, the y-axis in the LDA plot was inverted for this optimized experiment. ERK1 was clearly distinguished on the bottom left quadrant of the plot, while p38γ was placed on the top left quadrant.

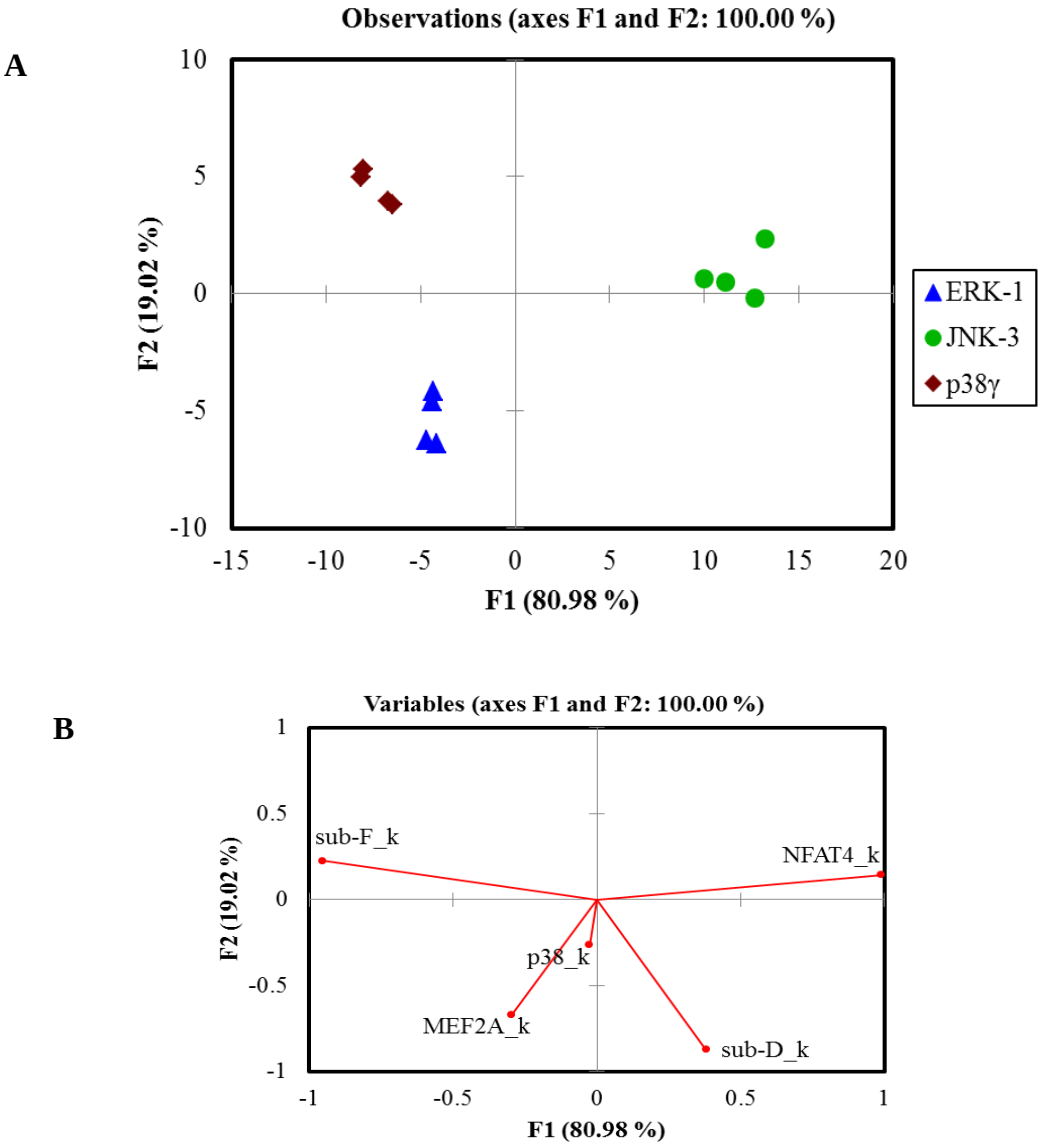

Figure 3.15: *LDA score plots of the response from the SOX-peptides showing in vitro differentiation of MAPK sub-families*. (A) LDA score plot and (B) loading plot of the fluorescence response pattern of three MAP kinases with 100% jack knife analysis. Kinase concentrations: ERK1 (0.5 nM), JNK3 (5 nM) and p38γ (2.5 nM) with five SOX-peptides (2 µM). Data collected with 96-well plate half area, plate reader with λ_{ex} filter of 340 ± 35 nm and λ_{em} filter of 485 ± 20 nm. Assay buffer: (25mM HEPES, 50mM KCl, 0.1 mM EDTA, 0.1 mM EGTA pH 7.4) with 2 mM DTT, 2.5 µg/mL BSA, 5mM $MgCl_2$, 500 µM ATP at 25°C.

3.7 ARRAY REPRODUCIBILITY OF NINE MAPKS

The previous results demonstrated that the methodology was improved by using the new plate reader which had the capability of dispensing the ATP aliquots to the entire plate in less than 20 seconds. In addition, the fixed fluorescence endpoints in the equation and the extension of the time range further improved the kinetic data, increasing the reliability of the obtained rate constants. After showing the successful differentiation of MAPK groups using the previous sensing array, the rest of the MAPK isoforms were subjected to the same sensing ensemble to investigate the reproducibility of the optimized kinase assay.

3.7.1 Optimizing SOX-p38 Peptide Concentration

In this assay the concentration of SOX-p38 peptide was increased to improve the fluorescence signal. The optimal SOX-p38 peptide concentration for the sensing ensemble was found by increasing the concentration of peptide in the presence of p38γ MAPK at a fixed concentration of 8 nM. Fluorescent changes of SOX-p38 were detected using a well-plate reader under the same buffer conditions for 60 minutes. The graph in **Figure 3.16** showed that the peptide is efficiently phosphorylated by p38γ using a concentration close to 10 μM. Higher concentrations were not considered due to the possible overflow of the fluorescence signal which was observed at 50 μM concentration. From this experiment, a final concentration of 8 μM of SOX-p38 peptide was chosen for the following sensing ensemble.

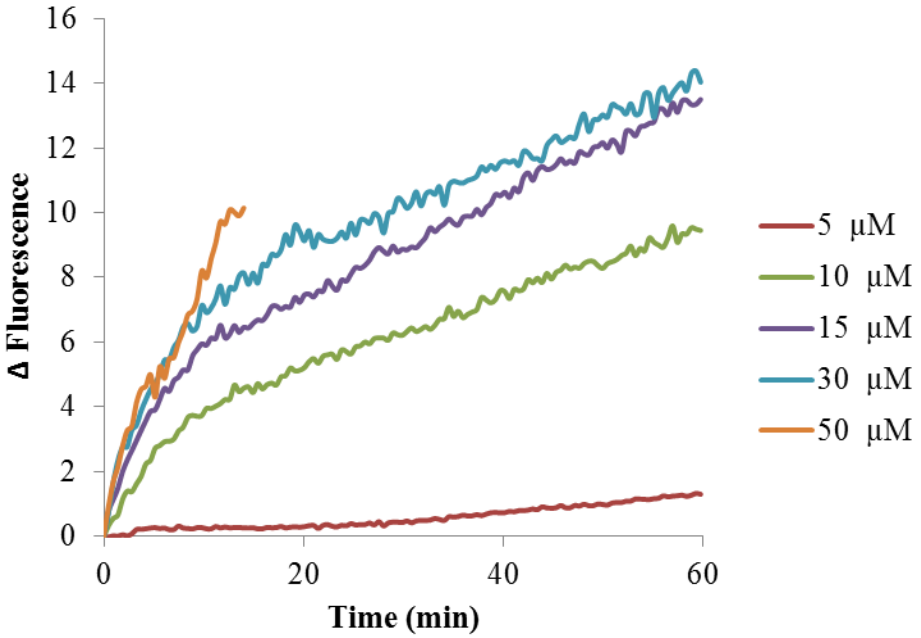

Figure 3.16: *Fluorescent* increase *of SOX-p38 peptide upon phosphorylation.* Plots showed emission changes at different SOX-p38 concentrations in the presence of p38γ MAPK at a fixed concentration of 8 nM. Data collected with 96-well plate half area, plate reader with λ_{ex} filter of 340 ± 35 nm and λ_{em} filter of 485 ± 20 nm. Assay buffer: (25mM HEPES, 50mM KCl, 0.1 mM EDTA, 0.1 mM EGTA pH 7.4) with 2 mM DTT, 2.5 µg/mL BSA, 5mM $MgCl_2$, 500 µM ATP at 25℃.

3.7.2 Reproducible Fingerprint of Nine MAPKs

The experiment with the nine MAPK analytes was replicated in its entirety using the previous low concentrations of ERK1/2 (0.5 nM), JNK1/2/3 (5 nM) and p38α/β/γ/δ (2.5 nM) in the sensing ensemble. A final concentration of SOX-peptide (2 µM) was also used in this sensing array, with the exception of SOX-p38 peptide (8 µM) concentration. The resulting kinetic plots showed comparable rates of phosphorylation of SOX-peptides with respect to the preliminary experiment (Supplementary information **Figures 3.43, 3.44, 3.45** and **3.46**). SOX-p38 peptide was phosphorylated by all p38 isoforms at the given

concentrations ((Supplementary information **Figures 3.47**), while lower fluorescence increase was detected in the presence of the ERK and JNK groups. The LDA plot in **Figure 3.17** was acquired from this array, showing a similar pattern response with respect to the previous LDA plot with nine MAPKs. The data presented 62.99% differentiation along the F1 axes and 33.24% separation along the F2 axes, showing a jack-knife analysis of 86.11%. The JNK sub-family was found on the right side of the plot. The y-axis was also inverted in this LDA plot where the ERK isoforms were found on the bottom left quadrant along with p38α. The isoforms p38δ and p38γ were placed on the top left quadrant. Interestingly, p38β was located on the right side of the LDA plot, along with the JNK group. Despite most of the MAPKs being differentiated along the F1 axes some overlap was observed between JNK2 and p38β on the right side of the plot. In addition, the ERK isoforms showed close approximation between each other. In contrast to the formerly obtained LDA plot (**Figure 3.11**) with nine MAPKs, this sensing ensemble presented a slight decrease of discriminatory power. From these results, it was hypothesized that the addition of more discriminatory variables to the array may improve the differentiation of the MAPK isoforms.

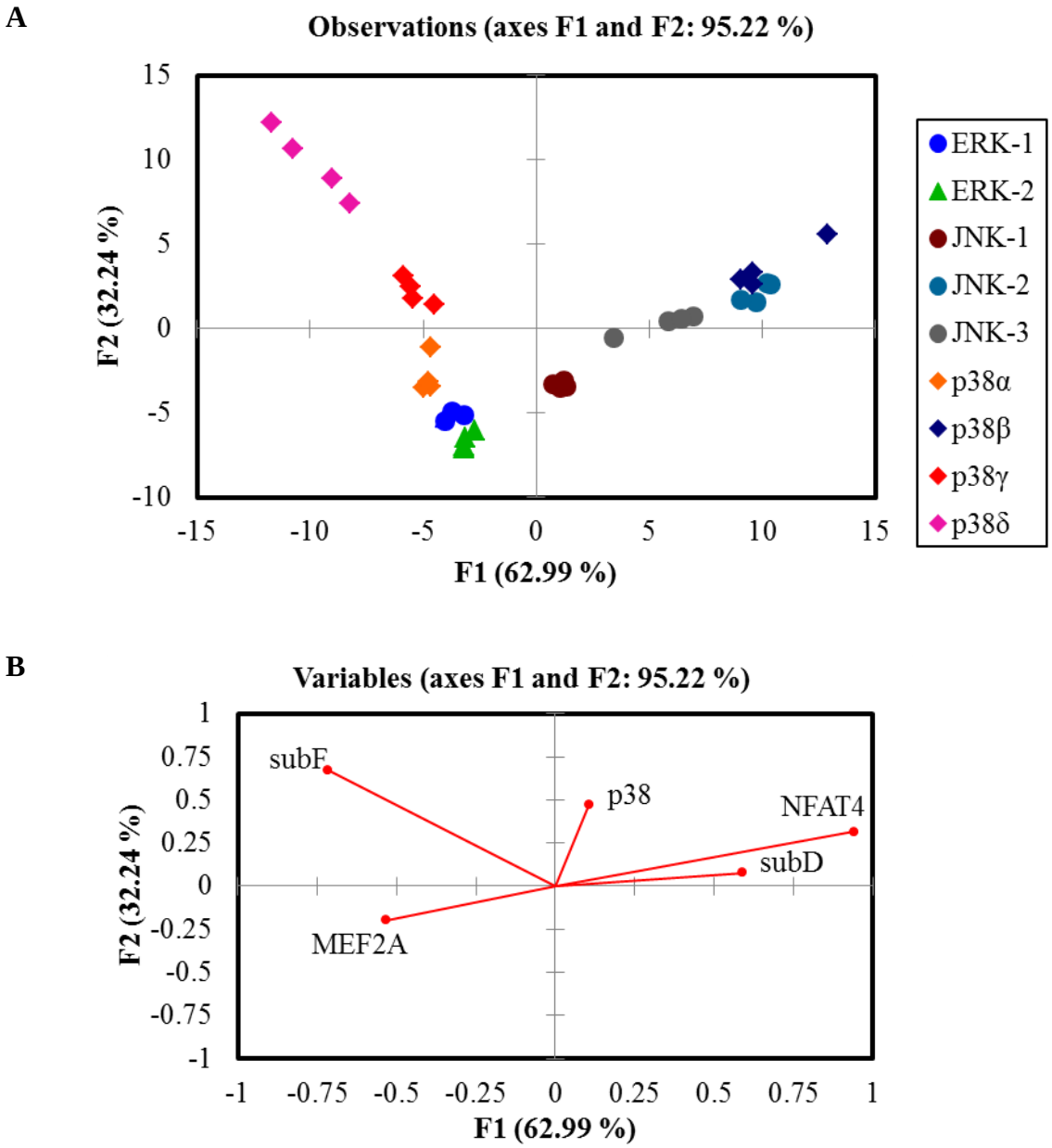

Figure 3.17: *LDA score plots of the response from the SOX-peptides showing in vitro differentiation of nine MAP kinases*. (A) LDA score plot and (B) loading plot of the fluorescence response pattern of phosphorylated MAP kinases with of 86.11% jack-knife analysis. Kinase concentrations: ERK1/2 (0.5 nM), JNK1/2/3 (5 nM) and p38α/β/γ/δ (2.5 nM) with Sox-peptides (2 µM) and SOX-p38 peptide (8 µM). Data collected with 96-well plate half area, plate reader with λ_{ex} filter of 340 ± 35 nm and λ_{em} filter of 485 ± 20 nm. Assay buffer: (25mM HEPES, 50mM KCl, 0.1 mM EDTA, 0.1 mM EGTA pH 7.4) with 2 mM DTT, 2.5 µg/mL BSA, 5mM $MgCl_2$, 500 µM ATP at 25℃.

3.7.3 Additional Discriminatory Variables

Our group has previously shown that spectrophotometric changes at different wavelengths for a given sensor can be used to increase the number of discriminatory variables in a sensing array.[131] In the case of kinetic assays more variables could be added to the array by using additional kinetic parameters from the previously obtained data. The additional kinetic parameters considered were the initial and final fluorescence of the product. However, the initial and final fluorescence values were fixed in the equation for a particular SOX-peptide to obtain the rate constants. Thereby, it was investigated whether a randomly chosen fluorescence value could be used to improve the differentiation of this sensing array. From the previously acquired kinetic data in the sensing array for nine MAPKs, the fluorescence values at 20 minutes were chosen to be included in the input data in combination with the rate constants (supplementary information **Table 3.9**). The LDA plot in **Figure 3.18** was obtained using the same sensing ensemble with additional fluorescence variables. The nine MAPK kinases were differentiated with 55.13% of the variance along the F1 axes, and 26.09% of the variance along the F2 axes. In this LDA plot, eight analyte groups were classified into respective sets with 94.44% accuracy according to the jack-knife analysis. The analyte clustering was improved in comparison to the previously discussed LDA plot in **Figure 3.17**. In addition, each of the MAPK isoforms was classified into their corresponding sub-family group with the exception of p38β which was found in close proximity to the JNK group. The JNK group was placed on the left side of the LDA plot, whereas the ERK and p38

sub-families were found on the right side. ERK isoforms were found in the top right quadrant, presenting further separation along both axes. The isoforms p38δ and p38γ are located on the bottom right quadrant. Finally the discriminating variables (rate constants and fluorescence values) obtained from each SOX-peptide showed the contribution to the differentiation of the enzymes in the loading plot (**Figure 3.18B**). The peptide-based sensors presented excellent cross-reactivity properties, allowing for further separation of the enzymes. A three-dimensional plot was also obtained from this data (**Figure 3.19**), carrying an additional 14.19% of differentiation in the third axis. This sensing array was reproduced and demonstrated to be effective to assess for the detection and differentiation of MAPK groups and isoforms.

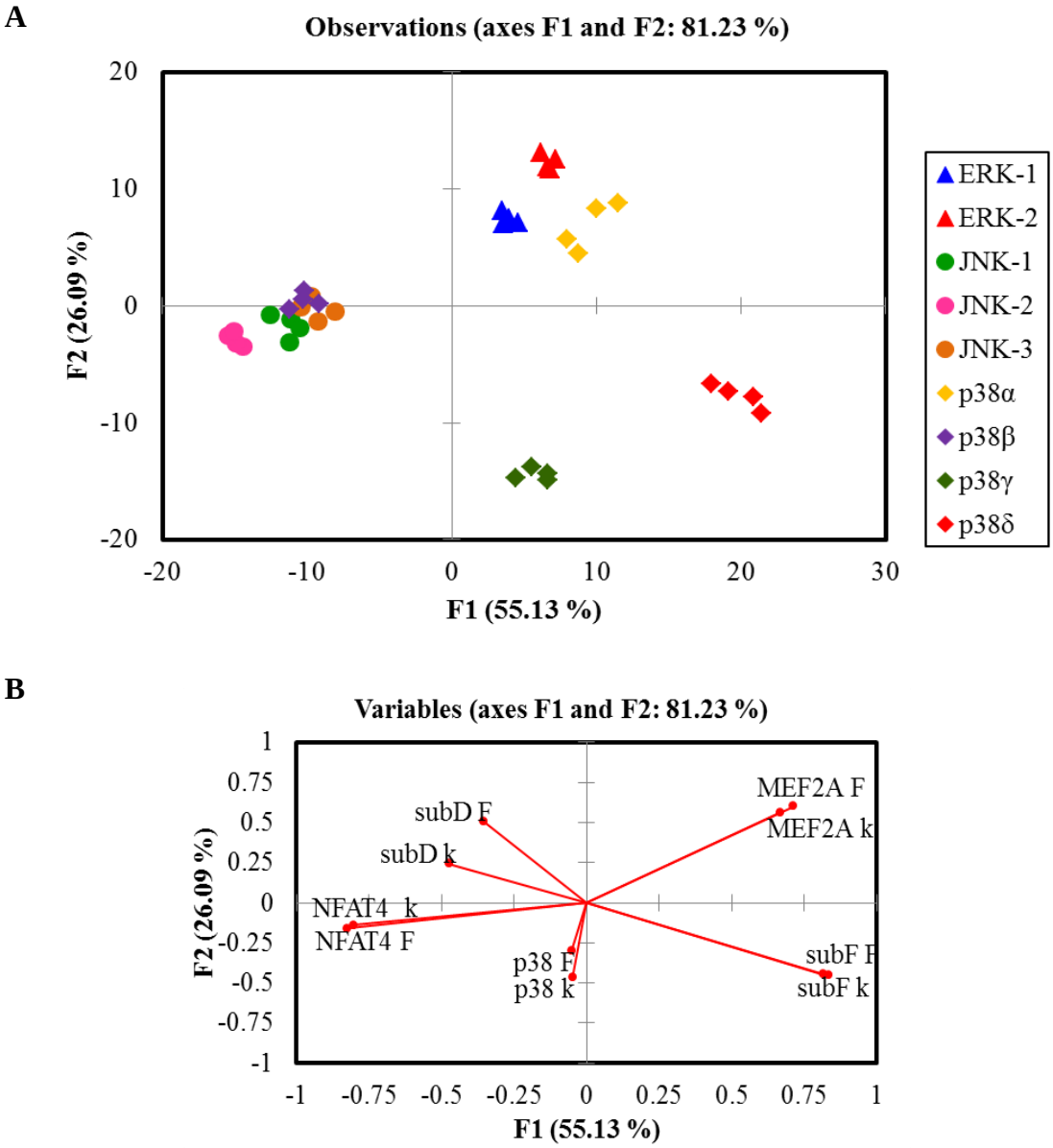

Figure 3.18: *LDA score plot of the response from the SOX-peptides showing in vitro differentiation of nine MAP kinases*. (A) LDA score plot and (B) loading plot obtained with 94.44% jack knife analysis. Kinase concentrations: ERK1/2 (0.5 nM), JNK1/2/3 (5 nM) and p38α/β/γ/δ (2.5 nM). Sox-Sub-D, SOX-MEF2A, SOX-NFAT4 and SOX-Sub-F (2 µM) and SOX-p38 peptide (8 µM). Data collected with 96-well plate half area, plate reader with λ_{ex} filter of 340 ± 35 nm and λ_{em} filter of 485 ± 20 nm. Assay buffer: (25mM HEPES, 50mM KCl, 0.1 mM EDTA, 0.1 mM EGTA pH 7.4) with 2 mM DTT, 2.5 µg/mL BSA, 5mM $MgCl_2$, 500 µM ATP at 25℃.

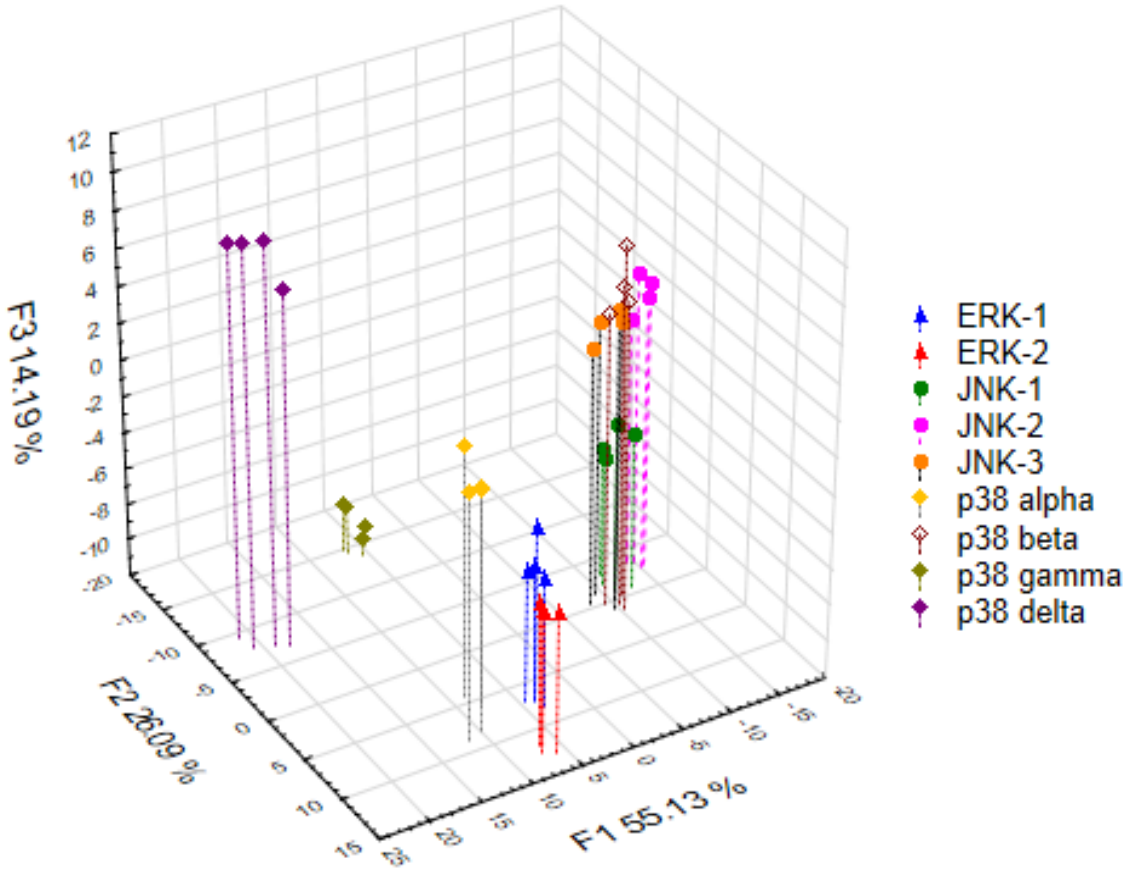

Figure 3.19: *Three-dimensional LDA plot score plot showing in vitro differentiation of nine MAP kinases*. Fluorescence response pattern of *SOX-peptides* in the presence of nine active MAP kinases obtained from **Figure 3.18**.

3.8 SEMIQUANTITATIVE ANALYSIS OF MAPKS

After it was corroborated that a sensing array composed of five SOX-peptides was capable of qualitatively recognizing the studied MAPKs, the semiquantitative determination of mixtures of MAPK groups was explored. MAPKs are intrinsically found in different concentrations in complex mixtures such as cell lysates. In addition, uncontrolled activity of upper kinases can lead to overexpression of aberrant MAPKs, causing altered kinase concentrations. A semiquantitative assay with structurally related MAPK groups was investigated *in vitro* by using a mixture of three MAPKs at different nanomolar concentrations.

3.8.1 Detecting Increasing ERK1 Concentrations

The aforementioned peptide-based sensing ensemble was used to detect increasing concentrations of ERK1 in the presence of fixed concentrations of JNK3 and p38γ. The plate layout of the sensing ensemble for each SOX-peptide and the mixture of ERK1, JNK3 and p38γ analytes is shown in **Figure 3.20**. For this kinase assay, eight kinase solutions were prepared using the following fixed concentration of JNK3 (10 nM) and p38γ (5 nM). Each kinase stock was prepared with increasing concentrations of ERK1 as described in the supplementary information. The following final concentrations of ERK1 were estimated in each well as follows 0 nM, 0.05 nM, 0.1 nM, 0.2 nM, 0.4 nM, 0.8 nM, 1.6 nM and 3.2 nM ERK1 in the presence of JNK3 (5 nM) and p38γ (2.5 nM). The SOX-peptide concentrations were correspondingly used for this assay as previously described.

Sensing Array to Semi-quantitatively Detect Increasing [ERK1] in the Presence of JNK3 and p38γ										
	Well plate	1	2	3	4	5	6	7	8	9
	Analyte nM	**ERK = 0** JNK = 5 p38 = 2.5	**ERK = 0.05** JNK = 5 p38 = 2.5	**ERK = 0.1** JNK = 5 p38 = 2.5	**ERK = 0.2** JNK = 5 p38 = 2.5	**ERK = 0.4** JNK = 5 p38 = 2.5	**ERK = 0.8** JNK = 5 p38 = 2.5	**ERK = 1.6** JNK = 5 p38 = 2.5	**ERK = 3.2** JNK = 5 p38 = 2.5	Buffer
SOX-Sub-F	A	*Smix= 25 Pep= 20 ATP=5*	*Smix= 25 Pep= 20 ATP=5*	*Smix= 25 Pep= 20 ATP=5*	*Smix= 25 Pep= 20 ATP=5*	*Smix= 25 Pep= 20 ATP=5*	*Smix= 25 Pep= 20 ATP=5*	*Smix= 25 Pep= 20 ATP=5*	*Smix= 25 Pep= 20 ATP=5*	B= 50
	B	*Smix= 25 Pep= 20 ATP=5*	*Smix= 25 Pep= 20 ATP=5*	*Smix= 25 Pep= 20 ATP=5*	*Smix= 25 Pep= 20 ATP=5*	*Smix= 25 Pep= 20 ATP=5*	*Smix= 25 Pep= 20 ATP=5*	*Smix= 25 Pep= 20 ATP=5*	*Smix= 25 Pep= 20 ATP=5*	B= 50
	C	*Smix= 25 Pep= 20 ATP=5*	*Smix= 25 Pep= 20 ATP=5*	*Smix= 25 Pep= 20 ATP=5*	*Smix= 25 Pep= 20 ATP=5*	*Smix= 25 Pep= 20 ATP=5*	*Smix= 25 Pep= 20 ATP=5*	*Smix= 25 Pep= 20 ATP=5*	*Smix= 25 Pep= 20 ATP=5*	B= 50
	D	*Smix= 25 Pep= 20 ATP=5*	*Smix= 25 Pep= 20 ATP=5*	*Smix= 25 Pep= 20 ATP=5*	*Smix= 25 Pep= 20 ATP=5*	*Smix= 25 Pep= 20 ATP=5*	*Smix= 25 Pep= 20 ATP=5*	*Smix= 25 Pep= 20 ATP=5*	*Smix= 25 Pep= 20 ATP=5*	B= 50

Figure 3.20: *Schematic representation of the sensing ensemble.* Sensing array for the semi-quantitatively detection of increasing ERK1 concentration in the presence of JNK3 and p38γ with SOX-Sub-F peptide.

3.8.1.1 Analyzing Kinetic Data

An average of the four experimental replicates was obtained for each ERK1-catalyzed reaction at each different concentration to clearly visualize the kinetic trend with each SOX-peptide. In contrast, the rate constants were individually obtained from each replicate using the same equation. The fluorescence endpoint (F_∞) was obtained as an average value from the highest ERK-1 concentration (3.2 nM) for each SOX-peptide and this F_∞ value was considered a constrained variable. The resulting kinetic data in **Figure 3.21** was obtained from this array, showing emission changes that were dependent on increasing ERK1 concentration for three SOX-peptides. SOX-Sub-D peptide was initially phosphorylated by JNK3 and p38γ, showing an initial fluorescence increase at 0 nM of ERK1 concentration (**Figure 3.21A**). The rate of phosphorylation was clearly

enhanced after the addition of 0.2 nM ERK1, reaching saturation after 0.4 nM concentration. SOX-MEF2A was also firstly phosphorylated by JNK3 and p38γ. A slower fluorescence increase was observed upon addition of increasing ERK1 concentration with respect to SOX-Sub-D (**Figure 3.21B**). Saturation kinetics were achieved in the presence of 1.6 nM ERK1 concentration. These results were consistent with the previously obtained kinetic data where the five SOX-peptides were phosphorylated by individual MAPK groups. SOX-Sub-F presented a similar kinetic trend with respect to SOX-Sub-D and MEF2A peptides, showing a continuous enhancement of the fluorescence signal (**Figure 3.21C**). However, the initial fluorescence of SOX-Sub-F was higher at 0 nM ERK concentration, suggesting that the peptide was efficiently phosphorylated by p38γ. In contrast, SOX-NFAT4 and SOX-p38 peptides showed high specificity for JNK3 and p38γ, respectively. Thus, no change in the rate of phosphorylation was observed for these peptides (supplementary information **Figure 3.57**).

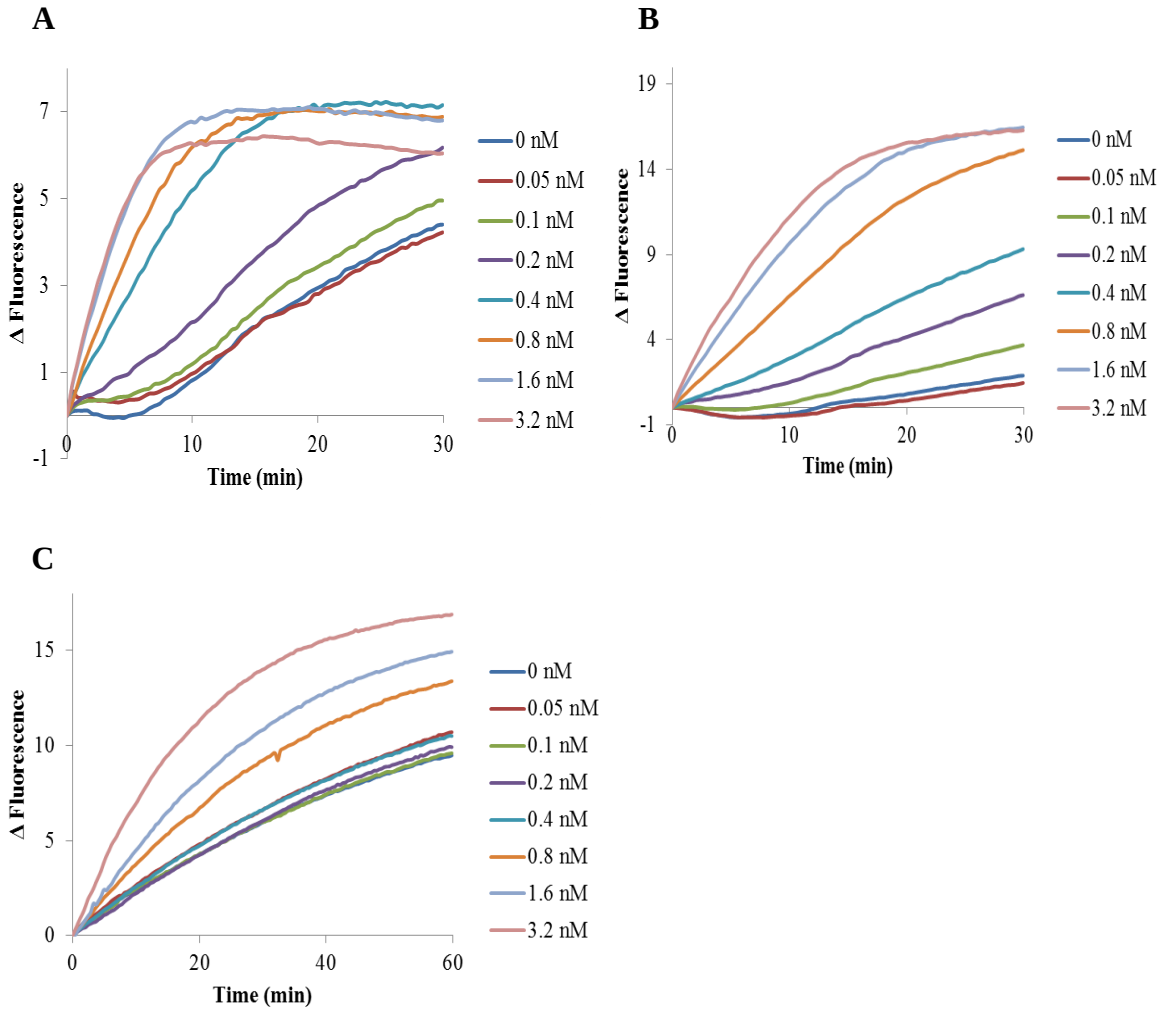

Figure 3.21: *Kinetic plots showing emission changes as a function of phosphorylated SOX-Sub-D, SOX-MEF2A and SOX-Sub-F peptides at different ERK1 concentrations in the presence of fixed JNK3 and p38γ concentrations.* (A) Fluorescence increase of SOX-Sub-D peptide. (B) Fluorescence increase of SOX-MEF2A peptide. (C) Fluorescence increase of SOX-Sub-F peptide. Final ERK1 concentrations: 0 nM, 0.05 nM, 0.1 nM, 0.2 nM, 0.4 nM, 0.8 nM, 1.6 nM and 3.2 nM. Final fixed concentrations of JNK3 (5 nM) and p38γ (2.5 nM). Sox-Sub-D, SOX-MEF2A, and SOX-Sub-F (2 µM). Data collected with 96-well plate half area, plate reader with λ_{ex} filter of 340 ± 35 nm and λ_{em} filter of 485 ± 20 nm. Assay buffer: (25mM HEPES, 50mM KCl, 0.1 mM EDTA, 0.1 mM EGTA pH 7.4) with 2 mM DTT, 2.5 µg/mL BSA, 5mM $MgCl_2$, 500 µM ATP at 25°C.

3.8.1.2 Semiquantitative Analysis Using Pattern Recognition

From the aforementioned kinetic data, rate constants and fluorescence values at 20 minutes were obtained. This sensing array enabled the semiquantitative detection of a mixture of kinases at different concentrations. The LDA plot in **Figure 3.22A** was acquired from this sensing ensemble, showing a progression of the concentration changes in the array response. Interestingly, the LDA plot showed a strong dependence of the kinetic response on the increasing concentrations of ERK1. This LDA plot presumably showed the amount of ERK1 concentration in the presence of other MAPKs, displaying 82.09% of differentiation along the F1 axes, and 17.59% of separation along the F2 axes. The LDA plot was obtained with 100% jack-knife analysis. Interestingly, the previously discussed kinetic trends in **Figure 3.21** were represented by the discriminating variables from this array. The corresponding loading plot (**Figure 3.22B**) indicated that the discriminating variables from SOX-Sub-D, SOX-MEF2A and SOX-Sub-F similarly contributed to the concentration trend, whereas variables from SOX-NFAT4 and SOX-p38 peptides mainly contributed to concentration discrimination. The cross-reactive properties of this array demonstrated its capability to detect minor changes of the concentration of ERK1 in the presence of other MAPK groups. This sensing array presumably could be used for further quantitative determinations.

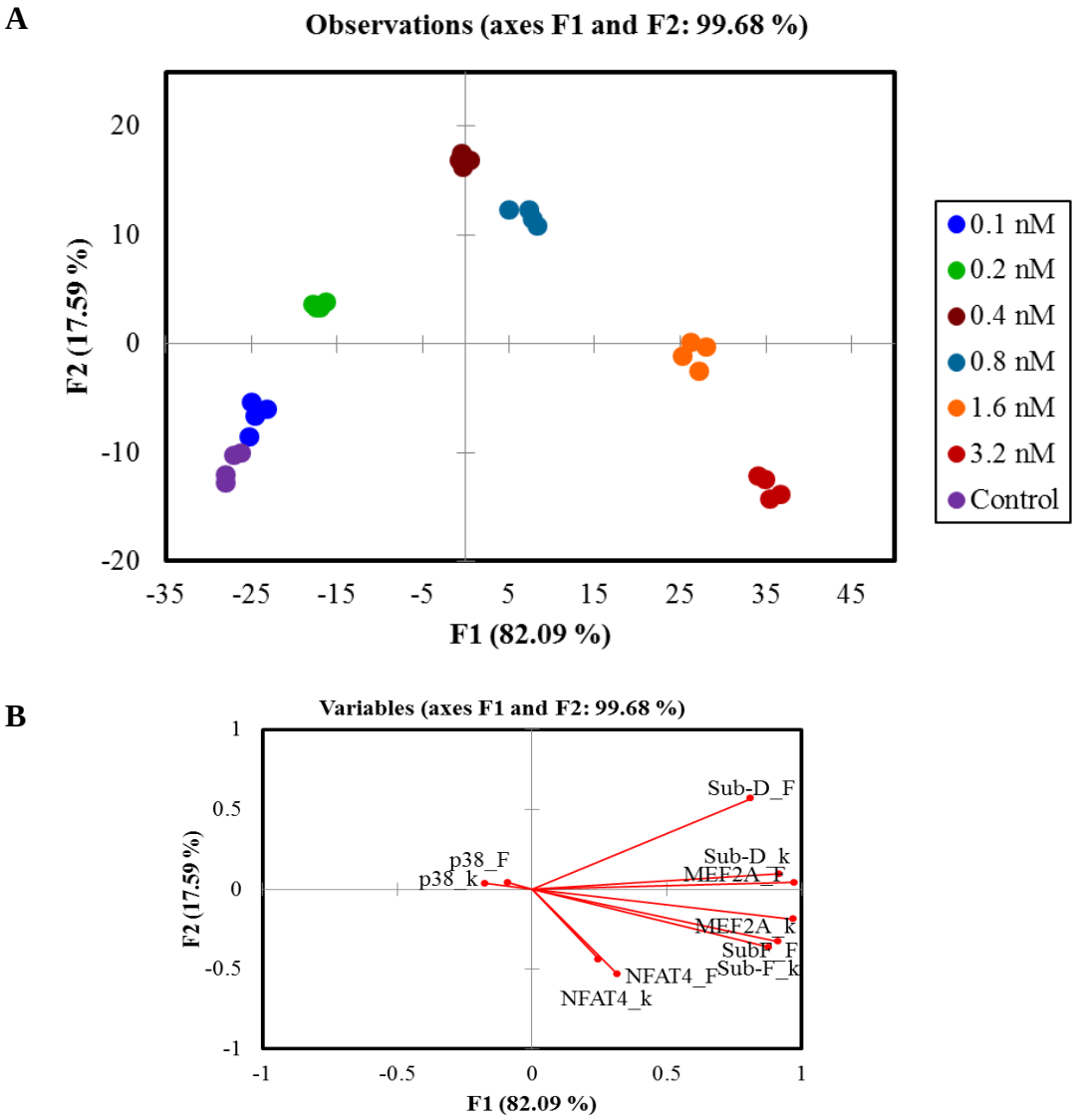

Figure 3.22: *LDA score plot of the kinetic response pattern from the SOX-peptides showing in vitro differentiation of ERK1 concentration changes in the presence of JNK3 and p38γ MAPKs.* (A) LDA plot and (B) loading plot showing 100% jack-knife analysis. Final ERK1 concentrations: 0 nM, 0.05 nM, 0.1 nM, 0.2 nM, 0.4 nM, 0.8 nM, 1.6 nM and 3.2 nM. Final fixed concentrations of JNK3 (5 nM) and p38γ (2.5 nM). Sox-Sub-D, SOX-MEF2A, and SOX-Sub-F (2 µM). Sox-peptides (2 µM). SOX-p38 peptide (8 µM). Data collected with 96-well plate half area, plate reader with λ_{ex} filter of 340 ± 35 nm and λ_{em} filter of 485 ± 20 nm. Assay buffer: (25mM HEPES, 50mM KCl, 0.1 mM EDTA, 0.1 mM EGTA pH 7.4) with 2 mM DTT, 2.5 µg/mL BSA, 5mM $MgCl_2$, 500 µM ATP at 25℃.

3.8.2 Detecting Increasing JNK3 Concentrations

The aforementioned sensing ensemble was also followed to detect increasing concentrations of JNK3 in the presence of ERK1 and p38γ. The following final concentrations of JNK3 were used in each well as follows 0, 0.5, 1, 2, 4, 8, 16 and 32 nM JNK-3 in the presence of 0.5 nM ERK1 and 2.5 nM p38γ. Four replicates were also performed for each JNK3-catalyzed reaction at each different concentration. The fluorescence endpoint was similarly obtained by using the previously described procedure. The kinetic data in **Figure 3.23** was acquired from this sensing array. Fluorescence changes of SOX-NFAT4 peptide were primarily observed by increasing JNK3 concentration. In contrast, the remaining SOX-peptides showed no fluorescence changes. SOX-MEF2A and SOX-Sub-D were efficiently phosphorylated by ERK1, showing saturation at 0 nM JNK3 concentration. Thus, no fluorescence changes were observed upon addition of JNK3 concentration. As expected no fluorescence increase of SOX-Sub-F was observed at high JNK3 concentration (supplementary information **Figure 3.49B**). This result strongly confirmed the lack of the F-recruitment site in the JNK group. In addition, SOX-p38 was initially phosphorylated by p38γ, showing no changes upon addition of JNK3.

A

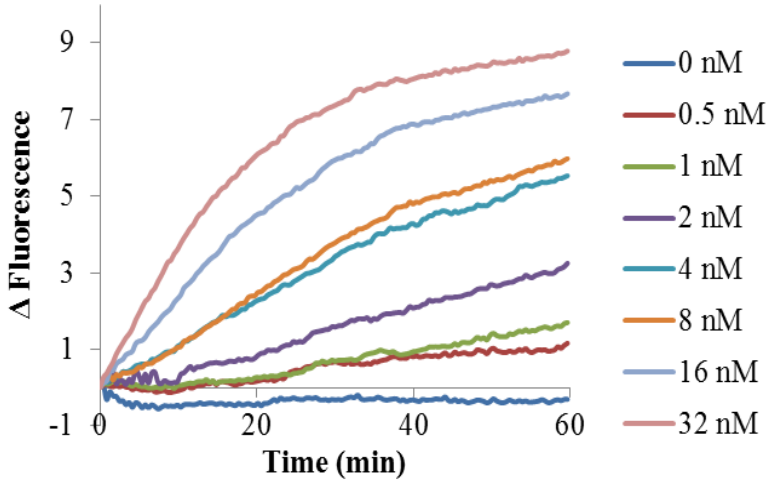

B

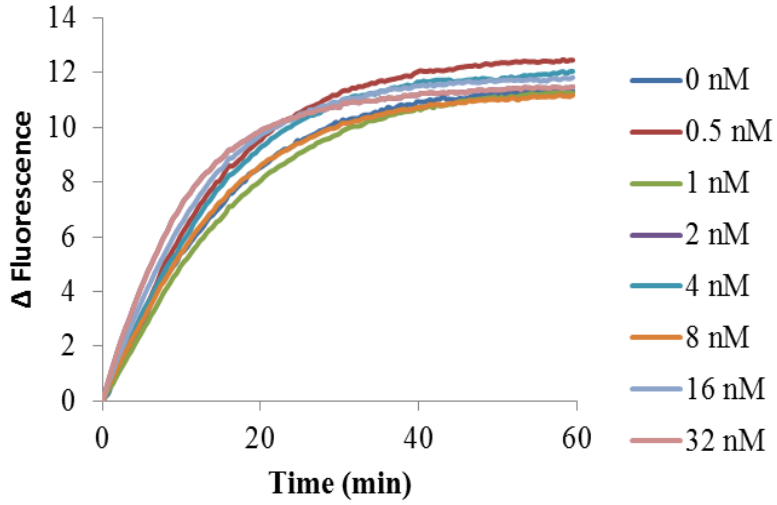

Figure 3.23: *Kinetic plots showing emission changes as a function of phosphorylated SOX-NFAT4 and SOX-MEF2A at different JNK3 concentrations in the presence of fixed ERK1 and p38γ concentrations.* (A) *Fluorescence* increase *of SOX-NFAT4 peptide*. (B) *Fluorescence* increase *of SOX-MEF2A peptide.* Final JNK3 concentrations: 0 nM, 0.5 nM, 1 nM, 2 nM, 4 nM, 8 nM, 16 nM and 32 nM. Final fixed concentrations of ERK (0.5 nM) and p38γ (2.5 nM). Sox-NFAT4 and SOX-MEF2A (2 µM). Data collected with 96-well plate half area, plate reader with λ_{ex} filter of 340 ± 35 nm and λ_{em} filter of 485 ± 20 nm. Assay buffer: (25mM HEPES, 50mM KCl, 0.1 mM EDTA, 0.1 mM EGTA pH 7.4) with 2 mM DTT, 2.5 µg/mL BSA, 5mM $MgCl_2$, 500 µM ATP at 25°C.

Unfortunately, most of the SOX-peptides were initially phosphorylated by either ERK1 or p38γ. Therefore, no differentiation was obtained from the rates of phosphorylation and fluorescence values at 20 min. The LDA plot in **Figure 3.24** showed that separation of each JNK3 concentration was only obtained along the F1 axes (100%). The use of additional cross-reactive peptides would be required to improve the discriminant properties of the array.

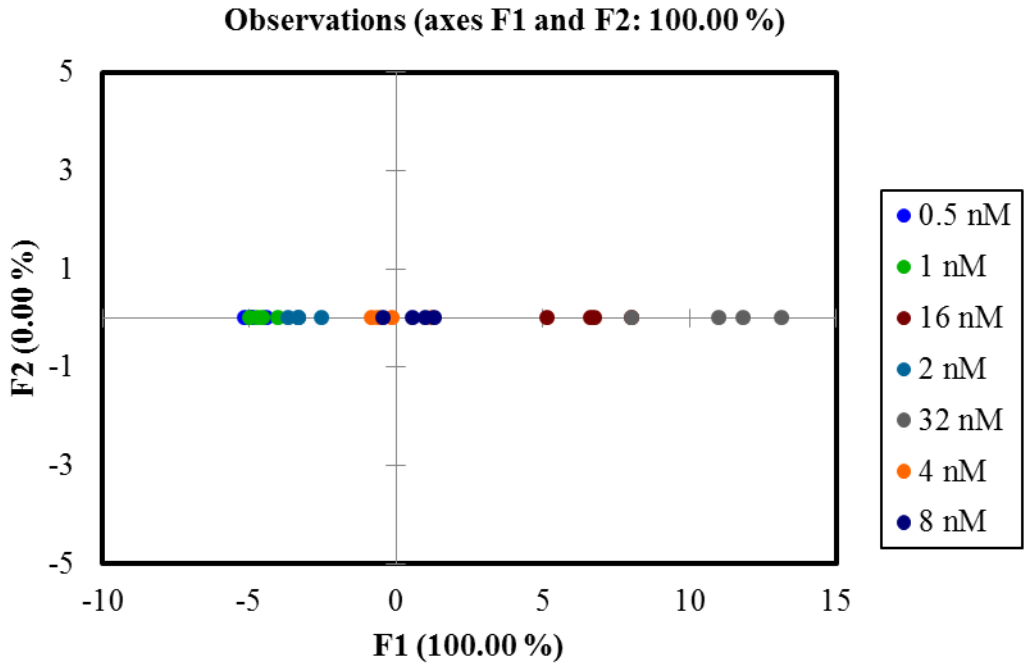

Figure 3.24: *LDA score plot of the kinetic response pattern from the SOX-peptides with increasing JNK3 concentrations in the presence of ERK1 and p38γ MAPKs.* Final JNK3 concentrations: 0 nM, 0.5 nM, 1 nM, 2 nM, 4 nM, 8 nM, 16 nM and 32 nM. Final fixed concentrations of ERK (0.5 nM) and p38γ (2.5 nM). Sox-peptides (2 µM) and SOX-p38 peptide (8 µM). Data collected with 96-well plate half area, plate reader with λ_{ex} filter of 340 ± 35 nm and λ_{em} filter of 485 ± 20 nm. Assay buffer: (25mM HEPES, 50mM KCl, 0.1 mM EDTA, 0.1 mM EGTA pH 7.4) with 2 mM DTT, 2.5 µg/mL BSA, 5mM $MgCl_2$, 500 µM ATP at 25°C.

3.8.3 Detecting Increasing p38γ Concentrations

The same sensing array was used to explore the semiquantitative detection of p38γ MAPK in the presence of ERK1 and JNK3. The p38γ kinase was used in each well at concentrations of 0 nM, 0.25 nM, 0.5 nM, 1 nM, 2 nM, 4 nM, 8 nM, and 16 nM in the presence of ERK1 (0.5 nM) and JNK3 (5 nM). Each p38γ-catalyzed reaction at each different kinase concentration was replicated four times. The fluorescence endpoint was obtained as previously described. The kinetic data in **Figure 3.25** was acquired from this array. SOX-Sub-F was initially phosphorylated by ERK1, showing an initial fluorescence change at 0 nM p38γ. However, the fluorescence intensity was clearly enhanced by increasing concentrations of p38γ, showing saturation at 8 nM concentration (**Figure 3.25A**). Interestingly, SOX-NFAT4 peptide presented a modest fluorescent enhancement after the addition of 0.5 nM concentration of p38γ (**Figure 3.25B**). This result suggested that SOX-NFAT4 was presumably recognized by the D-recruitment site of both JNK3 and p38γ which present close structural similarities at the DRS. In contrast, the resulting kinetic assays showed that the phosphorylation reaction of SOX-p38 was efficiently catalyzed by p38γ MAPK, showing high specificity for this peptide substrate. The p38γ-catalyzed reaction of SOX-p38 peptide showed continuous fluorescence changes with increasing p38γ concentrations (**Figure 3.25C**).

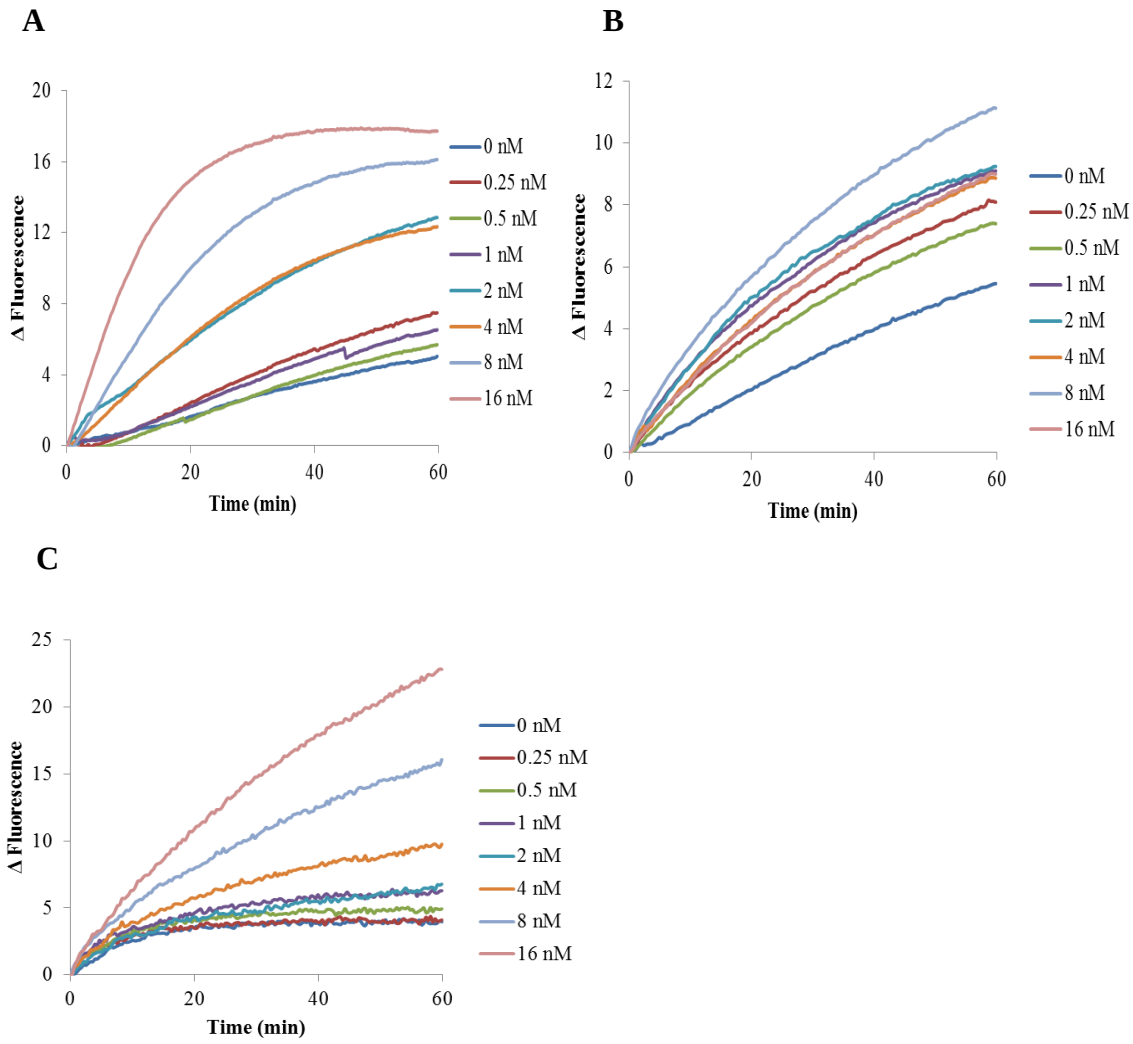

Figure 3.25: *Kinetic plots showing emission changes as a function of phosphorylated SOX-peptides at different p38γ concentrations in the presence of fixed ERK1 and JNK3 concentrations.* (A) Fluorescence increase of SOX-Sub-F peptide. (B) Fluorescence increase of SOX-NFAT4 peptide. (C) Fluorescence increase of SOX-p38 peptide. Final p38γ concentrations: 0 nM, 0.25 nM, 0.5 nM, 1 nM, 2 nM, 4 nM, 8 nM, and 16 nM. Final fixed concentrations: ERK (0.5 nM), and JNK3 (5 nM). SOX-Sub-F and Sox-NFAT4 (2 µM); SOX-p38 peptide (8 µM). Data collected with 96-well plate half area, plate reader with λ_{ex} filter of 340 ± 35 nm and λ_{em} filter of 485 ± 20 nm. Assay buffer: (25mM HEPES, 50mM KCl, 0.1 mM EDTA, 0.1 mM EGTA pH 7.4) with 2 mM DTT, 2.5 µg/mL BSA, 5mM $MgCl_2$, 500 µM ATP at 25°C.

3.8.3.1 Semiquantitative Detection of p38γ Using Pattern Recognition

The rate constants and fluorescence values at 20 minutes were obtained from the previously discussed kinetic data. The LDA plot in **Figure 3.26A** was acquired from this sensing ensemble, showing a modest progression of the concentration changes in the array response. Most of the data was classified along the F1 axes with 96.75% of the variance, and 2.58% of the variance along the F2 axes. The rate of phosphorylation of the SOX-peptides was quite similar from 0 to 4 nM p38γ concentrations, showing overlap of the concentration sets on the left side of the LDA plot. The clusters were classified with 59.38% jack-knife analysis due to the high similarity of the kinetic data at low concentrations. However, concentrations at 8 nM and 16 nM were differentiated from the other sets along the F1 axes, suggesting modest dependence of the kinetic response on increasing p38γ concentrations. The corresponding loading plot in **Figure 3.26B** was obtained. Most of the discriminating variables equally contributed to the modest concentration trend.

These semiquantitative kinase assays showed that this sensing array best detected nanomolar concentration changes of ERK1 in the presence of JNK3 and p38γ using a pattern recognition approach. The semiquantitative detection of the progression of the concentration changes was effectively followed by using the kinetic response of the SOX-peptides with increasing ERK1 concentrations. Nevertheless, no differentiation of JNK3 concentration changes was achieved due to the immediate response from the SOX-peptides to ERK1. A modest trend of p38γ concentration changes was also detected by

using this array. It should be pointed out, however, that this kinase assay could potentially be optimized to improve the differentiation patterns by adding more discriminating variables to the sensing ensemble.

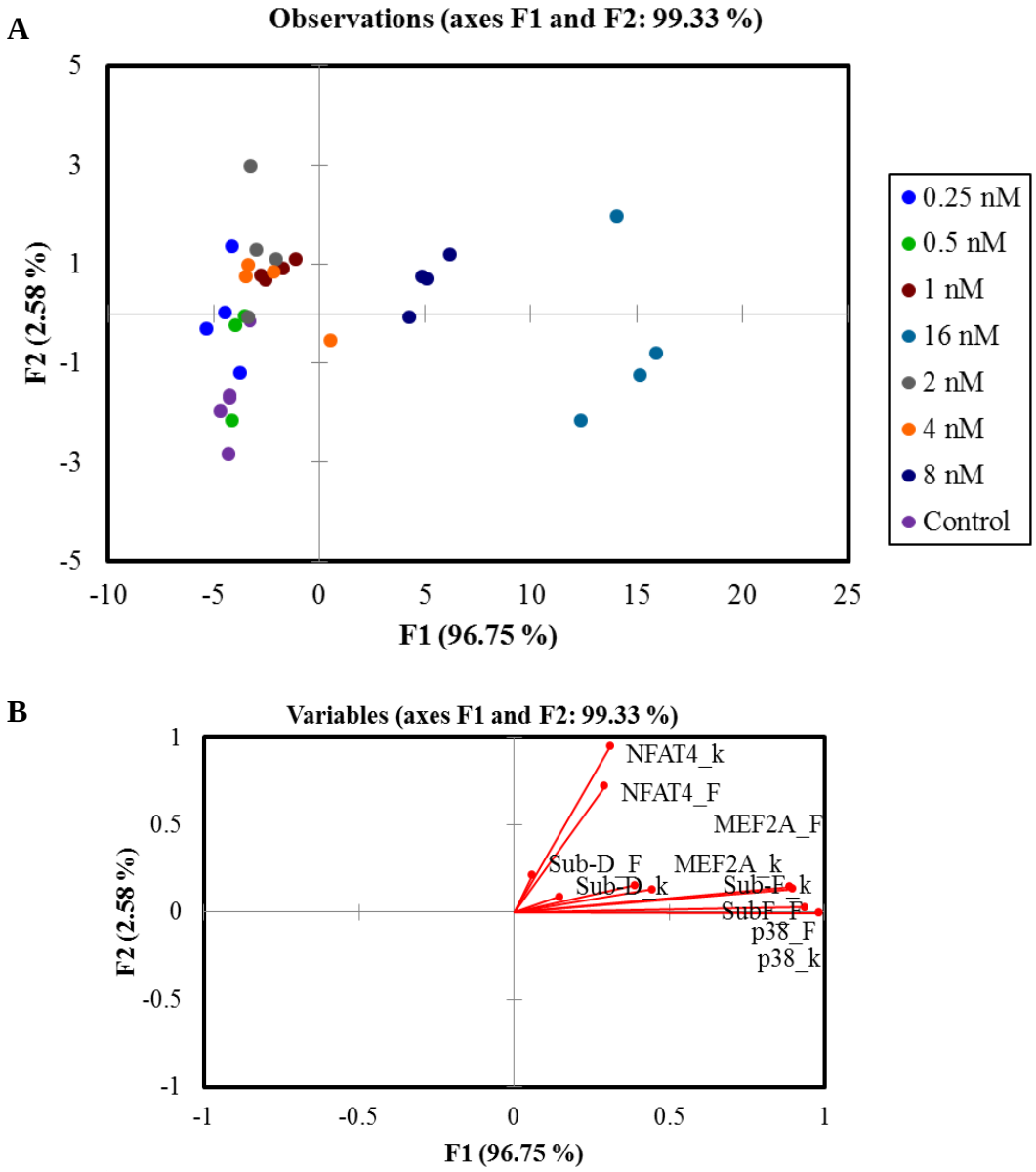

Figure 3.26: *LDA score plot of the kinetic response pattern from the SOX-peptides showing modest differentiation of p38γ concentration changes in the presence of ERK1 and JNK3.* (A) LDA plot with eight *p38γ* concentrations. (B) Corresponding loading plot for (A). Final p38γ concentrations: 0 nM, 0.25 nM, 0.5 nM, 1 nM, 2 nM, 4 nM, 8 nM, and 16 nM. Final fixed concentrations: ERK (0.5 nM), and JNK3 (5 nM). SOX-peptides (2 µM); SOX-p38 peptide (8 µM). Data collected with 96-well plate half area, plate reader with λ_{ex} filter of 340 ± 35 nm and λ_{em} filter of 485 ± 20 nm. Assay buffer: (25mM HEPES, 50mM KCl, 0.1 mM EDTA, 0.1 mM EGTA pH 7.4) with 2 mM DTT, 2.5 µg/mL BSA, 5mM $MgCl_2$, 500 µM ATP at 25°C.

3.9 DETECTION OF INHIBITION KINETICS OF ERK1

A variety of small-molecule inhibitors have been developed to regulate the uncontrolled activity of the ERK pathway as described in Chapter 1. Pharmaceutical companies can screened over 2000 compounds involved in a cascade kinase assay to discover the initial efficiency of these inhibitors.[132] However, few detection methods can be applied for high-throughput screening to rapidly investigate the *in vitro* activity of several kinases or mixtures of kinases. Herein, a semiquantitative kinase assay was investigated to explore the inhibition of ERK1 activity by using the previously described sensing array.

3.9.1 VX-11e Inhibitor for ERKs

Aronov *et al.* recently reported the synthesis of a potent pyrimidylpyrrole ERK inhibitor called VX-11e (**3.20**).[133] The selectivity of **3.20** was assessed for kinases ERK2, Glycogen synthase kinase 3 (GSK3), cyclin-dependent kinase 2 (CDK2) and Aurora A. Compound **3.20** was found to present good selectivity for ERK2 with respect to the other kinases, showing a binding affinity of K_I < 2 nM. This inhibitor was used to show the utility of this sensing ensemble to differentiate inhibition kinetics of ERK1 alone, and ERK1 in the presence of other MAPK sub-families. Thus, a preliminary semiquantitative assay was initially performed *in vitro* with ERK1 in the presence of VX-11e inhibitor at different nanomolar concentrations. Subsequently, a second assay was performed to

detect the reduced activity of ERK1 in the presence of JNK3 and p38γ with increasing VX-11e inhibitor concentrations.

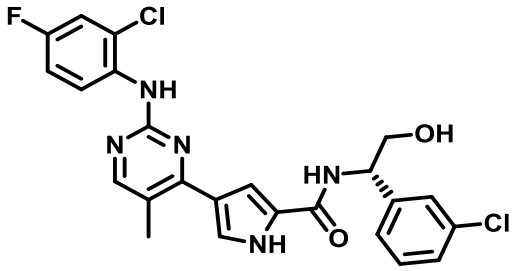

3.20

3.9.2 Sensing Array Using VX-11e Inhibitor

A quick preliminary assay was performed with this sensing ensemble to investigate the performance of the inhibitor at the chosen concentrations. This array was first used to detect the decreased activity of ERK1 with increasing VX-11e concentrations. The same SOX-peptide concentrations were correspondingly used for this assay. The plate layout of the sensing ensemble for each SOX-peptide is shown in **Figure 3.27**, presenting the corresponding inhibitor concentrations. For this kinase assay, stock solutions were prepared to obtain a final concentration of ERK1 (0.5 nM) in each well. Inhibitor stock solutions were separately prepared with increasing concentrations of **3.20** as described in supplementary information to obtain a final concentration of 0 nM, 1 nM, 8 nM, 16 nM, and 48 nM in each well. These concentrations were chosen based on the binding affinity K_I < 2 nM of the inhibitor.

ERK-1 inhibitor sensing array_ SOX-Sub-D peptide with ERK1								
	Well	1	2	3	4	5	6	7
	[Analyte] nM	**Inh = 0** ERK = 0.5	**Inh = 1** ERK = 0.5	**Inh = 8** ERK = 0.5	**Inh = 16** ERK = 0.5	**Inh = 48** ERK = 0.5	Buffer	Supermix
SOX Sub-D	A	*Pep= 20 Smix= 15 Inh = 10 ATP=5*	*Pep= 20 Smix= 15 Inh = 10 ATP=5*	*Pep= 20 Smix= 15 Inh = 10 ATP=5*	*Pep= 20 Smix= 15 Inh = 10 ATP=5*	*Pep= 20 Smix= 15 Inh = 10 ATP=5*	B= 50	*B =30 Smix= 15 ATP=5*
	B	*Pep= 20 Smix= 15 Inh = 10 ATP=5*	*Pep= 20 Smix= 15 Inh = 10 ATP=5*	*Pep= 20 Smix= 15 Inh = 10 ATP=5*	*Pep= 20 Smix= 15 Inh = 10 ATP=5*	*Pep= 20 Smix= 15 Inh = 10 ATP=5*	B= 50	*B =30 Smix= 15 ATP=5*
	C	*Pep= 20 Smix= 15 Inh = 10 ATP=5*	*Pep= 20 Smix= 15 Inh = 10 ATP=5*	*Pep= 20 Smix= 15 Inh = 10 ATP=5*	*Pep= 20 Smix= 15 Inh = 10 ATP=5*	*Pep= 20 Smix= 15 Inh = 10 ATP=5*	B= 50	*B =30 Smix= 15 ATP=5*
	D	*Pep= 20 Smix= 15 Inh = 10 ATP=5*	*Pep= 20 Smix= 15 Inh = 10 ATP=5*	*Pep= 20 Smix= 15 Inh = 10 ATP=5*	*Pep= 20 Smix= 15 Inh = 10 ATP=5*	*Pep= 20 Smix= 15 Inh = 10 ATP=5*	B= 50	*B =30 Smix= 15 ATP=5*

Figure 3.27: *Schematic representation of the sensing ensemble.* Sensing array for the semi-quantitatively detection of decreasing ERK1 activity by inhibition of VX-11e.

3.9.3 Differentiating Inhibition of ERK1

The four experimental replicates of each inhibitor concentration were used to obtain the corresponding rate constants and fluorescence values at 20 minutes. The resulting kinetic data shown in **Figure 3.28** was obtained from this sensing array, showing fluorescence changes that were dependent on inhibition concentrations. As expected, SOX-MEF2A and SOX-Sub-D peptides were efficiently phosphorylated by ERK1, showing saturation at the given concentration. The addition of increasing inhibitor concentrations decreased the rate of phosphorylation which was represented by a gradual drop of the fluorescence signal (**Figure 3.28A and B**). SOX-Sub-F showed an analogous diminution of the rate and a corresponding modest fluorescence drop (**Figure 3.28C**).

However, no fluorescence changes were observed for SOX-NFAT4 and SOX-p38 SOX-NFAT4 and SOX-p38 (supporting information). The LDA plot in **Figure 3.29A** was obtained with this array. A modest progression of the inhibition changes was observed in the plot. The group without inhibition (0 nM) was located on the bottom right quadrant, whereas the remaining groups were gradually placed on the right side of the LDA plot. The data was differentiated with 83.83% of the variance along the F1 axes, and 16.17% of the variance along the F2 axes. Although, the LDA presented 100% jack-knife analysis, considerable scattering was found within the analyte replicates. The corresponding loading plot in **Figure 3.29B** indicated the contribution of the SOX-peptides to the differentiation of the inhibitor concentrations. The discriminating variables obtained from SOX-Sub-D, SOX-MEF2A and SOX-Sub-F peptides mainly contributed to the concentration trend, whereas variables obtained from SOX-NFAT4 and SOX-p38 peptides contributed to the differentiation. The discriminating properties of this sensing ensemble enable the detection of inhibition changes in the catalytic activity of ERK1. This sensing array presumably could be used for the detection of ERK inhibition in the presence of other MAPK groups.

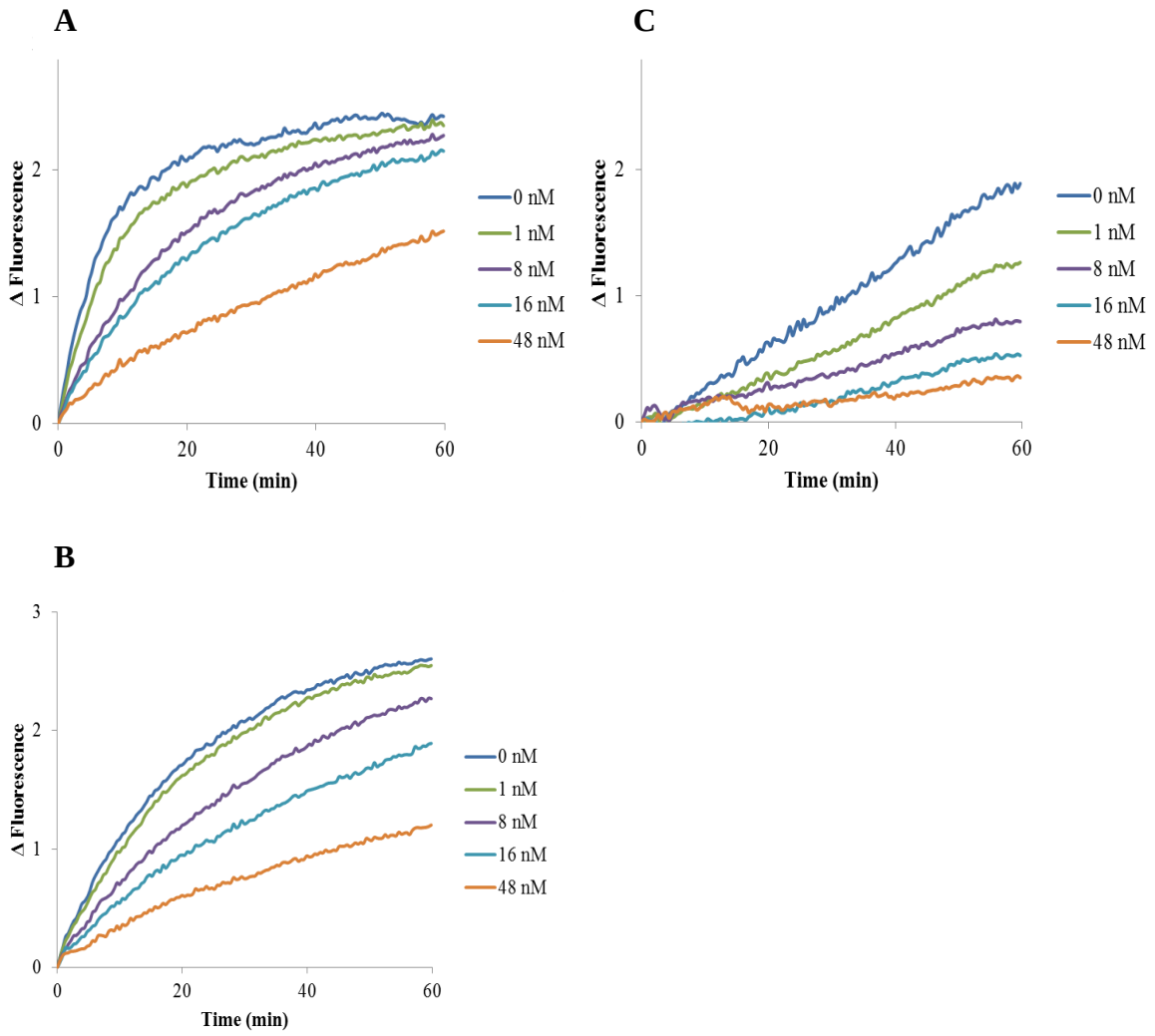

Figure 3.28: *Kinetic data showing the average of 4 experimental replicates of ERK-inhibitor concentrations.* (A) Fluorescence changes of SOX-MEF2A peptide. (B) Fluorescence changes of SOX-Sub-D peptide. (C) Fluorescence changes of SOX-Sub-F peptide. Inhibitor concentrations: 0 nM, 1 nM, 8 nM, 16 nM, and 48 nM. Fixed concentration: ERK1 (0.5 nM). Sox-MEF2A, SOX-Sub-F and SOX-Sub-D (2 µM). Data collected with 96-well plate half area, plate reader with λ_{ex} filter of 340 ± 35 nm and λ_{em} filter of 485 ± 20 nm. Assay buffer: (25mM HEPES, 50mM KCl, 0.1 mM EDTA, 0.1 mM EGTA pH 7.4) with 2 mM DTT, 2.5 µg/mL BSA, 5mM $MgCl_2$, 500 µM ATP at 25°C.

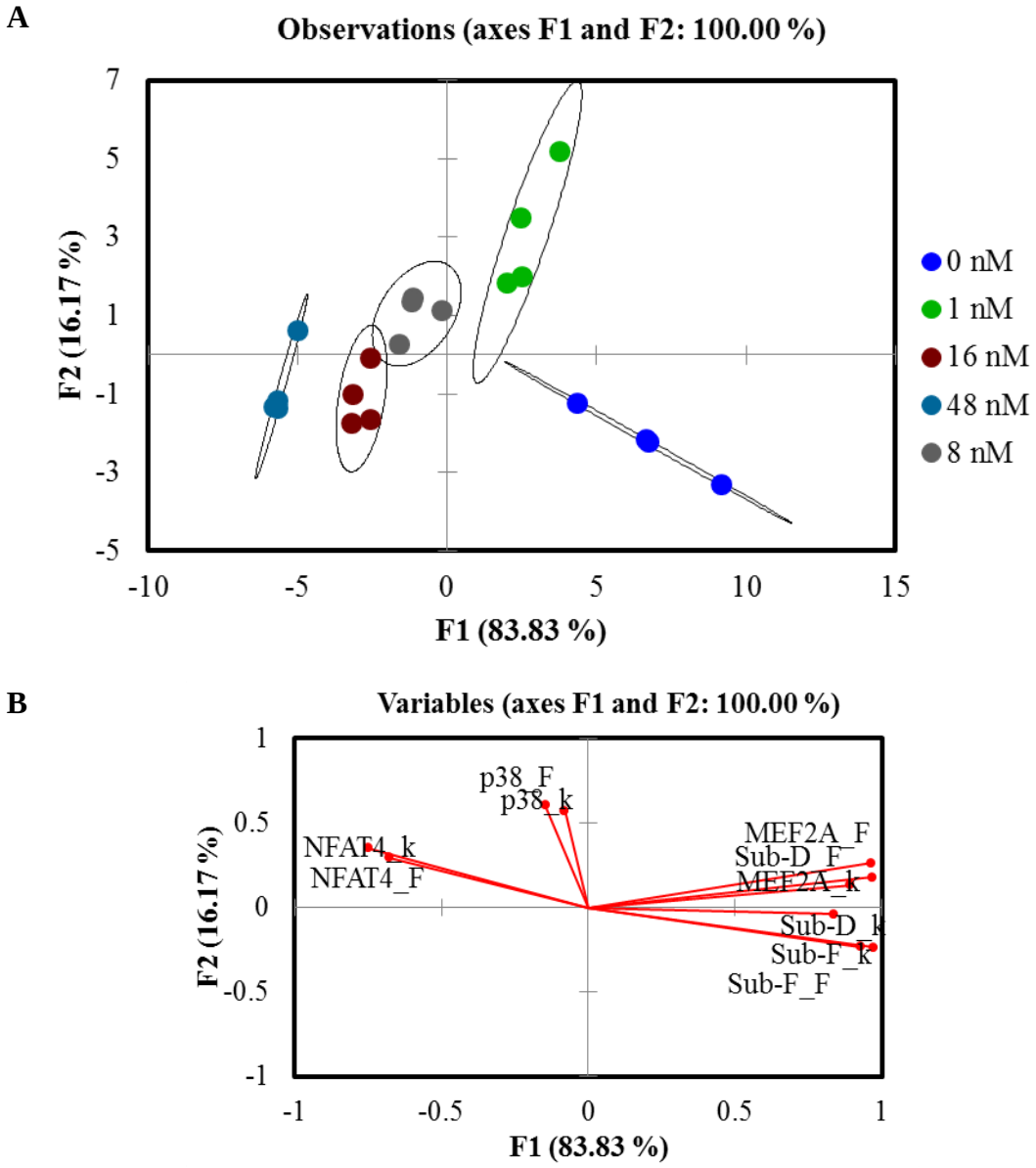

Figure 3.29: *LDA score plots of the kinetic response pattern from the SOX-peptides showing inhibition of ERK1 activity.* (A) LDA plot with ERK-inhibitor concentrations, showing 100% jack-knife analysis. (B) Corresponding loading plot for (A). Inhibitor concentrations: 0 nM, 1 nM, 8 nM, 16 nM, and 48 nM. Fixed concentration: ERK1 (0.5 nM). Sox-peptides (2 µM) and SOX-p38 peptide (8 µM). Data collected with 96-well plate half area, plate reader with λ_{ex} filter of 340 ± 35 nm and λ_{em} filter of 485 ± 20 nm. Assay buffer: (25mM HEPES, 50mM KCl, 0.1 mM EDTA, 0.1 mM EGTA pH 7.4) with 2 mM DTT, 2.5 µg/mL BSA, 5mM $MgCl_2$, 500 µM ATP at 25℃.

3.9.4 Detecting ERK1 Inhibition in Kinase Mixtures

In an effort to demonstrate the additional utility of this sensing array, the following kinase assay was performed to detect the inhibition of ERK1 activity in the presence of JNK3 and p38γ. The plate layout of the sensing ensemble for each SOX-peptide is shown in **Figure 3.30**, presenting the corresponding inhibitor concentrations with ERK1, JNK3 and p38γ analyte concentrations. The stock solutions were prepared to obtain a final concentration of ERK1 (0.5 nM), JNK3 (5 nM) and p38γ (2.5 nM) in each well. Additional inhibitor stocks were separately prepared with increasing concentrations of **3.20** as described in supplementary information to obtain a final concentration of 0 nM, 1 nM, 2 nM, 3 nM, 4 nM, 8 nM, 16 nM, and 48 nM in each well.

ERK-1 inhibitor sensing array_ SOX-Sub-D peptide with ERK1, JNK3 and p38γ										
	Well	1	2	3	4	5	6	7	8	9
	[Analyte] nM	**Inh = 0** ERK = 0.5 JNK = 5 P38 = 2.5	**Inh = 1** ERK = 0.5 JNK = 5 P38 = 2.5	**Inh = 2** ERK = 0.5 JNK = 5 P38 = 2.5	**Inh =3** ERK = 0.5 JNK = 5 P38 = 2.5	**Inh = 4** ERK = 0.5 JNK = 5 P38 = 2.5	**Inh = 8** ERK = 0.5 JNK = 5 P38 = 2.5	**Inh = 16** ERK = 0.5 JNK = 5 P38 = 2.5	**Inh = 48** ERK = 0.5 JNK = 5 P38 = 2.5	Buffer
SOX Sub-D	A	*Pep= 20* *Smix= 15* *Inh = 10* *ATP=5*	*Pep= 20* *Smix= 15* *Inh = 10* *ATP=5*	*Pep= 20* *Smix= 15* *Inh = 10* *ATP=5*	*Pep= 20* *Smix= 15* *Inh = 10* *ATP=5*	*Pep= 20* *Smix= 15* *Inh = 10* *ATP=5*	*Pep= 20* *Smix= 15* *Inh = 10* *ATP=5*	*Pep= 20* *Smix= 15* *Inh = 10* *ATP=5*	*Pep= 20* *Smix= 15* *Inh = 10* *ATP=5*	B= 50
	B	*Pep= 20* *Smix= 15* *Inh = 10* *ATP=5*	*Pep= 20* *Smix= 15* *Inh = 10* *ATP=5*	*Pep= 20* *Smix= 15* *Inh = 10* *ATP=5*	*Pep= 20* *Smix= 15* *Inh = 10* *ATP=5*	*Pep= 20* *Smix= 15* *Inh = 10* *ATP=5*	*Pep= 20* *Smix= 15* *Inh = 10* *ATP=5*	*Pep= 20* *Smix= 15* *Inh = 10* *ATP=5*	*Pep= 20* *Smix= 15* *Inh = 10* *ATP=5*	B= 50
	C	*Pep= 20* *Smix= 15* *Inh = 10* *ATP=5*	*Pep= 20* *Smix= 15* *Inh = 10* *ATP=5*	*Pep= 20* *Smix= 15* *Inh = 10* *ATP=5*	*Pep= 20* *Smix= 15* *Inh = 10* *ATP=5*	*Pep= 20* *Smix= 15* *Inh = 10* *ATP=5*	*Pep= 20* *Smix= 15* *Inh = 10* *ATP=5*	*Pep= 20* *Smix= 15* *Inh = 10* *ATP=5*	*Pep= 20* *Smix= 15* *Inh = 10* *ATP=5*	B= 50
	D	*Pep= 20* *Smix= 15* *Inh = 10* *ATP=5*	*Pep= 20* *Smix= 15* *Inh = 10* *ATP=5*	*Pep= 20* *Smix= 15* *Inh = 10* *ATP=5*	*Pep= 20* *Smix= 15* *Inh = 10* *ATP=5*	*Pep= 20* *Smix= 15* *Inh = 10* *ATP=5*	*Pep= 20* *Smix= 15* *Inh = 10* *ATP=5*	*Pep= 20* *Smix= 15* *Inh = 10* *ATP=5*	*Pep= 20* *Smix= 15* *Inh = 10* *ATP=5*	B= 50

Figure 3.30: *Schematic representation of the sensing ensemble.* Sensing array for the semi-quantitatively detection of decreasing ERK1 activity by inhibition of VX-11e, in the presence of JNK3 and p38γ.

3.9.5 Inhibition Kinetics of ERK1 in Kinase Mixtures

The previously described protocol was followed to obtain the rate constants and fluorescence values at 20 minutes. For this experiment, however, the rate constants were obtained by using the fluorescence endpoints (F_∞) from the previously obtained kinetic data with increasing kinase (ERK1, JNK3 and p38γ) concentrations. For instance, an average fluorescence endpoint of F_∞ = 7228 was obtained for SOX-Sub-D peptide with ERK1 at 1.6 nM concentration (**Figure 3.21A**). SOX-MEF2A (**Figure 3.21B)** and SOX-Sub-F peptides **(Figure 3.21C)** yielded fluorescence endpoints of 16303 and 17903 with ERK1 at 3.2 nM concentration, respectively. In addition, a fluorescence endpoint of 8790 was found from the assay of SOX-NFAT4 peptide with 32 nM JNK3 (**Figure 3.23A**). Finally, a fluorescence endpoint of 22819 was found from the assay of SOX-p38 peptide with 16 nM p38γ (**Figure 3.25C**). The rate constants were then obtained from each kinetic replicate using the same equation, constraining the aforementioned final fluorescence values for each corresponding SOX-peptide. The resulting kinetic data in **Figure 3.31** was obtained from this array, showing emission changes that were dependent on increasing inhibitor concentration. SOX-MEF2A was mainly phosphorylated by ERK1, showing saturation at the given concentration in the presence of JNK3 and p38γ (**Figure 3.31A**). The rate of phosphorylation gradually decreased upon addition of increasing ERK-inhibitor concentrations. A comparable kinetic trend was observed with SOX-Sub-F, showing a modest fluorescence drop (**Figure 3.31B**). Interestingly, no fluorescence change was observed for SOX-Sub-D (**Figure 3.31C**). This result

corroborated with the reported high selectivity of the inhibitor which only affected the catalytic activity of ERK1, whereas no inhibition was observed for JNK3 even at high 48 nM inhibitor concentration. As expected, no significant fluorescence changes were observed for SOX-NFAT4 and SOX-p38 (supporting information **Figure 3.61**).

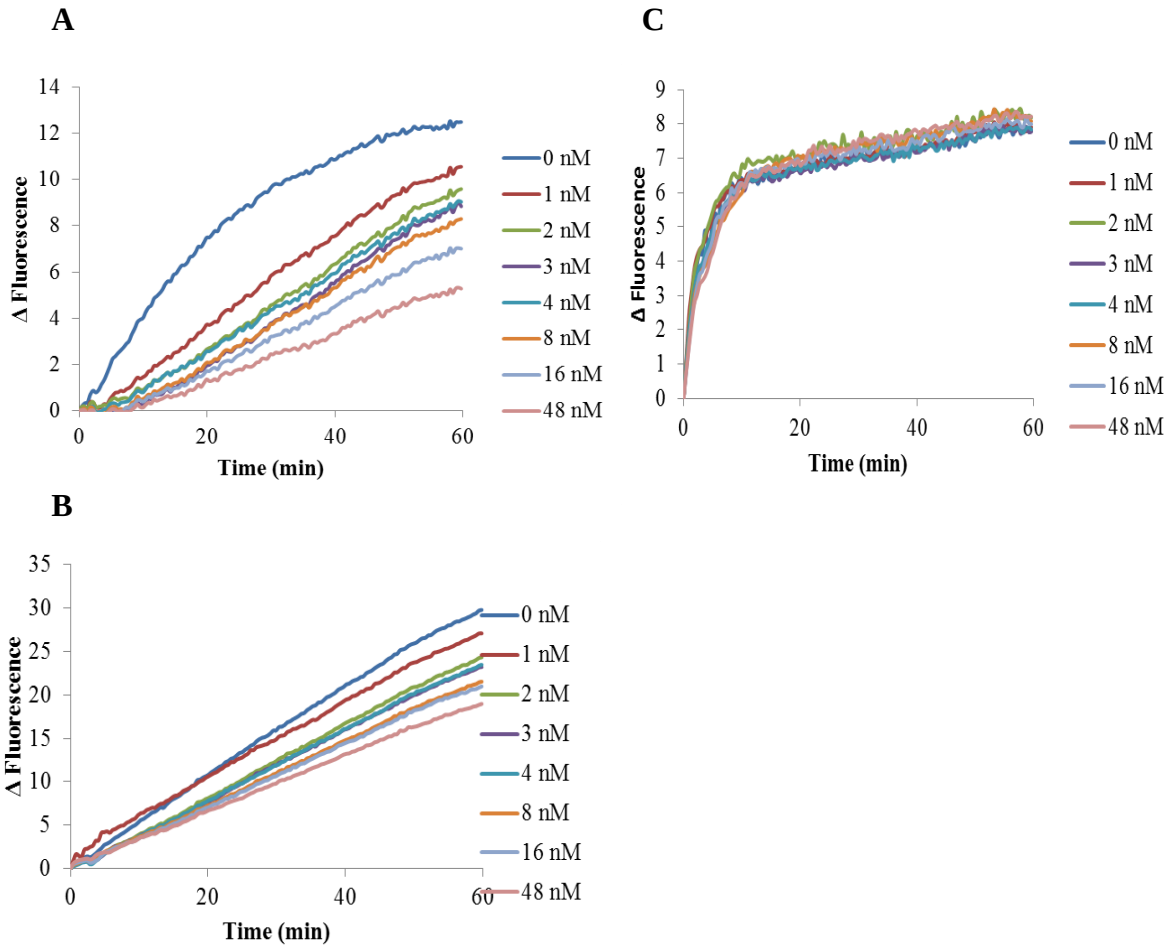

Figure 3.31: *Kinetic data showing the average of 4 experimental replicates of ERK-inhibitor concentration in the presence of ERK1, JNK3 and p38γ.* (A) Fluorescence changes of SOX-MEF2A peptide. (B) Fluorescence changes of SOX-Sub-F peptide. (C) Fluorescence changes of SOX-Sub-D peptide. Inhibitor concentrations: 0 nM, 1 nM, 2 nM, 3 nM, 4 nM, 8 nM, 16 nM, and 48 nM. Fixed concentration: ERK1 (0.5 nM), JNK3 (5 nM) and p38γ (2.5 nM). SOX-MEF2A, SOX-Sub-F and SOX-Sub-D (2 µM). Data collected with 96-well plate half area, plate reader with λ_{ex} filter of 340 ± 35 nm and λ_{em} filter of 485 ± 20 nm. Assay buffer: (25mM HEPES, 50mM KCl, 0.1 mM EDTA, 0.1 mM EGTA pH 7.4) with 2 mM DTT, 2.5 µg/mL BSA, 5mM $MgCl_2$, 500 µM ATP at 25°C.

3.9.6 Differentiating Inhibition of ERK1 in the Presence of MAPK Groups

This kinase assay encompassed the differential sensing of three MAPK groups (0.5 nM ERK1, 5 nM JNK3 and 2.5 nM p38γ) with increasing ERK-inhibitor concentrations. The array enabled the semiquantitative detection of ERK inhibition using the aforementioned kinetic data. The LDA plot in **Figure 3.32A** was acquired from this sensing ensemble, showing progression of the inhibition changes in the array response. A control group was used in this LDA plot by including the kinetic data of SOX-peptides with 5 nM JNK3 and 2.5 nM p38γ (no ERK1 was added). This LDA presented a linear trend in the inhibition data, showing dependence of the kinetic response on the increasing inhibitor concentrations. The total catalytic activity of ERK1 in the presence of JNK3 and p38γ is represented by the analyte group at 0 nM inhibitor concentration which is located on the top right quadrant. The increasing inhibitor concentrations are diagonally placed on the left side of the LDA plot. The control group was expected to be located on the far bottom left side of the LDA plot. The ERK-inhibition patterns were classified with 83.96% of the variance along the F1 axes, and 14.85% of the variance along the F2 axes. However, the groups were classified with 69.44% jack-knife analysis due to the analogous response of ERK1 to four inhibitor concentrations. The analyte groups in the range of 2 nM to 8 nM inhibitor concentrations presented considerable overlap. The corresponding loading plot shown in **Figure 3.32B** indicated the contribution of each SOX-peptide towards the differentiation of inhibitor concentrations in the array. The cross-reactive properties of this array demonstrated its utility to differentiate inhibition of

ERK1 activity in the presence of other MAPK groups. The semiquantitative detection of the progression of the inhibition changes was followed by using the kinetic response of the SOX-peptides in the array.

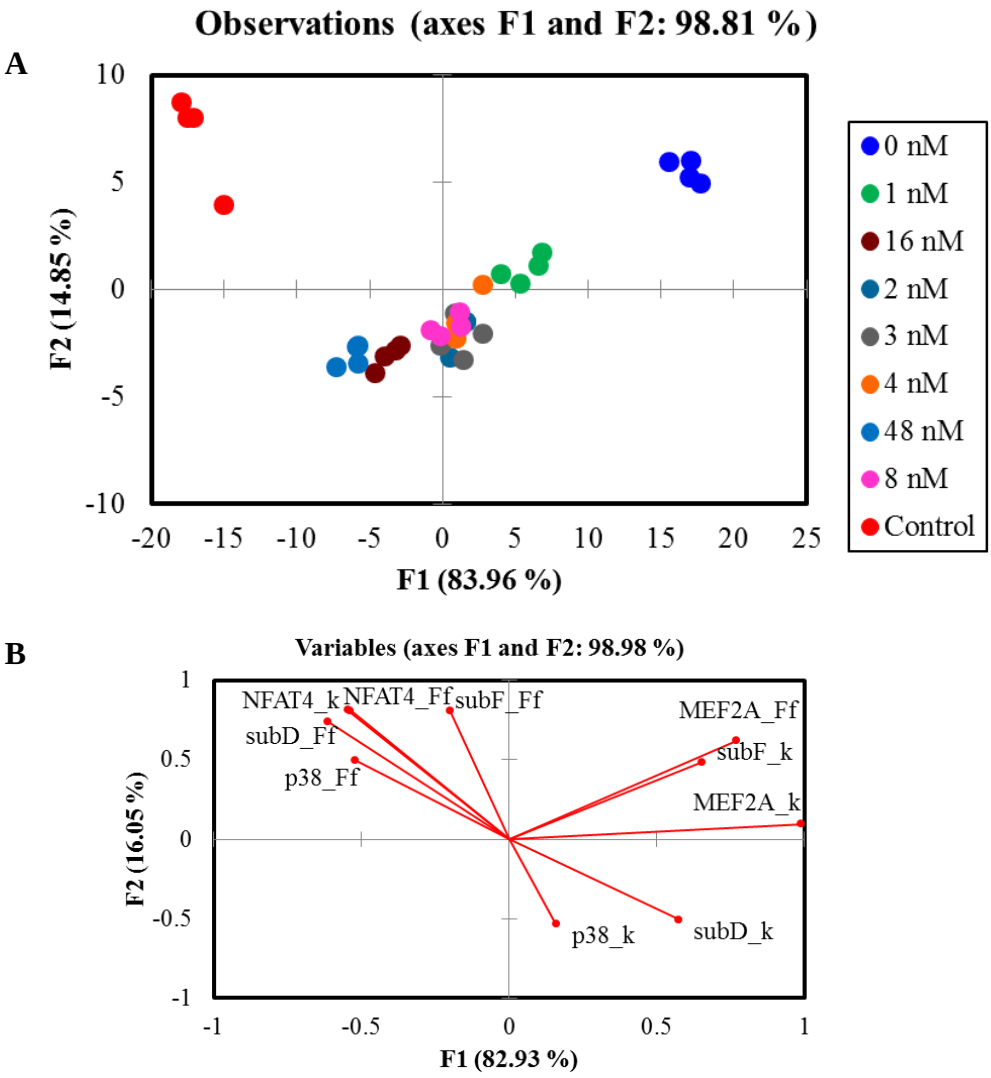

Figure 3.32: *LDA score plots of the kinetic response pattern from the SOX-peptides showing inhibition of ERK1 activity in the presence of JNK3 and p38γ.* (A) LDA plot with eight ERK-inhibitor concentrations and control, showing 69.44% jack-knife analysis. (B) LDA plot with five ERK-inhibitor concentrations and control, showing 91.67% jack-knife analysis. (C) Corresponding loading plot for (B). Inhibitor concentrations: 0 nM, 1 nM, 2 nM, 3 nM, 4 nM, 8 nM, 16 nM, and 48 nM. Fixed concentration: ERK1 (0.5 nM), JNK3 (5 nM) and p38γ (2.5 nM). Sox-peptides (2 µM), and SOX-p38 peptide (8 µM). Data collected with 96-well plate half area, plate reader with λ_{ex} filter of 340 ± 35 nm and λ_{em} filter of 485 ± 20 nm. Assay buffer: (25mM HEPES, 50mM KCl, 0.1 mM EDTA, 0.1 mM EGTA pH 7.4) with 2 mM DTT, 2.5 µg/mL BSA, 5mM $MgCl_2$, 500 µM ATP at 25°C.

3.10 QUANTITATIVE ANALYSIS OF ERK1 ACTIVITY

In the field of pattern recognition, machine learning approaches have emerged as powerful chemometric tools to analyze complex datasets. The machine learning technique has focused on the construction and study of models that can learn the structure from the dataset to predict the properties of analogous unknowns.[59] Support vector machines (SVM) have been implemented for the classification and quantification of analytes as described in Chapter 1. For instance, this mathematical model has allowed for the simultaneous prediction of guest concentrations in complex mixtures.[134,135] SVM is a supervised method that uses kernel functions to classify analyte groups with non-linear behavior by mapping the input data into a different dimensional space, obtaining linear correlations between the variables.[62] The SVM functions can be additionally used to solve regression problems. SVM algorithms use training sets and prediction (test) models to generate a linear classification plot of the original dataset. The training set or calibration set uses input (x) and output (y) sets to tune the parameters of the predicting model. The classes of the input and output sets in the training set are known in advanced. The result of running the training set can be expressed as a function y(x) which considers the new data (x) as input and that produces an output vector.

3.10.1 Detecting Unknown ERK Concentrations

In this study, SVM analysis was performed to improve the utility of this sensing array for the quantitative sensing of ERK1 activity. This SVM model was applied to the previously obtained response data from the sensing array. From the semiquantitative assay of increasing ERK1 concentrations in the presence of JNK3 (5 nM) and p38γ (2.5 nM) shown in **Figure 3.21**, the obtained rate constants and fluorescence values at 20 min were used as input data. To assess the quantitative response of this array, the following concentrations 0 nM, 0.1nM, 0.4 nM, 1.6 nM and 3.2 nM of ERK1 were used as input data and the corresponding kinetic data were used as output data for the calibration and prediction model development (**Table 3.1**). In addition, the remaining ERK1 concentrations 0.2 nM and 0.8 nM and the corresponding kinetic data were used as unknown samples for the cross-validation analysis (**Table 3.2**). Solo software was used to generate the SVM regression analysis.

Different error values are generated to assess the confidence level of the SVM regression analysis. The training set produces a root mean square error of calibration (RMSEC) value. Once the SVM analysis is implemented, cross-validation analysis will be added along with the calibration and prediction results. This model validation is used to test the calibration and prediction models validity, producing a root mean square error of cross validation (RMSECV) value. The test model used to assess the utility and validation of the calibration model produces a root mean square error of prediction

(RMSEP) value, which gives a measure of the calibration model performance when presented with unknown data.

ERK1	SOX-Sub-D		SOX-MEF2A		SOX-NFAT4		SOX-Sub-F		SOX-p38	
(nM)	k	F	k	F	k	F	k	F	k	F
0.0	0.02695	3082	0.00251	809	0.02119	3732	0.01187	4143	0.00841	3501
0.0	0.02621	3121	0.00281	912	0.01857	3471	0.01408	4430	0.00633	2310
0.0	0.02285	2797	0.00218	594	0.01482	2998	0.01372	4362	0.00367	1022
0.0	0.02322	2830	0.00307	935	0.01819	3400	0.01330	4275	0.00393	1490
0.1	0.03118	3543	0.00740	2286	0.02010	3464	0.01023	3539	0.00939	4340
0.1	0.03209	3505	0.00808	2596	0.01672	3124	0.01683	5330	0.00310	1010
0.1	0.02847	3219	0.00685	2006	0.01532	3201	0.01431	4550	0.00356	1303
0.1	0.03142	3510	0.00433	1370	0.01160	2142	0.01243	3806	0.00247	2218
0.4	0.12623	6954	0.03423	8329	0.01718	3103	0.01365	4431	0.00616	2288
0.4	0.14153	7386	0.01005	2946	0.01655	2944	0.01422	4432	0.00506	2372
0.4	0.12427	6923	0.03437	8297	0.00908	1752	0.01707	5104	0.00524	3268
0.4	0.13120	7000	0.02622	6524	0.01144	1917	0.01611	4983	0.00363	2143
1.6	0.20445	6967	0.10476	15243	0.02116	3794	0.03020	7931	0.00281	1435
1.6	0.21434	6840	0.10928	15602	0.02084	3793	0.03004	8135	0.00280	510
1.6	0.22317	6853	0.10012	15307	0.01454	3002	0.03314	8561	0.00458	1938
1.6	0.30674	7605	0.09087	14459	0.01423	2863	0.02972	8104	0.00405	1857
3.2	0.13687	5902	0.13607	16128	0.02454	4194	0.05340	11624	0.00765	3738
3.2	0.15254	5912	0.12148	15529	0.01669	3267	0.05927	12193	0.00647	2388
3.2	0.28457	6589	0.11248	15263	0.01788	3709	0.04932	11187	0.00476	2248
3.2	0.26009	6659	0.11899	15417	0.01683	3312	0.04106	10328	0.00629	2792

Table 3.1: *ERK1 concentrations and kinetic data used as input data for the calibration set.*

ERK1	SOX-Sub-D		SOX-MEF2A		SOX-NFAT4		SOX-Sub-F		SOX-p38	
(nM)	k	F	k	F	k	F	k	F	k	F
0.2	0.04540	4646	0.01519	4226	0.01634	2884	0.01162	3816	0.00866	3775
0.2	0.04820	4717	0.01520	4325	0.01541	2860	0.01547	4493	0.00412	1594
0.2	0.04607	4660	0.01394	3955	0.01151	2303	0.01434	4360	0.00709	4205
0.2	0.04460	4618	0.01478	4169	0.01221	2498	0.01374	4329	0.00662	3191
0.8	0.13508	6601	0.06279	12120	0.01768	3185	0.02591	7072	0.00577	2112
0.8	0.14544	6702	0.05765	11668	0.01696	3234	0.02596	7297	0.00657	3073
0.8	0.15627	6839	0.05682	11655	0.01377	2851	0.02231	6468	0.00500	1776
0.8	0.14498	6666	0.05335	11228	0.01609	3267	0.02125	6078	0.00418	1210

Table 3.2: *ERK1 concentrations (0.2 nM and 0.8 nM) and kinetic data treated as unknown samples.*

This sensing array yielded a very accurate quantitative analysis of the mixtures of ERK1 in the presence of other MAPK groups at different concentrations. The result of the SVM regression method is shown in **Figure 3.33.** The nonlinear behavior of the original dataset from the sensing array was successfully detected and differentiated by the SVM functions, obtaining a linear relationship of the actual and predicted ERK1 concentrations. The plot in **Figure 3.33** additionally showed the correct quantification of two unknown samples (ERK1 at 0.2 and 0.8 nM) which are shown in red dots. The values of the root mean square errors of calibration RMSEC = 0.044, cross-validation RMSECV = 0.256, and prediction RMSEP = 0.151 showed good confidence levels of the generated calibration and test models.

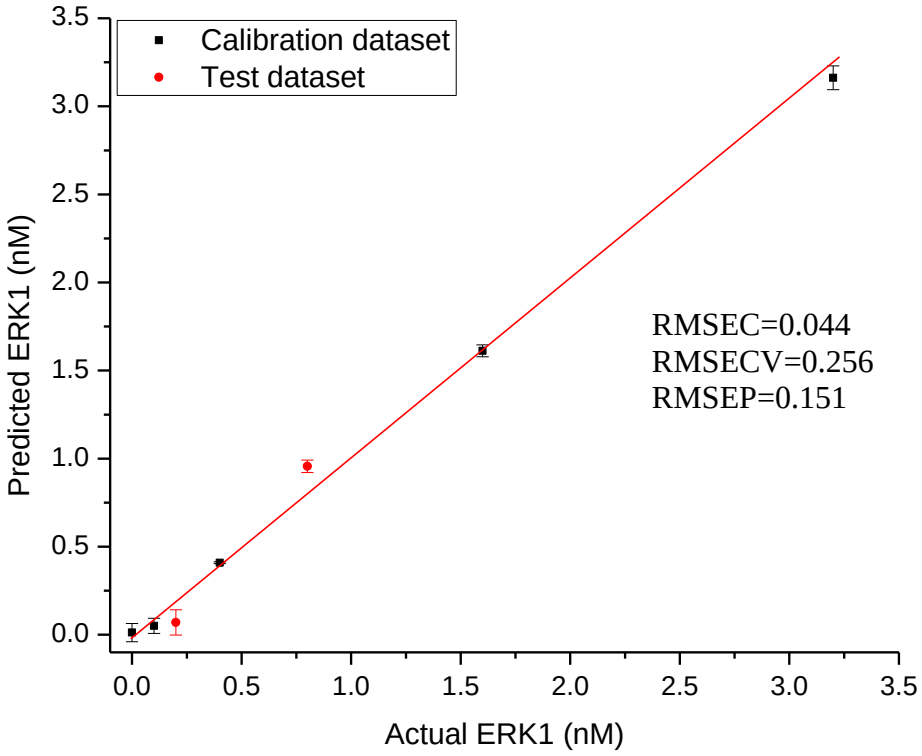

Figure 3.33: *Quantitative analysis of the kinetic data of ERK1 in the presence of JNK3 (5 nM) and p38γ (2.5 nM).* Linear regression using a support vector machine (SVM) method allowed for the quantitative analysis of ERK1 activity. The plot of actual and predicted concentrations showed high confidence level of the prediction of two unknown samples (red dots).

An additional SVM regression analysis was performed with different type of data to explore the application of the predicted dataset. From the same kinase assay with increasing concentrations of ERK1, the obtained score factors from the LDA in **Figure 3.22** were used as input and output datasets (**Table 3.3** and **Table 3.4**) for the calibration and prediction models, respectively. The result of this SVM analysis is shown in **Figure**

3.34. An analogous linear relationship was found between the actual and predicted ERK1 concentrations. The values of the root mean square errors of calibration RMSEC = 0.070, cross-validation RMSECV = 0.362, and prediction RMSEP = 0.130 showed similar confidence levels of the generated calibration and test models with respect to the previously described plot.

ERK1	LDA Score factors				
(nM)	F1	F2	F3	F4	F5
0.0	-27.068	-10.266	0.046	-0.679	0.027
0.0	-26.243	-10.019	0.357	-0.139	0.220
0.0	-27.958	-12.774	0.081	-0.264	0.258
0.0	-27.952	-12.104	-0.250	-0.182	0.219
0.1	-24.912	-5.334	-0.765	-0.602	-0.348
0.1	-23.210	-6.047	-0.147	1.081	0.423
0.1	-25.305	-8.577	-0.415	0.287	0.181
0.1	-24.556	-6.679	0.329	-0.512	-0.066
0.4	-0.400	17.490	-0.099	-0.446	-0.354
0.4	-0.760	16.865	5.044	-2.125	0.553
0.4	0.486	16.921	0.423	0.299	-0.047
0.4	-0.313	16.207	1.803	-0.472	0.238
1.6	26.249	0.095	-1.341	-1.713	-1.192
1.6	27.203	-2.510	-1.772	-2.141	-1.194
1.6	25.278	-1.110	-1.623	-0.396	0.131
1.6	28.052	-0.297	-1.168	-1.646	2.116
3.2	36.699	-13.822	1.904	0.556	-2.539
3.2	34.052	-12.171	2.394	3.408	-0.318
3.2	35.464	-14.271	0.709	0.802	2.432
3.2	34.930	-12.537	0.039	-1.714	0.309

Table 3.3: *Input data used for the calibration dataset of the SVM model.* LDA score factors obtained from the sensing array of five SOX-peptides in the presence of different ERK1 concentrations with JNK3 (5 nM) and p38γ (2.5 nM) kinases.

ERK1	LDA Score factors				
(nM)	F1	F2	F3	F4	F5
0.2	-17.742	3.663	-0.415	-0.210	-0.672
0.2	-16.267	3.782	0.155	0.692	-0.207
0.2	-17.016	3.297	0.235	0.318	-0.336
0.2	-17.373	3.291	-0.101	0.293	-0.429
0.8	8.402	10.783	-1.308	1.616	-0.195
0.8	7.787	11.498	-1.040	1.847	0.371
0.8	7.425	12.350	-1.479	0.988	0.259
0.8	5.044	12.276	-1.597	1.052	0.159

Table 3.4: *Input data treated as unknown samples for the prediction dataset of the SVM model.* LDA score factors obtained from the sensing array of five SOX-peptides in the presence of different ERK1 concentrations with JNK3 (5 nM) and p38γ (2.5 nM) kinases.

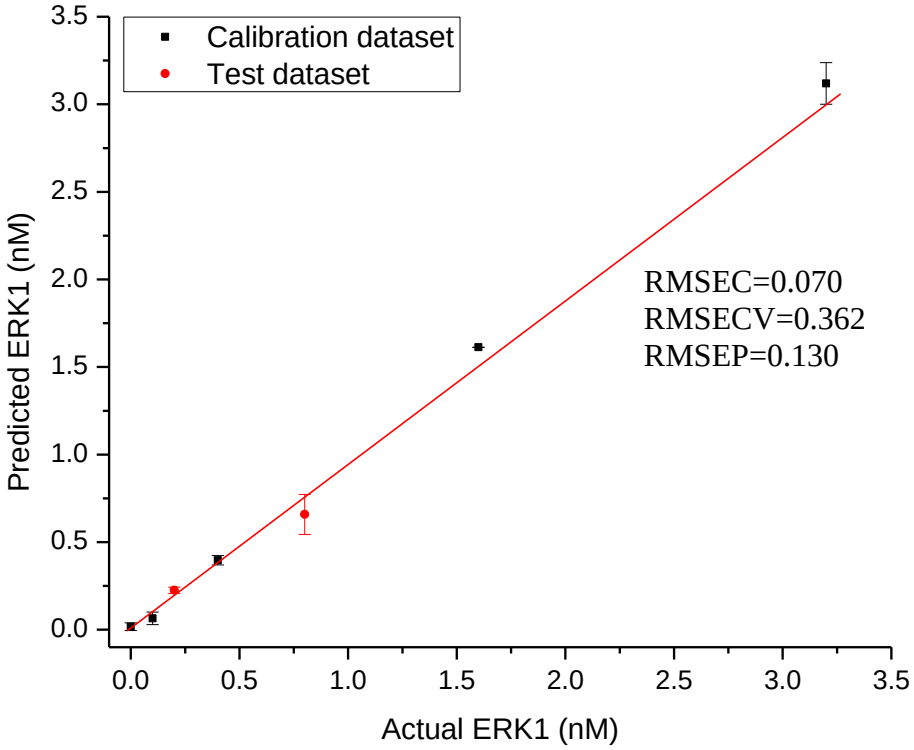

Figure 3.34: *Quantitative analysis of the LDA score data from the kinetic response of five SOX-peptides in the presence of increasing ERK1 concentrations in the presence of JNK3 (5 nM) and p38γ (2.5 nM).* Linear regression using a support vector machine (SVM) method allowed for the quantitative analysis of ERK1 concentrations. The plot of actual and predicted concentrations showed high confidence level of the prediction of two unknown samples at 0.2 and 0.8 nM (red dots).

3.10.2 Detecting Unknown ERK-Inhibitor Concentrations

The successful SVM analysis of either the raw kinetic dataset or the LDA score factors allowed for the simultaneous prediction of two unknown concentrations of ERK1 in the presence of other MAP kinases. After the quantification of ERK1 concentrations in the presence of other MAPK groups was accomplished, the following study involved the quantification of ERK1-inhibitor concentrations. From the semiquantitative assay of inhibition of ERK1 (0.5 nM) in the presence of JNK3 (5 nM) and p38γ (2.5 nM) shown in **Figure 3.32**, the obtained LDA score factors from the response data of the array were used as input/output datasets. The following inhibitor concentrations 0 nM, 1 nM, 4 nM, 8 nM, 16 nM and 48 nM of ERK1 were chosen as input data and the corresponding score factors were used as output data for the calibration and prediction model development (**Table 3.5**). The inhibitor concentration at 2 nM and the corresponding LDA score data were used as unknown samples for the cross-validation analysis (**Table 3.6**).

Inhibitor	LDA Score factors			
(nM)	F1	F2	F3	F4
0	17.083	5.996	-0.783	0.896
0	17.686	4.943	-1.727	0.466
0	16.995	5.193	-1.336	-0.703
0	15.554	5.954	-0.017	-0.613
1	6.571	1.124	1.579	0.043
1	5.315	0.279	1.878	0.201
1	6.866	1.731	0.395	-0.267
1	4.021	0.707	0.458	-0.874
4	2.798	0.204	-1.434	0.063
4	0.898	-2.281	0.202	0.518
4	0.911	-1.575	0.148	-0.776
4	0.878	-2.189	1.489	-0.947
8	1.296	-1.752	1.228	-0.434
8	1.174	-1.066	0.822	-0.339
8	-0.127	-2.199	0.959	-0.497
8	-0.776	-1.885	0.302	-1.237
16	-2.882	-2.635	-0.349	1.367
16	-4.603	-3.904	-2.608	1.801
16	-3.998	-3.137	-0.595	-0.274
16	-3.214	-2.862	-0.529	-1.507
48	-5.825	-2.647	-1.361	0.519
48	-5.855	-2.680	-1.202	-0.659
48	-7.300	-3.647	-1.665	-0.291
48	-5.833	-3.439	-0.752	-1.574

Table 3.5: *Input data used for the calibration dataset of the SVM model.* LDA score factors obtained from the sensing array of five SOX-peptides in the presence of different ERK1-inhibitor concentrations with ERK1 (0.5 nM), JNK3 (5 nM) and p38γ (2.5 nM) kinases.

Inhibitor	LDA Score factors			
(nM)	F1	F2	F3	F4
2	1.327	-1.597	0.217	1.654
2	0.541	-3.192	-1.638	2.173
2	1.604	-1.535	-0.719	-0.214
2	1.568	-1.510	0.439	-1.020

Table 3.6: *Input data treated as unknown sample for the prediction dataset of the SVM model.* LDA score factors obtained from the sensing array of five SOX-peptides in the presence of different ERK1-inhibitor concentrations with ERK1 (0.5 nM), JNK3 (5 nM) and p38γ (2.5 nM) kinases.

This sensing array additionally generated a correct quantitative analysis of ERK1-inhibitor in the presence of ERK1 (0.5 nM), JNK3 (5 nM) and p38γ (2.5 nM) kinases at different concentrations. The result of the SVM analysis is shown in **Figure 3.35.** The kinetic response of ERK1 with different inhibitor concentrations produced from this array was quantified by the SVM functions, obtaining a linear relationship of the actual and predicted ERK1-inhibitor concentrations. The plot in **Figure 3.35** showed the correct quantification of the unknown sample (ERK1-inhibitor at 2 nM) which is shown as a red dot. The values of the root mean square errors of calibration RMSEC = 4.48, cross-validation RMSECV = 7.25, and prediction RMSEP = 2.06 were also obtained from this SVM analysis. Although the accuracy was diminished, the obtained calibration curve was still useful for the correct identification of the unknown sample.

This sensing array along with a SVM model demonstrated its utility to construct a calibration model for the quantitative detection of ERK1 and ERK-inhibitor concentrations in the presence of other MAPK groups. This study demonstrated the

applicability of LDA score factors from the kinetic response of five SOX-peptides to be used as input dataset. The SVM analysis of the LDA score factors allowed for the construction of a calibration and prediction model, allowing for the detection of unknown concentrations of either ERK1 or inhibitor in the presence of other MAP kinases.

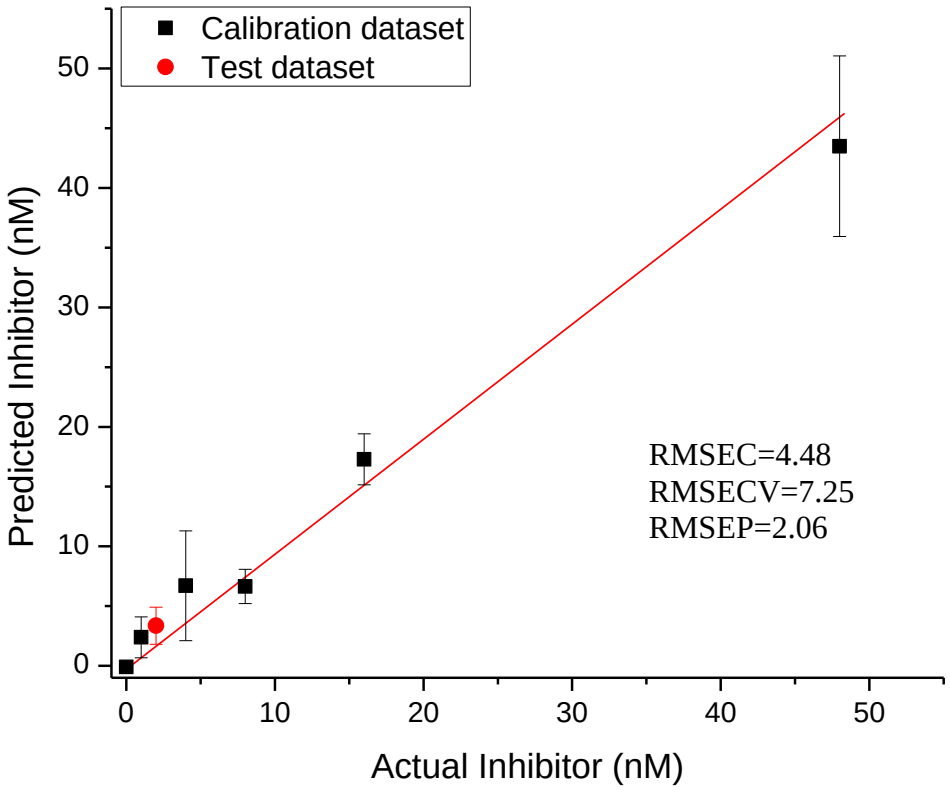

Figure 3.35: *Quantitative analysis of the LDA score data from the kinetic response of five SOX-peptides in the presence of ERK1-inhibitor with ERK1 (0.5 nM), JNK3 (5 nM) and p38γ (2.5 nM).* Linear regression using a support vector machine (SVM) method allowed for the quantitative analysis of inhibitor concentrations. The plot of actual and predicted concentrations showed correct prediction of the unknown sample at 2 nM (red dot).

3.11 CONCLUSIONS

From these kinase assays the following has been determined: (1) MAPK sub-families and isoforms can be differentiated using cross-reactive SOX-peptides with docking sites that present different selectivity and affinity towards this class of analytes. (2) This sensing array can be further applied to the semiquantitative detection of concentration changes of ERKs in a mixture of MAPKs at different nanomolar concentrations. (3) Inhibition of the catalytic activity of ERKs can be additionally detected in the presence of other MAPK groups using this array sensing approach. (4) This sensing array further allowed for the quantitative analysis of ERK1 and inhibition concentrations using a calibration and prediction model.

In summary, this study showed that the discriminating properties of the docking sites on MAPK substrates can be used to develop a pattern recognition approach for this class of analytes. The enzymatic activity of nine different MAPK isoforms was detected and differentiated by using a high-throughput screening protocol in parallel with a differential sensing approach. The fluorescence changes of the chosen SOX-peptide substrates were consistent with previous studies, showing similar specificity for corresponding MAPKs. From these results, SOX-peptides proved to be not very selective or specific when used in a sensing array.

3.12 FUTURE WORK

The developed kinase protocols in this project have contributed to the rapid detection of MAPK activity which may assist in developing diagnostic techniques associated with kinase malfunction and early-onset cancer. The ability of this sensing array to detect and differentiate semiquantitative changes in kinase concentration and inhibition of catalytic activity has opened the possibility to extrapolate this assay to the quantitative detection of MAP kinases. Additional assays are still left on this project. Important future experiments consist of exploring the quantitative detection of MAPK concentration changes in real-life biological mixtures, detecting cell lysates with differing kinase expression, and testing how cells from healthy, metastatic and carcinoma tissues respond to the sensing ensemble.

3.13 CONTRIBUTIONS AND EXPERIMENTAL INFORMATION

The research presented here was developed in collaboration with the Dalby group. Special acknowledgments are given to Dr. Tamer S. Kaoud who has supplied the kinase analytes assessed in this project, and has given valuable insight. Jorge Luis Martinez, an undergraduate Chemistry major at the University of Texas at El Paso, received a NSF REU fellowship, and worked under my supervision during the summer 2012. His assistance with the synthetic procedure toward fluorophore **3.13** is gratefully acknowledged. Jorge graduated in 2014 and is currently a graduate student at the University of Texas at Austin.

3.13.1 Materials and Methods

Starting materials were purchased from Aldrich Chemical Co., Acros Organics, EM, or TCI, and used without further purification. All solvents were of reagent grade quality and purchased commercially. All compounds were prepared according to previous literature *Imperiali et al*.[128] All reactions were performed in standard glassware. Evaporation was done by rotatory evaporation using a standard rotovap equipped with dry ice condenser. TLC analyses were carried out using Silica TLC Plates Aluminum Backing 20 by 20 cm sheet UV active. Column chromatography (CC) was performed using silica gel 60 (230 ± 400 mesh, 0.040 ± 0.063 mm) from Dynamic Adsorbents. ^{1}H and ^{13}C spectra were recorded on Varian DirectDrive or Varian INOVA NMR spectrometers. The NMR spectra were referenced to solvent and the spectroscopic solvents were purchased from Cambridge Isotope Laboratories. Finnigan MAT-VSQ 700 and DSQ spectrometers were used to obtain mass spectra. HR electrospray ionization (ESI) mass spectra were recorded on Agilent 6530 Accurate-Mass Q-TOF LC/MS.

3.13.2 Peptide Synthesis

Peptides were synthesized using standard SPPS protocol. Peptide Sub-D and MEF2A were synthesized on rink resin (NovaSyn TGR resin) using a peptide synthesizer (CEM Liberty Automated Microwave). Peptides Sub-F and p38 were synthesized on NovaSyn Wang resin with a different peptide synthesizer (Prelude by Protein Technology**,** Inc)**.** NFAT4 peptide was purchased from Bio-Synthesis. Coupling reactions

used Fmoc-L-amino acid/ HBTU/DIPEA (5:5:10 eq) relative to 1 eq. of pre-loaded resin. The N-terminus of each peptide was acetylated using a solution of 1.2 M of NMM in DMF (2 mL), acetic acid (1 mL) and CH_2Cl_2 (1 mL). Few beads were taken to corroborate the presence of the desired peptide. Crude peptide was cleaved from the resin using a solution of 5 mL TFA/ H_2O/TIS (95/2.5/2.5 % v/v) for 2 h. Crude peptides were characterized by mass spectrometry using a either MALDI-TOF (Vogayer, PerSeptive Biosystem) or ESI (LCQ, Thermo Finnigan).

Peptide	Peptide Sequence	Molecular Formula	MALDI-TOF $[M]^+$ Calcd.	MALDI-TOF $[M]^+$ Found
3.2	FQRKTLQRRNLKGLNLNL XXXTGPLSP**C**PF	$C_{157}H_{267}N_{47}O_{38}S$	3451.01	3451.6
			MALDI-TOF $[M]^+$ Calcd.	MALDI-TOF $[M]^+$ Found
3.3	NLGMNSRKPDLRVVIPPGX XXTGPLSP**C**PF	$C_{147}H_{246}N_{40}O_{38}S_2$	$[M+2H]^{2+}$ 1622.4 $[M+3H]^{3+}$ 1081.9	$[M+2H]^{2+}$ 1691.4 $[M+3H]^{3+}$ 1043.4
			MALDI-TOF $[M]^+$ Calcd.	MALDI-TOF $[M]^+$ found
3.4	LERPSRDHLYLPLSGRYRE S**C**LSPSPA	$C_{137}H_{217}N_{41}O_{42}S$	3141.57	3141.92
			ESI $[M+H]^+$ Calcd.	ESI $[M+H]^+$ found
3.5	YAE**C**LTPRILAK WEWPA	$C_{99}H_{145}N_{23}O_{25}S$	$[M+1H]^{1+}$ 2089.1 $[M+2H]^{2+}$ 1045.0	$[M+1H]^{1+}$ 2088.6 $[M+2H]^{2+}$ 1044.6
3.6	I**C**TTPITTTYFFFKKK	$C_{101}H_{147}N_{23}O_{25}$	$[M+1H]^{1+}$ 1981.05 $[M+2H]^{2+}$ 991.53 $[M+3H]^{3+}$ 661.02	$[M+1H]^{1+}$ 1980.8 $[M+2H]^{2+}$ 990.6 $[M+3H]^{3+}$ 661.0

Table 3.7: *LCMS characterization data of the crude peptides.*

3.13.3 Synthesis of SOX-Br Fluorophore

8-hydroxy-N,N,2-trimethylquinoline-5-sulfonamide **(3.9)**

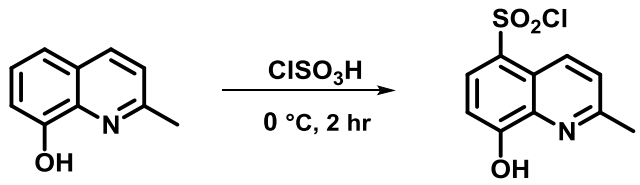

3.8 **3.9**

A solution of chlorosulfonic acid (50 mL, 0.751 moles, 11.9 eq) was cooled to 0 °C in a round bottom flask and **3.8** (10 g, 63 mmol, 1 eq) was added in portions while keeping the temperature between 0 °C – 5 °C. The reaction was stirred at 0 °C for 2 h. The reaction mixture was then extracted several times with CH_2Cl_2 (200 mL). The organic layers were joined and washed with $NaHCO_3$, brine and dried over Na_2SO_4. The solution was filtered and the solvent evaporated to dryness. Crude product **3.9** (3.51 g, 13.6 mmol, 21.6%) was obtained as a yellow solid, and it was used in the next reaction without further purification. ^{1}H NMR (400 MHz, $CDCl_3$) δ 8.99 (d, *J* = 8.9 Hz, 1H), 8.29 (d, *J* = 8.5 Hz, 1H), 7.63 (d, *J* = 8.9 Hz, 1H), 7.23 (d, *J* = 9.7 Hz, 1H), 2.83 (s, 3H).

8-hydroxy-*N*,*N*,2-trimethylquinoline-5-sulfonamide **(3.10)**

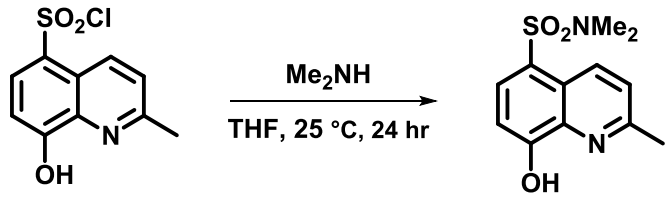

3.9 **3.10**

A solution of **3.9** (3 g, 12 mmol, 1 eq) in dry THF (45 mL) was stirred at room temperature. N,N-dimethylamine (30 mL, 2 M in THF, 60 mmol, 4.57 eq) was carefully added drop wise over a period of 15 minutes. The reaction was then stirred at room temperature overnight. The crude product after evaporation was purified by normal phase column chromatography (hexane:ethylacetate, 1:1 v/v) to yield compound **3.10** (1.33 g, 5 mmol, 41.6%) as a pale yellow solid. ^{1}H NMR (499 MHz, $CDCl_3$) δ 8.95 (d, J = 8.9 Hz, 1H), 8.07 (d, J = 8.3 Hz, 1H), 7.44 (d, J = 8.9 Hz, 1H), 7.15 (d, J = 8.3 Hz, 1H), 2.73 (d, J = 3.6 Hz, 9H); ^{13}C NMR (126 MHz, $CDCl_3$) δ 157.86 (s), 156.27 (s), 137.51 (s), 134.47 (s), 132.11 (s), 124.41 (s), 123.63 (s), 121.69 (s), 108.02 (s), 37.40 (s), 24.70 (s). HRMS (m/z): $[M+H]^+$ calcd. for $C_{12}H_{15}N_2O_3S$ 267.0797; Found 267.07977. $[M+Na]^+$ calcd. for $C_{12}H_{14}N_2O_3SNa$ $[M+Na]^+$ 289.06173; Found 289.06172.

8-((*tert*-butyldiphenylsilyl)oxy)-*N*,*N*,2-trimethylquinoline-5-sulfonamide **(3.11)**

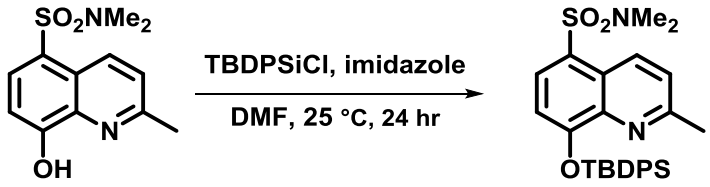

3.10 **3.11**

Compound **3.10** (1.33 g, 5 mmol, 1 eq) and imidazole (0.83 g, 12.2 mmol, 2.44 eq) were added in dry DMF (15 mL) and stirred at 25 °C for 10 minutes. A solution of TBDPSCl (2.17 mL, 8.33 mmol, 1.66 eq) was added drop wise to the reaction mixture and stirred for 24 h at 25 °C. The reaction mixture was neutralized with water and a saturated ammonium chloride solution. The reaction mixture was extracted with ethyl acetate. The organic layer was washed with brine and dried over Na_2SO_4. The filtrate was evaporated under reduced pressure at 25 °C. The crude product after evaporation was dissolved in solution (2 mL) of MeOH:CH_2Cl_2 1:1 v/v. This solution was slowly evaporated to approximately half of its volume. The precipitate was filtered and the solvent evaporated to dryness. Product **3.11** (1.83 g, 3.62 mmol, 72.7%) was obtained as a white crystalline solid. ^{1}H NMR (499 MHz, $CDCl_3$) δ 8.79 (d, J = 8.8 Hz, 1H), 7.95 (d, J = 8.3 Hz, 1H), 7.73 (d, J = 6.7 Hz, 4H), 7.34 (t, J = 7.4 Hz, 2H), 7.30 – 7.25 (m, 5H), 7.17 (d, J = 8.9 Hz, 1H), 7.13 (d, J = 8.3 Hz, 1H), 2.70 (s, 6H), 2.18 (s, 3H), 1.15 (s, 9H). ^{13}C NMR (126 MHz, $CDCl_3$) δ 157.54 (s), 156.82 (s), 140.61 (s), 134.83 (s), 133.98 (s), 133.13 (s), 131.04 (s), 129.35 (s), 127.35 (s), 124.53 (s), 123.47 (s), 115.04 (s), 37.35 (s), 26.65 (s), 23.67 (s), 20.22 (s). LRMS (m/z): $[M+H]^+$ calcd. for $C_{28}H_{33}N_2O_3SSi$ 505.19; Found 505.2. $[M+Na]^+$ calcd. for $C_{28}H_{32}N_2O_3SSiNa$ 527.71; Found 527.2.

8-((*tert*-butyldiphenylsilyl)oxy)-2-formyl-*N*,*N*-dimethylquinoline-5-sulfonamide **(3.12)**

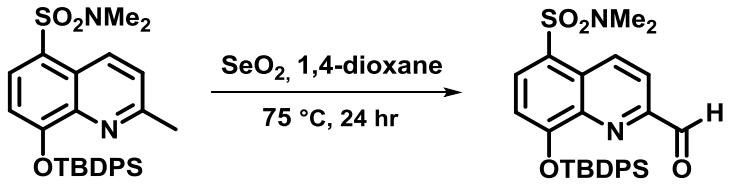

3.11 **3.12**

SeO_2 (0.23 g, 2.10 mmol, 1.02 eq) was dissolved in 1,4-dioxane (10 mL) and the reaction mixture was heated to 60 °C. A solution of **3.11** (1.04 g, 2.06 mmol, 1 eq) was added to the SeO_2 solution. After the solution became homogenous, it was stirred at 75 °C for 24 h. The reaction mixture was then allowed to cool to room temperature. The mixture was filtered through celite to remove a dark brown residue. The solvent was evaporated by rotary evaporation, covering the flask to avoid direct light to yield a pale yellow solid **3.12** (1.57 g). This crude material was used in the next step without further purification.

8-((*tert*-butyldiphenylsilyl)oxy)-2-(hydroxymethyl)-*N*,*N*-dimethylquinoline-5-sulfonamide **(3.13)**

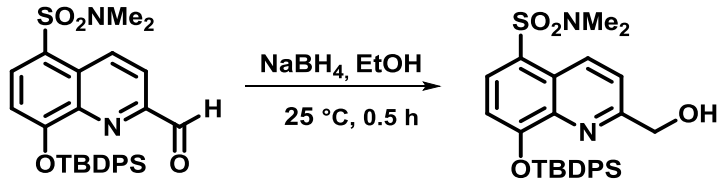

3.12 **3.13**

Crude product **3.12** (1.5 g) was dissolved in dry CH_2Cl_2 (10 mL) and the reaction was cooled to 0 °C. $NaBH_4$ (1.09 g, 28.92 mmol) was dissolved in EtOH and was slowly added to the reaction mixture containing **5**. The reaction mixture was stirred at 0 °C for 0.5 h. Diethyl ether (30 mL) was added to the reaction mixture and the organic layer was extracted with saturated ammonium chloride, H_2O, and brine. The organic layer was dried over Na_2SO_4. The solution was filtered and the solvent was evaporated to dryness. Crude material **3.13** (0.51 g) was obtained as a pale yellow thick oil. This crude product was used in the subsequent reaction without further purification. ^{1}H NMR (400 MHz, $CDCl_3$) δ 8.96 (d, *J* = 8.9 Hz, 1H), 7.93 (d, *J* = 8.3 Hz, 1H), 7.73 (dd, *J* = 8.1, 1.4 Hz, 4H), 7.40 – 7.30 (m, 7H), 7.03 (d, *J* = 8.3 Hz, 1H), 4.64 (s, 2H), 2.70 (s, 6H), 1.17 (s, 9H).

2-(bromomethyl)-8-((*tert*-butyldiphenylsilyl)oxy)-*N*,*N*-dimethylquinoline-5-sulfonamide **(3.14)**

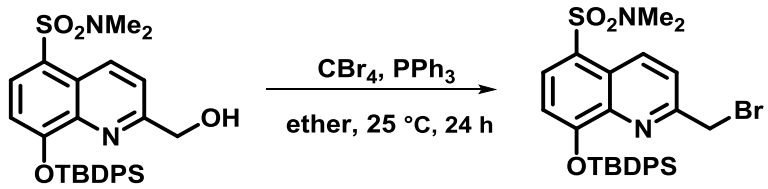

3.13 **3.14**

All glassware and syringes were oven-dried before use. CBr_4 (0.71 g, 2.14 mmol) and **3.13** (0.99 g, 1.90 mmol) were added to a round bottom flask, and the flask was purged with nitrogen. Fresh ether (20 mL) was added and the reaction mixture was cooled to 0 °C. PPh_3 (0.55 g, 2.09 mmol) was dissolved in ether (5 mL) and slowly added to the reaction mixture. The reaction was stirred at room temperature overnight under nitrogen. A yellow precipitate was filtered and the solvent was evaporated. The crude product was purified by flash chromatography (hexane:ethylacetate, 9:1 v/v). Product **3.14** (1.20 g, 2.05 mmol, 34.7% over three steps) was obtained as a pale yellow sticky oil. ^{1}H NMR (400 MHz, $CDCl_3$) δ 8.91 (d, *J* = 9.0 Hz, 1H), 8.00 (d, *J* = 8.3 Hz, 1H), 7.72 (d, *J* = 1.4 Hz, 2H), 7.70 (d, *J* = 1.5 Hz, 2H), 7.49 (d, *J* = 9.0 Hz, 1H), 7.33 (t, *J* = 1.6 Hz, 1H), 7.31 – 7.29 (m, 2H), 7.28 (t, *J* = 1.5 Hz, 2H), 7.26 – 7.25 (m, 1H), 7.13 (d, *J* = 8.3 Hz, 1H), 4.10 (s, 2H), 2.70 (s, 6H), 1.15 (s, 9H). HRMS (m/z): $[M+H]^+$ calcd. for $C_{28}H_{32}BrN_2O_3SSi$ 585.10639; Found 585.10677. $[M+Na]^+$ calcd. for $C_{28}H_{31}BrN_2NaO_3SSi$ 607.08834; Found 607.08913.

3.13.4 Alkylation Reaction of Peptides with SOX-Br

The resin-bound peptides were dried for at least 4 h under vaccum prior to the alkylation reaction. The resin-bound peptide (0.077 g, 0.0084 mmol, 1 eq) was swelled with dry DMF for 30 min. The Mmt protecting group was cleaved by exposing the resin to a solution of 1% TFA and 5% TIS in CH_2Cl_2 for 30 min. This previous step was repeated until the yellowish solution changed to a transparent color. The resin was thoroughly washed with CH_2Cl_2 and DMF. A solution of SOX-Br (0.010 g, 0.0184 mmol, 2 eq) and tetramethylguanidine (5 µL, 0.042 mmol, 5 eq) in dried DMF (6 mL) was stirred at room temperature. The solution was then added to the resin-bound peptide. The reaction mixture was allowed to shake for 24 h under argon. The reagents were filtered and the resin was thoroughly washed with DMF, CH_2Cl_2 and MeOH. The resin was then dried under vacuum for 4 h. A cleaving solution of 5 mL of TFA/ H_2O/TIS (95/2.5/2.5 % v/v) was added to the resin. The crude SOX-peptides were purified using preparative HPLC. Pure SOX-peptides were analyzed by analytical HPLC (Shimadzu HPLC) equipped with Gemini C18 column (250 X 10 mm, 5 µm) or Vydac 218MS C18 (250 mm X 4.6 mm) with UV detection at 220 and 316 nm. Solvent A: H_2O with 0.1% v/v TFA; solvent B: CH_3CN with 0.1% v/v TFA. Rate flow: 4 mL/min or 1 mL/min. Purified peptides were characterized by mass spectrometry using a either MALDI-TOF (Vogayer, PerSeptive Biosystem) or ESI (LCQ, Thermo Finnigan).

SOX-Peptide	Peptide sequence	Molecular Formula	HPLC t_R (min)	ESI $[M+H]^+$ Calcd.	ESI $[M+H]^+$ Found
3.15	FQRKTLQRRNL KGLNLNLXXXTGPL SP**CSOX**PF	$C_{171}H_{279}N_{49}O_{42}S_2$	13.56	$[M+6H]^{6+}$ 627.0 $[M+5H]^{5+}$ 752.2 $[M+4H]^{4+}$ 940.0	$[M+6H]^{6+}$ 627.1 $[M+5H]^{5+}$ 752.6 $[M+4H]^{4+}$ 940.5
				MALDI-TOF $[M]^+$ Calcd.	MALDI-TOF $[M]^+$ Found
3.16	NLGMNSRKPDL RVVIPPGXXXTGPLS P**CSOX**PF	$C_{159}H_{256}N_{42}O_{41}S_3$	10.58	3505.84	3505.85
3.17	LERPSRDHLYL PLSGRYRES**CSOX**LS PSPA	$C_{149}H_{233}N_{43}O_{45}S_2$	26.28	3408.67	3408.54
				ESI $[M+H]^+$ Calcd.	ESI $[M+H]^+$ found
3.18	YAE**CSOX**LTPRILAK WEWPA	$C_{111}H_{157}N_{25}O_{28}S_2$	26.6	$[M+2H]^{2+}$ 1177.6 $[M+3H]^{3+}$ 785.37	$[M+2H]^{2+}$ 1177.6 $[M+3H]^{3+}$ 785.4
3.19	I**CSOX**TTPITTTYFFF KKK	$C_{108}H_{157}N_{21}O_{27}S_2$	31.56	$[M+2H]^{2+}$ 1123.6 $[M+3H]^{3+}$ 749.4	$[M+2H]^{2+}$ 1123.9 $[M+3H]^{3+}$ 749.4

Table 3.8: *LCMS characterization data of the purified SOX-peptides.*

3.13.5 Experimental Information

The fluorescence measurements were taken with a Biotek Synergy 2 Multi-Mode Microplate Reader or a Tecan Infinite 500 Microplate Reader at 25°C with assay buffer: 25 mM HEPES, 50 mM KCl, 0.1 mM EDTA, 0.1 mM EGTA pH 7.4 with 2 mM DTT, 2.5 µg/mL BSA, 5 mM $MgCl_2$. The phosphorylation reaction was initiated upon addition of 5µL of 5 mM ATP stock to 45 µL well assay, obtaining a final concentration of 500 µM ATP. The kinetic assays were measured with a 96-well half area flat bottom, non-binding surface, and black polystyrene. A final reaction volume of 50 µL was used in each well for all assays. Four experimental replicates were measured for each kinase-peptide in well assay. The well plate reader was blanked with HEPES buffer. The 96-well plates half area were read with λ_{ex} filter of 340 ± 35 nm and λ_{em} filter of 485 ± 20 nm, using a top 400 mirror. Speed 300 µL/sec. The collected kinetic data was analyzed by using IgorPro 6.04 or OriginPro 8.5.1. The rate constants and fluorescence values at 20 min were analyzed by linear discriminant analysis using XLSTAT 2011 software package. SOX-peptide concentrations were determined by UV-Vis (DU 800 Spectrophotometer) based on the extinction coefficient of the fluorophore ε355 = 8247 M^{-1} cm^{-1} in 0.1 M NaOH with 1 mM Na_2EDTA as previously reported. Stock kinase solutions were prepared to obtain a final concentration of 1 µM MAPK. Kinase solutions were prepared by adding the corresponding aliquot (µL) of 1 µM MAPK stock to the corresponding volume of assay buffer according to each kinase assay.

Preliminary sensing array experiment. Nine individual kinase solutions with the following final concentrations 2.5 nM ERK1/2, 25 nM JNK1/2/3 and 12.5 nM p38α/β/γ/δ (final volume 880 µL) were prepared in buffer assay. Kinase aliquots of 40 µL were then added to obtain the following final concentration 2 nM ERK1/2, 20 nM JNK1/2/3 and 10 nM p38α/β/γ/δ in the sensing ensemble. Stock peptide aliquots of 5 µL (20 µM) were added to obtain a final concentration of 2 µM SOX-peptide in the array.

Optimizing sensing array experiment. Three different kinase solutions with the following final concentrations 0.6 nM ERK1, 6.4 nM JNK3 and 3.1 nM p38γ (final volume 588 µL) were prepared in buffer assay. Kinase aliquots of 40 µL were then added to obtain the following final concentrations 0.5 nM ERK1, 5 nM JNK3 and 2.5 nM p38γ in the sensing ensemble. Stock peptide solutions of 5 µL (20 µM) were added to obtain a final concentration of 2 µM SOX-peptide.

Optimizing SOX-p38 peptide concentration assay. A kinase solution with the following final concentration 27 nM p38γ (final volume 300 µL) was prepared in buffer assay. Kinase aliquots of 15 µL were then added to obtain the following final concentration 8 nM p38γ in the sensing ensemble. Different SOX-p38 peptide solutions (final volume 40 µL) were prepared to obtain the following final concentrations 3.5 nM, 8.3 nM, 16.6 nM, 25 nM, 50 nM and 83 nM in buffer assay. Peptide aliquots of 30 µL were then added to obtain the following final concentrations 2 µM, 5 µM, 10 µM, 15 µM, 30 µM and 50 µM in the sensing ensemble, respectively.

Array reproducibility for nine MAPKs experiment. Nine individual kinase solutions with the following final concentrations 1 nM ERK1/2, 10 nM JNK1/2/3 and 5 nM p38α/β/γ/δ (final volume 460 µL) were prepared in buffer assay. Kinase aliquots of 25 µL were then added to obtain the following final concentration 0.5 nM ERK1/2, 5 nM JNK1/2/3 and 2.5 nM p38α/β/γ/δ in the sensing ensemble. Peptide aliquots of 20 µL (5 µM) were added to obtain a final concentration of 2 µM SOX-peptide in the array. SOX-p38 peptide aliquots of 20 µL (20 µM) were added into the corresponding wells to obtain a final concentration of 8 µM.

Increasing ERK1 concentration assay. ERK1 stock solution (1 µM) was diluted to obtain a final concentration of 0.1 µM. Eight different kinase solutions (final volume 550 µL) were prepared to obtain the following final concentrations 10 nM JNK3 and 5 nM p38γ with 0 nM, 0.1 nM, 0.2 nM, 0.4 nM, 0.8 nM 1.6 nM, 3.2 nM and 6.4 nM ERK1 in buffer assay, respectively. Kinase aliquots of 25 µL were then added to obtain the following final concentrations 5 nM JNK3, 2.5 nM p38γ and 0 nM, 0.05 nM, 0.1 nM, 0.2 nM, 0.4 nM, 0.8 nM, 1.6 nM and 3.2 nM ERK1 in the sensing ensemble, respectively. Peptide aliquots of 20 µL (5 µM) were added to obtain a final concentration of 2 µM SOX-peptide in the array. SOX-p38 peptide aliquots of 20 µL (20 µM) were added into the corresponding wells to obtain a final concentration of 8 µM.

Increasing JNK3 concentration assay. Eight different kinase solutions (final volume 550 µL) were prepared to obtain the following final concentrations 1 nM ERK1 and 5 nM p38γ with 0 nM, 1 nM, 2 nM, 4 nM, 8 nM 16 nM, 32 nM and 64 nM JNK3 in

buffer assay, respectively. Kinase aliquots of 25 µL were then added to obtain the following final concentrations 0.5 nM ERK1, 2.5 nM p38γ and 0 nM, 0.5 nM, 1 nM, 2 nM, 4 nM, 8 nM, 16 nM and 32 nM JNK3 in the sensing ensemble, respectively. Peptide aliquots of 20 µL (5 µM) were added to obtain a final concentration of 2 µM SOX-peptide in the array. SOX-p38 peptide aliquots of 20 µL (20 µM) were added into the corresponding wells to obtain a final concentration of 8 µM.

Increasing p38γ concentration assay. Eight different kinase solutions (final volume 575 µL) were prepared to obtain the following final concentrations 1 nM ERK1 and 10 nM JNK3 with 0 nM, 0.5 nM, 1 nM, 2 nM, 4 nM, 8 nM 16 nM, and 32 nM p38γ in buffer assay, respectively. Kinase aliquots of 25 µL were then added to obtain the following final concentrations 0.5 nM ERK1, 5 nM JNK3 and 0 nM, 0.25 nM, 0.5 nM, 1 nM, 2 nM, 4 nM, 8 nM, and 16 nM p38γ in the sensing ensemble, respectively. Peptide aliquots of 20 µL (5 µM) were added to obtain a final concentration of 2 µM SOX-peptide in the array. SOX-p38 peptide aliquots of 20 µL (20 µM) were added into the corresponding wells to obtain a final concentration of 8 µM.

ERK1 inhibitor experiment. A kinase solution with the following final concentration 1.65 nM ERK1 (final volume 2760 µL) was prepared in buffer assay. Kinase aliquots of 15 µL were then added to obtain the following final concentration 0.5 nM ERK1 in the sensing ensemble. Different inhibitor solutions (final volume 300 µL) were prepared to obtain the following final concentrations 0 nM, 5 nM, 40 nM, 80 nM and 240 nM with 25% DMSO in buffer assay. Inhibitor aliquots of 10 µL were then

added to obtain the following final concentrations 0 nM, 1 nM, 8 nM, 16 nM, and 48 nM in the sensing ensemble, respectively. Peptide aliquots of 20 µL (5 µM) were added to obtain a final concentration of 2 µM SOX-peptide. SOX-p38 peptide aliquots of 20 µL (20 µM) were added into the corresponding wells to obtain a final concentration of 8 µM.

ERK1 inhibition in kinase mixtures experiment. A kinase solution with the following final concentrations 1.65 nM ERK1, 16.7 nM JNK3 and 8.4 nM p38γ (final volume 2760 µL) was prepared in buffer assay. Kinase aliquots of 15 µL were then added to obtain the following final concentration 0.5 nM ERK1, 5 nM JNK3 and 2.5 nM p38γ in the sensing ensemble. Different inhibitor solutions (final volume 450 µL) were prepared to obtain the following final concentrations 0 nM, 5 nM, 10 nM, 15 nM, 20 nM 40 nM, 80 nM and 240 nM with 25% DMSO in buffer assay. Inhibitor aliquots of 10 µL were then added to obtain the following final concentrations 0 nM, 1 nM, 2 nM, 3 nM, 4 nM, 8 nM, 16 nM, and 48 nM in the sensing ensemble, respectively. Peptide aliquots of 20 µL (5 µM) were added to obtain a final concentration of 2 µM SOX-peptide. SOX-p38 peptide aliquots of 20 µL (20 µM) were added into the corresponding wells to obtain a final concentration of 8 µM.

Expression, Purification and Activation of Tagless MAP Kinases – Tagless *N*-terminal truncated human JNK3α2 (amino acids 39-422 with alanine inserted between amino acids 39 and 40, GenBank accession number NM_138982) was expressed, purified and activated as described previously.[112,113] Activated tagless ERK2 (Rattus norvegicus mitogen activated protein kinase 1, GenBank accession number NM_053842)

was expressed, purified and activated as described in *Kaoud et al*.[114] Activated ERK1 were expressed, purified and activated as described in *Callaway et al*.[115] p38MAPKγ was expressed, purified and activated as described previously.[116,117] The activated kinases were all stored in buffer S [25 mM HEPES (pH 7.5), 50 mM KCl, 0.1 mM EDTA, 0.1 mM EGTA, 2 mM DTT and 10-20% (v/v) glycerol] at -80 ºC.

3.13.6 Supplementary Figures

3.13.6.1 Preliminary Assay

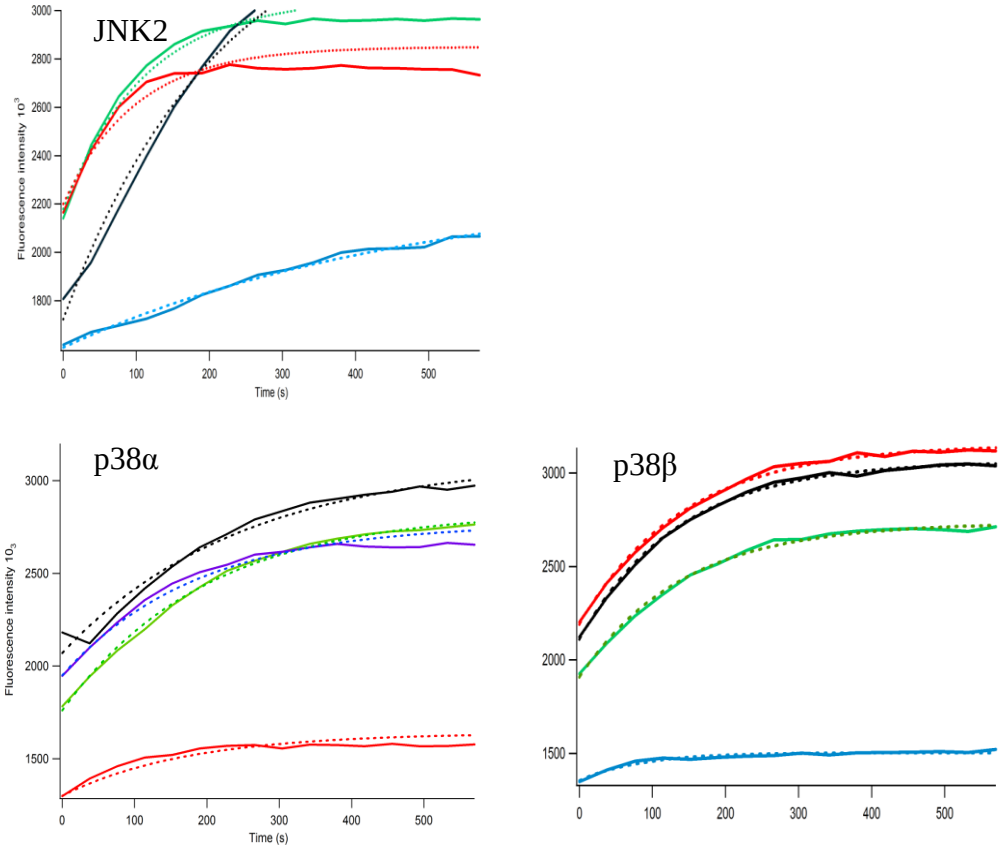

Figure 3.36: *Fit curves of the fluorescence changes of SOX-Sub-D peptide upon phosphorylation with three different MAPKs, showing 4 experimental replicates*. Kinase concentrations: ERK1/2 (2 nM), JNK1/2/3 (20 nM) and p38α/β/γ/δ (10 nM) with SOX-peptide (2 µM).Data collected with 96-well plate half volume, plate reader with λ_{ex} filter of 360 ± 10 nm and λ_{em} filter of 485 ± 10 nm, using a top 400 mirror. Assay buffer: (25mM HEPES, 50mM KCl, 0.1 mM EDTA, 0.1 mM EGTA pH 7.4) with 2 mM DTT, 2.5 µg/mL BSA, 5mM $MgCl_2$, 500 µM ATP at 25°C.

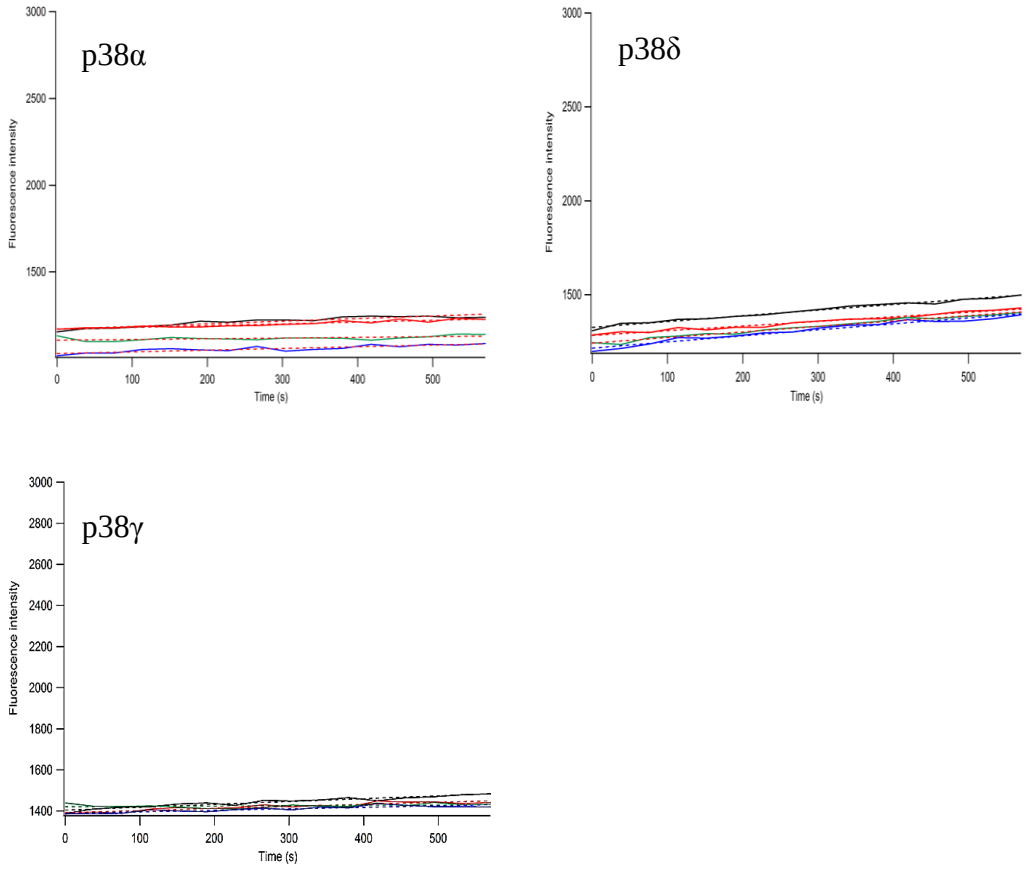

Figure 3.37: *Fit curves of the fluorescence changes of SOX-NFAT4 peptide upon phosphorylation with three different MAPKs, showing 4 experimental replicates*. Kinase concentrations: ERK1/2 (2 nM), JNK1/2/3 (20 nM) and p38α/β/γ/δ (10 nM) with SOX-peptide (2 µM). Data collected with 96-well plate half area, plate reader with λ_{ex} filter of 360 ± 10 nm and λ_{em} filter of 485 ± 10 nm, using a top 400 mirror. Assay buffer: (25mM HEPES, 50mM KCl, 0.1 mM EDTA, 0.1 mM EGTA pH 7.4) with 2 mM DTT, 2.5 µg/mL BSA, 5mM $MgCl_2$, 500 µM ATP at 25°C.

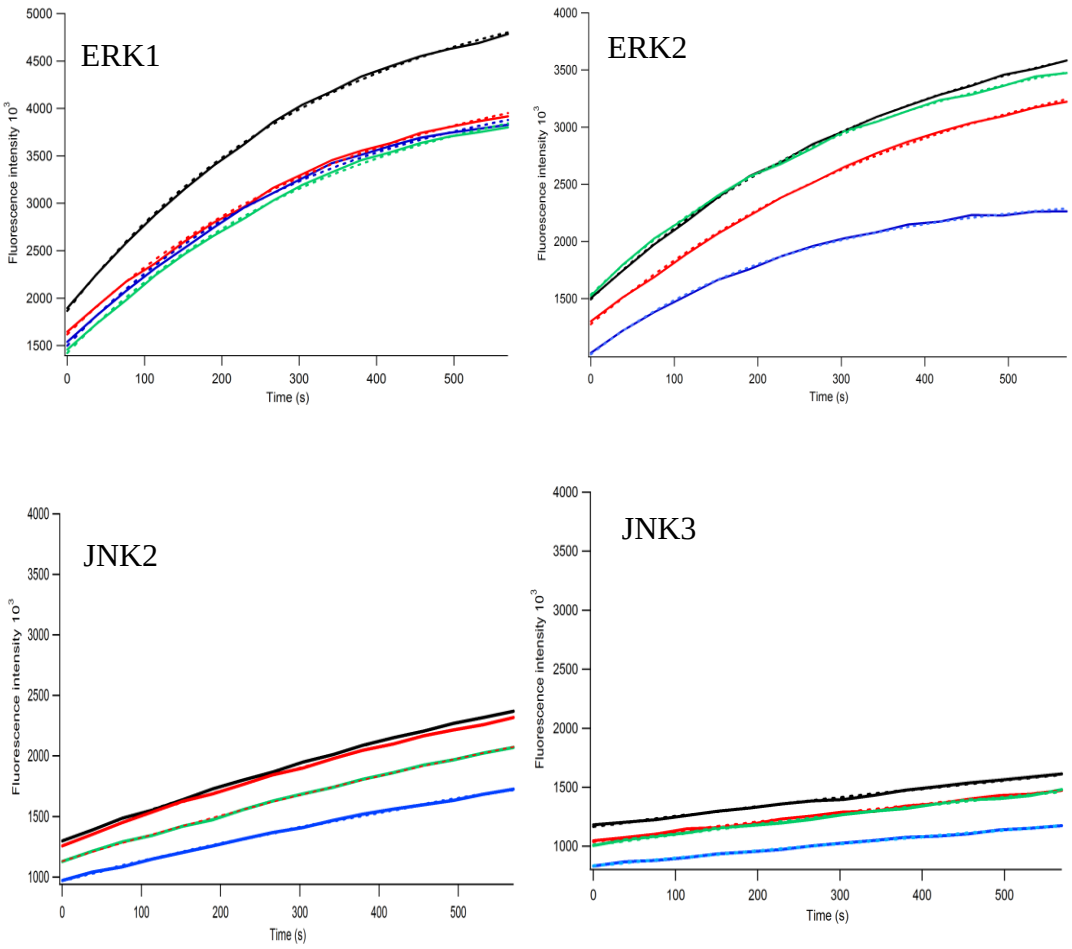

Figure 3.38: *Fit curves of the fluorescence changes of SOX-MEF2A peptide upon phosphorylation with different MAPKs, showing 4 experimental replicates.* Kinase concentrations: ERK1/2 (2 nM), JNK/2/3 (20 nM) with SOX-peptide (2 µM). Data collected with 96-well plate half area, plate reader with λ_{ex} filter of 360 ± 10 nm and λ_{em} filter of 485 ± 10 nm, using a top 400 mirror. Assay buffer: (25mM HEPES, 50mM KCl, 0.1 mM EDTA, 0.1 mM EGTA pH 7.4) with 2 mM DTT, 2.5 µg/mL BSA, 5mM $MgCl_2$, 500 µM ATP at 25℃.

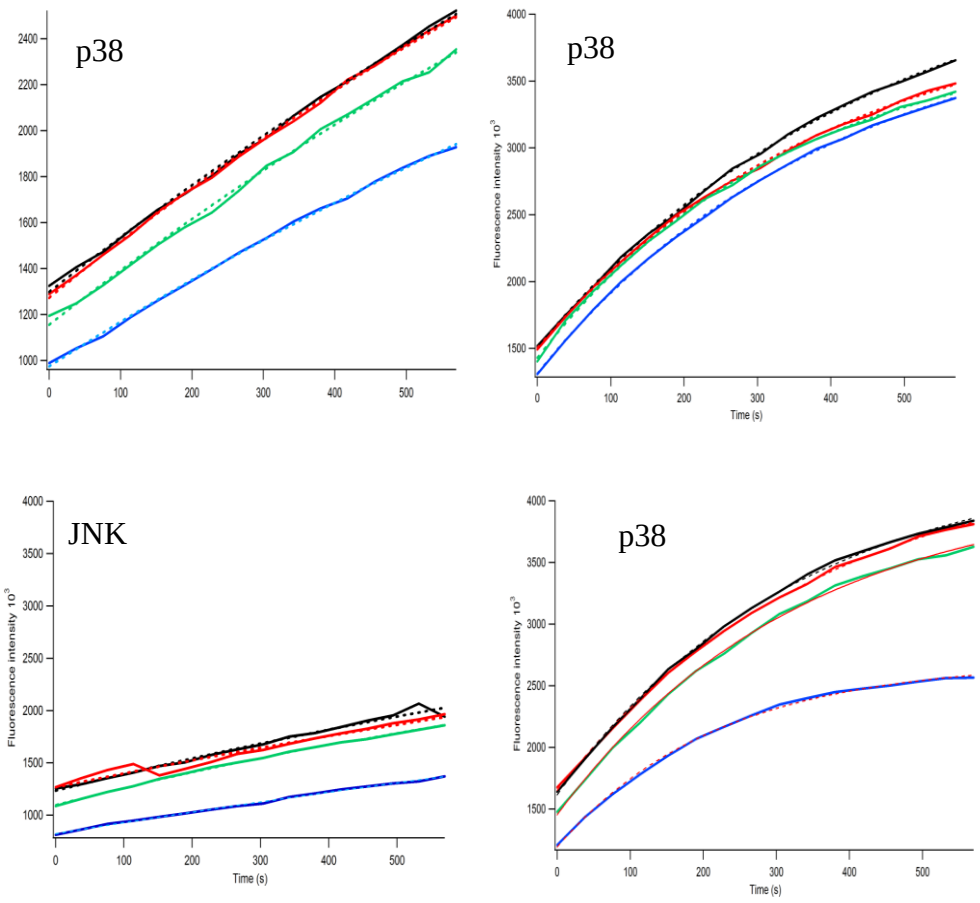

Figure 3.39: *Fit curves of the fluorescence changes of SOX-MEF2A peptide upon phosphorylation with different MAPKs, showing 4 experimental replicates.* Kinase concentrations: JNK1 (20 nM) and p38α/β/δ (10 nM) with SOX-peptide (2 µM). Data collected with 96-well plate half area, plate reader with λ_{ex} filter of 360 ± 10 nm and λ_{em} filter of 485 ± 10 nm, using a top 400 mirror. Assay buffer: (25mM HEPES, 50mM KCl, 0.1 mM EDTA, 0.1 mM EGTA pH 7.4) with 2 mM DTT, 2.5 µg/mL BSA, 5mM $MgCl_2$, 500 µM ATP at 25°C.

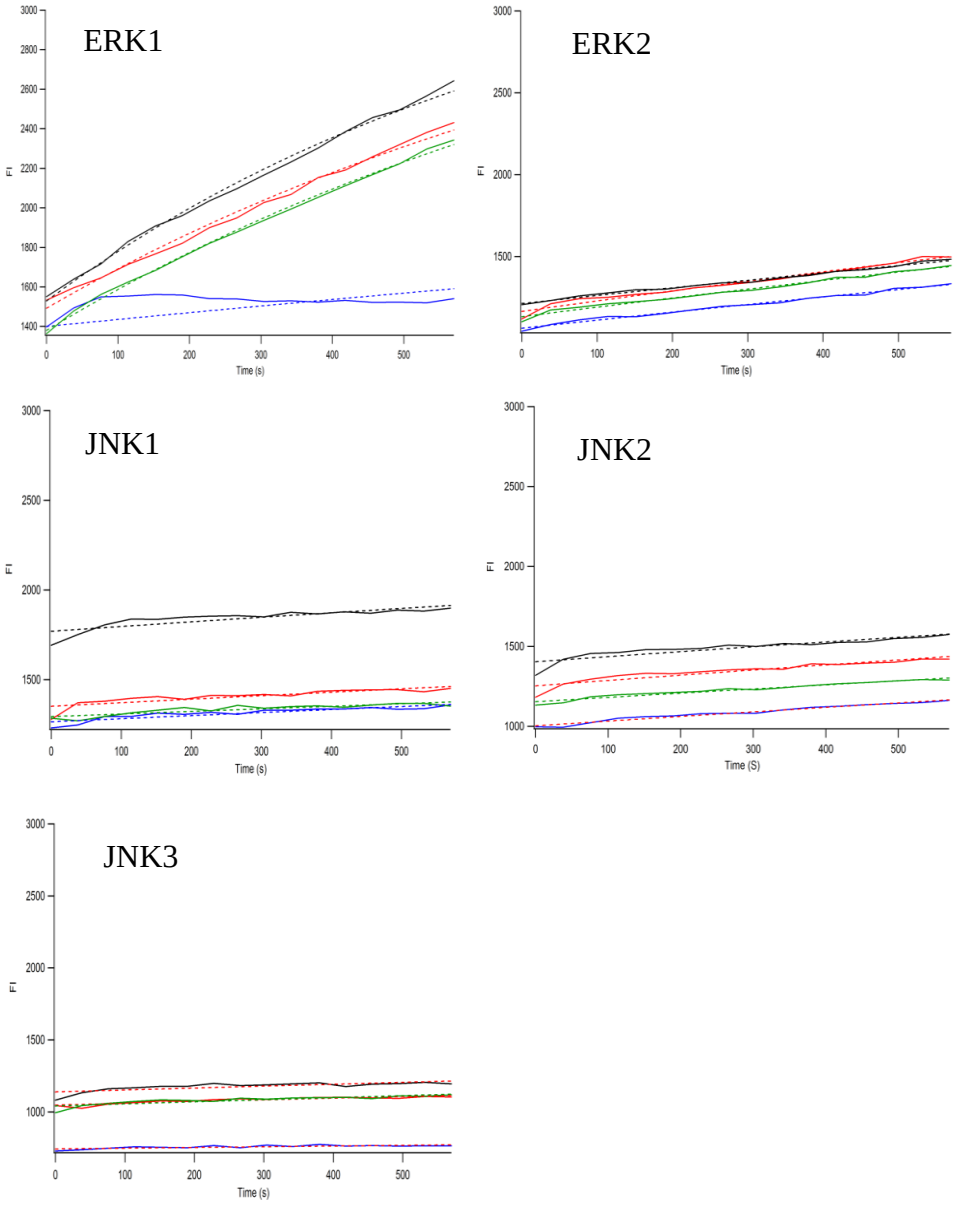

Figure 3.40: *Fit curves of the fluorescence changes of SOX-Sub-F peptide upon phosphorylation with different MAPKs, showing 4 experimental replicates.* Kinase concentrations: ERK1/2 (2 nM) and JNK1/2/3 (20 nM) with SOX-peptide (2 µM). Data collected with 96-well plate half area, plate reader with λ_{ex} filter of 360 ± 10 nm and λ_{em} filter of 485 ± 10 nm, using a top 400 mirror. Assay buffer: (25mM HEPES, 50mM KCl, 0.1 mM EDTA, 0.1 mM EGTA pH 7.4) with 2 mM DTT, 2.5 µg/mL BSA, 5mM $MgCl_2$, 500 µM ATP at 25℃.

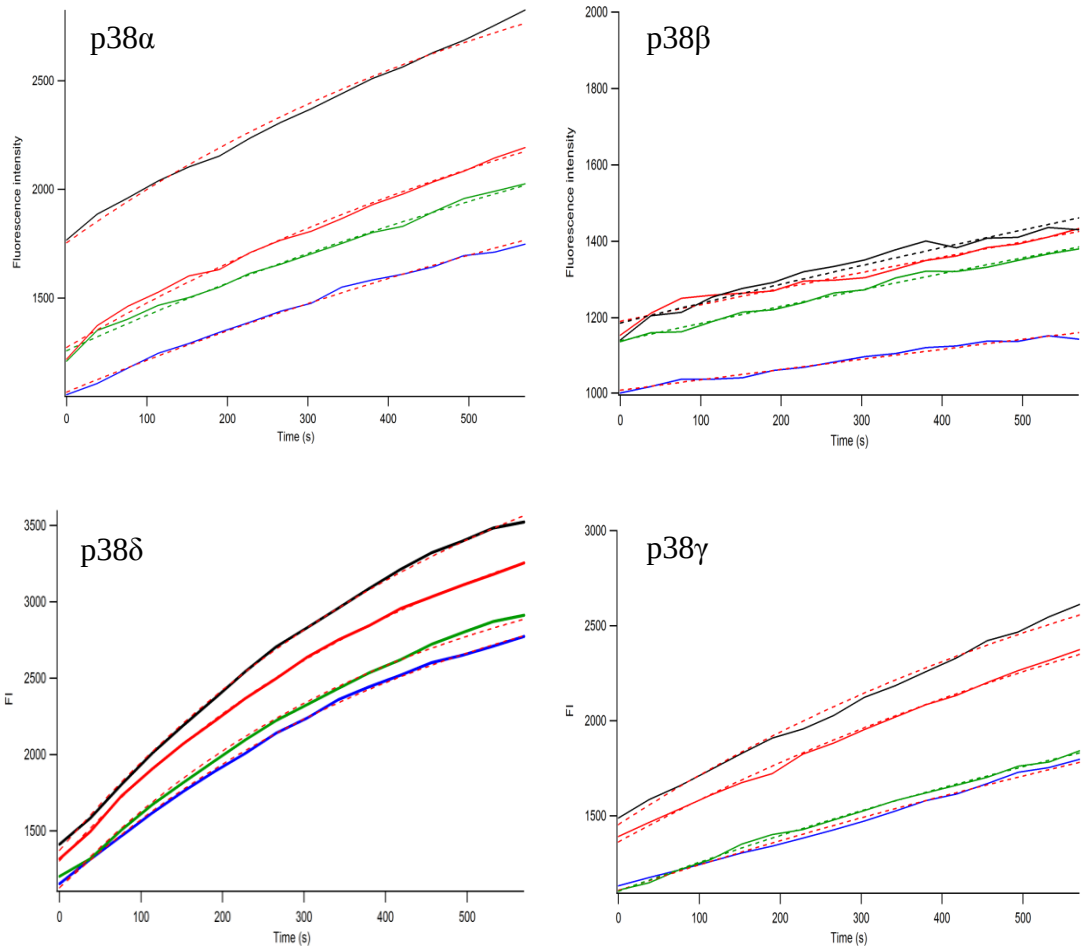

Figure 3.41: *Fit curves of the fluorescence changes of SOX-Sub-F peptide upon phosphorylation with different MAPKs, showing 4 experimental replicates.* Kinase concentrations: p38α/β/γ/δ (10 nM) with SOX-peptide (2 µM). Data collected with 96-well plate half area, plate reader with λ_{ex} filter of 360 ± 10 nm and λ_{em} filter of 485 ± 10 nm, using a top 400 mirror. Assay buffer: (25mM HEPES, 50mM KCl, 0.1 mM EDTA, 0.1 mM EGTA pH 7.4) with 2 mM DTT, 2.5 µg/mL BSA, 5mM $MgCl_2$, 500 µM ATP at 25°C.

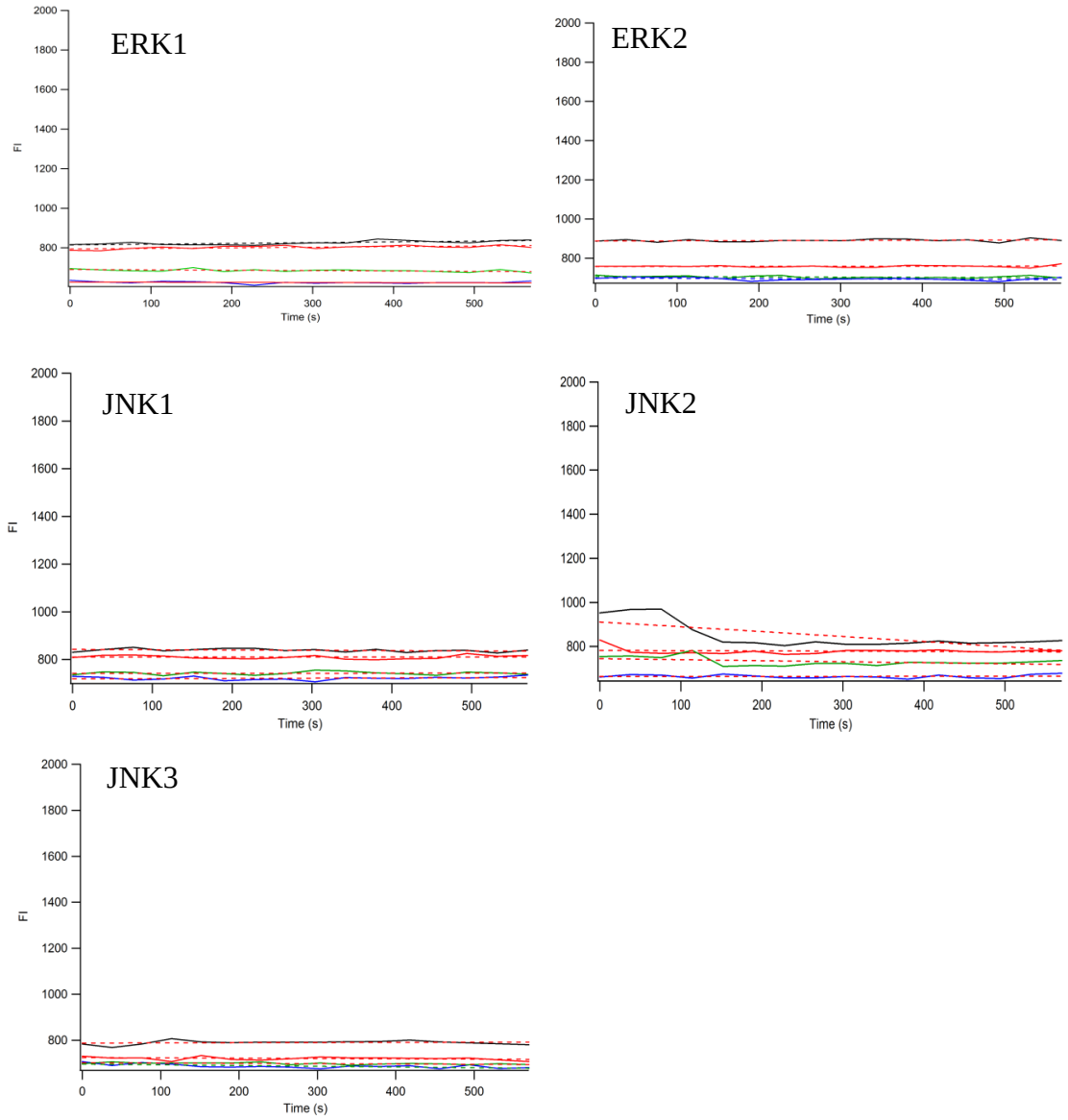

Figure 3.42: *Fit curves of the fluorescence changes of SOX-p38 peptide upon phosphorylation with different MAPKs, showing 4 experimental replicates.* Kinase concentrations: ERK1/2 (2 nM) and JNK1/2/3 (20 nM) with SOX-peptide (2 µM). Data collected with 96-well plate half area, plate reader with λ_{ex} filter of 360 ± 10 nm and λ_{em} filter of 485 ± 10 nm, using a top 400 mirror. Assay buffer: (25mM HEPES, 50mM KCl, 0.1 mM EDTA, 0.1 mM EGTA pH 7.4) with 2 mM DTT, 2.5 µg/mL BSA, 5mM $MgCl_2$, 500 µM ATP at 25℃.

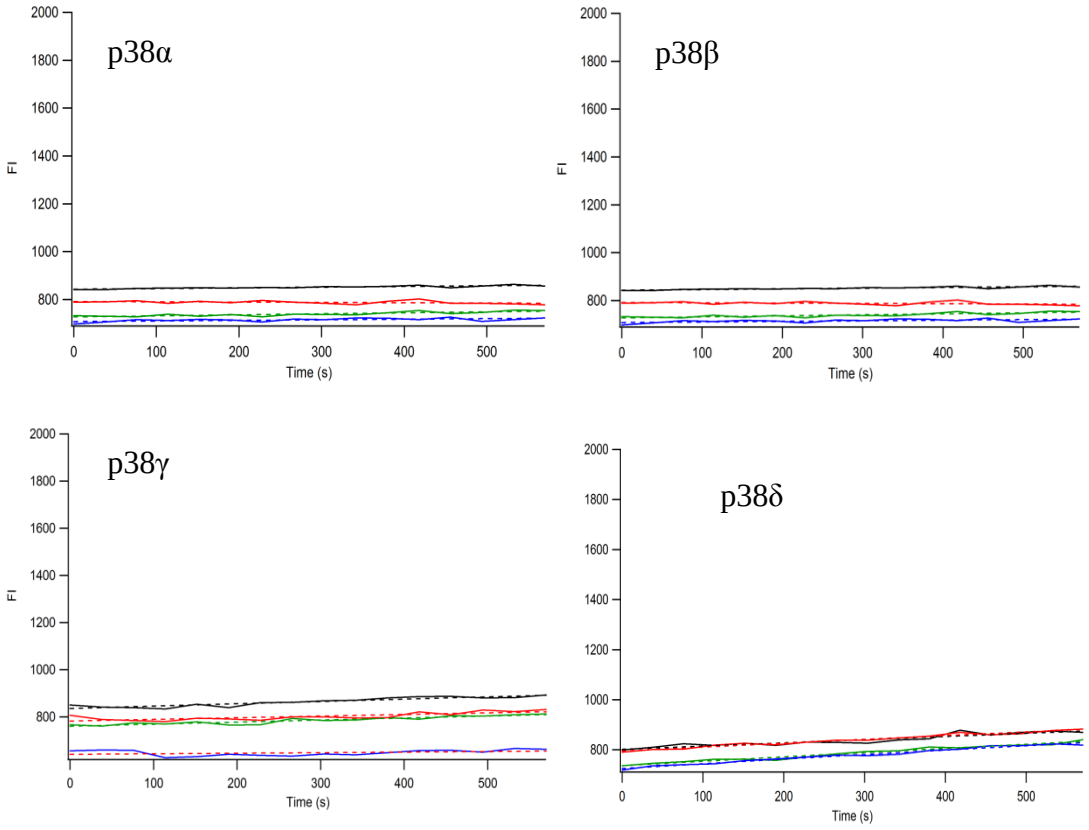

Figure 3.43: *Fit curves of the fluorescence changes of SOX-p38 peptide upon phosphorylation with different MAPKs, showing 4 experimental replicates.* Kinase concentrations: p38α/β/γ/δ (10 nM) with SOX-peptide (2 µM). Data collected with 96-well plate half area, plate reader with λ_{ex} filter of 360 ± 10 nm and λ_{em} filter of 485 ± 10 nm, using a top 400 mirror. Assay buffer: (25mM HEPES, 50mM KCl, 0.1 mM EDTA, 0.1 mM EGTA pH 7.4) with 2 mM DTT, 2.5 µg/mL BSA, 5mM $MgCl_2$, 500 µM ATP at 25°C.

3.13.6.2 Fluorescence Changes o of Three MAPK Groups

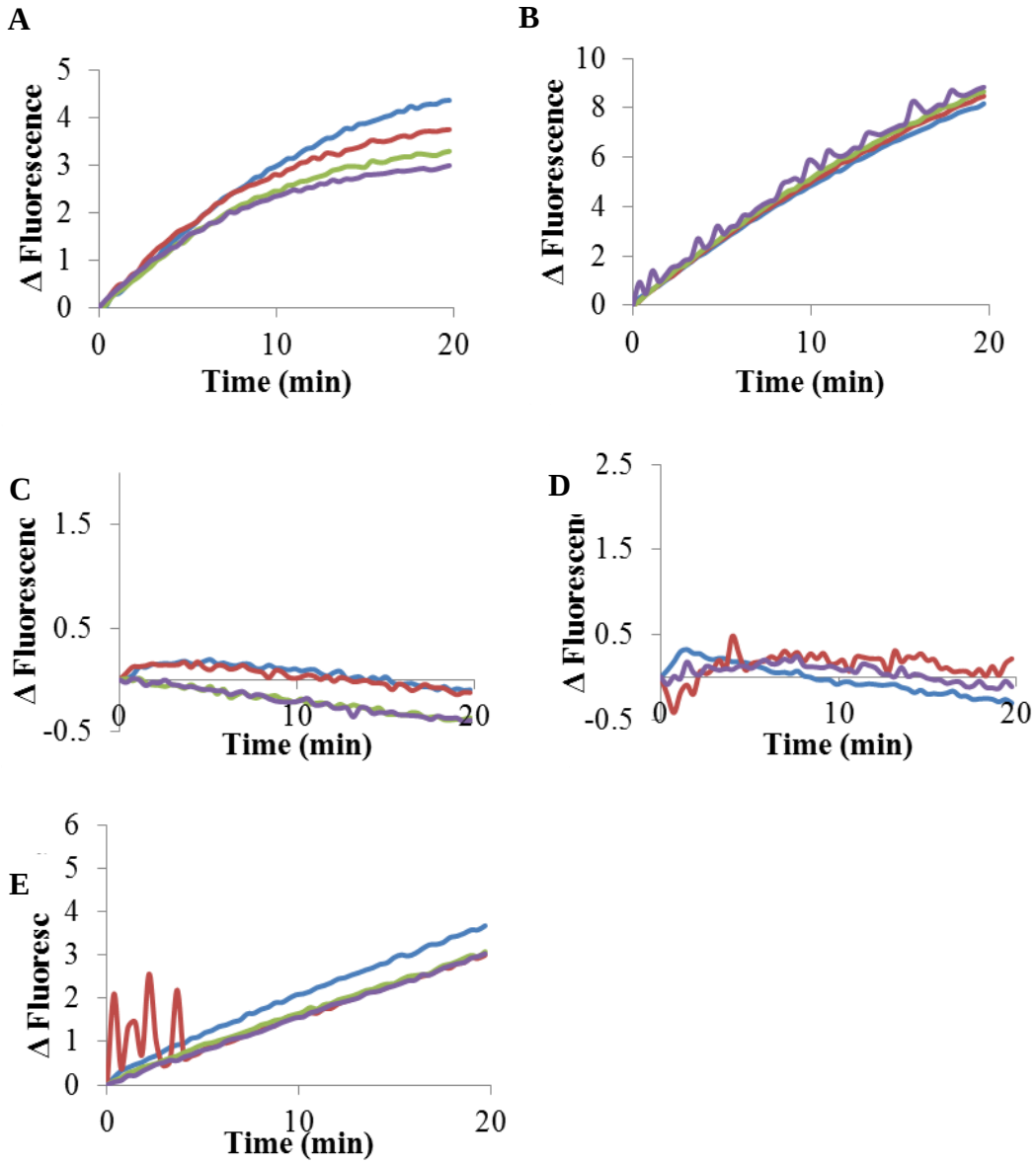

Figure 3.44: *Fluorescence changes of SOX-peptides upon phosphorylation with ERK1, showing 4 experimental replicates.* A) SOX-Sub-D. (B) SOX-MEF2A. (C) SOX-NFAT4. (D) SOX-Sub-F. (E) SOX-p38. Concentrations: ERK1 (0.5 nM); SOX-peptides (2 µM). Data collected with 96-well plate half area, plate reader with λ_{ex} filter of 340 ± 35 nm and λ_{em} filter of 485 ± 20 nm. Assay buffer: (25mM HEPES, 50mM KCl, 0.1 mM EDTA, 0.1 mM EGTA pH 7.4) with 2 mM DTT, 2.5 µg/mL BSA, 5mM $MgCl_2$, 500 µM ATP at 25°C.

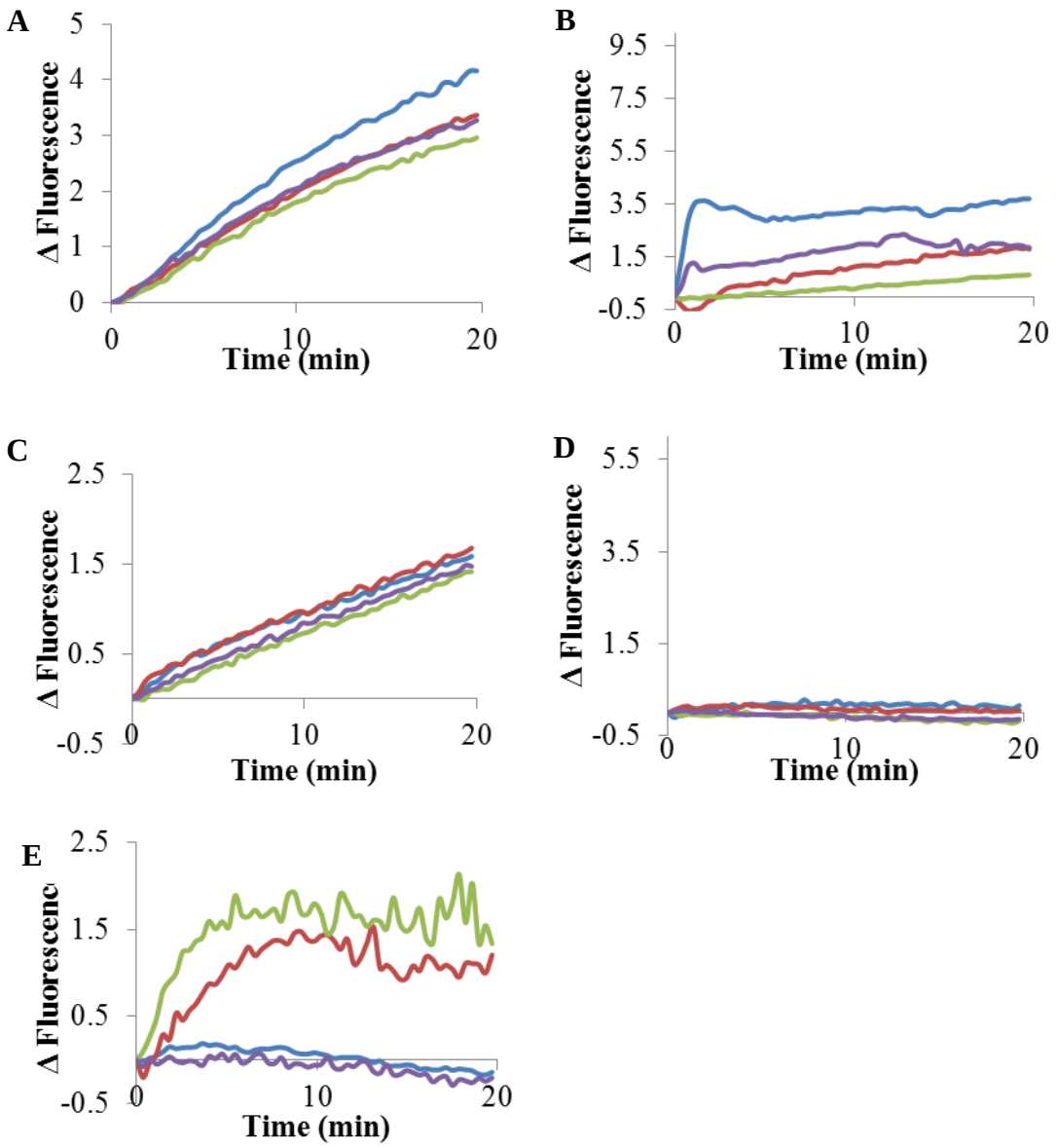

Figure 3.45: *Fluorescence changes of SOX-peptides upon phosphorylation with JNK3, showing 4 experimental replicates.* A) SOX-Sub-D. (B) SOX-MEF2A. (C) SOX-NFAT4. (D) SOX-Sub-F. (E) SOX-p38. Concentrations: JNK3 (5 nM); SOX-peptides (2 µM). Data collected with 96-well plate half area, plate reader with λ_{ex} filter of 340 ± 35 nm and λ_{em} filter of 485 ± 20 nm. Assay buffer: (25mM HEPES, 50mM KCl, 0.1 mM EDTA, 0.1 mM EGTA pH 7.4) with 2 mM DTT, 2.5 µg/mL BSA, 5mM $MgCl_2$, 500 µM ATP at 25℃.

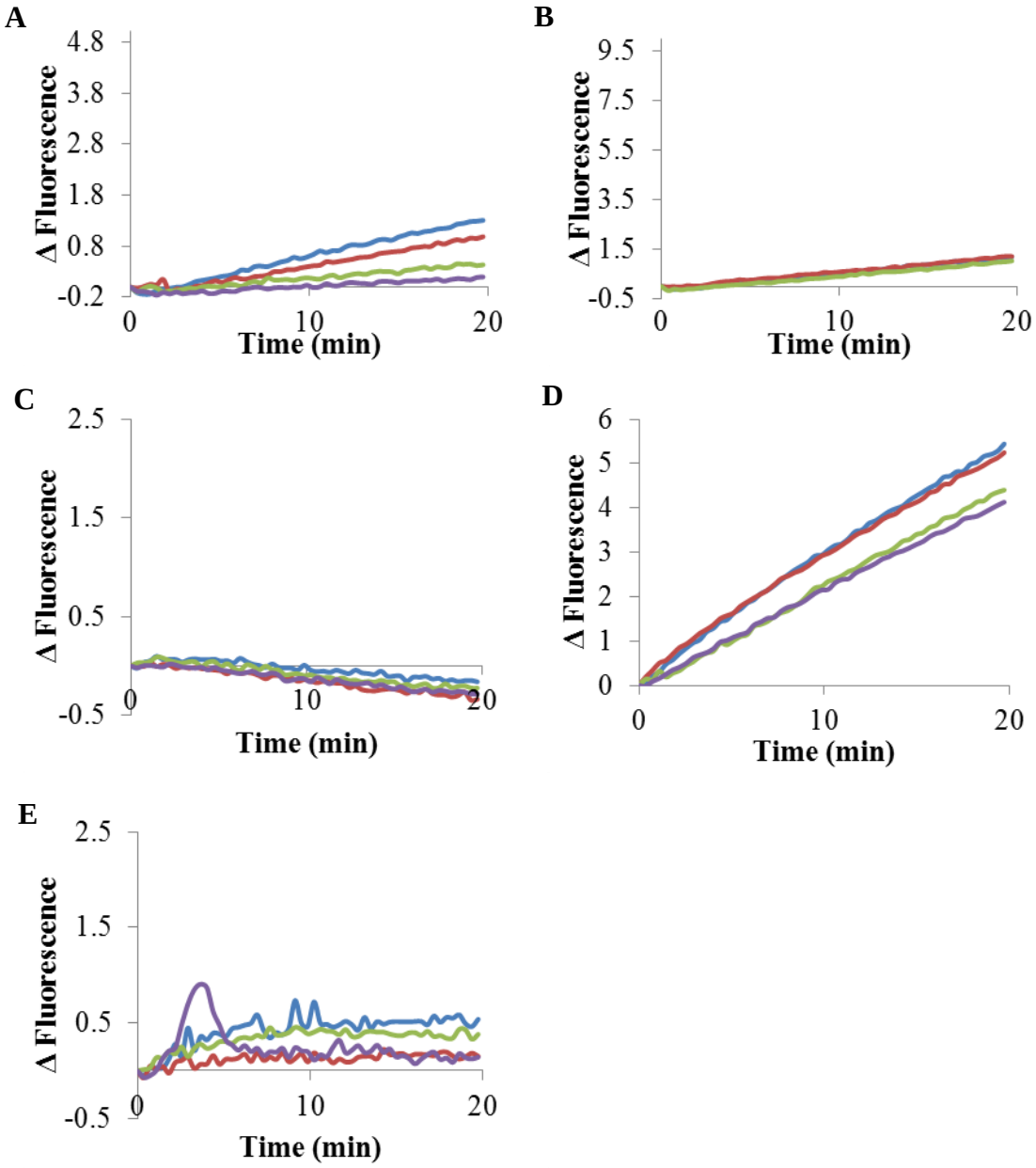

Figure 3.46: *Fluorescence changes of SOX-peptides upon phosphorylation with p38γ, showing 4 experimental replicates.* A) SOX-Sub-D. (B) SOX-MEF2A. (C) SOX-NFAT4. (D) SOX-Sub-F. (E) SOX-p38. Concentrations: *p38γ* (2.5 nM); SOX-peptides (2 µM). Data collected with 96-well plate half area, plate reader with λ_{ex} filter of 340 ± 35 nm and λ_{em} filter of 485 ± 20 nm. Assay buffer: (25mM HEPES, 50mM KCl, 0.1 mM EDTA, 0.1 mM EGTA pH 7.4) with 2 mM DTT, 2.5 µg/mL BSA, 5mM $MgCl_2$, 500 µM ATP at 25℃.

3.13.6.3 Reproducible Fluorescence Changes of MAPKs

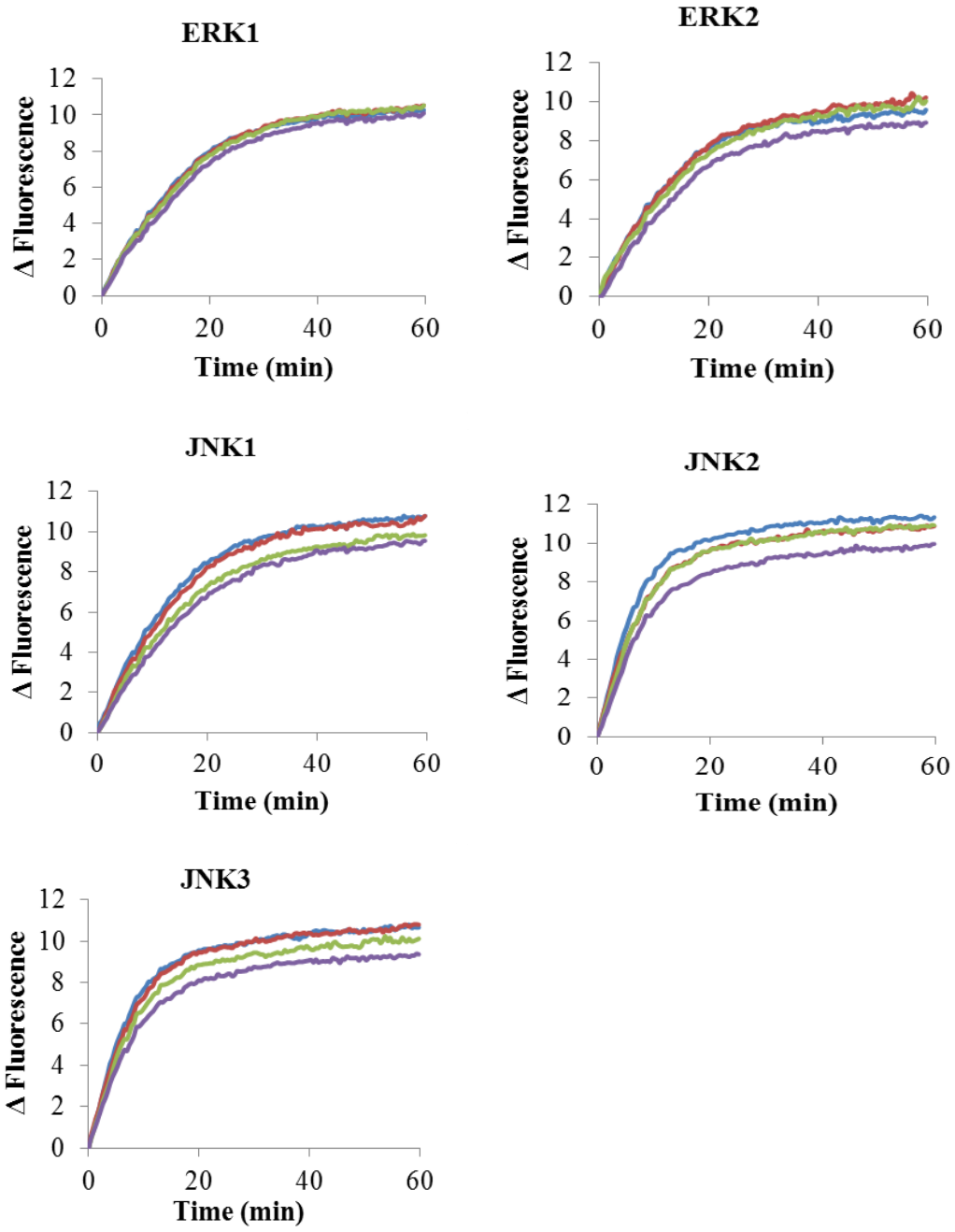

Figure 3.47: *Fluorescence changes of SOX-Sub-D peptide upon phosphorylation with different MAPKs, showing 4 experimental replicates.* Kinase concentrations: ERK1/2 (0.5 nM), JNK1/2/3 (5 nM) with SOX-Sub-D peptide (2 µM).

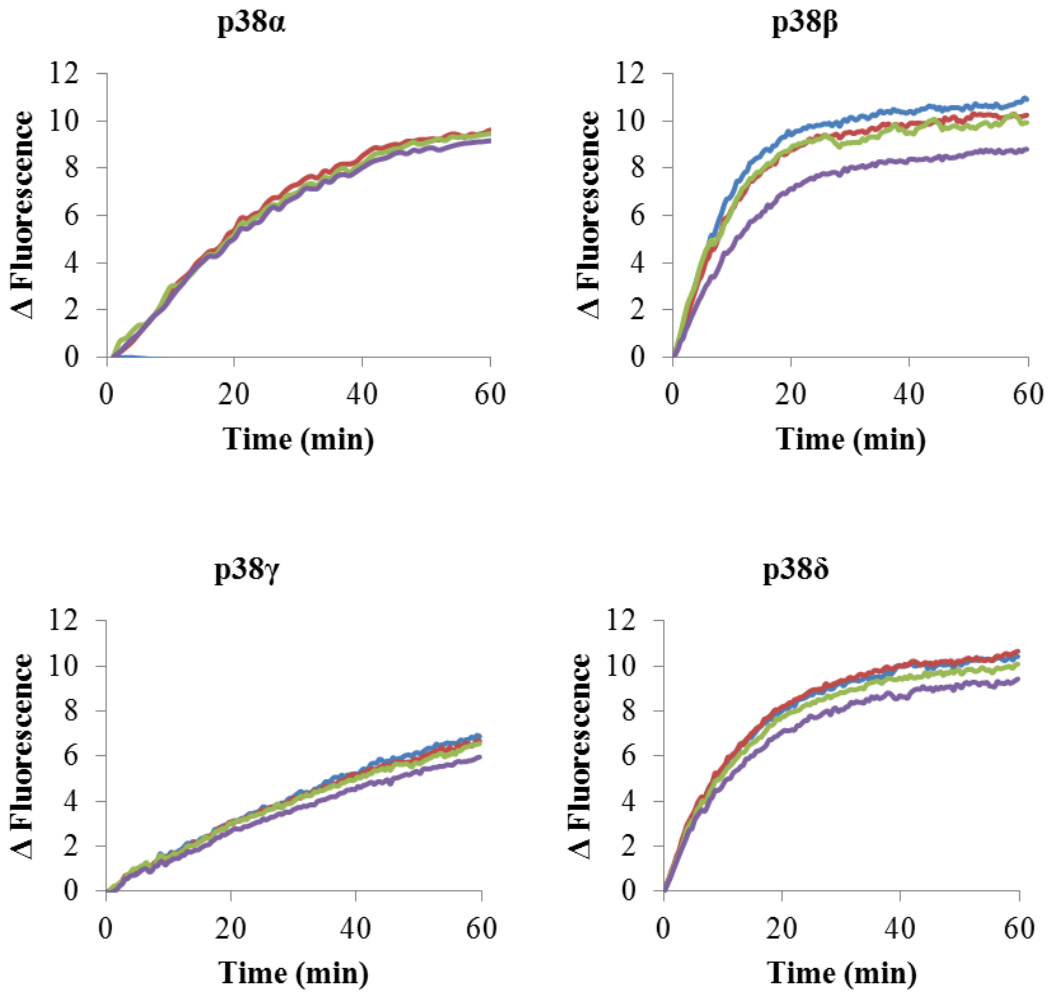

Figure 3.48: *Fluorescence changes of SOX-Sub-D peptide upon phosphorylation with different MAPKs, showing 4 experimental replicates.* Kinase concentrations: p38α/β/γ/δ (2.5 nM) with SOX-Sub-D peptide (2 µM). Data collected with 96-well plate half area, plate reader with λ_{ex} filter of 360 ± 10 nm and λ_{em} filter of 485 ± 10 nm, using a top 400 mirror. Assay buffer: (25mM HEPES, 50mM KCl, 0.1 mM EDTA, 0.1 mM EGTA pH 7.4) with 2 mM DTT, 2.5 µg/mL BSA, 5mM $MgCl_2$, 500 µM ATP at 25°C.

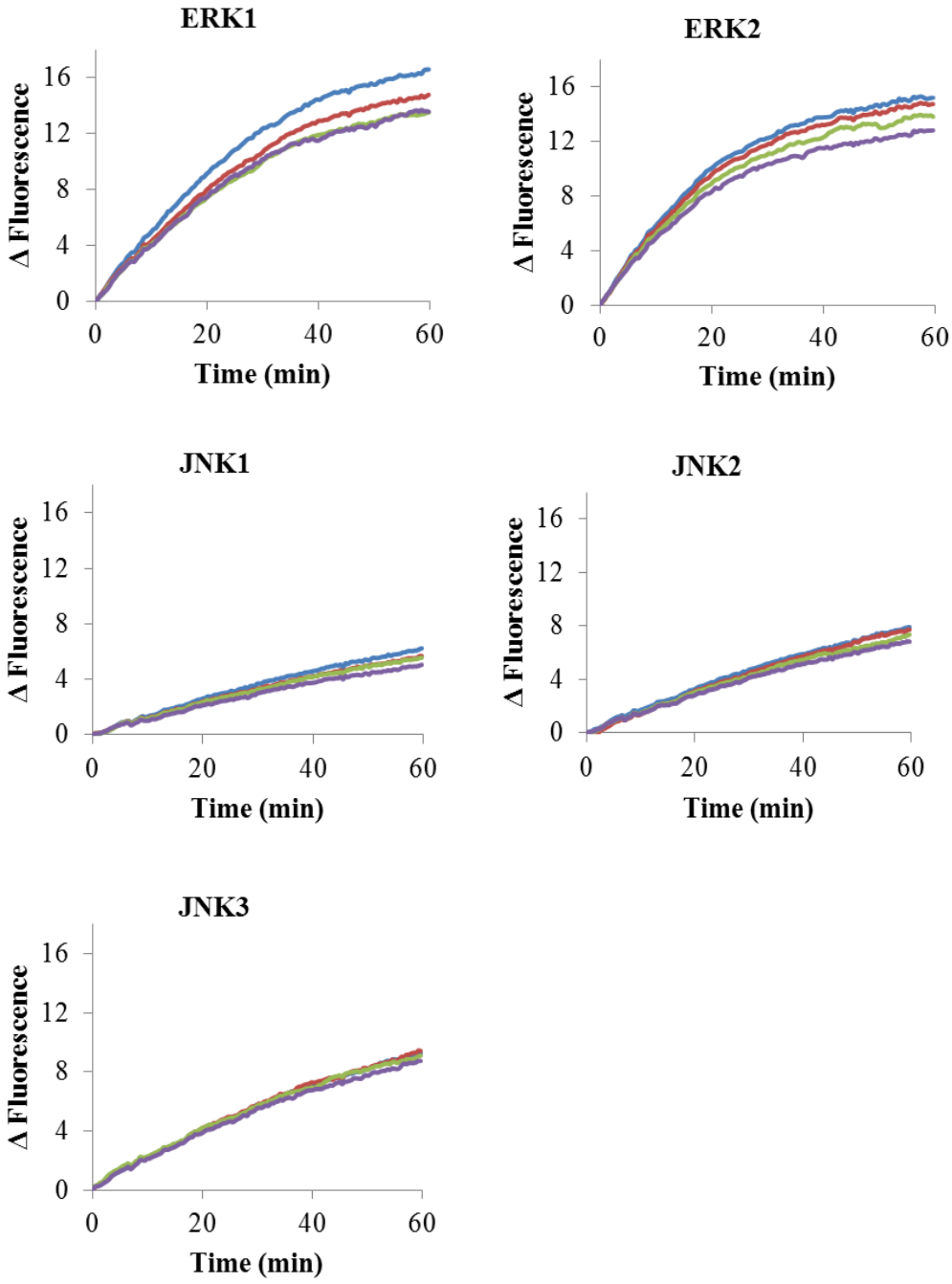

Figure 3.49: *Fluorescence changes of SOX-MEF2A peptide upon phosphorylation with different MAPKs, showing 4 experimental replicates.* Kinase concentrations: ERK1/2 (0.5 nM), and JNK1/2/3 (5 nM) with SOX-MEF2A peptide (2 µM).

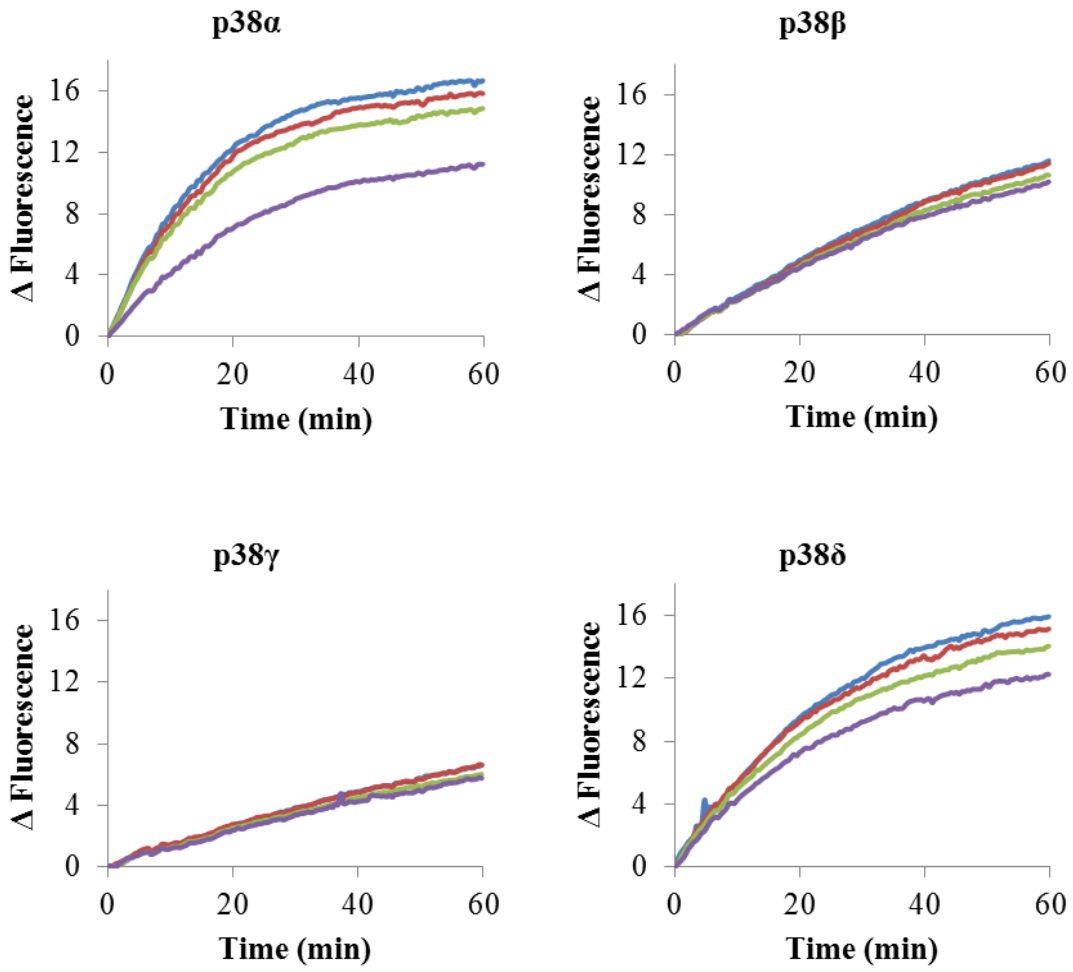

Figure 3.50: *Fluorescence changes of SOX-MEF2A peptide upon phosphorylation with different MAPKs, showing 4 experimental replicates.* Kinase concentrations: p38α/β/γ/δ (2.5 nM) with SOX-MEF2A peptide (2 µM). Data collected with 96-well plate half area, plate reader with λ_{ex} filter of 360 ± 10 nm and λ_{em} filter of 485 ± 10 nm, using a top 400 mirror. Assay buffer: (25mM HEPES, 50mM KCl, 0.1 mM EDTA, 0.1 mM EGTA pH 7.4) with 2 mM DTT, 2.5 µg/mL BSA, 5mM $MgCl_2$, 500 µM ATP at 25°C.

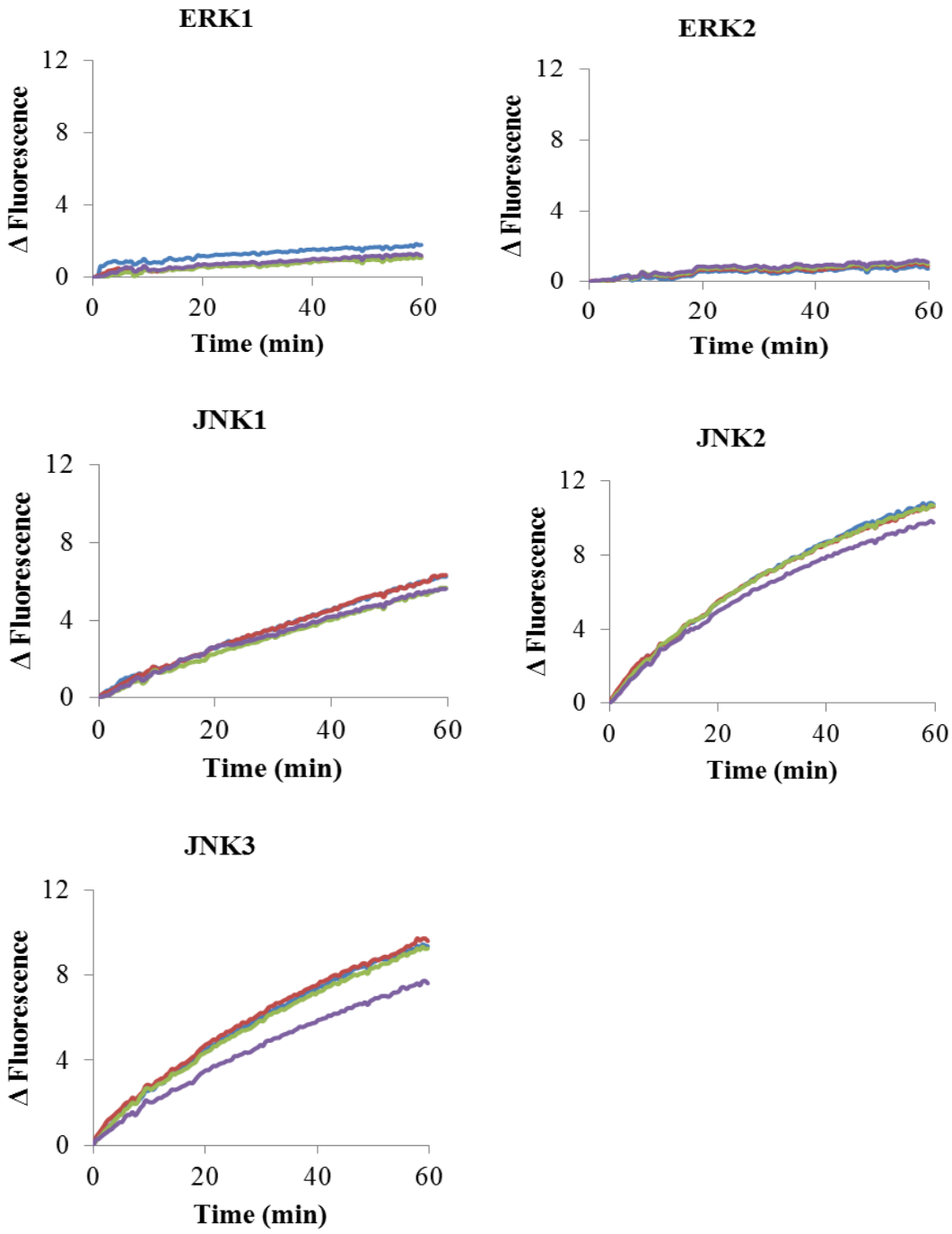

Figure 3.51: *Fluorescence changes of SOX-NFAT4 peptide upon phosphorylation with different MAPKs, showing 4 experimental replicates.* Kinase concentrations: ERK1/2 (0.5 nM), and JNK1/2/3 (5 nM) with SOX-NFAT4 peptide (2 µM).

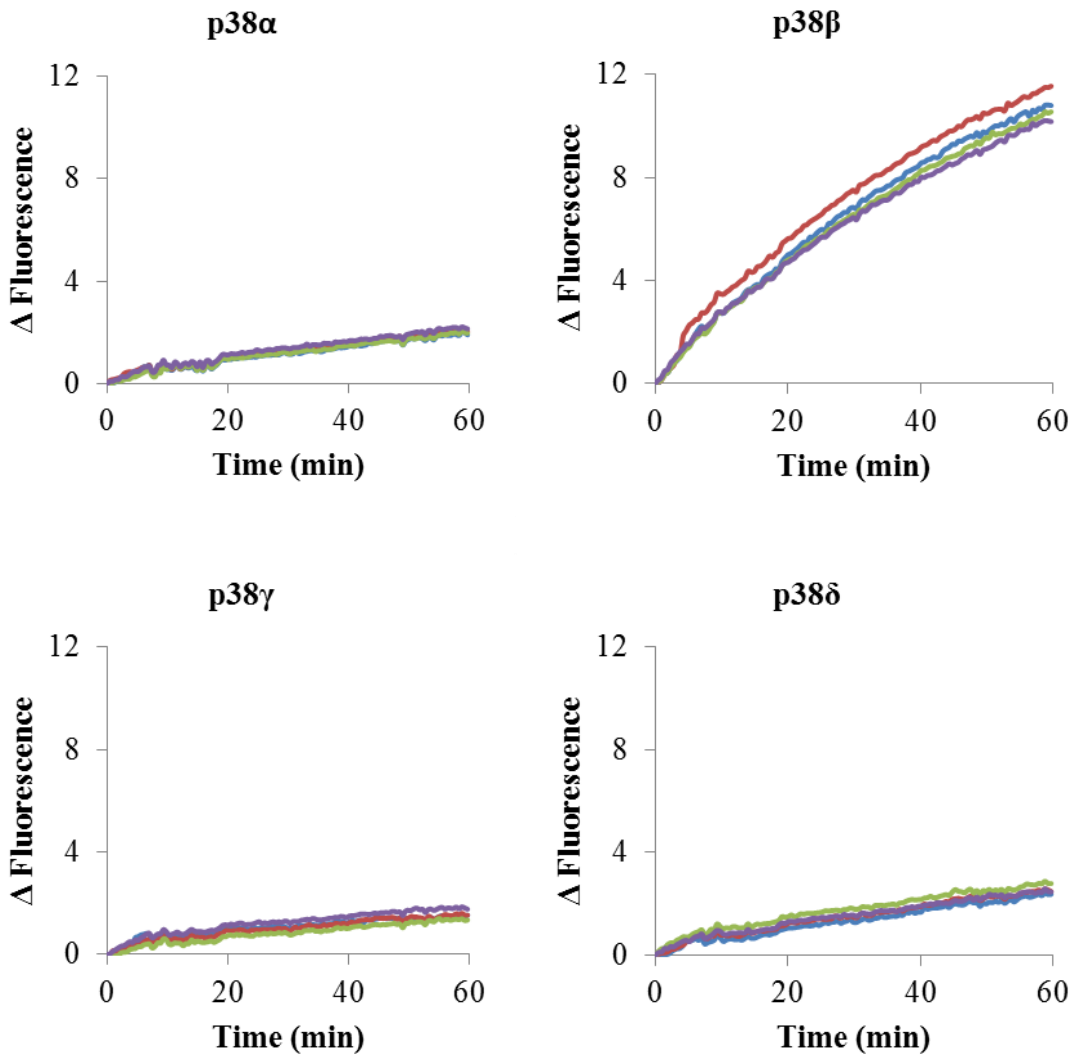

Figure 3.52: *Fluorescence changes of SOX-NFAT4 peptide upon phosphorylation with different MAPKs, showing 4 experimental replicates.* Kinase concentrations: p38α/β/γ/δ (2.5 nM) with SOX-NFAT4 peptide (2 µM). Data collected with 96-well plate half area, plate reader with λ_{ex} filter of 360 ± 10 nm and λ_{em} filter of 485 ± 10 nm, using a top 400 mirror. Assay buffer: (25mM HEPES, 50mM KCl, 0.1 mM EDTA, 0.1 mM EGTA pH 7.4) with 2 mM DTT, 2.5 µg/mL BSA, 5mM $MgCl_2$, 500 µM ATP at 25°C.

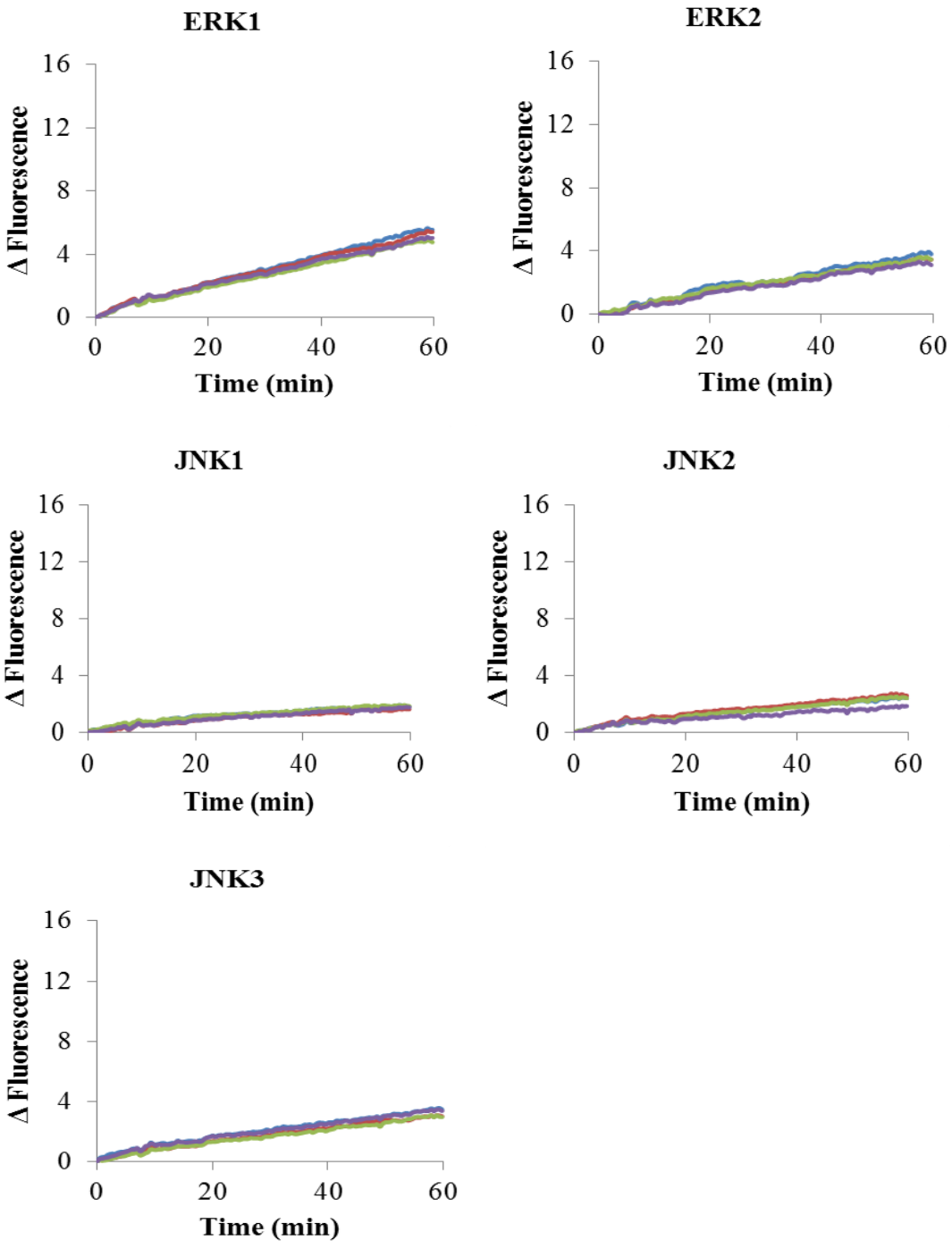

Figure 3.53: *Fluorescence changes of SOX-Sub-F peptide upon phosphorylation with different MAPKs, showing 4 experimental replicates.* Kinase concentrations: ERK1/2 (0.5 nM), and JNK1/2/3 (5 nM) with SOX-Sub-F peptide (2 µM).

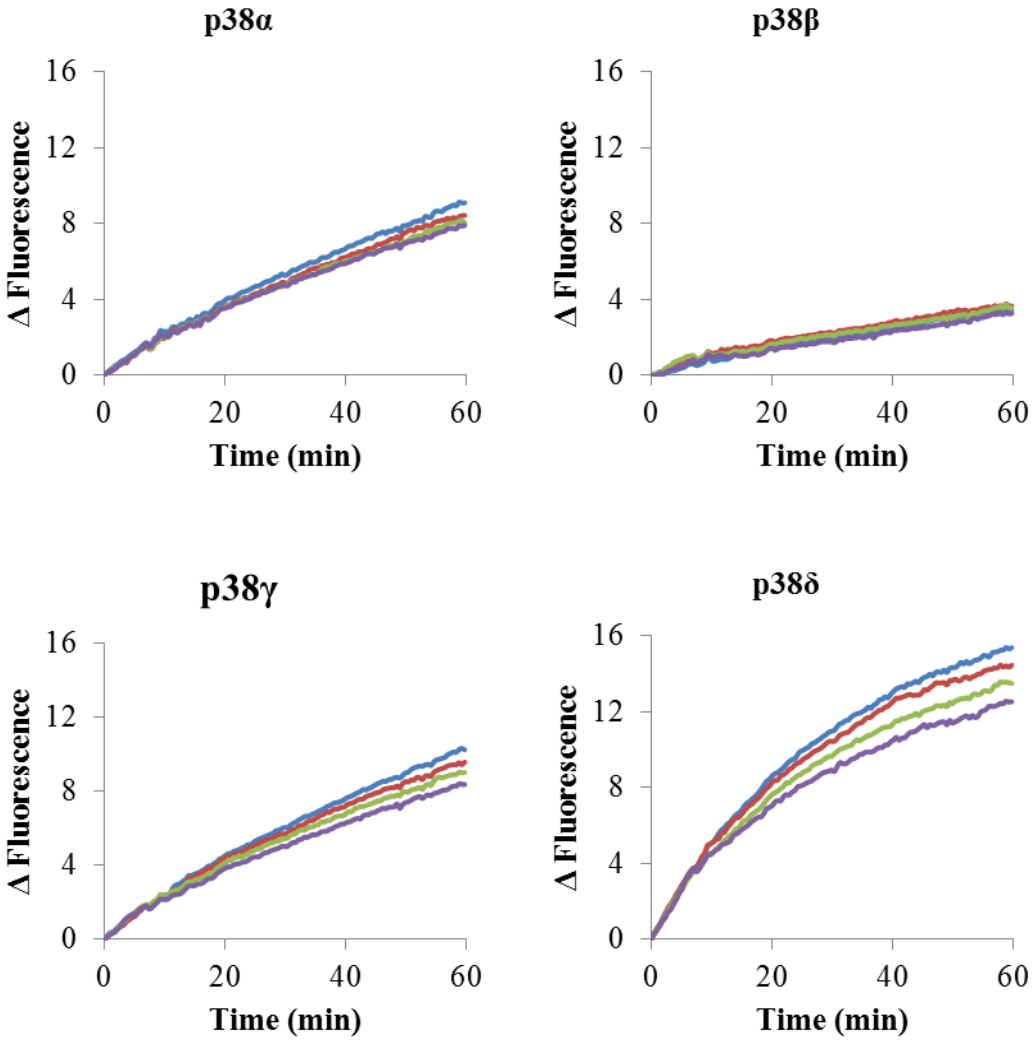

Figure 3.54: *Fluorescence changes of SOX-Sub-F peptide upon phosphorylation with different MAPKs, showing 4 experimental replicates.* Kinase concentrations: p38α/β/γ/δ (2.5 nM) with SOX-Sub-F peptide (2 µM). Data collected with 96-well plate half area, plate reader with λ_{ex} filter of 360 ± 10 nm and λ_{em} filter of 485 ± 10 nm, using a top 400 mirror. Assay buffer: (25mM HEPES, 50mM KCl, 0.1 mM EDTA, 0.1 mM EGTA pH 7.4) with 2 mM DTT, 2.5 µg/mL BSA, 5mM $MgCl_2$, 500 µM ATP at 25°C.

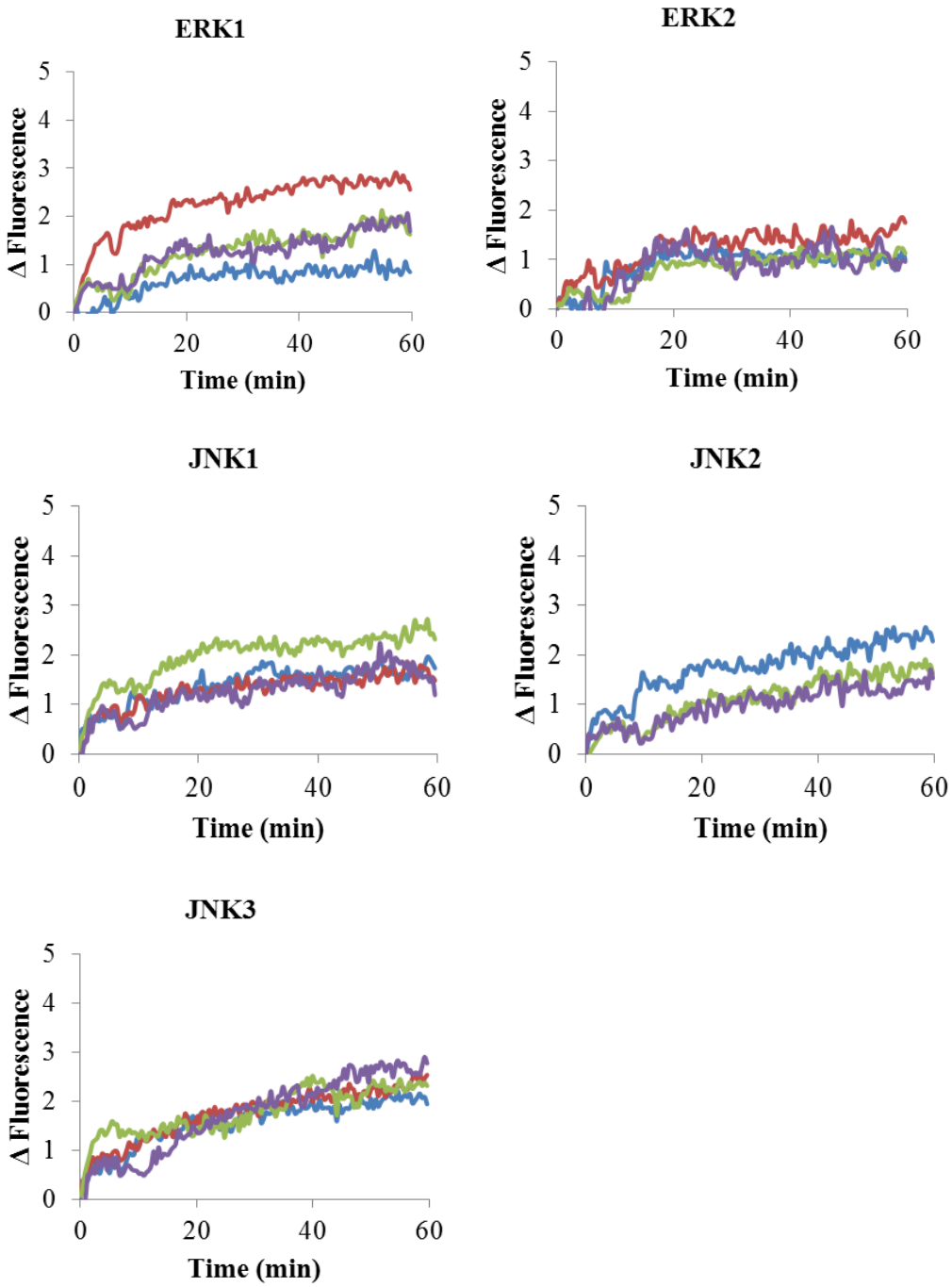

Figure 3.55: *Fluorescence changes of SOX-p38 peptide upon phosphorylation with different MAPKs, showing 4 experimental replicates.* Kinase concentrations: ERK1/2 (0.5 nM), and JNK1/2/3 (5 nM) with SOX-p38 peptide (8 µM).

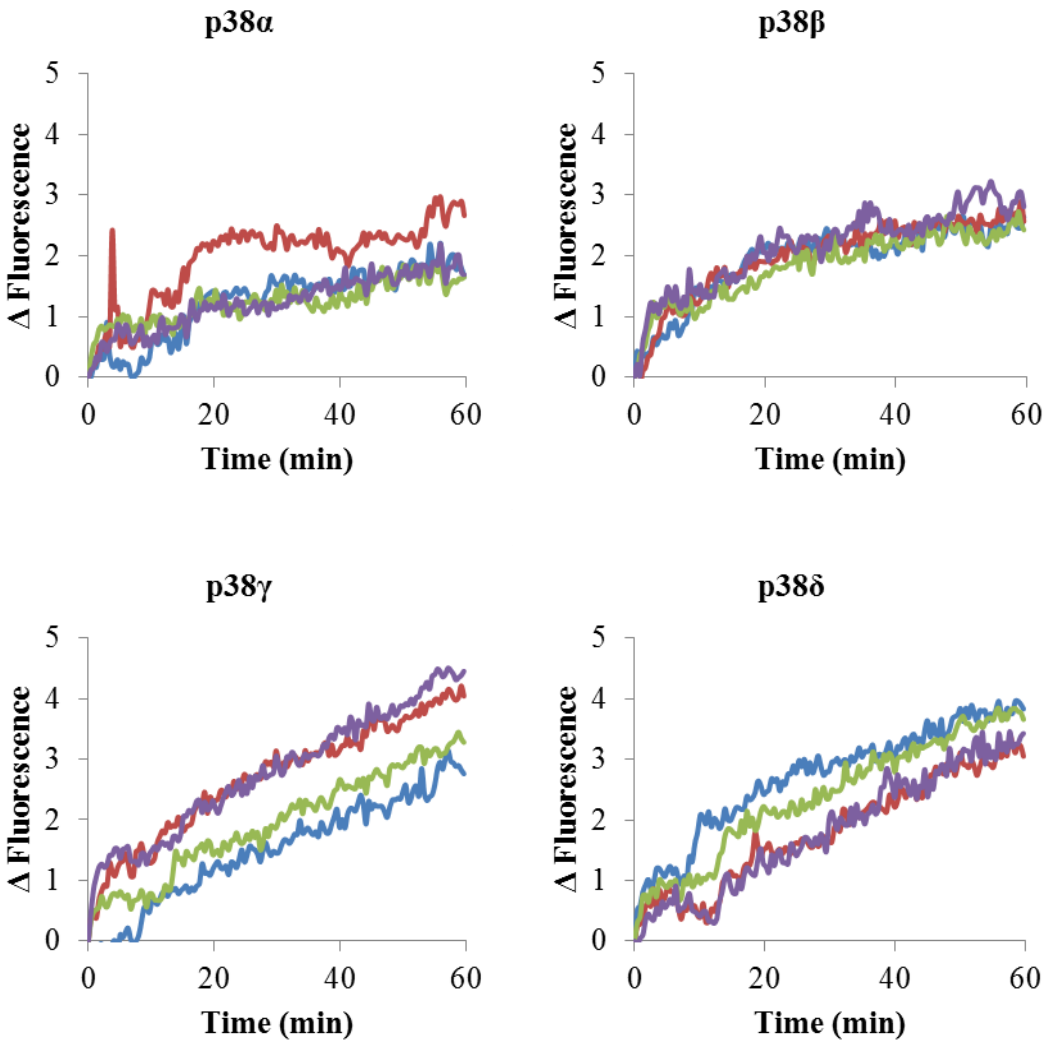

Figure 3.56: *Fluorescence changes of SOX-p38 peptide upon phosphorylation with different MAPKs, showing 4 experimental replicates.* Kinase concentrations: p38α/β/γ/δ (2.5 nM) with SOX-p38 peptide (8 µM). Data collected with 96-well plate half area, plate reader with λ_{ex} filter of 360 ± 10 nm and λ_{em} filter of 485 ± 10 nm, using a top 400 mirror. Assay buffer: (25mM HEPES, 50mM KCl, 0.1 mM EDTA, 0.1 mM EGTA pH 7.4) with 2 mM DTT, 2.5 µg/mL BSA, 5mM $MgCl_2$, 500 µM ATP at 25°C.

MAPK	SOX-Sub-D		SOX-MEF2A		SOX-NFAT4		SOX-Sub-F		SOX-p38	
Kinetic Param.	k	F	k	F	k	F	k	F	k	F
ERK-1	0.06342	7958	0.04593	9109	0.00381	1190	0.00630	2222	0.00093	804
ERK-1	0.06345	7869	0.03598	7951	0.00218	666	0.00603	2177	0.00301	2337
ERK-1	0.06172	7791	0.03107	7404	0.00204	622	0.00538	1917	0.00175	1196
ERK-1	0.05399	7300	0.03110	7422	0.00244	689	0.00566	2127	0.00171	1528
ERK-2	0.05517	7577	0.04626	9997	0.00155	577	0.00416	1803	0.00117	1086
ERK-2	0.05899	7736	0.04222	9519	0.00185	700	0.00379	1487	0.00163	1407
ERK-2	0.05349	7309	0.03680	8862	0.00205	777	0.00390	1629	0.00112	963
ERK-2	0.04153	6690	0.03142	8253	0.00229	868	0.00349	1354	0.00115	1272
JNK-1	0.07438	8415	0.00827	2628	0.01401	2570	0.00218	1146	0.00181	1456
JNK-1	0.06794	8220	0.00743	2396	0.01404	2598	0.00185	805	0.00168	1243
JNK-1	0.05223	7283	0.00730	2363	0.01194	2230	0.00223	1107	0.00260	2085
JNK-1	0.04603	6745	0.00650	2140	0.01245	2609	0.00191	860	0.00168	1307
JNK-2	0.14811	10132	0.01121	3259	0.03953	5336	0.00268	1122	0.00237	1587
JNK-2	0.11530	9614	0.01070	3121	0.03880	5394	0.00295	1277	0.00883	4080
JNK-2	0.11312	9598	0.01005	3031	0.03884	5364	0.00267	1091	0.00159	1063
JNK-2	0.07529	8430	0.00938	2822	0.03272	4885	0.00199	930	0.00135	866
JNK-3	0.11423	9550	0.01424	4126	0.02902	4362	0.00399	1684	0.00211	1554
JNK-3	0.10671	9466	0.01444	4199	0.03055	4635	0.00338	1347	0.00236	1539
JNK-3	0.08365	8849	0.01416	4210	0.02779	4299	0.00326	1318	0.00236	1349
JNK-3	0.06233	8100	0.01325	3866	0.01985	3443	0.00387	1652	0.00254	1431
p38α	0.08633	9152	0.07057	12244	0.00365	925	0.01185	3838	0.00178	1421
p38α	0.08202	8984	0.06110	11740	0.00400	1021	0.01081	3583	0.00267	2240
p38α	0.07584	8619	0.05007	10734	0.00371	994	0.01033	3521	0.00161	1157
p38α	0.05471	7759	0.02427	7048	0.00425	1142	0.01011	3515	0.00170	1151
p38β	0.10025	9420	0.01946	4991	0.03635	4883	0.00379	1519	0.00264	2081
p38β	0.07974	8784	0.01882	4752	0.04315	5533	0.00426	1819	0.00274	1906
p38β	0.07895	8862	0.01728	4561	0.03396	4716	0.00400	1615	0.00250	1659
p38β	0.04437	7145	0.01636	4441	0.03260	4674	0.00346	1394	0.00297	2062
p38γ	0.01683	3033	0.00883	2741	0.00311	968	0.01401	4388	0.00231	1184
p38γ	0.01606	3080	0.00881	2789	0.00306	937	0.01302	4342	0.00390	2288
p38γ	0.01559	3024	0.00794	2545	0.00255	691	0.01209	4057	0.00285	1425
p38γ	0.01362	2660	0.00754	2391	0.00378	1164	0.01092	3750	0.00409	2317
p38δ	0.06713	8001	0.04565	9506	0.00438	1039	0.03229	8436	0.00388	2422
p38δ	0.06994	8186	0.04199	9248	0.00492	1180	0.02962	8078	0.00271	1502
p38δ	0.05931	7733	0.03526	8392	0.00574	1479	0.02561	7493	0.00353	2223
p38δ	0.04772	7060	0.02690	7289	0.00496	1242	0.02249	6938	0.00279	1280

Table 3.9: *Rate constants (k) corresponding to delta fluorescence of SOX-peptides and fluorescence values (F) at 20 min.*

3.13.6.4 Increasing ERK1 Concentrations

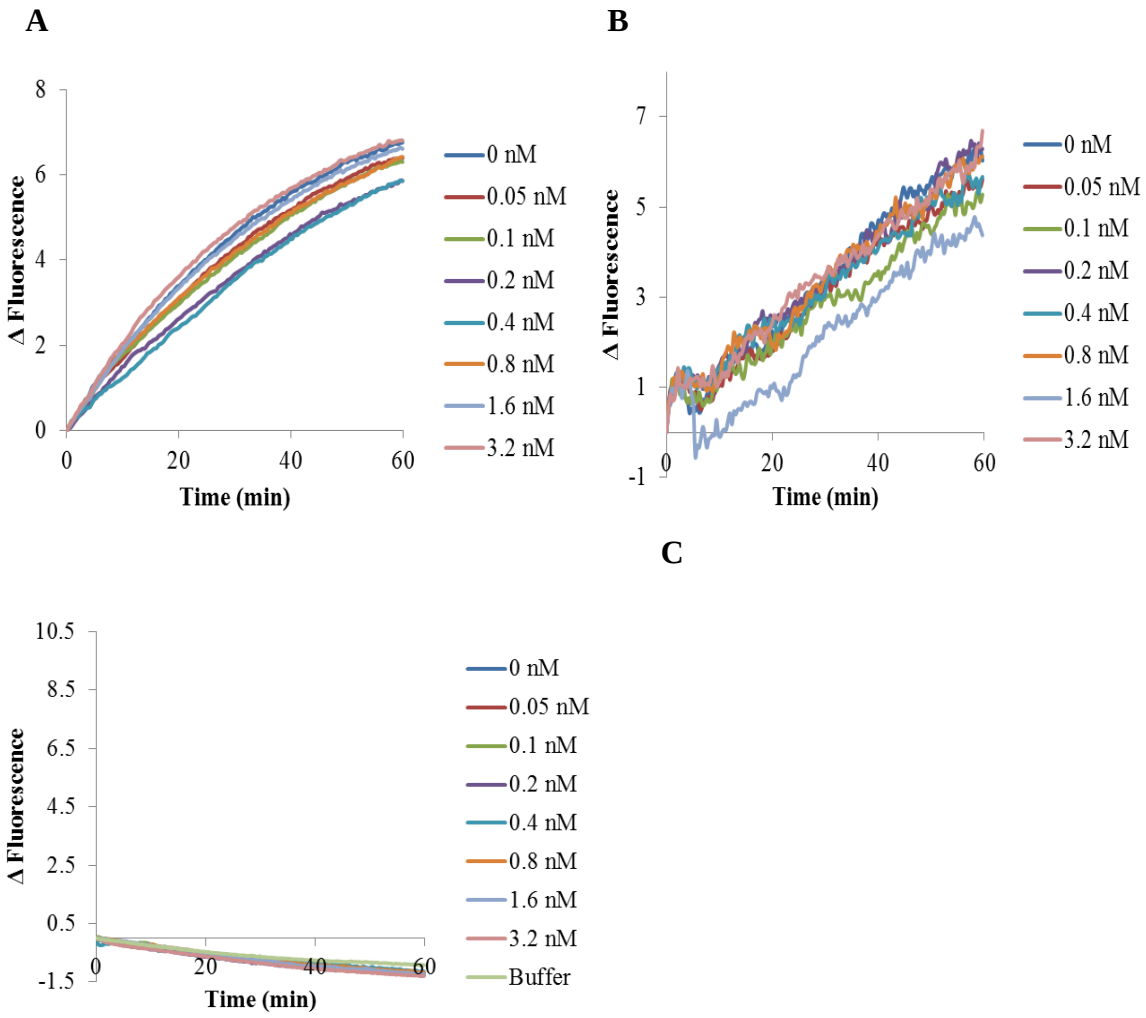

Figure 3.57: *Kinetic data showing the average of 4 experimental replicates of each ERK concentration in the presence of JNK3 and p38γ*. (A) Fluorescence increase of SOX-NFAT4 peptide. (B) Fluorescence increase of SOX-p38 peptide. (C) Control experiment showing the fluorescence background from kinase solutions and buffer. Final ERK1 concentrations: 0 nM, 0.05 nM, 0.1 nM, 0.2 nM, 0.4 nM, 0.8 nM, 1.6 nM and 3.2 nM. Fixed concentrations of JNK3 (5 nM) and p38γ (2.5 nM). Sox-NFAT4 (2 µM) and SOX-p38 (8 µM). Data collected with 96-well plate half area, plate reader with λ_{ex} filter of 340 ± 35 nm and λ_{em} filter of 485 ± 20 nm. Assay buffer: (25mM HEPES, 50mM KCl, 0.1 mM EDTA, 0.1 mM EGTA pH 7.4) with 2 mM DTT, 2.5 µg/mL BSA, 5mM $MgCl_2$, 500 µM ATP at 25°C.

3.13.6.5 Increasing JNK3 Concentrations

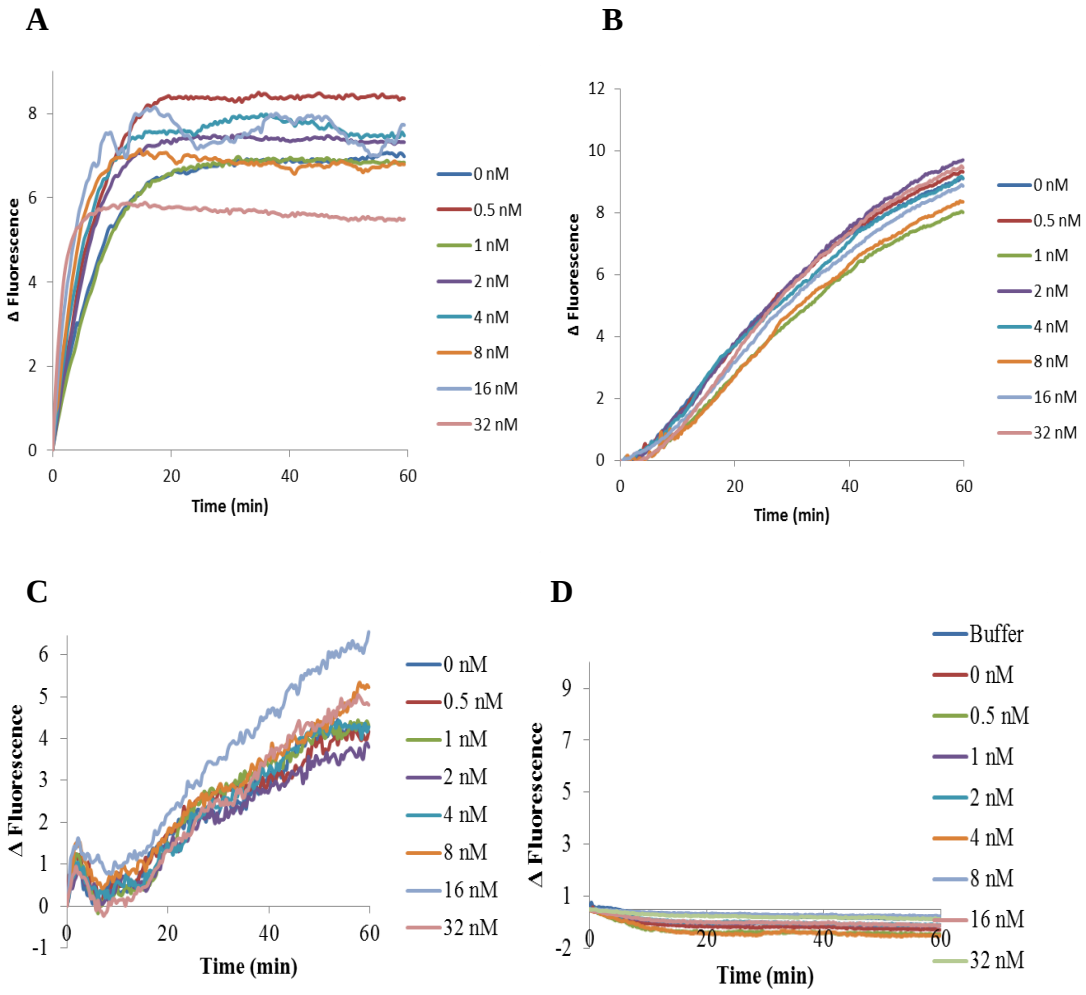

Figure 3.58: *Kinetic data showing the average of 4 experimental replicates of each JNK3 concentration in the presence of ERK and p38γ.* (A) Fluorescence increase of SOX-Sub-D peptide. (B) Fluorescence increase of SOX-Sub-F peptide. (C) Fluorescence increase of SOX-p38 peptide. (D) Control experiment showing the fluorescence background from kinase solutions and buffer. Final JNK3 concentrations: 0 nM, 0.5 nM, 1 nM, 2 nM, 4 nM, 8 nM, 16 nM and 32 nM. Final fixed concentrations of ERK (0.5 nM) and p38γ (2.5 nM). Sox-Sub-D and SOX-Sub-F (2 µM); SOX-p38 peptide (8 µM). Data collected with 96-well plate half area, plate reader with λ_{ex} filter of 340 ± 35 nm and λ_{em} filter of 485 ± 20 nm. Assay buffer: (25mM HEPES, 50mM KCl, 0.1 mM EDTA, 0.1 mM EGTA pH 7.4) with 2 mM DTT, 2.5 µg/mL BSA, 5mM $MgCl_2$, 500 µM ATP at 25°C.

3.13.6.6 Increasing p38γ Concentrations

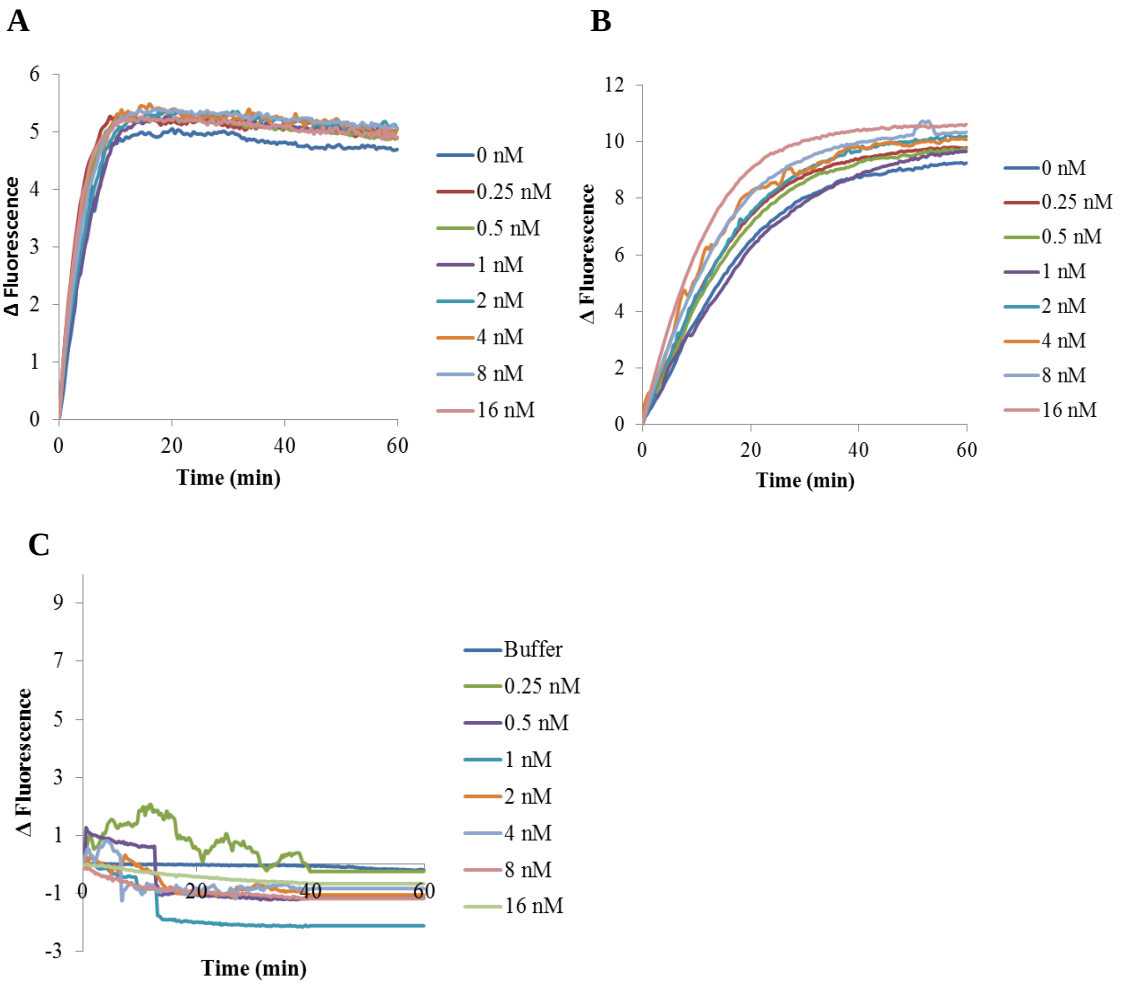

Figure 3.59: *Kinetic data showing the average of 4 experimental replicates of each p38γ concentration in the presence of ERK and JNK3.* (A) Fluorescence increase of SOX-Sub-D peptide. (B) Fluorescence increase of SOX-MEF2A peptide. (C) Control experiment showing the fluorescence background from kinase solutions and buffer. Final p38γ concentrations: 0 nM, 0.25 nM, 0.5 nM, 1 nM, 2 nM, 4 nM, 8 nM, and 16 nM. Final fixed concentrations: ERK (0.5 nM), and JNK3 (5 nM). SOX-Sub-D and Sox-MEF2A (2 µM). Data collected with 96-well plate half area, plate reader with λ_{ex} filter of 340 ± 35 nm and λ_{em} filter of 485 ± 20 nm. Assay buffer: (25mM HEPES, 50mM KCl, 0.1 mM EDTA, 0.1 mM EGTA pH 7.4) with 2 mM DTT, 2.5 µg/mL BSA, 5mM $MgCl_2$, 500 µM ATP at 25°C.

3.13.6.7 ERK-Inhibitor Concentrations

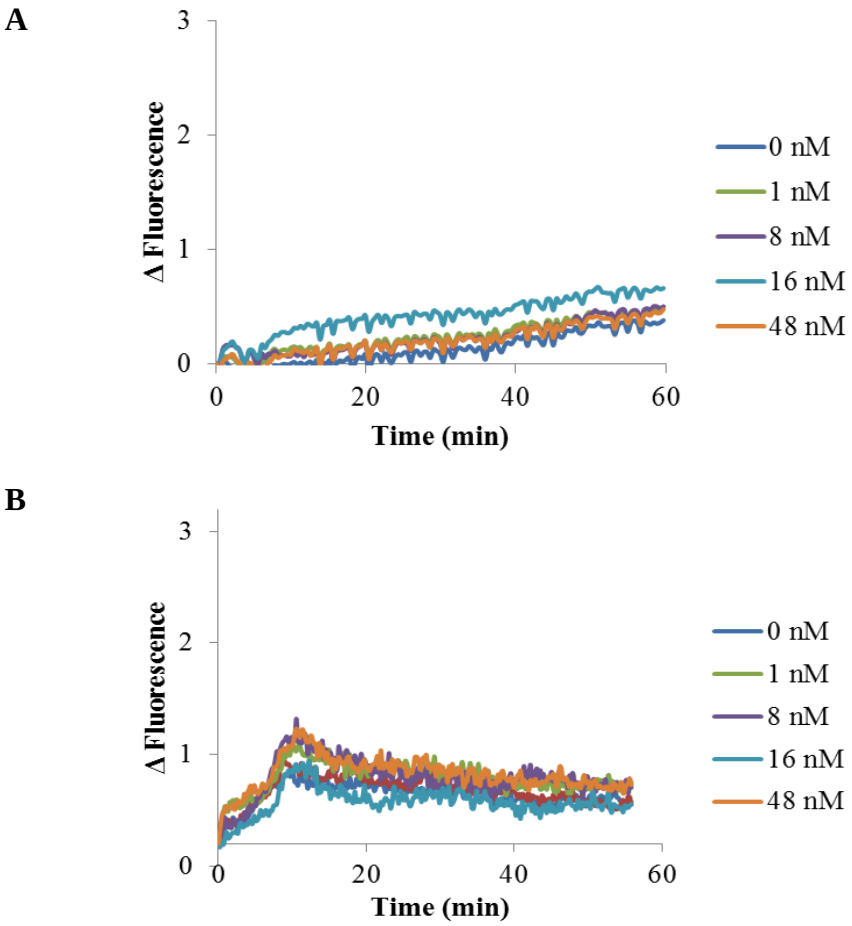

Figure 3.60: *Kinetic data showing the average of 4 experimental replicates of ERK-inhibitor concentration.* (A) Fluorescence changes of SOX-NFAT4 peptide. (B) Fluorescence changes of SOX-p38 peptide. Inhibitor concentrations: 0 nM, 1 nM, 8 nM, 16 nM, and 48 nM. Fixed concentration: ERK1 (0.5 nM). Sox-NFAT4 (2 µM) and SOX-p38 peptide (8 µM). Data collected with 96-well plate half area, plate reader with λ_{ex} filter of 340 ± 35 nm and λ_{em} filter of 485 ± 20 nm. Assay buffer: (25mM HEPES, 50mM KCl, 0.1 mM EDTA, 0.1 mM EGTA pH 7.4) with 2 mM DTT, 2.5 µg/mL BSA, 5mM $MgCl_2$, 500 µM ATP at 25°C.

3.13.6.8 ERK-Inhibitor Concentrations with MAPK groups

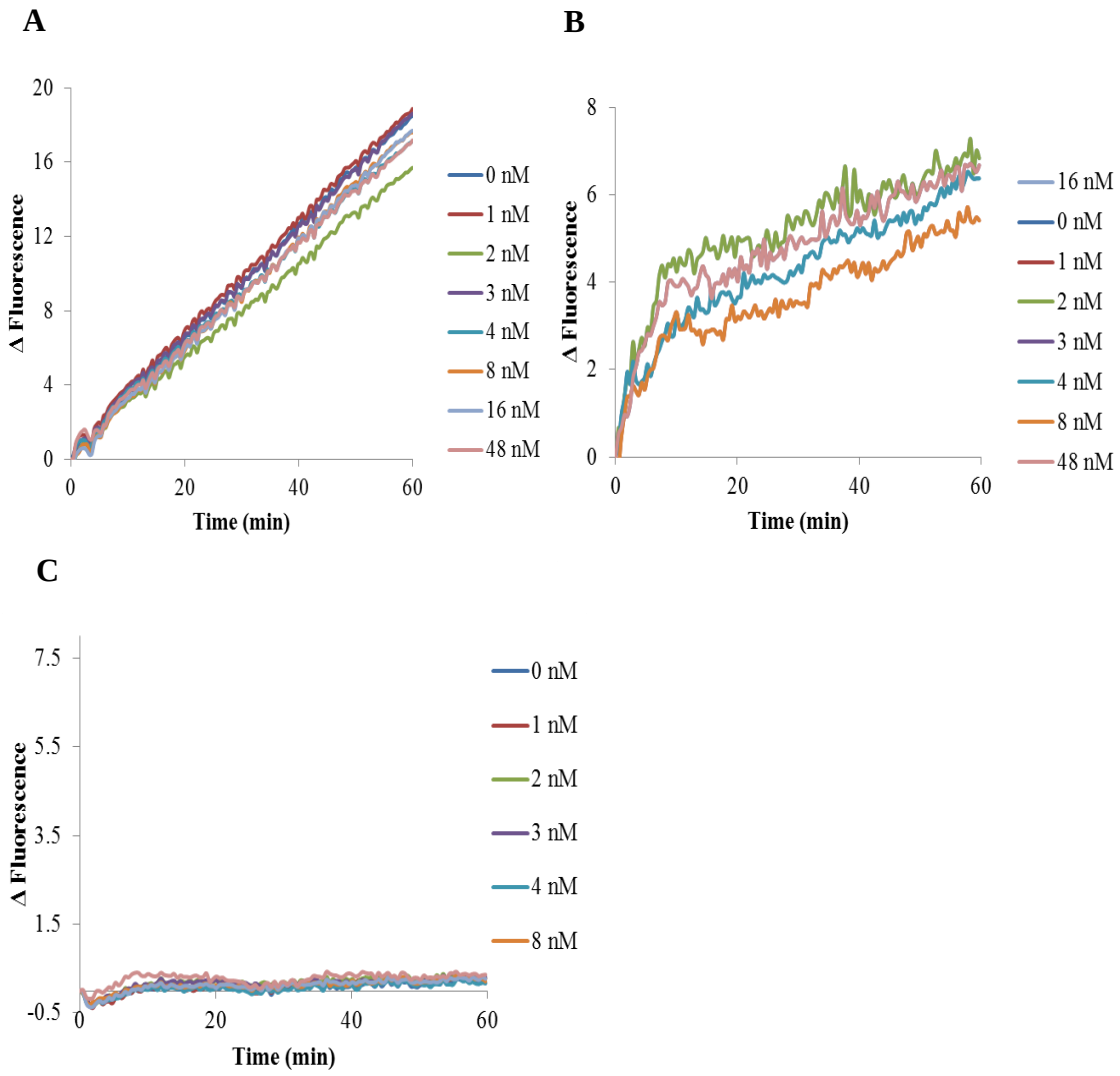

Figure 3.61: *Kinetic data showing the average of 4 experimental replicates of ERK-inhibitor concentration in the presence of ERK1, JNK3 and p38γ.* (A) Fluorescence changes of SOX-NFAT4 peptide. (B) Fluorescence changes of SOX-p38 peptide. (C) Control experiment showing the fluorescence background from kinase solutions. Inhibitor concentrations: 0 nM, 1 nM, 2 nM, 3 nM, 4 nM, 8 nM, 16 nM, and 48 nM. Fixed concentration: ERK1 (0.5 nM), JNK3 (5 nM) and p38γ (2.5 nM). SOX-NFAT4 (2 µM) and SOX-p38 peptide (8 µM). Data collected with 96-well plate half area, plate reader with λ_{ex} filter of 340 ± 35 nm and λ_{em} filter of 485 ± 20 nm. Assay buffer: (25mM HEPES, 50mM KCl, 0.1 mM EDTA, 0.1 mM EGTA pH 7.4) with 2 mM DTT, 2.5 µg/mL BSA, 5mM $MgCl_2$, 500 µM ATP at 25°C.

3.13.6.9 Control Experiments

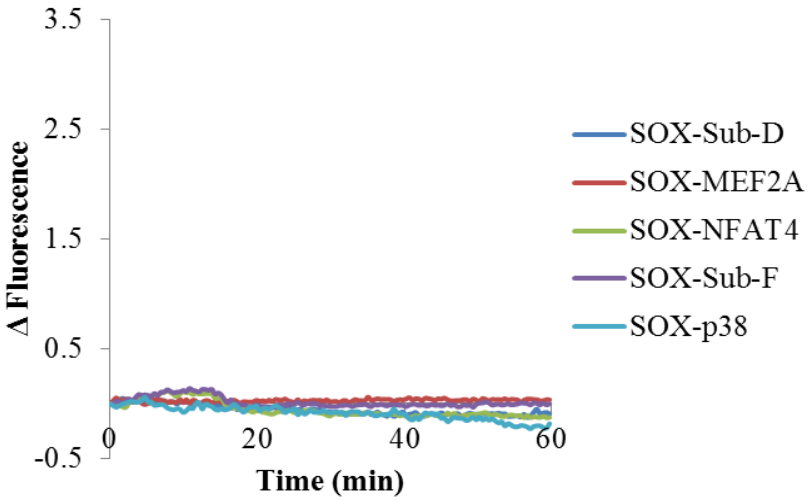

Figure 3.62: *Control experiments without MAP kinases.* Fluorescence changes during the presence of SOX-peptides with ATP. Concentrations: SOX-Sub-D (2 µM); SOX-MEF2A (2 µM), SOX-NFAT4 (2 µM), SOX-Sub-F (2 µM), SOX-p38 peptide (8 µM). Data collected with 96-well plate half area, plate reader with λ_{ex} filter of 360 ± 10 nm and λ_{em} filter of 485 ± 10 nm, using a top 400 mirror. Assay buffer: (25mM HEPES, 50mM KCl, 0.1 mM EDTA, 0.1 mM EGTA pH 7.4) with 2 mM DTT, 2.5 µg/mL BSA, 5mM $MgCl_2$, 500 µM ATP at 25°C.

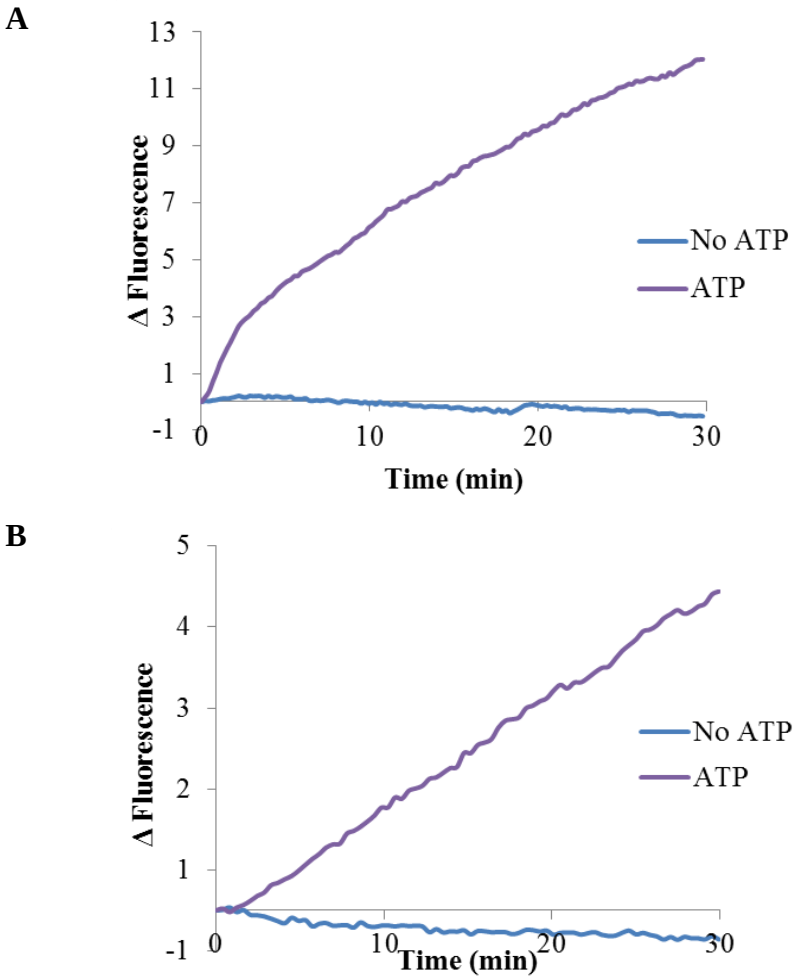

Figure 3.63: *Control experiments without ATP*. (A) Fluorescence changes of SOX-Sub-F peptide (2 µM) with ERK1 (1.6 nM) with and without ATP. (B) Fluorescence changes of SOX-NFAT4 peptide (2 µM) with ERK1 (0.4 nM) with and without ATP. Data collected with 96-well plate half area, plate reader with λ_{ex} filter of 360 ± 10 nm and λ_{em} filter of 485 ± 10 nm, using a top 400 mirror. Assay buffer: (25mM HEPES, 50mM KCl, 0.1 mM EDTA, 0.1 mM EGTA pH 7.4) with 2 mM DTT, 2.5 µg/mL BSA, 5mM $MgCl_2$, 500 µM ATP at 25℃.

Appendix A: ^{1}H NMR Spectra of New Compounds

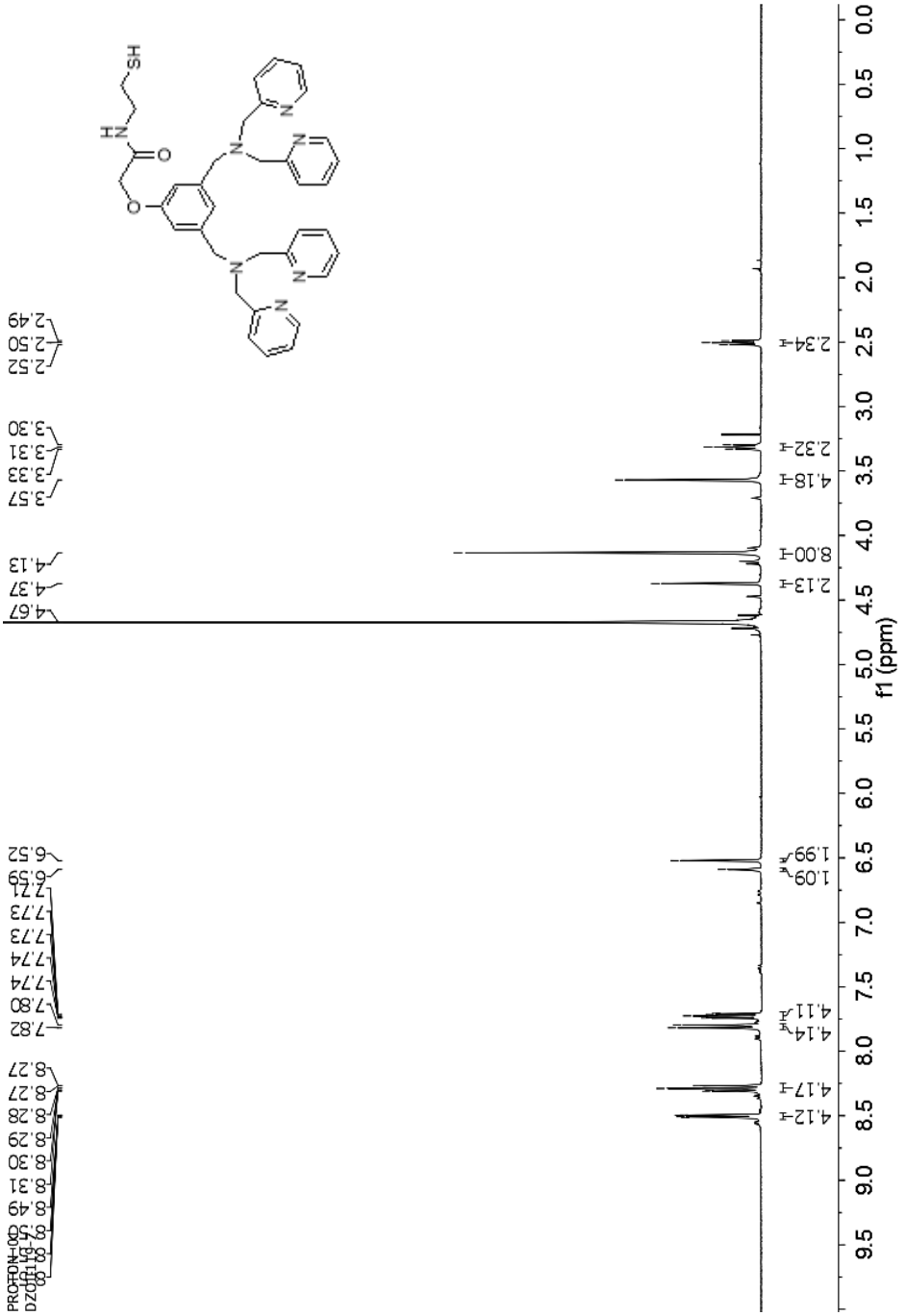

Figure A.1: 400 MHz ^{1}H NMR spectrum of compound **2.19** in D_2O (D, 99.9%).

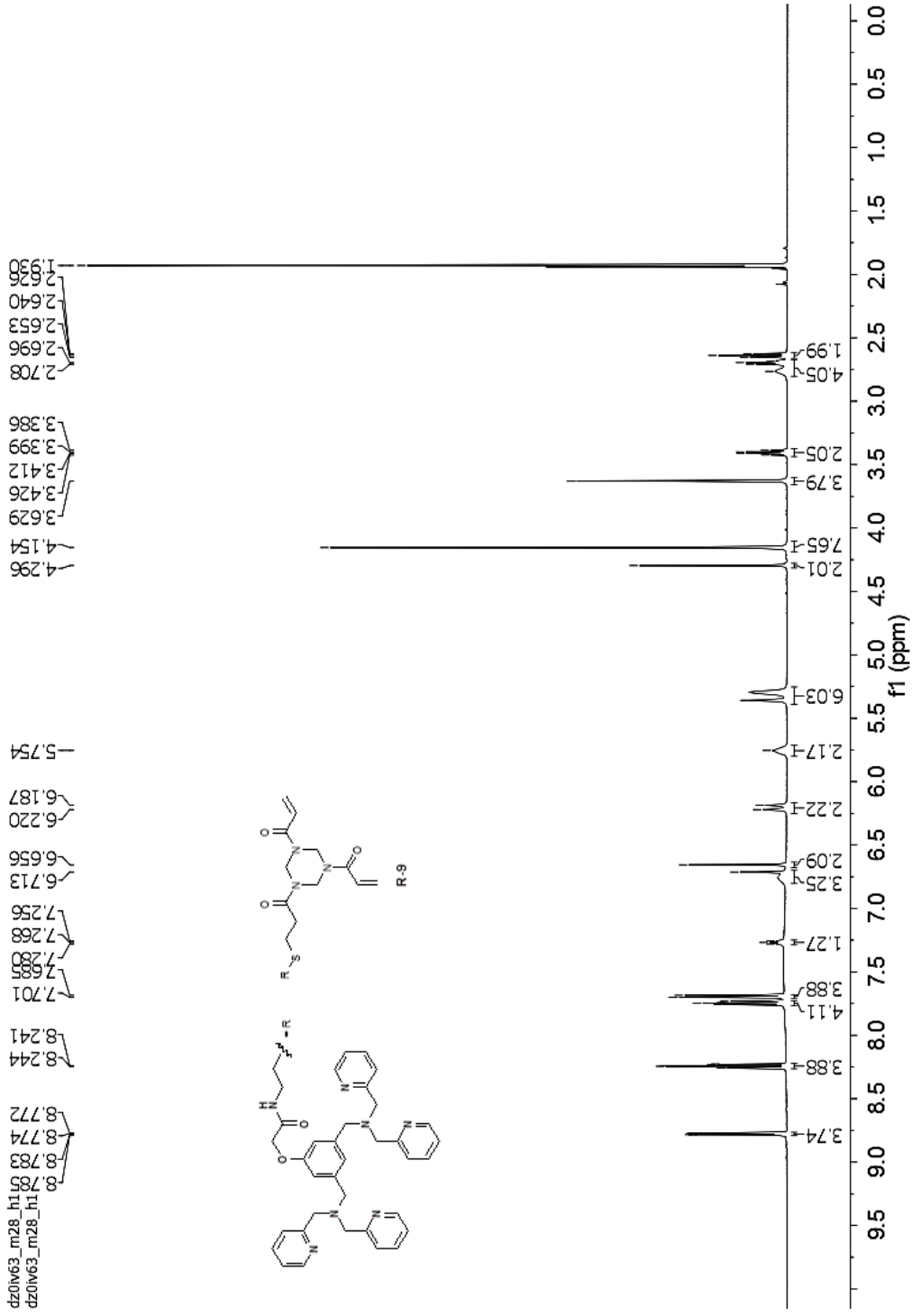

Figure A.2: 500 MHz ^{1}H NMR spectrum of compound **R-9** in CD_3CN (D, 99.8%).

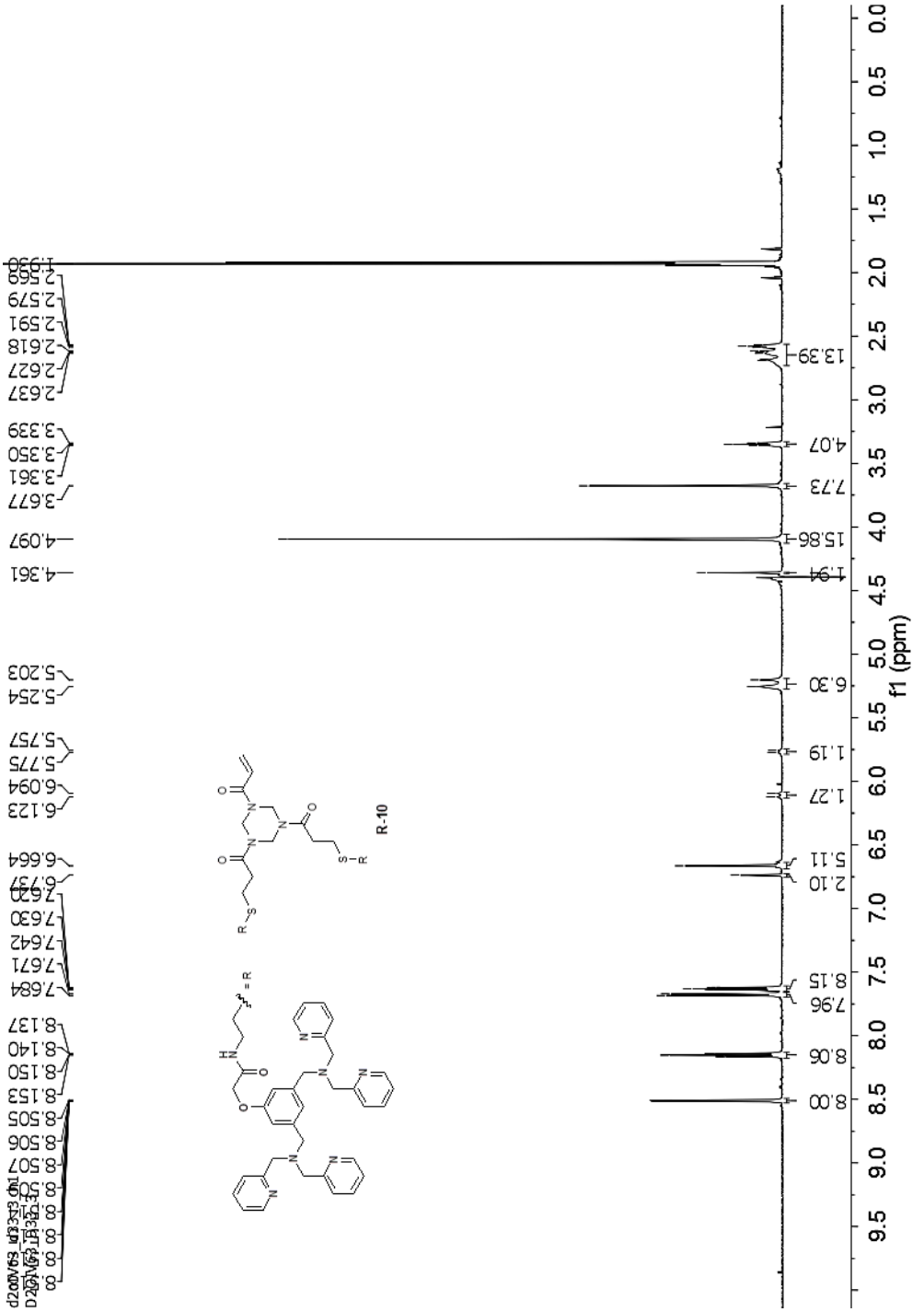

Figure A.3: 600 MHz ^{1}H NMR spectrum of compound **R-10** in D_2O, 30% CD_3CN (D, 99.8%).

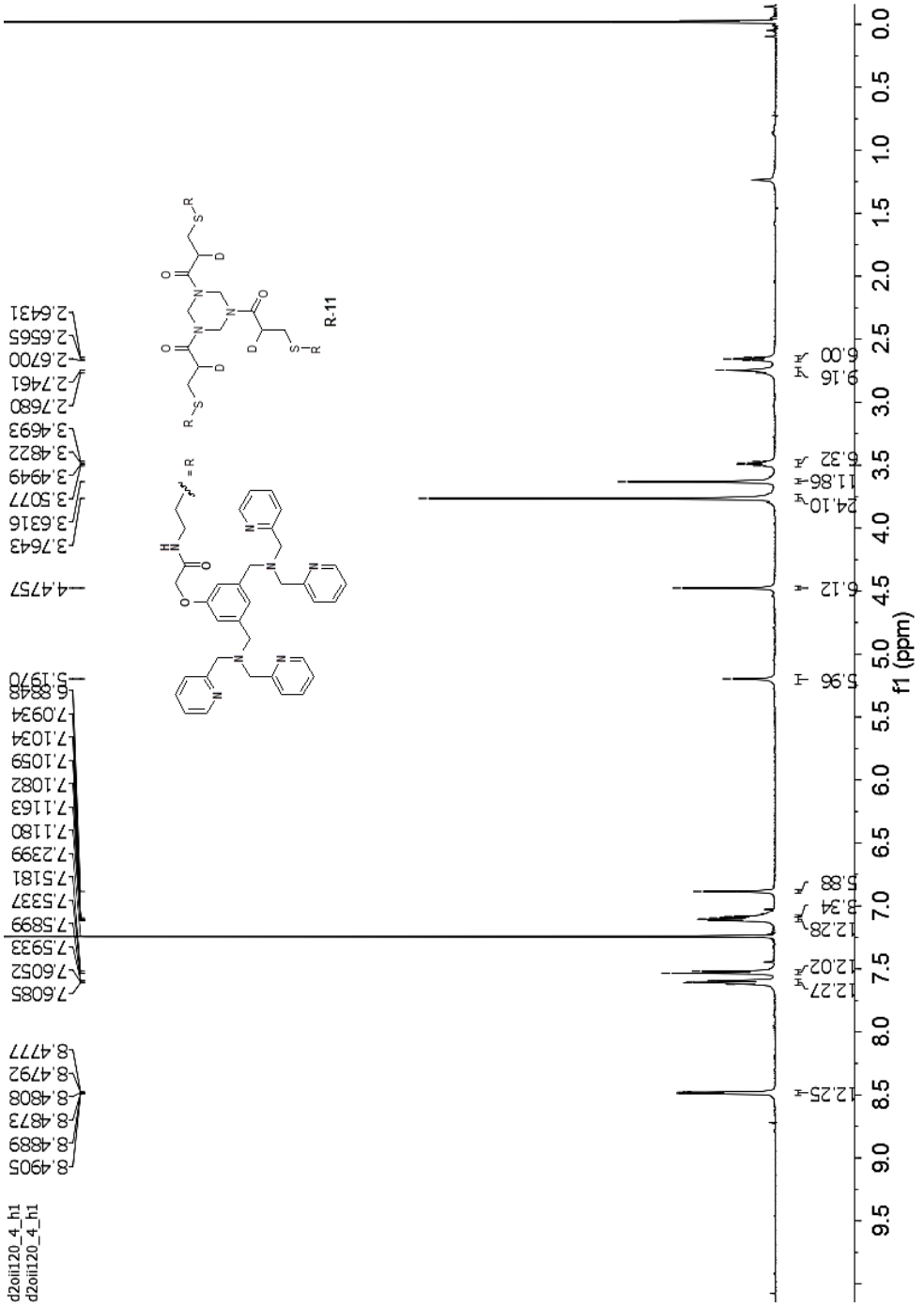

Figure A.4. 500 MHz ^{1}H NMR spectrum of compound **R-11** in $CDCl_3$ (D, 99.8%).

Appendix B: Characterization data of SOX-peptides

SOX-Sub-D peptide

A

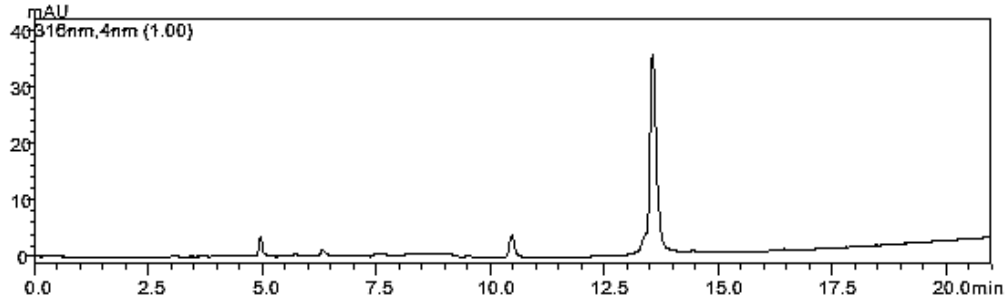

B

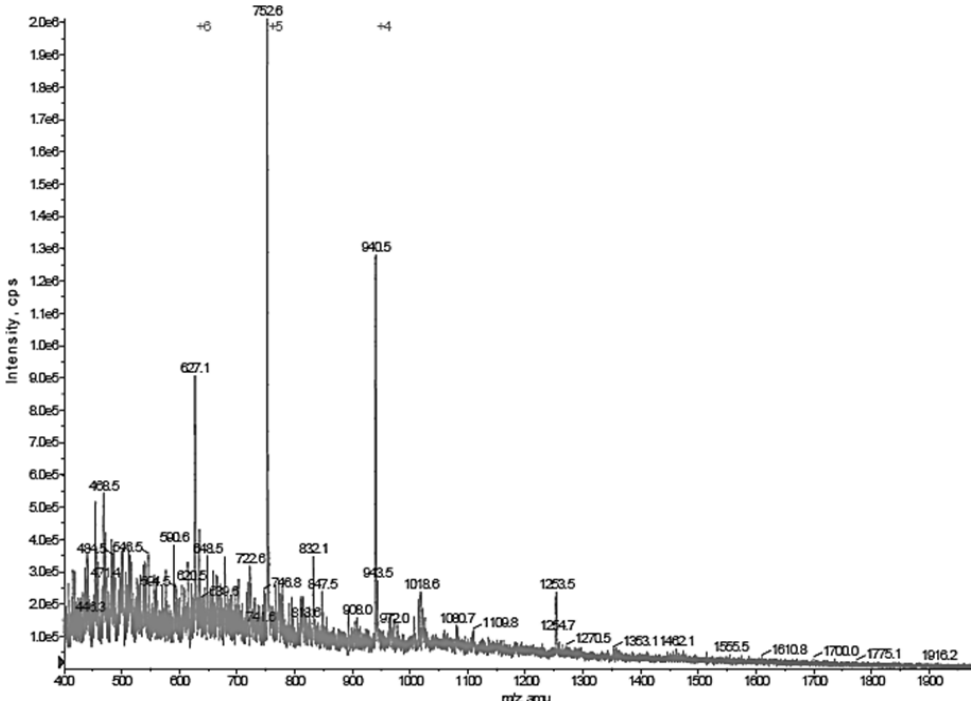

Figure B.1: *HPLC and MS analysis of SOX-Sub-D peptide* (A) HPLC t_R (gradient: 5 to 90% B over 20 min) = 13.56 min. (B) ESI obsd m/z = $[M+6H]^{6+}$ 627.1; $[M+5H]^{5+}$ 752.6; $[M+4H]^{4+}$ 940.5. Calculated $[M+6H]^{6+}$ 627.0; $[M+5H]^{5+}$ 752.2; $[M+4H]^{4+}$ 940.0.

SOX-MEF2A peptide

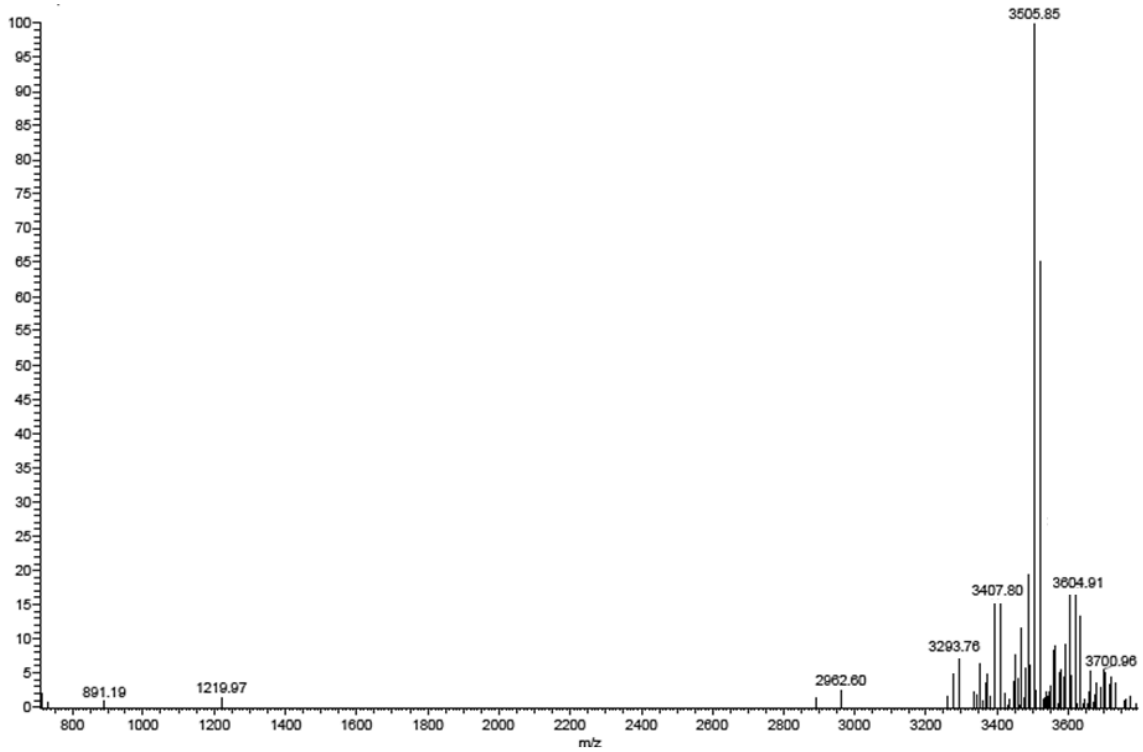

Figure B.2: *MS analysis of SOX-MEF2A peptide*. MALDI-TOF $[M]^+$ obsd m/z = 3505.85, calculated 3505.84.

SOX-NFAT4 peptide

A

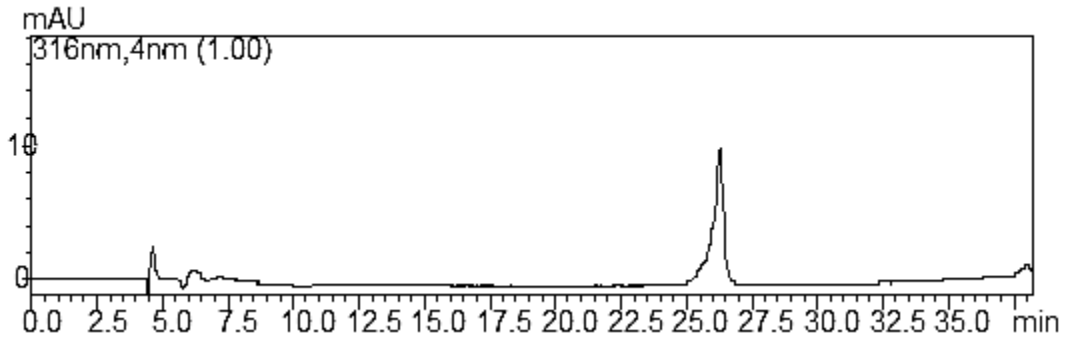

B

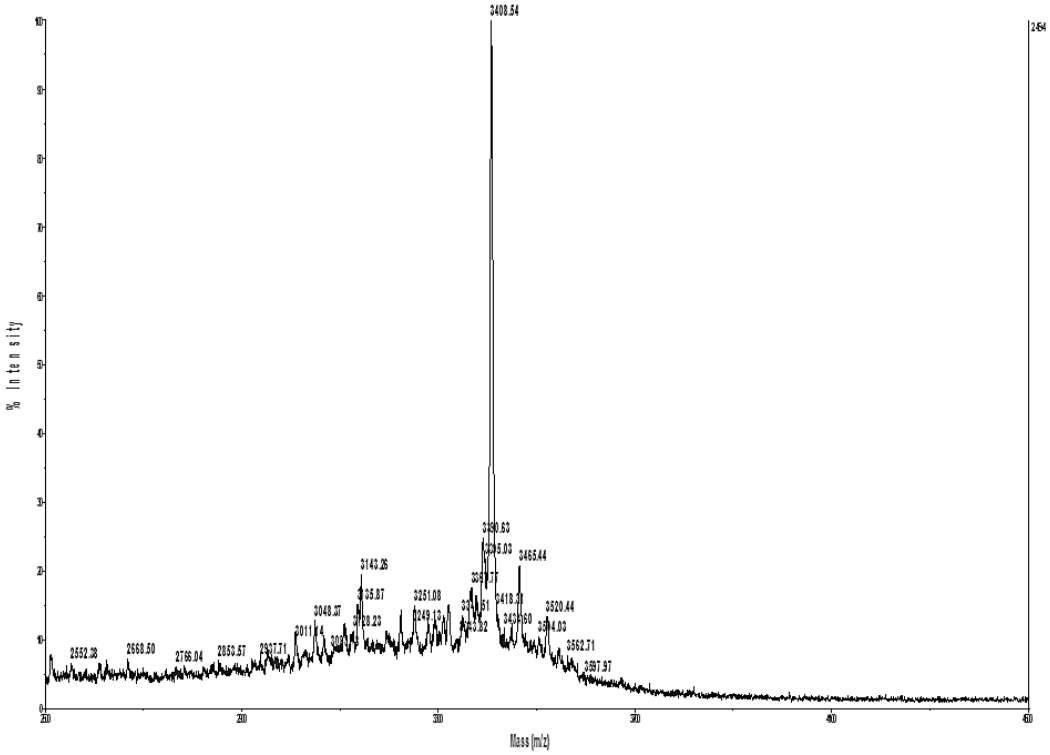

Figure B.3: *HPLC and MS analysis of SOX-NFAT4 peptide* (A) HPLC t_R (gradient: 5 to15% B over 5 min, 15 to 40% B over 35 min, 40 to 95% over 5 min) = 26.28 min. (B) MALDI-TOF $[M]^+$ obsd m/z = 3408.54, calculated 3408.67.

SOX-Sub-F peptide

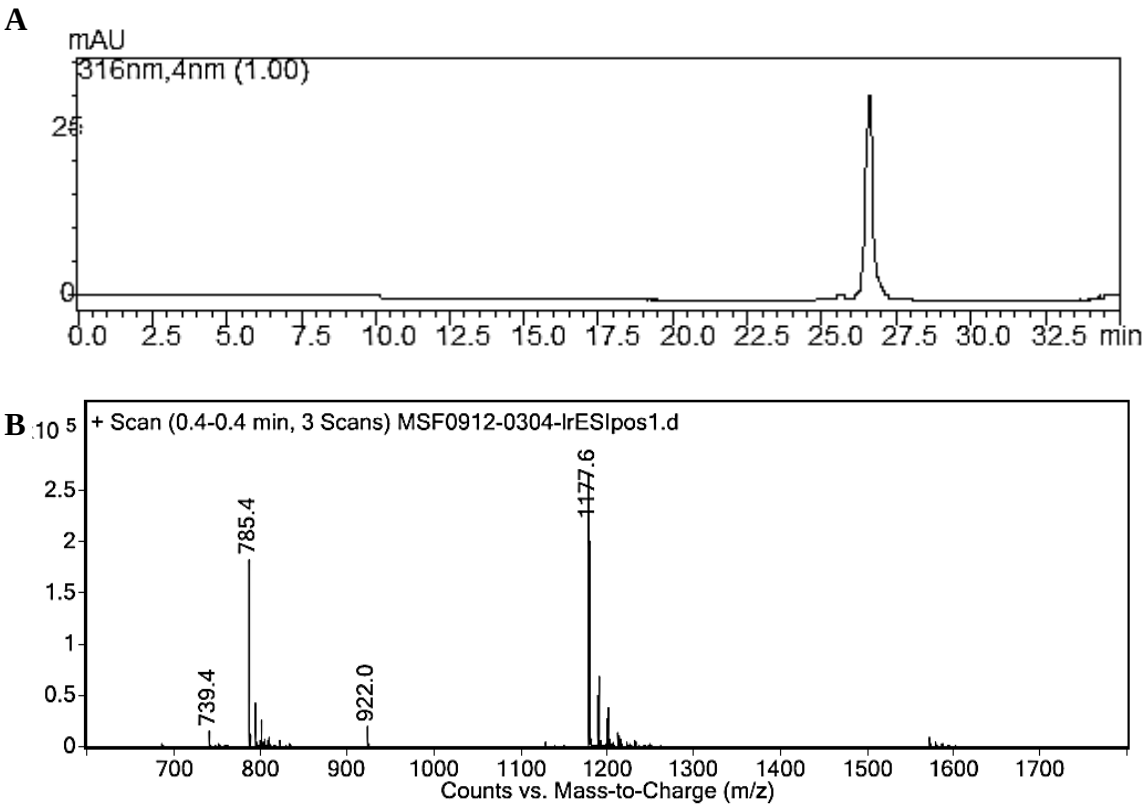

Figure B.4: *HPLC and MS analysis of SOX-Sub-F peptide.* (A) HPLC t_R (gradient: 5 to15% B over 5 min, 15 to 55% B over 25 min, 55 to 95% over 5 min) = 26.6 min. (B) ESI obsd m/z $[M+2H]^{2+}$ = 1177.6; $[M+3H]^{3+}$ 785.37, calculated $[M+2H]^{2+}$1177.8; $[M+3H]^{3+}$ 785.4.

SOX-p38 peptide

A

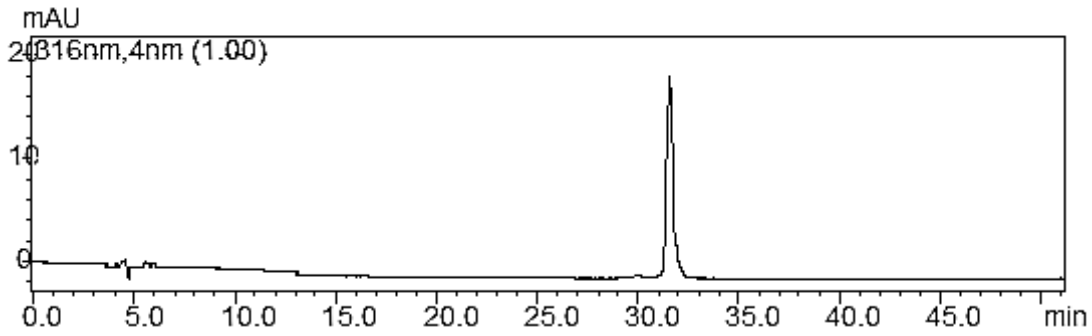

B

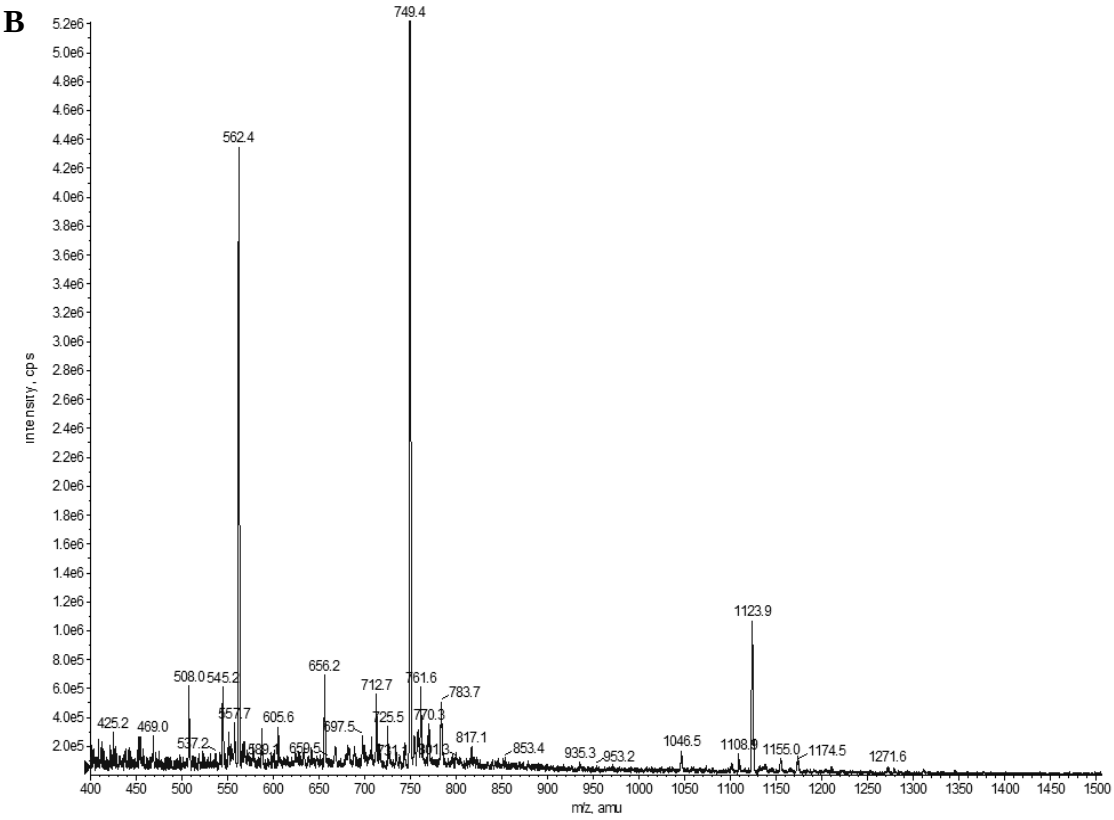

Figure B.5: *HPLC and MS analysis of SOX-p38 peptide.* (A) HPLC t_R (gradient: 5 to 20% B over 5 min, 20 to 70% B over 45 min) = 31.56 min. (B) ESI obsd m/z $[M+2H]^{2+}$ =1123.9; $[M+3H]^{3+}$ 749.4, calculated $[M+2H]^{2+}$1123.6; $[M+3H]^{3+}$ 749.4.

BIBLIOGRAPHY

(1) H. S. Lu, C.; Liu, K.; Tan, L. P.; Yao, S. Q. *Chemistry – A European Journal* **2012**, *18*, 28.
(2) Matthews, D. J.; Gerritsen, M. E.; 1 ed.; Wiley: Hoboken, 2010.
(3) Junttila, M. R.; Li, S.-P.; Westermarck, J. *The FASEB Journal* **2008**, *22*, 954.
(4) Cohen, P. *Nat Rev Drug Discov* **2002**, *1*, 309.
(5) Platanias, L. C. *Blood* **2003**, *101*, 4667.
(6) Burnett, G.; Kennedy, E. P. *Journal of Biological Chemistry* **1954**, *211*, 969.
(7) Kresge, N.; Simoni, R. D.; Hill, R. L. *Journal of Biological Chemistry* **2011**, *286*, e1.
(8) Cohen, P. *Nat Cell Biol* **2002**, *4*, E127.
(9) Hunter, T. *Current Opinion in Cell Biology* **2009**, *21*, 140.
(10) Kishimoto, A.; Takai, Y.; Mori, T.; Kikkawa, U.; Nishizuka, Y. *Journal of Biological Chemistry* **1980**, *255*, 2273.
(11) Manning, G.; Whyte, D. B.; Martinez, R.; Hunter, T.; Sudarsanam, S. *Science* **2002**, *298*, 1912.
(12) Raman, M.; Chen, W.; Cobb, M. H. *Oncogene* **2007**, *26*, 3100.
(13) Johnson, G. L.; Lapadat, R. *Science* **2002**, *298*, 1911.
(14) Huse, M.; Kuriyan, J. *Cell* **2002**, *109*, 275.
(15) Seth, A.; Gonzalez, F. A.; Gupta, S.; Raden, D. L.; Davis, R. J. *Journal of Biological Chemistry* **1992**, *267*, 24796.
(16) Davis, R. J. *Journal of Biological Chemistry* **1993**, *268*, 14553.
(17) Murphy, L. O.; Blenis, J. *Trends in Biochemical Sciences* **2006**, *31*, 268.
(18) Canagarajah, B. J.; Khokhlatchev, A.; Cobb, M. H.; Goldsmith, E. J. *Cell* **1997**, *90*, 859.
(19) Wada, T.; Penninger, J. M. *Oncogene* **2004**, *23*, 2838.
(20) Kaoud, T. S.; Mitra, S.; Lee, S.; Taliaferro, J.; Cantrell, M.; Linse, K. D.; Van Den Berg, C. L.; Dalby, K. N. *ACS Chemical Biology* **2011**, *6*, 658.
(21) Zhang, Y.; Dong, C. *Cellular and Molecular Life Sciences* **2007**, *64*, 2771.
(22) Stalheim, L.; Johnson, G. In *Stress-Activated Protein Kinases*; Posas, F., Nebreda, A., Eds.; Springer Berlin Heidelberg: 2008; Vol. 20, p 1.
(23) Roger, K. J. N. D. J. *Cell Cycle* **2003**, *2*, 198.
(24) Mathas, S.; Hinz, M.; Anagnostopoulos, I.; Krappmann, D.; Lietz, A.; Jundt, F.; Bommert, K.; Mechta-Grigoriou, F.; Stein, H.; Dorken, B.; Scheidereit, C. *EMBO J* **2002**, *21*, 4104.
(25) Shibata, W.; Maeda, S.; Hikiba, Y.; Yanai, A.; Sakamoto, K.; Nakagawa, H.; Ogura, K.; Karin, M.; Omata, M. *Cancer Research* **2008**, *68*, 5031.
(26) Stadheim, T. A.; Kucera, G. L. *Leukemia Research* **2002**, *26*, 55.

(27) Lechner, C.; Zahalka, M. A.; Giot, J. F.; Møller, N. P.; Ullrich, A. *Proceedings of the National Academy of Sciences* **1996**, *93*, 4355.
(28) Seger, R.; Krebs, E. G. *The FASEB Journal* **1995**, *9*, 726.
(29) Huang, C.; Jacobson, K.; Schaller, M. D. *Journal of Cell Science* **2004**, *117*, 4619.
(30) Campbell, P. M.; Der, C. J. *Seminars in Cancer Biology* **2004**, *14*, 105.
(31) Bos, J. L. *Cancer Research* **1989**, *49*, 4682.
(32) Hodgson, D. R. W.; Schroder, M. *Chemical Society Reviews* **2011**, *40*, 1211.
(33) Knight, J. D. R.; Pawson, T.; Gingras, A.-C. *Journal of Proteomics* **2013**, *81*, 43.
(34) Zhang, Q.; Nottke, A.; Goodman, R. H. *Proceedings of the National Academy of Sciences of the United States of America* **2005**, *102*, 2802.
(35) Towbin, H.; Staehelin, T.; Gordon, J. *Proceedings of the National Academy of Sciences* **1979**, *76*, 4350.
(36) Burnette, W. N. *Analytical Biochemistry* **1981**, *112*, 195.
(37) O'Neill, R. A.; Bhamidipati, A.; Bi, X.; Deb-Basu, D.; Cahill, L.; Ferrante, J.; Gentalen, E.; Glazer, M.; Gossett, J.; Hacker, K.; Kirby, C.; Knittle, J.; Loder, R.; Mastroieni, C.; MacLaren, M.; Mills, T.; Nguyen, U.; Parker, N.; Rice, A.; Roach, D.; Suich, D.; Voehringer, D.; Voss, K.; Yang, J.; Yang, T.; Vander Horn, P. B. *Proceedings of the National Academy of Sciences* **2006**, *103*, 16153.
(38) Gonzalez-Vera, J. A. *Chemical Society Reviews* **2012**, *41*, 1652.
(39) Parkesh, R.; Veale, E. B.; Gunnlaugsson, T. In *Chemosensors*; John Wiley & Sons, Inc.: 2011, p 229.
(40) Pazos, E.; Vazquez, O.; Mascarenas, J. L.; Eugenio Vazquez, M. *Chemical Society Reviews* **2009**, *38*, 3348.
(41) Martic, S.; Kraatz, H.-B. *Chemical Science* **2013**, *4*, 42.
(42) Randriamampita, C.; Mouchacca, P.; Malissen, B.; Marguet, D.; Trautmann, A.; Lellouch, A. C. *PLoS ONE* **2008**, *3*, e1521.
(43) Sharma, V.; Wang, Q.; Lawrence, D. S. *Biochimica et Biophysica Acta (BBA) - Proteins and Proteomics* **2008**, *1784*, 94.
(44) Wang, Q.; Lawrence, D. S. *Journal of the American Chemical Society* **2005**, *127*, 7684.
(45) Wong, B. A.; Friedle, S.; Lippard, S. J. *Journal of the American Chemical Society* **2009**, *131*, 7142.
(46) Sakamoto, T.; Ojida, A.; Hamachi, I. *Chemical Communications* **2009**, 141.
(47) Tamaru, S.-i.; Hamachi, I. In *Recognition of Anions*; Vilar, R., Ed.; Springer Berlin / Heidelberg: 2008; Vol. 129, p 95.
(48) Ojida, A.; Mito-oka, Y.; Sada, K.; Hamachi, I. *Journal of the American Chemical Society* **2004**, *126*, 2454.

(49) Ojida, A.; Kohira, T.; Hamachi, I. *Chemistry Letters* **2004**, *33*, 1024.
(50) Anai, T.; Nakata, E.; Koshi, Y.; Ojida, A.; Hamachi, I. *J. Am. Chem. Soc.* **2007**, *129*, 6232.
(51) Drewry, J. A.; Gunning, P. T. *Coordination Chemistry Reviews* **2011**, *255*, 459.
(52) Sakamoto, T.; Inoue, M.-a.; Ojida, A.; Hamachi, I. *Bioorganic & Medicinal Chemistry Letters* **2009**, *19*, 4175.
(53) Ojida, A.; Sakamoto, T.; Inoue, M.-a.; Fujishima, S.-h.; Lippens, G.; Hamachi, I. *Journal of the American Chemical Society* **2009**, *131*, 6543.
(54) Shults, M. D.; Carrico-Moniz, D.; Imperiali, B. *Analytical Biochemistry* **2006**, *352*, 198.
(55) Luković, E.; González-Vera, J. A.; Imperiali, B. *Journal of the American Chemical Society* **2008**, *130*, 12821.
(56) Lavigne, J. J.; Anslyn, E. V. *Angewandte Chemie International Edition* **2001**, *40*, 3118.
(57) Collins, B. E.; Anslyn, E. V. *Chem.– Eur. J.* **2007**, *13*, 4700.
(58) Wright, A. T.; Griffin, M. J.; Zhong, Z.; McCleskey, S. C.; Anslyn, E. V.; McDevitt, J. T. *Angewandte Chemie International Edition* **2005**, *44*, 6375.
(59) Brereton, R. G. In *Chemometrics for Pattern Recognition*; John Wiley & Sons, Ltd: 2009, p 47.
(60) Anzenbacher, P.; Palacios, M. A. In *Chemosensors*; John Wiley & Sons, Inc.: 2011, p 345.
(61) Bartlett, P. *Statistics in Medicine* **1997**, *16*, 2385.
(62) Hamel, L. In *Knowledge Discovery with Support Vector Machines*; John Wiley & Sons, Inc.: 2009, p 89.
(63) Umali, A. P.; Anslyn, E. V. *Current Opinion in Chemical Biology* **2010**, *14*, 685.
(64) Zhou, H.; Baldini, L.; Hong, J.; Wilson, A. J.; Hamilton, A. D. *J. Am. Chem. Soc.* **2006**, *128*, 2421.
(65) Moyano, D. F.; Rana, S.; Bunz, U. H. F.; Rotello, V. M. *Faraday Discuss.* **2011**, *152*, 33.
(66) Margulies, D.; Hamilton, A. D. *Angew. Chem., Int. Ed.* **2009**, *48*, 1771.
(67) De, M.; Rana, S.; Akpinar, H.; Miranda, O. R.; Arvizo, R. R.; Bunz, U. H. F.; Rotello, V. M. *Nat. Chem.* **2009**, *1*, 461.
(68) Roskoski Jr, R. *Pharmacol. Res.* **2012**, *66*, 105.
(69) Junttila, M. R.; Li, S.-P.; Westermarck, J. *FASEB J.* **2008**, *22*, 954.
(70) Pearson, G.; Robinson, F.; Beers Gibson, T.; Xu, B.-e.; Karandikar, M.; Berman, K.; Cobb, M. H. *Endocrine Rev.* **2001**, *22*, 153.
(71) Bonetta, L. *Nat. Meth.* **2005**, *2*, 225.
(72) Kinoshita, E.; Kinoshita-Kikuta, E.; Koike, T. *Nat. Protocols* **2009**, *4*, 1513.

(73) Takahashi, M.; Kawamura, A.; Kato, N.; Nishi, T.; Hamachi, I.; Ohkanda, J. *Angew. Chem., Int. Ed.* **2012**, *51*, 509.
(74) Wang, Q.; Lawrence, D. S. *J. Am. Chem. Soc.* **2005**, *127*, 7684.
(75) H. S. Lu, C.; Liu, K.; Tan, L. P.; Yao, S. Q. *Chem.–Eur. J.* **2012**, *18*, 28.
(76) Hargrove, A. E.; Nieto, S.; Zhang, T.; Sessler, J. L.; Anslyn, E. V. *Chem. Rev.* **2011**, *111*, 6603.
(77) Shults, M. D.; Carrico-Moniz, D.; Imperiali, B. *Anal. Biochem.* **2006**, *352*, 198.
(78) Luković, E.; González-Vera, J. A.; Imperiali, B. *J. Am. Chem. Soc.* **2008**, *130*, 12821.
(79) Drewry, J. A.; Gunning, P. T. *Coord. Chem. Rev.* **2011**, *255*, 459.
(80) Sakamoto, T.; Ojida, A.; Hamachi, I. *Chem. Commun.* **2009**, 141.
(81) Ojida, A.; Mito-oka, Y.; Inoue, M.-a.; Hamachi, I. *J. Am. Chem. Soc.* **2002**, *124*, 6256.
(82) Ojida, A.; Mito-oka, Y.; Sada, K.; Hamachi, I. *J. Am. Chem. Soc.* **2004**, *126*, 2454.
(83) Wright, A. T.; Anslyn, E. V. *Chem. Soc. Rev.* **2006**, *35*, 14.
(84) Anslyn, E. V. *J. Org. Chem.* **2007**, *72*, 687.
(85) Wright, A. T.; Griffin, M. J.; Zhong, Z.; McCleskey, S. C.; Anslyn, E. V.; McDevitt, J. T. *Angew. Chem., Int. Ed.* **2005**, *44*, 6375.
(86) Zhang, T.; Edwards, N. Y.; Bonizzoni, M.; Anslyn, E. V. *J. Am. Chem. Soc.* **2009**, *131*, 11976.
(87) Shi, B.; Stevenson, R.; Campopiano, D. J.; Greaney, M. F. *J. Am. Chem. Soc.* **2006**, *128*, 8459.
(88) Shi, B.; Greaney, M. F. *Chem. Commun.* **2005**, 886.
(89) Schmidt, T. J.; Lyß, G.; Pahl, H. L.; Merfort, I. *Bioorg. Med. Chem.* **1999**, *7*, 2849.
(90) Rim, C.; Lahey, L. J.; Patel, V. G.; Zhang, H.; Son, D. Y. *Tetrahedron Lett.* **2009**, *50*, 745.
(91) Umali, A. P.; Anslyn, E. V. *Curr. Opin. Chem. Biol.* **2010**, *14*, 685.
(92) Waas, W. F.; Dalby, K. N. *J. Biol. Chem.* **2002**, *277*, 12532.
(93) Callaway, K.; Waas, W. F.; Rainey, M. A.; Ren, P.; Dalby, K. N. *Biochemistry* **2010**, *49*, 3619.
(94) Lee, S.; Warthaka, M.; Yan, C.; Kaoud, T. S.; Ren, P.; Dalby, K. N. *Biochemistry* **2011**, *50*, 9500.
(95) Nguyen, B. T.; Anslyn, E. V. *Coord. Chem. Rev.* **2006**, *250*, 3118.
(96) Piątek, A. M.; Bomble, Y. J.; Wiskur, S. L.; Anslyn, E. V. *J. Am. Chem. Soc.* **2004**, *126*, 6072.
(97) Kitamura, M.; Shabbir, S. H.; Anslyn, E. V. *J. Org. Chem.* **2009**, *74*, 4479.
(98) Hanshaw, R. G.; Hilkert, S. M.; Jiang, H.; Smith, B. D. *Tetrahedron Lett.* **2004**, *45*, 8721.
(99) Horie, S.; Kubo, Y. *Chem. Lett.* **2009**, *38*, 616.

(100) Lefloch, R.; Pouysségur, J.; Lenormand, P. *Mol. Cell. Biol.* **2008**, *28*, 511.
(101) Sivasankar; Oxford University Press: New Delhi, 2012.
(102) Petrozzi, S. In *Practical Instrumental Analysis*; Wiley-VCH Verlag GmbH & Co. KGaA: 2012, p 1.
(103) Hughes, I.; Hase, T.; OUP Oxford: Oxford, 2010.
(104) Brand, U.; Vahrenkamp, H. *Chem. Ber.* **1996**, *129*, 435.
(105) Jurs, P. C.; Bakken, G. A.; McClelland, H. E. *Chem. Rev.* **2000**, *100*, 2649.
(106) Gong, G. *J. Am. Stat. Assoc.* **1986**, *81*, 108.
(107) Rosser, E. M.; Morton, S.; Ashton, K. S.; Cohen, P.; Hulme, A. N. *Org. Biomol. Chem.* **2004**, *2*, 142.
(108) zu Schwabedissen, H. E. M.; Grube, M.; Dreisbach, A.; Jedlitschky, G.; Meissner, K.; Linnemann, K.; Fusch, C.; Ritter, C. A.; Völker, U.; Kroemer, H. K. *Drug Metab. Dispos.* **2006**, *34*, 524.
(109) Zamora-Olivares, D.; Kaoud, T. S.; Dalby, K. N.; Anslyn, E. V. *J. Am. Chem. Soc.* **2013**, *135*, 14814.
(110) Felder, D.; Gutiérrez Nava, M.; del Pilar Carreón, M.; Eckert, J.-F.; Luccisano, M.; Schall, C.; Masson, P.; Gallani, J.-L.; Heinrich, B.; Guillon, D.; Nierengarten, J.-F. *Helvetica Chimica Acta* **2002**, *85*, 288.
(111) Hanshaw, R. G.; Hilkert, S. M.; Jiang, H.; Smith, B. D. *Tetrahedron Letters* **2004**, *45*, 8721.
(112) Madsen, J. A.; Kaoud, T. S.; Dalby, K. N.; Brodbelt, J. S. *Proteomics* **2011**, *11*, 1329.
(113) Yan, C.; Kaoud, T.; Lee, S.; Dalby, K. N.; Ren, P. *J. Phys. Chem. B* **2011**, *115*, 1491.
(114) Kaoud, T. S.; Devkota, A. K.; Harris, R.; Rana, M. S.; Abramczyk, O.; Warthaka, M.; Lee, S.; Girvin, M. E.; Riggs, A. F.; Dalby, K. N. *Biochemistry* **2011**, *50*, 4568.
(115) Callaway, K.; Abramczyk, O.; Martin, L.; Dalby, K. N. *Biochemistry* **2007**, *46*, 9187.
(116) Szafranska, A. E.; Luo, X.; Dalby, K. N. *Anal. Biochem.* **2005**, *336*, 1.
(117) Keesler, G. A.; Bray, J.; Hunt, J.; Johnson, D. A.; Gleason, T.; Yao, Z.; Wang, S.-W.; Parker, C.; Yamane, H.; Cole, C.; Lichenstein, H. S. *Protein Expression Purif.* **1998**, *14*, 221.
(118) Caffrey, D. R.; O'Neill, L. A. J.; Shields, D. C. *Journal of Molecular Evolution* **1999**, *49*, 567.
(119) Akella, R.; Moon, T. M.; Goldsmith, E. J. *Biochimica et biophysica acta* **2008**, *1784*, 48.
(120) Lee, T.; Hoofnagle, A. N.; Kabuyama, Y.; Stroud, J.; Min, X.; Goldsmith, E. J.; Chen, L.; Resing, K. A.; Ahn, N. G. *Molecular cell* **2004**, *14*, 43.
(121) Zhou, T.; Sun, L.; Humphreys, J.; Goldsmith, E. J. *Structure (London, England : 1993)* **2006**, *14*, 1011.

(122) Zhang, F.; Strand, A.; Robbins, D.; Cobb, M. H.; Goldsmith, E. J. *Nature* **1994**, *367*, 704.
(123) Sheridan, D. L.; Kong, Y.; Parker, S. A.; Dalby, K. N.; Turk, B. E. *Journal of Biological Chemistry* **2008**, *283*, 19511.
(124) Lee, S.; Warthaka, M.; Yan, C.; Kaoud, T. S.; Piserchio, A.; Ghose, R.; Ren, P.; Dalby, K. N. *PLoS ONE* **2011**, *6*, e18594.
(125) Stains, C. I.; Luković, E.; Imperiali, B. *ACS Chemical Biology* **2010**, *6*, 101.
(126) Garai, A.; Zeke, A.; Gogl, G.; Toro, I.; Fordos, F.; Blankenburg, H.; Barkai, T.; Varga, J.; Alexa, A.; Emig, D.; Albrecht, M.; Remenyi, A. *Sci. Signal.* **2012**, *5*, ra74.
(127) Chen, G.; Porter, M. D.; Bristol, J. R.; Fitzgibbon, M. J.; Pazhanisamy, S. *Biochemistry* **2000**, *39*, 2079.
(128) Pearce, D. A.; Jotterand, N.; Carrico, I. S.; Imperiali, B. *Journal of the American Chemical Society* **2001**, *123*, 5160.
(129) Shults, M. D.; Pearce, D. A.; Imperiali, B. *Journal of the American Chemical Society* **2003**, *125*, 10591.
(130) Fersht, A. *Structure and mechanism in protein science: a guide to enzyme catalysis and protein folding*; Macmillan, 1999.
(131) Joyce, L. A.; Canary, J. W.; Anslyn, E. V. *Chemistry – A European Journal* **2012**, *18*, 8064.
(132) Yap, J. L.; Worlikar, S.; MacKerell, A. D.; Shapiro, P.; Fletcher, S. *ChemMedChem* **2011**, *6*, 38.
(133) Aronov, A. M.; Tang, Q.; Martinez-Botella, G.; Bemis, G. W.; Cao, J.; Chen, G.; Ewing, N. P.; Ford, P. J.; Germann, U. A.; Green, J.; Hale, M. R.; Jacobs, M.; Janetka, J. W.; Maltais, F.; Markland, W.; Namchuk, M. N.; Nanthakumar, S.; Poondru, S.; Straub, J.; ter Haar, E.; Xie, X. *Journal of Medicinal Chemistry* **2009**, *52*, 6362.
(134) Minami, T.; Esipenko, N. A.; Akdeniz, A.; Zhang, B.; Isaacs, L.; Anzenbacher, P. *Journal of the American Chemical Society* **2013**.
(135) Minami, T.; Esipenko, N. A.; Zhang, B.; Kozelkova, M. E.; Isaacs, L.; Nishiyabu, R.; Kubo, Y.; Anzenbacher, P. *Journal of the American Chemical Society* **2012**, *134*, 20021.